Methods in Molecular Biology 1199

Springer Protocols

Adriana Fontes
Beate Saegesser Santos *Editors*

Quantum Dots: Applications in Biology

Second Edition

Humana Press

METHODS IN MOLECULAR BIOLOGY

Series Editor
John M. Walker
School of Life Sciences
University of Hertfordshire
Hatfield, Hertfordshire, AL10 9AB, UK

For further volumes:
http://www.springer.com/series/7651

Quantum Dots: Applications in Biology

Second Edition

Edited by

Adriana Fontes

Research Group on Biomedical Nanotechnology,
Biophysics and Radiobiology Department,
Federal University of Pernambuco, Recife, Pernambuco, Brazil

Beate Saegesser Santos

Research Group on Biomedical Nanotechnology, Pharmaceutical Sciences Department,
Federal University of Pernambuco, Recife, Pernambuco, Brazil

Humana Press

Editors
Adriana Fontes
Research Group on Biomedical Nanotechnology
Biophysics and Radiobiology Department
Federal University of Pernambuco
Recife, Pernambuco, Brazil

Beate Saegesser Santos
Research Group on Biomedical Nanotechnology
Pharmaceutical Sciences Department
Federal University of Pernambuco
Recife, Pernambuco, Brazil

ISSN 1064-3745 ISSN 1940-6029 (electronic)
ISBN 978-1-4939-1279-7 ISBN 978-1-4939-1280-3 (eBook)
DOI 10.1007/978-1-4939-1280-3
Springer New York Heidelberg Dordrecht London

Library of Congress Control Number: 2014944737

© Springer Science+Business Media New York 2014
This work is subject to copyright. All rights are reserved by the Publisher, whether the whole or part of the material is concerned, specifically the rights of translation, reprinting, reuse of illustrations, recitation, broadcasting, reproduction on microfilms or in any other physical way, and transmission or information storage and retrieval, electronic adaptation, computer software, or by similar or dissimilar methodology now known or hereafter developed. Exempted from this legal reservation are brief excerpts in connection with reviews or scholarly analysis or material supplied specifically for the purpose of being entered and executed on a computer system, for exclusive use by the purchaser of the work. Duplication of this publication or parts thereof is permitted only under the provisions of the Copyright Law of the Publisher's location, in its current version, and permission for use must always be obtained from Springer. Permissions for use may be obtained through RightsLink at the Copyright Clearance Center. Violations are liable to prosecution under the respective Copyright Law.
The use of general descriptive names, registered names, trademarks, service marks, etc. in this publication does not imply, even in the absence of a specific statement, that such names are exempt from the relevant protective laws and regulations and therefore free for general use.
While the advice and information in this book are believed to be true and accurate at the date of publication, neither the authors nor the editors nor the publisher can accept any legal responsibility for any errors or omissions that may be made. The publisher makes no warranty, express or implied, with respect to the material contained herein.

Cover designed by the Biomedical Nanotechnology Research Group
Cover illustration: Mammary fibroadenoma tissue labeled with CdTe quantum dots conjugated to Concanavalin A. Quantum dots present an orange emission.

Printed on acid-free paper

Humana Press is a brand of Springer
Springer is part of Springer Science+Business Media (www.springer.com)

Preface

Fluorescence provides a unique method for understanding how biomolecules interact with each other in many levels, from single cell to whole organisms. Researchers commonly use techniques based on Fluorescence mainly due to its high sensitivity (capable of detecting even a single molecule) and specificity. The development of new techniques (such as Multiphoton Microscopy and Fluorescence Correlation Spectroscopy), new lasers, and new fluorophores (presenting new features in respect to the traditional organic dyes), have allowed researchers to take advantages of the full potential of Fluorescence. Semiconductor nanoparticles, with typical dimensions ranging from 2 to 10 nm, also called Quantum Dots (QDs) are an active and integral part of these advances.

Due to their unique optical properties QDs have been increasingly applied as fluorescent probes in Life Sciences since the late 1990s. Over the years, QDs have offered considerable benefits and complementary characteristics when compared to the conventional organic dyes. Besides the tunable emission according to their size, some major advantages offered by QDs are: (1) a broad absorption band, allowing a flexible cross section, for example for FRET (Förster Energy Transfer) applications; (2) an active surface for chemical bioconjugation: QDs can be conjugated to a variety of different biomolecules and become inorganic–organic hybrid nanoparticles combining characteristics of both materials, that is, the fluorescence of QDs with the biochemical properties of the biomolecules; and (3) a high resistance to photobleaching: the most important feature of QDs over conventional organic dyes.

QDs belong to the class of the modern tools which provide a great contribution to Optical Microscopy and Life Sciences. However, even after approximately 16 years of the first QDs' report for biological purposes, this new class of fluorophores still continues to be applied in new procedures. Nevertheless the development of new protocols for QDs' characterization and applications, there are still aspects of QDs–biological systems interactions to be understood and drawbacks to be overcome.

In this context, after approximately 7 years from the first edition, the second edition of the Quantum Dots book (Applications in Biology) brings 18 chapters addressing consolidated approaches as well as new trends in the field. The book is organized in five parts. The first part comprises an introduction on QDs as fluorescent probes in Life Sciences. The second part covers some important features about QDs' preparative processes and characterizations for their successful application as fluorophores. The third part presents main aspects related to QDs methods applied to live cells and tissues. The fourth part comprises QDs experiments in small animals. By the end, the last part demonstrates the versatility of QDs in a set of FRET applications. The editors hope that the book can be a good reference material for people who already work or intend to work with QDs by providing information about methods and protocols helping, in this way, to widely expand their research.

Recife, Brazil

Adriana Fontes
Beate Saegesser Santos

Contents

Preface . . . . . *v*
Contributors . . . . . *ix*

PART I INTRODUCTION TO QUANTUM DOTS

1 Quantum Dots as Biophotonics Tools 3
Carlos L. Cesar

PART II QUANTUM DOTS' PREPARATIVE PROCESSES AND CHARACTERIZATIONS

2 Photoligation Combined with Zwitterion-Modified Lipoic Acid Ligands Provides Compact and Biocompatible Quantum Dots 13
Naiqian Zhan, Goutam Palui, Henry Grise, and Hedi Mattoussi

3 Analysis of Quantum Dots and Their Conjugates by Capillary Electrophoresis with Detection of Laser-Induced Luminescence 33
Karel Klepárník, Vladimíra Datinská, Ivona Voráčová, and Marcela Lišková

4 Advanced Procedure for Oriented Conjugation of Full-Size Antibodies with Quantum Dots 55
Kristina Brazhnik, Igor Nabiev, and Alyona Sukhanova

5 Quantum Dot–Antibody Conjugates via Carbodiimide-Mediated Coupling for Cellular Imaging 67
Daniel Alistair East, Michael Todd, and Ian James Bruce

6 Measuring the Hydrodynamic Radius of Quantum Dots by Fluorescence Correlation Spectroscopy 85
André A. de Thomaz, Diogo B. Almeida, and Carlos L. Cesar

7 Quantum Dots Fluorescence Quantum Yield Measured by Thermal Lens Spectroscopy 93
Carlos Estupiñán-López, Christian Tolentino Dominguez, Paulo E. Cabral Filho, Adriana Fontes, and Renato E. de Araujo

8 Semiquantitative Fluorescence Method for Bioconjugation Analysis. 103
Aluízio G. Brasil Jr., Kilmara H.G. Carvalho, Elisa S. Leite, Adriana Fontes, and Beate Saegesser Santos

PART III QUANTUM DOTS FOR LIVE CELLS AND TISSUES APPLICATIONS

9 Assembly, Characterization, and Delivery of Quantum Dot Labeled Biotinylated Lipid Particles 113
Valeria Sigot

10 Oriented Conjugation of Single-Domain Antibodies and Quantum Dots 129
Kristina Brazhnik, Igor Nabiev, and Alyona Sukhanova

11 Functional Integration of Quantum Dot Labeled Mesenchymal Stem Cells in a Cardiac Microenvironment 141
Maria C. Collins, Philip R. Gunst, and Barbara J. Muller-Borer

12 In Vitro Approaches to Assessing the Toxicity of Quantum Dots 155
Ryan S. McMahan, Vivian Lee, William C. Parks, Terrance J. Kavanagh, and David L. Eaton

13 Basics for the Preparation of Quantum Dots and Their Interactions with Living Cells 165
Xiue Jiang, Jing Bai, and Tiantian Wang

PART IV QDs FOR SMALL ANIMALS APPLICATIONS

14 In Vivo Approaches to Assessing the Toxicity of Quantum Dots 179
David K. Scoville, Christopher M. Schaupp, François Baneyx, and Terrance J. Kavanagh

15 Quantum Dots for Imaging Neural Cells In Vitro and In Vivo 191
Angela O. Choi, Kevin D. Neibert, and Dusica Maysinger

16 A Short-Term Inhalation Study Protocol: Designed for Testing of Toxicity and Fate of Nanomaterials 207
Lan Ma-Hock, Thomas Hofmann, Robert Landsiedel, and Bennard van Ravenzwaay

PART V QUANTUM DOTS FOR FRET APPLICATIONS

17 Quantitative Measurement of Proteolytic Rates with Quantum Dot-Peptide Substrate Conjugates and Förster Resonance Energy Transfer 215
Miao Wu, Eleonora Petryayeva, Igor L. Medintz, and W. Russ Algar

18 Solid-Phase Supports for the in situ Assembly of Quantum Dot-FRET Hybridization Assays in Channel Microfluidics 241
Anthony J. Tavares, M. Omair Noor, Uvaraj Uddayasankar, Ulrich J. Krull, and Charles H. Vannoy

Index *257*

Contributors

W. Russ Algar • *Department of Chemistry, University of British Columbia, Vancouver, BC, Canada*

Diogo B. Almeida • *Quantum Electronics Department, Institute of Physics Gleb Wataghin, State University of Campinas/UNICAMP, Campinas, São Paulo, Brazil*

Renato E. de Araujo • *Laboratory of Biomedical Optics and Imaging, Federal University of Pernambuco, Recife, Pernambuco, Brazil*

Jing Bai • *State Key Laboratory of Electroanalytical Chemistry, Changchun Institute of Applied Chemistry, Chinese Academy of Sciences, Changchun, China*

François Baneyx • *Department of Chemical Engineering, University of Washington, Seattle, WA, USA*

Aluízio G. Brasil Jr. • *Research Group on Biomedical Nanotechnology, Federal University of Pernambuco, Recife, Pernambuco, Brazil; Exact Sciences and Technology Institute, Federal University of Amazonas, Itacoatiara, Amazonas, Brazil*

Kristina Brazhnik • *Laboratory of Nano-Bioengineering, National Research Nuclear University MEPhI "Moscow Engineering Physics Institute", Moscow, Russian Federation*

Ian James Bruce • *School of Physical Sciences, University of Kent, Canterbury, Kent, UK*

Paulo E. Cabral Filho • *Research Group on Biomedical Nanotechnology, Federal University of Pernambuco, Recife, Pernambuco, Brazil*

Kilmara H.G. Carvalho • *Research Group on Biomedical Nanotechnology, Federal University of Pernambuco, Recife, PE, Brazil; Superior School of Health Sciences, State University of Amazonas, Manaus, Amazonas, Brazil*

Carlos L. Cesar • *Quantum Electronics Department, Institute of Physics Gleb Wataghin, State University of Campinas/UNICAMP, Campinas, São Paulo, Brazil*

Angela O. Choi • *Department of Pharmacology and Therapeutics, Faculty of Medicine, McGill University, Montreal, QC, Canada*

Maria C. Collins • *Department of Cardiovascular Sciences, East Carolina Heart Institute, East Carolina University Brody School of Medicine, Greenville, NC, USA*

Vladimíra Datinská • *Institute of Analytical Chemistry, Czech Academy of Sciences, Brno, Czech Republic*

Christian Tolentino Dominguez • *Laboratory of Biomedical Optics and Imaging, Federal University of Pernambuco, Recife, Pernambuco, Brazil*

Daniel Alistair East • *Royal Veterinary College, London, UK*

David L. Eaton • *Department of Environmental and Occupational Health Sciences, University of Washington, Seattle, WA, USA*

Carlos Estupiñán-López • *Laboratory of Biomedical Optics and Imaging, Federal University of Pernambuco, Recife, Pernambuco, Brazil*

Adriana Fontes • *Research Group on Biomedical Nanotechnology, Biophysics and Radiobiology Department, Federal University of Pernambuco, Recife, Pernambuco, Brazil*

Henry Grise • *Department of Biological Science, Florida State University, Tallahassee, FL, USA*

Philip R. Gunst • *Metabolon Inc., Durham, NC, USA*

Thomas Hofmann • *Experimental Toxicology and Ecology, BASF SE, Ludwigshafen, Germany*
Xiue Jiang • *State Key Laboratory of Electroanalytical Chemistry, Changchun Institute of Applied Chemistry, Chinese Academy of Sciences, Changchun, China*
Terrance J. Kavanagh • *Department of Environmental and Occupational Health Sciences, University of Washington, Seattle, WA, USA*
Karel Klepárník • *Institute of Analytical Chemistry, Czech Academy of Sciences, Brno, Czech Republic*
Ulrich J. Krull • *Chemical Sensors Group, Department of Chemical and Physical Sciences, University of Toronto Mississauga, Mississauga, ON, Canada*
Robert Landsiedel • *Experimental Toxicology and Ecology, BASF SE, Ludwigshafen, Germany*
Vivian Lee • *Department of Cell Biology & Physiology, Washington University School of Medicine in St. Louis, MO, USA*
Elisa S. Leite • *Research Group on Biomedical Nanotechnology, Chemical Engineering Department, Federal University of Pernambuco, Recife, Pernambuco, Brazil*
Marcela Lišková • *Institute of Analytical Chemistry, Czech Academy of Sciences, Brno, Czech Republic*
Lan Ma-Hock • *Experimental Toxicology and Ecology, BASF SE, Ludwigshafen, Germany*
Hedi Mattoussi • *Department of Chemistry and Biochemistry, Florida State University, Tallahassee, FL, USA*
Dusica Maysinger • *Department of Pharmacology and Therapeutics, Faculty of Medicine, McGill University, Montreal, QC, Canada*
Ryan S. McMahan • *Department of Environmental and Occupational Health Sciences, University of Washington, Seattle, WA, USA*
Igor L. Medintz • *Center for Bio/Molecular Science and Engineering, U.S. Naval Research Laboratory, Washington, DC, USA*
Barbara J. Muller-Borer • *Department of Engineering, East Carolina University, Greenville, NC, USA*
Igor Nabiev • *Laboratory of Nano-Bioengineering, National Research Nuclear University MEPhI "Moscow Engineering Physics Institute", Moscow, Russian Federation; European Technological Platform "Semiconductor Nanocrystals", EA4682-Laboratory of Research in Nanosciences, Université de Reims Champagne-Ardenne, Reims, France*
Kevin D. Neibert • *Department of Pharmacology and Therapeutics, Faculty of Medicine, McGill University, Montreal, QC, Canada*
M. Omair Noor • *Chemical Sensors Group, Department of Chemical and Physical Sciences, University of Toronto Mississauga, Mississauga, ON, Canada*
Goutam Palui • *Department of Chemistry and Biochemistry, Florida State University, Tallahassee, FL, USA*
William C. Parks • *Department of Medicine, Cedars-Sinai Medical Center, Los Angeles, CA, USA*
Eleonora Petryayeva • *Department of Chemistry, University of British Columbia, Vancouver, BC, Canada*
Bennard van Ravenzwaay • *Experimental Toxicology and Ecology, BASF SE, Ludwigshafen, Germany*
Beate Saegesser Santos • *Research Group on Biomedical Nanotechnology, Pharmaceutical Sciences Department, Federal University of Pernambuco, Recife, Pernambuco, Brazil*

Christopher M. Schaupp • *Department of Environmental and Occupational Health Sciences, University of Washington, Seattle, WA, USA*
David K. Scoville • *Department of Environmental and Occupational Health Sciences, University of Washington, Seattle, WA, USA*
Valeria Sigot • *Laboratory of Cellular Dynamics, Max Planck Institute for Biophysical Chemistry, Götingen, Germany; Microscopy Laboratory Applied to Molecular and Cellular Studies, School of Bioengineering, National University of Entre Ríos, Oro Verde, Entre Ríos, Argentina*
Alyona Sukhanova • *Laboratory of Nano-Bioengineering, National Research Nuclear University MEPhI "Moscow Engineering Physics Institute", Moscow, Russian Federation; European Technological Platform "Semiconductor Nanocrystals", EA4682-Laboratory of Research in Nanosciences, Université de Reims Champagne-Ardenne, Reims, France*
Anthony J. Tavares • *Chemical Sensors Group, Department of Chemical and Physical Sciences, University of Toronto Mississauga, Mississauga, ON, Canada*
André A. de Thomaz • *Quantum Electronics Department, Institute of Physics Gleb Wataghin, State University of Campinas/UNICAMP, Campinas, São Paulo, Brazil*
Michael Todd • *School of Science, University of Greenwich, Chatham Maritime Kent, UK*
Uvaraj Uddayasankar • *Chemical Sensors Group, Department of Chemical and Physical Sciences, University of Toronto Mississauga, Mississauga, ON, Canada*
Charles H. Vannoy • *Chemical Sensors Group, Department of Chemical and Physical Sciences, University of Toronto Mississauga, Mississauga, ON, Canada; McColl-Lockwood Laboratory for Muscular Dystrophy Research, Neuromuscular/ALS Center, Carolinas Medical Center, Charlotte, NC, USA*
Ivona Voráčová • *Institute of Analytical Chemistry, Czech Academy of Sciences, Brno, Czech Republic*
Tiantian Wang • *State Key Laboratory of Electroanalytical Chemistry, Changchun Institute of Applied Chemistry, Chinese Academy of Sciences, Changchun, China*
Miao Wu • *Department of Chemistry, University of British Columbia, Vancouver, BC, Canada*
Naiqian Zhan • *Department of Chemistry and Biochemistry, Florida State University, Tallahassee, FL, USA*

Part I

Introduction to Quantum Dots

Chapter 1

Quantum Dots as Biophotonics Tools

Carlos L. Cesar

Abstract

This chapter provides a short review of quantum dots (QDs) physics, applications, and perspectives. The main advantage of QDs over bulk semiconductors is the fact that the size became a control parameter to tailor the optical properties of new materials. Size changes the confinement energy which alters the optical properties of the material, such as absorption, refractive index, and emission bands. Therefore, by using QDs one can make several kinds of optical devices. One of these devices transforms electrons into photons to apply them as active optical components in illumination and displays. Other devices enable the transformation of photons into electrons to produce QDs solar cells or photodetectors. At the biomedical interface, the application of QDs, which is the most important aspect in this book, is based on fluorescence, which essentially transforms photons into photons of different wavelengths. This chapter introduces important parameters for QDs' biophotonic applications such as photostability, excitation and emission profiles, and quantum efficiency. We also present the perspectives for the use of QDs in fluorescence lifetime imaging (FLIM) and Förster resonance energy transfer (FRET), so useful in modern microscopy, and how to take advantage of the usually unwanted blinking effect to perform super-resolution microscopy.

Key words Quantum dots, Biophotonics, Optical properties, Photostability, Fluorescence, FLIM, FRET, FCS, Blinking, Super resolution, Bioconjugation

Quantum dots (QDs) are semiconductor nanoparticles, so small that quantum confinement effects play a differential role in their physicochemical properties. The major difference between QDs and bulk semiconductors is that the QDs' optical properties depend upon the size and can, thus, be tailored to desired conditions, opening several opportunities to develop photonic devices and to establish biophotonic applications. From optics point of view, a particle is called a dot when its electronic levels and its fluorescence consequently change according to the small size, which happens to particles up to sizes of the order of 5 nm of radius, depending on the semiconductor material. In this way, QDs' typical diameters range from 2 to 10 nm. QDs made from the same material, but with different sizes, can present emission from the ultraviolet to the infrared light (Fig. 1a). This is a consequence of the energy level discretization, as well as of the bandgap energy

Adriana Fontes and Beate Saegesser Santos (eds.), *Quantum Dots: Applications in Biology*, Methods in Molecular Biology, vol. 1199, DOI 10.1007/978-1-4939-1280-3_1, © Springer Science+Business Media New York 2014

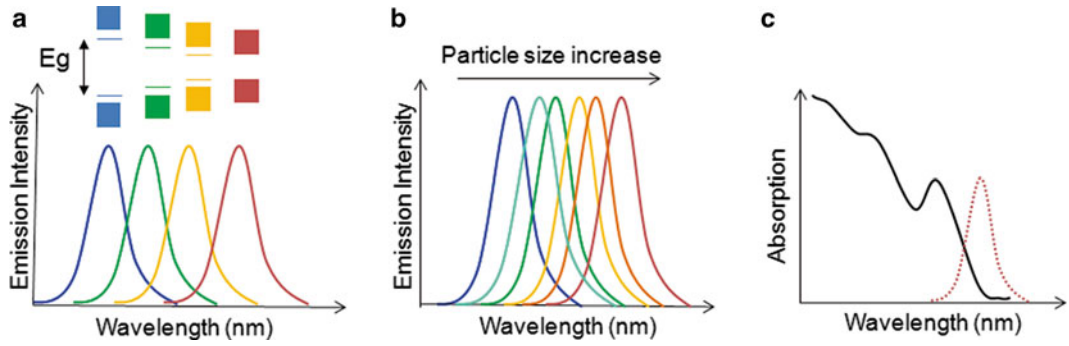

Fig. 1 Some of the unique optical properties of quantum dots: (**a** and **b**) bandgap (Eg) dependence on the size of the particle and (**c**) their multispectral capability of emission

which is higher as smaller is the size of the QD. Thus, as energy is inversely proportional to wavelength of the fluorescence, this means that the larger the QD, the smaller is the bandgap energy and the more towards to the red end of the spectrum is its corresponding fluorescence emission (Fig. 1b).

The first quantum dots were mentioned in the literature in 1981–1982 [1, 2], but the term quantum dot was applied only in 1988 [3]. Before the QDs' appearance the only way to control the optical property was by changing the semiconductor bandgap. Ternary or quaternary alloys were commonly used for a fine bandgap tuning. The ternary HgCdTe alloy, for example, was very important for night vision cameras [4]. Other option was to change temperature, but within a very narrow bandgap range. On the other hand, the first biological applications of QDs as fluorescent probes for Life Science application was reported in literature in 1998 simultaneously by Bruchez et al. [5] and Chan et al. [6].

We are living in a nanotechnology era and there are several nanomaterials that look promising in terms of devices and biological applications. An editorial from Nature Nanotechnology [7] called attention for the advantages of the QDs compared to today's other fashion nanomaterials, such as fullerenes, nanotubes, graphenes, and others. This paper argues that QDs exist for a longer time; thus, more basic science was produced with them. There are even optical devices based on QDs at the market, or very close to it, as one can observe by the number of patents associated with the material.

Today, QDs are considered photonic tools and their applications can be classified in terms of their characteristic optical properties. For example, we can have light-emitting devices such as illuminators, displays, lasers, LEDs [8], or fluorescent probes for Life Science [9]. One can also use light-absorbing devices to develop solar cells, or photovoltaics, and photodetectors. Finally, it is possible to use the fast optical nonlinearities of the QDs to develop optical switches and or other kinds of devices to manipulate light with light [10, 11].

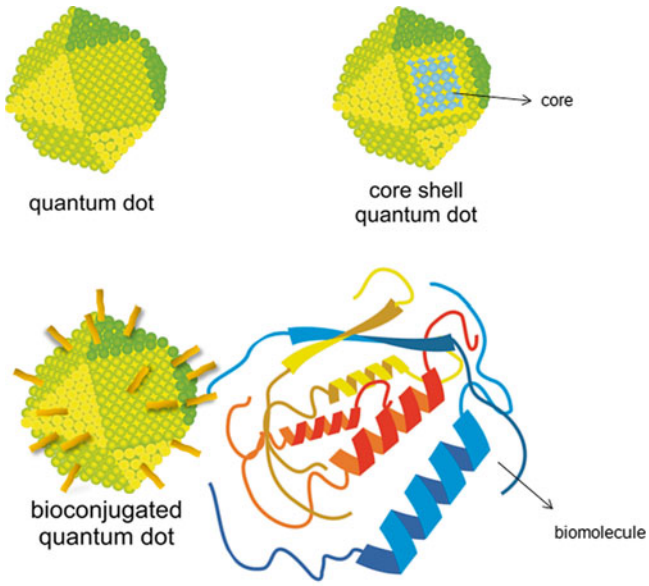

Fig. 2 Quantum dots are nanosized crystals. They may be composed of a core material coated by a shell of a different material, resulting in a core-shell structure. They may also be associated to functionalizing chemical species which may allow their conjugation to specific biomolecules

For all QDs light emission devices, such as QDs as fluorescent biological tools, it is mandatory to avoid as much as possible the presence of surfaces traps in order to enhance the emission efficiency. Due to this reason, QDs are usually core/shell nanoparticles (Fig. 2).

The core is responsible for the QDs' fundamental optical properties (electronic absorption the fluorescence spectral region) and the shell (made up of some monolayers of another semiconductor material) is used to passivate the defects of the surface of the core with the goal to improve the fluorescence intensity and decrease the linewidth of the emission band. The shell reduces the number of surface dangling bonds, which can act as trap states for electrons minimizing the QDs' emission quality. In general the shell is made of a semiconductor which has a greater bandgap than the bandgap of the core. For Life Science purposes, in which fluorescence in the visible region is usually required, both core and shell are composed of elements from the II B and VI A groups of the Periodic Table. Figure 3 relates the bandgap energy region and the size of the crystals. The major examples applied are CdSe/ZnS, CdTe/CdS and ZnSe/ZnS QDs [12, 13]. Moreover, most II–VI QDs crystallize either in the cubic zinc blend or in the hexagonal wurtzite type structure.

The importance of QDs for biophotonic applications is their use as fluorescent probes in the place the commonly used organic dyes [9]. For this, one needs a suspension of highly efficient

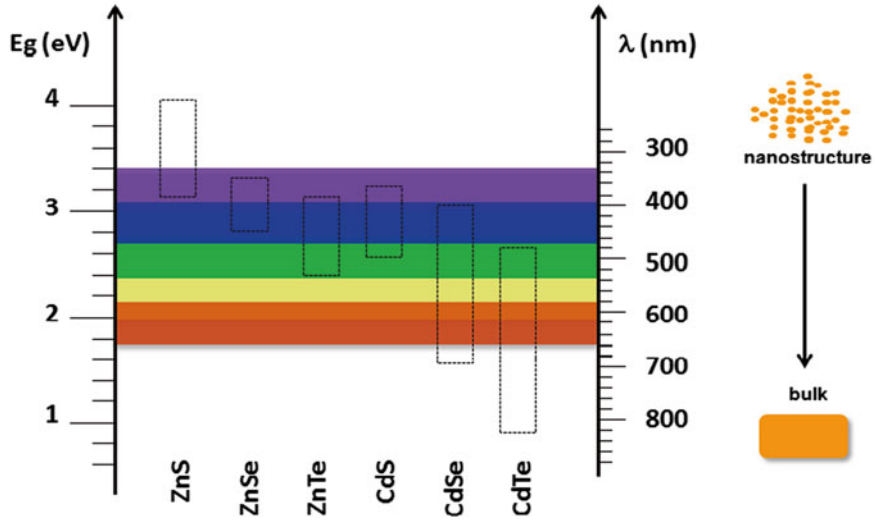

Fig. 3 Bandgap energy interval of some II–VI quantum dots ranging from nanosized to bulk crystals and the correlation with their spectral region

emitter colloidal QDs, chemically bound to some molecule, that is, bioconjugated, to provide bio-specificity, highlighting only the desired biomolecules (Fig. 2). The bioconjugation can be accomplished by simple adsorption or by covalent attachment following guidelines adapted from known bioconjugation methodologies [14]. For the aqueous synthetic QDs' procedures the stabilizing agents used present carboxyl, thiol or amine terminals which can be used as chemical bridges to bioconjugate biomolecules and confer more specificity for biological applications. Some common examples of stabilizing agents are: mercaptopropionic acid (MPA), mercaptoacetic acid (MAA), mercaptosuccinic acid (MSA), Dihydrolipoic acid (DHLA), cysteine (CYS) and cysteamine (CYSAM).

There are several advantages of the QDs when compared to organic dyes which may be described as follows:

1. The main one is photostability, the QDs resilience to photobleaching, which can be 100 times larger than organic fluorescent dyes [15–17]. This allows the Life Science researches to follow in time several long lasting biological processes, impossible with less stable markers.
2. Colloidal QDs 20 times brighter than organic dyes have been reported [15], although the emission efficiency for most used probes is not an issue today.
3. QDs' large excitation (absorption) bandwidth is also an advantage because only one laser line at the UV/blue can be used to excited several different color probes, which is impossible with organic dyes (Fig. 1c).

4. QDs' emission linewidths are more symmetric, and narrower, than organic dyes meaning they can provide more colors in multistaining methods (Fig. 1b). For multicolor staining procedures the narrow emission linewidth is also important to avoid cross talk. The wavelength range covered by different sizes with the same semiconductor QDs is much broader than the one obtained with different dye molecules, from the blue to the near infrared region.
5. There is also another difference between QDs and organic dyes which have not being fully exploited. The fluorescence lifetime of typical organic labels is around 1–5 ns while QDs fluorescence lifetime can be of order of 20 to a few hundred ns. This means that they can be used together with organic probes and then be discriminated by the fluorescence lifetime using fluorescence lifetime imaging (FLIM) [18].
6. Other important application in Life Science is FRET (Förster or fluorescence resonance energy transfer) [19]. The use of QDs in this application will involve more research to understand the FRET process in the presence of the cap layers and its efficiency dependence on the cap layer thickness. In the particular case, QDs can be efficient FRET donors due to their broad absorption band combined with their size-tunable emission and their larger physical size (when compared to conventional organic dyes). The use of QDs for FRET can allow (1) optimization of the spectral overlap with any potential FRET acceptor; (2) excitation at a wavelength far from the acceptor absorption peak (minimizing acceptor direct excitation), and (3) the ability to use multiple acceptors around QDs cores to increase the overall FRET efficiency [20].
7. Blinking [21, 22] was considered an undesirable QDs property. The emission of the QDs disappears/appears for some random time intervals. However, today, the microscopy community discovered that this can be used to perform super-resolution microscopy, because a subtraction between two frames in subsequent short times can reveal the light spot of a single QD source necessary for the localization of a microscopy processing below the diffraction limit.

In conclusion, this chapter presented some fundamental features related to QDs, focused specially in QDs as biophotonic tools. Although some QDs' drawbacks (such as toxicity and efficient label of specific cell/tissue organelles as well as other intracellular structures) have still to be overcome [23, 24], the fact is since the first mention in the literature, QDs have been studied and applied extensively. Today, these fluorescent nanoparticles can be employed in a variety of experiments ranging from imaging of fixed and live cells (and tissues) and photodynamic therapy all the way to fluoroimmunoassays and biosensors [25–27]. Taken together, all

these findings show that a deeper understanding of the QDs basis and mechanisms underlying QDs and biological systems interactions is helpful for researchers avoiding side effects and improving the quality of labeling by QDs, rendering innovative methodologies which can be applied for the comprehension of biological process as well as for diagnostics and therapeutic purposes.

References

1. Ekimov A, Onushchenko A (1981) Quantum size effect in 3-dimensional microscopic semiconductor crystals. JETP Lett 34(6):345–349
2. Rossetti R, Brus L (1982) Electron-hole recombination emission as a probe of surface-chemistry in aqueous CdS colloids. J Phys Chem 86(23):4470–4472
3. Reed MA, Randall JN, Aggarwal RJ, Matyi RJ, Moore TM, Wetsel AE (1988) Observation of discrete electronic states in a zero-dimensional semiconductor nanostructure. Phys Rev Lett 60(6):535–537
4. Rogalski A (2003) Infrared detectors: status and trends. Progr Quant Electron 27(2–3): 59–210
5. Bruchez M Jr, Morrone M, Gin P, Weiss S, Alivisatos AP (1998) Semiconductor nanocrystals as fluorescent biological labels. Science 281:2013–2016
6. Chan WCW, Nie S (1998) Quantum dot bioconjugates for ultrasensitive nonisotopic detection. Science 281:2016–2018
7. Nature Nanotechnology Editorial (2010) The many aspects of quantum dots. Nat Nanotechnol 5(6):381
8. Anikeeva P, Halpert J, Bawendi M, Bulovic V (2009) Quantum dot light-emitting deices with electroluminescence tunable over the entire visible spectrum. Nano Lett 9(7):2532–2536
9. Michalet X, Pinaud FF, Bentolila LA, Tsay JM, Doose S, Li JJ, Sundaresan G, Wu AM, Gambhir SS, Weiss S (2005) Quantum dots for live cells, in vivo imaging, and diagnostics. Science 307(5709):538–544
10. Cotter D (1986) High-contrast ultrafast phase conjugation in semiconductor-doped glass. J Opt Soc Am B 3(8):246
11. Loss D, Di Vincenzo D (1998) Quantum computation with quantum dots. Phys Rev A 57(1):120–126
12. Dabbousi BO, Rodriguez VJ, Mikulec FV, Heine JR, Mattoussi H, Ober R (1997) CdSe/ZnS core-shell quantum dots: synthesis and characterization of a size series of highly luminescent nanocrystallites. J Phys Chem B 101(46):9463–9475
13. Santos BS, Farias PMA, Fontes A (2008) Semiconductor quantum dots for biological applications. In: Henine M (ed) Handbook of self assembled semiconductor nanostructures novel devices in photonics and electronics. Elsevier, Amsterdam, pp 773–798
14. Goldman ER, Anderson GP, Tran PT, Mattoussi H, Charles PT, Mauro JM (2002) Conjugation of luminescent quantum dots with antibodies using an engineered adaptor protein to provide new reagents for fluoroimmunoassays. Anal Chem 74(4):841–847
15. Walling M, Novak J, Shepard JRE (2009) Quantum dots for live cell and in vivo imaging. Int J Mol Sci 10(2):441–491
16. Jamieson T, Bakhshi R, Petrova D, Pocock R, Imani M, Seifalian AM (2007) Biological applications of quantum dots. Biomaterials 28(31):4717–4732
17. Wu X, Liu H, Liu J, Haley KN, Treadway JA, Larson JP, Ge N, Peale F, Bruchez MP (2003) Immunofluorescent labeling of cancer marker Her2 and other cellular targets with semiconductor quantum dots. Nat Biotechnol 21(1): 41–46
18. Becker W (2005) Advanced time-correlated single photon counting techniques, vol 81, Springer series in chemical physics. Springer, Berlin
19. Wallrabe H, Periasamy A (2005) Imaging protein molecules using FRET and FLIM microscopy. Curr Opin Biotechnol 16(1):19–27
20. Medintz IL, Mattoussi H (2009) Quantum dot-based resonance energy transfer and its growing application in biology. Phys Chem Chem Phys 11:17–45
21. Shimizu KT, Neuhauser RG, Leatherdale CA, Empedocles SA, Woo WK, Bawendi MG (2001) Blinking statistics in single semiconductor nanocrystal quantum dots. Phys Rev B 3:205316-1–205316-5
22. Wang X, Ren X, Kahen K, Hahn MA, Rajeswaran M, Maccagnano-Zacher S, Silcox J, Cragg GE, Efros AL, Krauss TD (2009) Non-blinking semiconductor nanocrystals. Nature 459(7247):686–689

23. Vieira CS, Almeida DB, de Thomaz AA, Menna-Barreto RF, dos Santos-Mallet JR, Cesar CL, Gomes SA, Feder D (2011) Studying nanotoxic effects of CdTe quantum dots in Trypanosoma cruzi. Mem Inst Oswaldo Cruz 106(2):158–165
24. Lira RB, Seabra MABL, Matos ALL, Vasconcelos JV, Bezerra DP, de Paula E, Santos BS, Fontes A (2013) Studies on intracellular delivery of carboxyl-coated CdTe quantum dots mediated by fusogenic liposomes. J Mat Chem B 1:4297–4305
25. Samia ACS, Dayal S, Clemens B (2006) Quantum dot-based energy transfer: perspectives and potential for applications in photodynamic therapy. Photochem Photobiol 82(3):617–625
26. Stringer RC, Hoehn D, Grant SA (2008) Quantum dot-based biosensor for detection of human cardiac troponin I using a liquid-core waveguide. Sensors J 8(3):295–300
27. Vannoy CH, Tavares AJ, Noor MO, Uddayasankar U, Krull UJ (2011) Biosensing with quantum dots: a microfluidic approach. Sensors 11:9732–9763

Part II

Quantum Dots' Preparative Processes and Characterizations

Chapter 2

Photoligation Combined with Zwitterion-Modified Lipoic Acid Ligands Provides Compact and Biocompatible Quantum Dots

Naiqian Zhan, Goutam Palui, Henry Grise, and Hedi Mattoussi

Abstract

We describe the design and synthesis of a series of compact ligands made of lipoic acid (LA)-based coordinating anchors and hydrophilic zwitterion groups. This ligand design is combined with a novel photoligation strategy to promote the transfer of QDs to polar and buffer media. This approach has provided hydrophilic QDs that exhibit great colloidal stability over a broad range of pHs and in the presence of cell culture media. Our photoligation strategy drastically improves previous phase transfer methods by eliminating the need for chemical reduction of the dithiolane ring using $NaBH_4$ prior to the cap exchange, and it is adapted to several LA-based ligands. We also found that QDs stabilized with these compact zwitterionic ligands are fully compatible with metal-histidine-driven self-assembly where the protein activity is maintained after forming conjugation with the QDs.

Key words Semiconductor quantum dots, Compactness, Zwitterion ligands, Photo-induced ligand exchange, Protein conjugation

1 Introduction

Semiconductor quantum dots (QDs) possess remarkable photo and chemical stability, and exhibit unique optical and spectroscopic properties such as high quantum yields, size- and composition-dependent absorption, and narrow emission profiles. Such unique properties are not easily shared by organic fluorophores and fluorescent proteins. This has generated a great interest to develop them as fluorescent platforms for use in a variety of bio- and nonbio-inspired applications, such as imaging, sensing, and light-emitting devices [1–4]. Preparation of high-quality QDs (i.e., with reduced size dispersity and high photoemission quantum yields) has widely relied on the pyrolysis of organometallic precursors in hot coordinating solutions [5–7]. In addition, it has been demonstrated that overcoating the core with a few monolayers of a wider band-gap semiconducting material, such as ZnS, ZnSeS, and

Adriana Fontes and Beate Saegesser Santos (eds.), *Quantum Dots: Applications in Biology*, Methods in Molecular Biology, vol. 1199, DOI 10.1007/978-1-4939-1280-3_2, © Springer Science+Business Media New York 2014

CdZnS, increases the photoluminescence quantum yield and enhances the long-term photostability of these materials [8, 9]. However, as-prepared these QDs are typically capped with a hydrophobic layer primarily composed of a mixture of alkylphosphines (trioctylphosphine/trioctylphosphine oxide, TOP/TOPO) and alkylamines; they are dispersible in aqueous media. Post-synthetic surface modifications are thus needed to render them hydrophilic and biocompatible.

Several approaches have been put forward to develop hydrophilic QDs that are colloidally stable over a broad range of biologically relevant conditions, reactive and with small hydrodynamic size [10–15]. One common and simple-to-implement approach has relied on cap exchange of the native ligands with bifunctional thiol-appended molecular ligands. Within this strategy (ligand exchange), it has been found that multi-dentate ligands, namely those presenting one or more dihydrolipoic acid-anchoring group (DHLA-based ligands with their multithiol groups), provide strong anchoring onto the semiconducting surface of the nanoparticles [12, 16–18]. In this family, the use of zwitterionic ligands is beneficial as these provide compact-size QDs with colloidal stability over a broad range of pHs. These ligands have been used in a variety of targeted studies such as cellular uptake and imaging. They also offer an efficient sensing platform based on fluorescence resonance energy transfer (FRET) [19–22].

With these ligands the solubility of the QDs is primarily driven by the hydrophilic nature of the zwitterionic heads while anchoring is promoted by the reduced form of the ligand (dihydrolipoic acid-appended zwitterion, DHLA-ZW). However, reduction of LA to produce DHLA-appended ligands requires a large excess of $NaBH_4$. This chemical reduction is also harsh and can alter the integrity of certain sensitive groups (such as azide and aldehyde). Additional purification steps after reduction and inert storage requirements make this approach tedious especially for zwitterion ligands; this is due to the limited solubility of such zwitterion ligands in organic media.

Recently, we have introduced a simple strategy for the photomediated phase transfer of ZnS-overcoated CdSe quantum dots to buffer media [23, 24]. Here, the ligand exchange and phase transfer are promoted photochemically, and involve the in situ photoreduction of lipoic acid in the presence of UV irradiation at 350 nm combined with tight and rapid anchoring on the QD surface [25]. Thus, this approach uses the stable, oxidized form of the ligand and entails in situ photoligation of the QDs.

In this chapter, we describe the design of multicoordinating, zwitterion ligands that we have developed for constructing hydrophilic QDs with small hydrodynamic size. These ligands are based on mono lipoic acid (LA), on which either a zwitterion group (-ZW) or a tetraethylene glycol-zwitterion group (-TEG-ZW) is appended

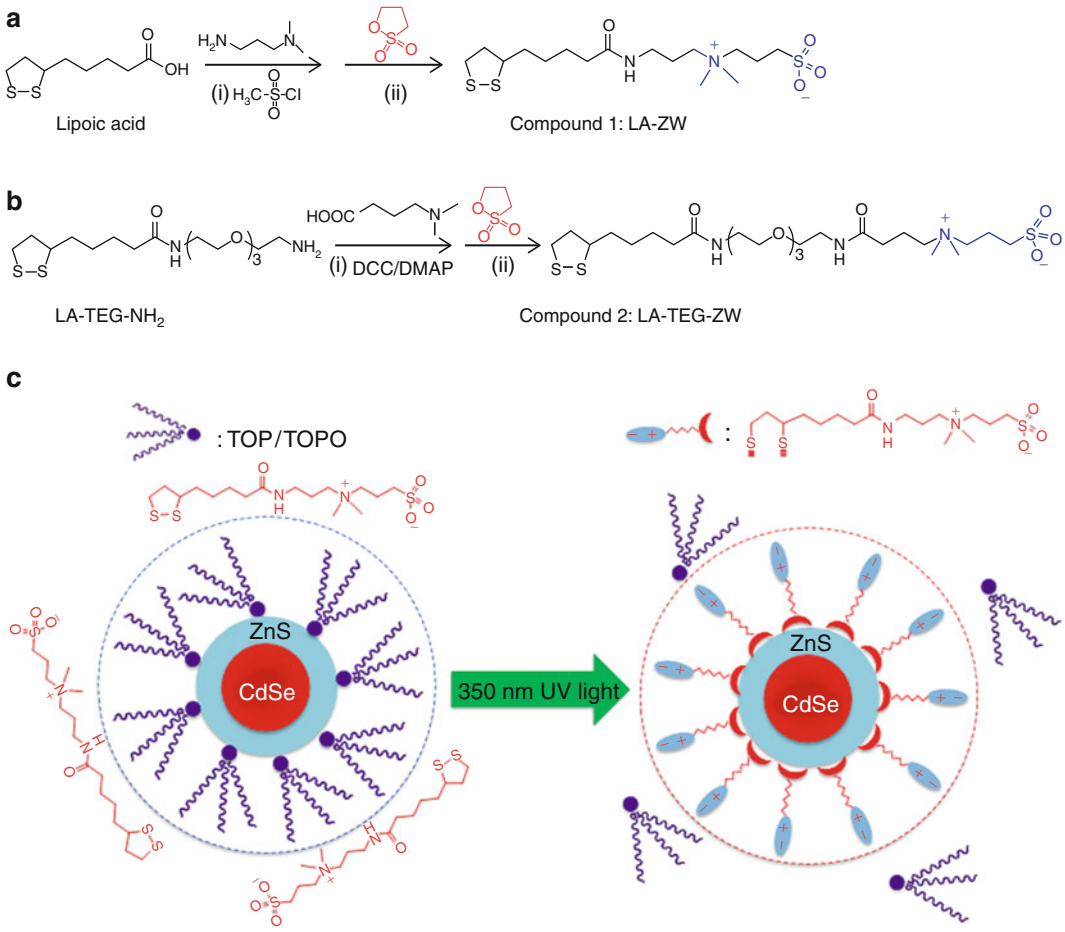

Fig. 1 Chemical structures and synthetic routes for the LA-based zwitterion ligands used. (**a**) Synthesis of LA-ZW was carried out in two steps. First, *N,N*-dimethyl-1,3-propane diamine was appended onto lipoic acid using methanesulfonyl chloride, and then coupled to 1,3-propanesultone to provide LA-ZW (compound 1). (**b**) Similarly, the synthesis of LA-TEG-ZW (compound 2) involved two steps. In the first, LA-TEG-NH_2 was coupled to 4-(dimethylamino)butyric acid hydrochloride in the presence of DCC and DMAP, followed by modification with sultone. (**c**) Schematic representation of the photoligation of TOP/TOPO-QDs with LA-zwitterion ligands, and transfer from hexane to buffer media

chemically (Fig. 1) [24]. This ligand design is combined with the photo-induced ligand exchange and phase transfer strategy to provide QDs that are compact and fully compatible with the ubiquitous metal-histidine conjugation to proteins expressed with a terminal polyhistidine tag. To implement this conjugation scheme, we further engineered a maltose-binding protein (MBP) expressing a C-terminal polyhistidine tag, MBP-His_n. We show that such protein can easily self-assemble on the surface of QDs photoligated with LA-ZW and LA-TEG-ZW alike. Conjugation of MBP onto the QDs can be confirmed by simple (and visual) amylose column assay which involves binding of the conjugate to the amylose gel loaded into a plastic column followed by release with soluble D-maltose.

Below we detail the protocols for the synthesis and purification of the zwitterion-appended lipoic acid ligand, photoligation, and phase transfer of CdSe-ZnS QDs using the stable oxidized form of the ligand. We also describe the protein expression and self-assembly on the QDs. The resulting QD-MBP-His_n conjugates will be tested using simple assay based on binding onto amylose gel and release with soluble maltose (the molecular substrate of MBP).

2 Materials

2.1 Synthesis of Quantum Dots

1. Selenium (99.99 %).
2. Cadmium acetylacetonate ($Cd(acac)_2$).
3. 1,2-Hexadecanediol (HDDO).
4. Trioctylphosphine (TOP, 90–95 %).
5. Trioctylphosphine (TOP, 98 %).
6. Trioctylphosphine oxide (TOPO, 90 %).
7. Trioctylphosphine oxide (TOPO, 98 %).
8. Hexadecylamine (HDA).
9. n-Hexylphosphonic acid (HPA).
10. Inert gas (nitrogen or argon).
11. Glove box.
12. Schlenk line.
13. Solvents (hexane, toluene, butanol, ethanol, methanol).
14. Diethylzinc ($ZnEt_2$).
15. Hexamethyldisilathiane (TMS_2S).
16. Tetramethylammonium hydroxide pentahydrate (TMAH).
17. Millipore hydrophilic and organic filters (PTFE).
18. Glass scintillation vials for cap exchange of TOP/TOPO-QDs.
19. Rubber septa.
20. Centrifugal filtration device, molecular weight cutoff of 50,000.
21. UV–Vis spectrophotometer (Shimadzu Spectrophotometer, UV 2450 model).
22. Photoreactor (Luzchem UV lamp, Model LZC-4V, Ottawa, ON, Canada).
23. Fluorolog-3 spectrometer (Jobin Yvon Inc., Edison, NJ, USA).

2.2 Synthesis of the Zwitterion Ligands

1. Lipoic acid, LA (or thioctic acid, TA).
2. Tetra-ethylene glycol (TEG).
3. Triethylamine (Et_3N).
4. Methanesulfonyl chloride (MsCl).

5. *N*,*N*-Dimethyl-1,3-propanediamine.
6. 4-(Dimethylamino)butyric acid hydrochloride.
7. 1,3-Propanesultone.
8. *N*,*N*′-Dicyclohexylcarbodiimide (DCC).
9. 4-Dimethylaminopyridine (DMAP).
10. Tris(2-aminoethyl)amine.
11. 1,1′-Carbonyldiimidazole (CDI).
12. Sodium carbonate (Na_2CO_3).
13. Sodium sulfate (Na_2SO_4), anhydrous.
14. Celite.
15. Silica gel (60 Å, 230–400 mesh).
16. Chloroform ($CHCl_3$).
17. Methanol (MeOH).
18. Deuterated dimethylsulfoxide (DMSO-d6).
19. Deuterated chloroform ($CDCl_3$).
20. Phosphoric acid.
21. Hydrochloric acid (HCl).
22. NMR spectrometer (Bruker SpectroSpin 600 MHz spectrometer).
23. Round-bottom flask, one and two necked.
24. Addition funnel.
25. Magnetic stirring bars.
26. Separatory funnels.
27. Rotary evaporator.
28. Glass funnels.
29. Filter papers.
30. Thin-layer chromatography (TLC) plates.
31. Iodine chamber to stain samples on TLC.

2.3 Expression and Purification of Proteins

1. pMal-c2 plasmid.
2. *Escherichia coli* BL21 cells.
3. Luria–Bertani broth base.
4. Isopropyl β-D-thiogalactoside.
5. Binding buffer: 50 mM sodium phosphate, pH 8.0, 300 mM NaCl, 10 mM imidazole.
6. Elution buffer: 50 mM sodium phosphate, pH 8.0, 300 mM NaCl, 250 mM imidazole.
7. Buffer for diafiltration: 20 mM Tris-HCl, pH 7.4, 2 mM EDTA.

8. Storage buffer: 12 mM phosphate buffer saline, pH 7.4, 137 mM NaCl, 2.7 mM KCl.
9. Nickel affinity gel.
10. Centricon units (10 kDa).
11. Syringe filter (0.22 μm) compatible with protein samples.

2.4 Construction of QD-Protein Conjugates, and Amylose Assay

1. Amylose resin.
2. D-(+)-Maltose monohydrate.
3. Disposable plastic columns (5 mL).
4. Microcentrifuge tubes.
5. Phosphate buffer salts.
6. Hand held UV light, 365 nm.

3 Methods

3.1 Synthesis of Zwitterion Ligands

We have designed and prepared a new set of lipoic acid-appended zwitterion ligands: LA-ZW and LA-TEG-ZW (*see* Fig. 1 for chemical structures). The protocol for synthesis of the ligand presenting a tetra-ethylene glycol-bridged zwitterion (LA-TEG-ZW) starts with LA-TEG-NH_2 previously described in reference [26]. All these ligands have been used for the photo-induced phase transfer of TOP/TOPO-QDs to buffer media.

1. LA-Zwitterion
   This involves two steps: synthesis of LA-*N*,*N*-dimethyl 1, 3-propanediamine followed by coupling to 1,3-propanesultone.
   - LA-*N*,*N*-dimethyl 1,3-propanediamine
     1. In a 250 mL three-necked round-bottom flask dissolve lipoic acid (6 g, ~30 mmol) and triethylamine (2.94 g, ~30 mmol) in 60 mL of CH_2Cl_2.
     2. Cool the reaction mixture to ~0 °C using an ice bath.
     3. Flush the content with nitrogen and let the reaction progress for 30 min with stirring.
     4. Add methanesulfonyl chloride (3.34 g, ~30 mmol) dropwise, slowly warm the reaction mixture up to room temperature, and leave it stirring for another 5 h.
     5. Load *N*,*N*-dimethyl-1,3-propanediamine (3.05 mL, ~24 mmol), triethylamine (1.22 g, ~12 mmol), and 40 mL of CH_2Cl_2 into an addition funnel.
     6. Add this solution to the reaction mixture dropwise (~over 30 min) under nitrogen while stirring.
     7. Once the addition is complete, leave the reaction vessel stirring overnight (or 10–12 h).

8. Transfer the reaction mixture to a separatory funnel, wash with water (60 mL, two times), and then with saturated Na_2CO_3 solution (two times).
9. Dry the organic layer over Na_2SO_4 (or $MgSO_4$) for 30 min while stirring, filter through a filter paper, and then evaporate the solvent using a rotary evaporator.
10. Dissolve the product in 10–20 mL CH_2Cl_2 (*see* **Note 1**) and store the product in refrigerator until further use.

- LA-Zwitterion
  1. Add LA-*N*,*N* dimethyl 1,3-propanediamine (4.0 g, ~14 mmol) and 60 mL $CHCl_3$ in a 100 mL one-necked round-bottom flask equipped with a septum, and a magnetic stirring bar.
  2. Purge the reaction vessel with nitrogen.
  3. In a separate vial, warm the 1,3-propanesultone until melting.
  4. Add 2.30 mL of the liquid 1,3-propanesultone into the reaction flask using a syringe, and leave the reaction mixture stirring for 3 days at room temperature. A slight turbidity builds up in the solution.
  5. Evaporate the solvent using a rotary evaporator and further dry the product under vacuum.
  6. Rinse the crude product with 50–60 mL of $CHCl_3$ three times (to remove any impurities), and dry under vacuum. The corresponding ^{1}HNMR spectrum of the compound in D_2O is shown in Fig. 2a.
  7. Store the product in refrigerator under nitrogen atmosphere until further use.

2. LA-TEG-Zwitterion
   - LA-TEG-*N*,*N*-dimethyl aminobutyric acid
     1. Add 4-(dimethylamino)butyric acid hydrochloride (0.33 g, ~2.0 mmol), triethylamine (0.29 g, ~3.0 mmol), and 30 mL $CHCl_3$ into a round-bottom flask mounted with an addition funnel, under ice-cold conditions The solution slowly becomes clear.
     2. Mix *N*,*N*′-dicylohexylcarbodiimide (0.41 g, ~2.0 mmol) and 4-dimethylaminopyridine (0.05 g, 0.4 mmol) under nitrogen and ice-cold conditions while stirring.
     3. Dissolve LA-TEG-NH_2 (0.5 g, 1.3 mmol) in 20 mL of $CHCl_3$ and transfer to the addition funnel.
     4. Add LA-TEG-NH_2 solution dropwise under nitrogen while stirring.

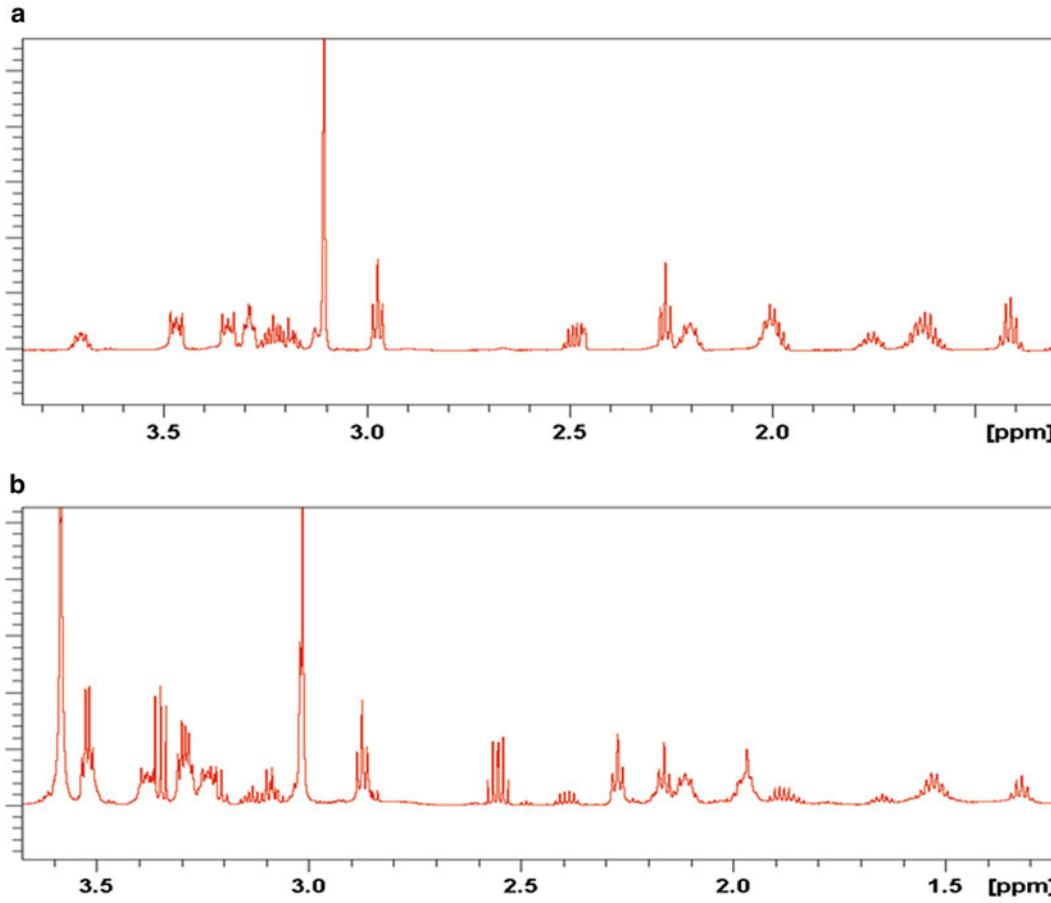

Fig. 2 (**a**) ^{1}H NMR spectra of LA-ZW (Compound 1); (**b**) ^{1}H NMR spectra of LA-TEG-ZW (Compound 2)

5. Once the addition is complete, let the reaction mixture warm up slowly to room temperature and leave it stirring for ~9 h.
6. Filter the mixture through celite.
7. Wash with 30 mL of water (twice) and with 30 mL of saturated Na_2CO_3 solution (twice).
8. Dry the chloroform layer over Na_2SO_4 (for 30 min), filter off the Na_2SO_4, and evaporate the chloroform using rotary evaporator.
9. Dry the product under vacuum, and store it under room temperature (*see* **Note 1**).

- LA-TEG-Zwitterion
  1. Add LA-TEG-*N*,*N*-dimethyl aminobutyric acid (0.3 g, ~0.6 mmol) and 30 mL $CHCl_3$ in a 100 mL one-neck round-bottom flask equipped with a septum and magnetic stir bar. These steps are similar to those detailed for LA-zwitterion above.

2. Purge the reaction vessel with nitrogen.
3. Warm the container of 1,3-propanesultone until melting.
4. Add 0.06 mL of this liquid reagent into the flask via syringe, and leave the reaction mixture stirring for 3 days at room temperature.
5. Evaporate the solvent using a rotary evaporator and dry the product under vacuum.
6. Rinse the crude product with 50–60 mL of ethyl acetate three times (to remove any impurities) and dry it under vacuum. The ^{1}H NMR spectrum of LA-TEG-Zwitterion in D_2O is shown in Fig. 2b.
7. Store the product in refrigerator under nitrogen atmosphere until further use.

3.2 Growth and Purification of CdSe-ZnS Quantum Dots

Different size luminescent CdSe-ZnS QDs with emission varying from 520 nm to 620 nm were used for photoligation with the zwitterion ligands. All QD samples were synthesized using high temperature reduction of organometallic precursors in a coordinating solvent mixture as reported in previous references [27, 28]. The QDs were prepared stepwise. The core CdSe was grown first followed by the overcoating with the ZnS layer.

3.2.1 CdSe Core

1. Prepare a 1.0 M stock solution of trioctylphosphine selenide (TOP:Se), by dissolving 7.9 g of selenium (99.99 %) into 100 mL of trioctylphosphine (90–95 %). Higher concentrations (1.5 or 2 M) can be used.
2. Load 2–3 g of TOPO (90 %), 1–2 g HDA, 0.1–0.5 g HPA, and 0.5–1.5 mL TOP (98 %) into a 50 mL three-neck round-bottom flask. Fit the flask with a thermocouple temperature sensor, a condenser, and a nitrogen/vacuum inlet adapter connected to an inert atmosphere line (Schlenk line).
3. Heat the content (TOP/TOPO along with HDA and HPA) to 140–160 °C for 2–3 h under vacuum while stirring. This allows degassing and removal of moisture.
4. Switch to nitrogen atmosphere and raise the temperature to 345–355 °C.
5. In parallel, mix $Cd(acac)_2$ (62 mg), HDDO (0.12 g), and TOP (90–95 %, 1–2 mL) in a separate scintillation vial.
6. Heat this precursor mixture to 100 °C under vacuum for ~1 h; the solution should slowly become homogeneous.
7. Cool the reaction mixture to 70–80 °C and add 1–3 mL of 1.0 M TOP:Se. Added amount depends on the target size/color of the materials desired.
8. Mix thoroughly before injection into the flask containing the preheated mixture (**step 4** above).

9. Rapidly inject the precursors into the hot coordinating solution mixture under continuous stirring.
10. Once the injection is complete, rapidly cool the round-bottom flask with its reaction mixture to ~100–120 °C; this stops any additional growth of the nanocrystals.
11. For further growth, for example to prepare red-emitting QDs, the solution can be further heated to 250–280 °C for several minutes.
12. Retrieve the growth solution, add a mixture of *n*-butanol and toluene (or hexane), and store until further use.

3.2.2 Purification

Purification is routinely carried out using precipitation/centrifugation to remove excess unreacted metal complexes and TOP/TOPO ligands; this step also provides a means to further select a narrow-size distribution set of nanocrystals.

1. Add ethanol or methanol to the hexane/QDs until the content becomes turbid.
2. Centrifuge at 1,577–1,840×*g* (or 3,000–3,500 RPM) for 10 min and collect the precipitate containing the QD materials. This allows removal of free TOP/TOPO and soluble impurities.
3. Redisperse the precipitate in toluene or hexane. A fraction of this "cleaned" solution can be used for overcoating.

3.2.3 ZnS-Overcoating

Overcoating the CdSe core with a few layers of wider band-gap semiconductor (ZnS or ZnSeS) provides a better passivation of surface states and subsequently enhances the QD photoluminescence quantum yield. Here we describe a typical overcoating with a few monolayers of ZnS following the original method using diethylzinc. However, other more "green" approaches and overcoating with additional blends (i.e., ZnSe, CdS, and ZnCdS) can be found in several reports [15, 27, 29, 30].

1. Load 20–30 g of TOPO (90 %) into a round-bottom flask (100 mL) equipped with a pressure-equalizing addition funnel.
2. Heat the content to 120–140 °C for 2–3 h under vacuum.
3. Cool the content to ~80 °C, and then add a solution of the purified solution of QDs in toluene (or hexane). For this it is recommended that the final Cd concentration be maintained to 0.1–1 mM.
4. Remove hexane or toluene under vacuum.
5. Increase the temperature of the QD solution in TOPO to 140–180 °C, depending on the size of the core materials. In general, a higher temperature is needed for the QDs having larger radius; for example, 180 °C is appropriate for red-color QDs.

6. Add 4–5 mL TOP solution containing equimolar amounts of diethylzinc ($ZnEt_2$) and hexamethyldisilathiane (TMS_2S) precursor mixed inside a glove box into the addition funnel using a syringe.
7. Slowly add the precursor solution into the QD/TOPO solution while stirring.
8. After complete addition, lower the temperature to 80–90 °C, and leave the solution stirring overnight.
9. Store the QDs after adding enough hexane or toluene (10–20ml) along with a small amount of 1-butanol to prevent the stock dispersion from solidifying.

3.3 Protein Expression and Purification

The MBP-His_8 was expressed using plasmid pMal-c2 vector where the sequence spanning from K1 to T366 was modified. This plasmid includes extra-NSSSHHHHHHHHSSGLVPRGSS residues at the C-terminus of MBP. The protein expression was done in BL21 cells. In brief, the bacteria Luria–Bertani broth is first inoculated at a 1:100 dilution with saturated culture and grown until the optical density of the culture at 600 nm (OD_{600}) reaches 0.6. Expression of the fusion proteins was then induced by addition of 0.4 mM isopropyl α-D-1-thiogalactopyranoside. Bacteria were harvested after 3-h induction and lysed in binding buffer using a microfluidizer. His-select Ni-NTA agarose column was performed as a first step to purify the clarified lysate. The histidine tag-containing proteins were extensively eluted with 250 mM imidazole in elution buffer. The collected fractions were diafiltrated into buffer (*see* Subheading 2.3) using YM-10 Centricon units and further purified through an anion-exchange HPLC using a linear gradient from 0 to 1 M NaCl, 20 mM Tris–HCl, and 2 mM EDTA buffer pH 7.4. Finally, tris buffer was replaced by PBS (11.9 mM sodium phosphate, 137 mM NaCl, 2.7 mM KCl, pH 7.4) using diafiltration and stored at 4 °C. Further details on the protein expression are provided in our previous publication [24].

3.4 Photoligation of QDs with Lipoic Acid-Zwitterion Ligands and Water Solubilization

The transfer of the TOP/TOPO-QDs to buffer media is achieved via cap exchange with the above lipoic acid-modified ligands. For this we rely on a recently developed photoligation strategy involving the UV irradiation (at 350 nm) of TOP/TOPO-QDs mixed in one- or two-phase solution reaction with the oxidized form of the LA-based ligands. The procedure involves the in situ reduction of lipoic acid to the reactive dihydrolipoic acid, combined with rapid anchoring on the QD surfaces concomitant with removal of the native cap (Fig. 1). This photoligation strategy eliminates the need for chemical reduction of the lipoic acid groups using $NaBH_4$, and has been found to effectively work with an array of ligands including pure LA, LA-PEG, and LA-zwitterion. Furthermore, this approach is more advantageous when cap exchange is implemented

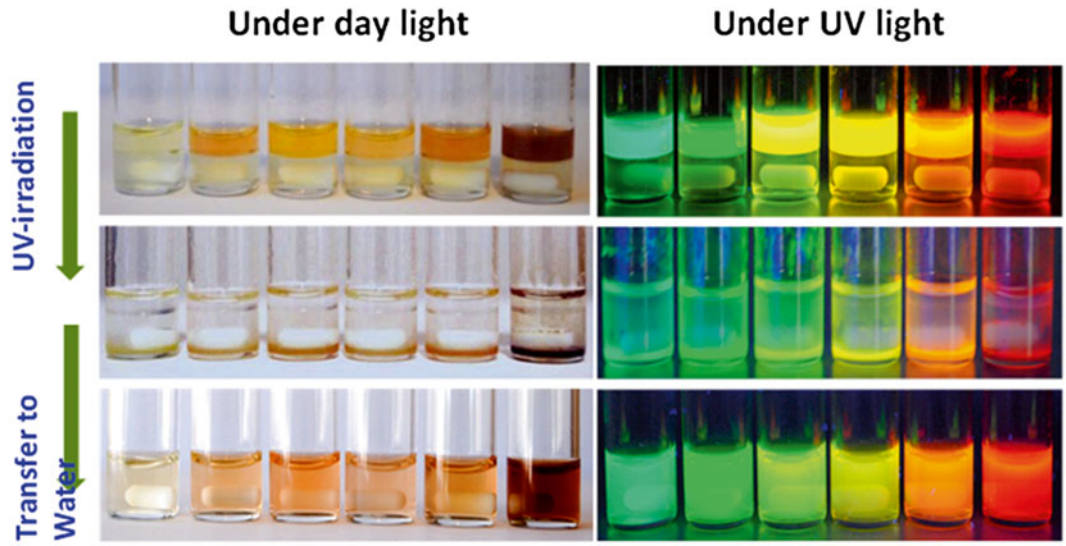

Fig. 3 White light and fluorescence images of five different size QDs transferred from organic solvent to water in the presence of UV irradiation. TOP/TOPO-QDs are dispersed in hexane (*top layer*), while the *bottom layer* contains LA-zwitterion ligand in MeOH. The zwitterion-capped QDs precipitate out of both phases, due to change in the solubility of the nanocrystals. Dispersions in water are shown in the *bottom*

using zwitterion-modified lipoic acid ligands, because preparation and purification of the chemically reduced form of LA-ZW are rather difficult [19, 31].

The photoligation with zwitterion-modified LA ligands is carried out using two-phase (hexane:methanol) reaction, because of the stringent solubility requirement of these ligands; LA-zwitterion ligands are soluble only in methanol or water (Fig. 3). The protocol described below is for photoligation of QDs with LA-ZW:

1. Precipitate 200 μL of a stock solution (~7 μM) of TOP/TOPO-QDs using ethanol or methanol.
2. Redisperse the precipitated QDs in 550 μL of hexane.
3. Solubilize 35 mg of LA-ZW ligand in a separate scintillation vial using 500 μL methanol; a slight heating (~50–60 °C) with stirring is needed to obtain a homogeneous ligand solution. The amount will vary for other zwitterion ligands (LA-TEG-ZW or bis(LA)-ZW) depending on their molecular weight.
4. Add catalytic amount (~10 mM) of tetramethyl ammonium hydroxide (TMAH) base to the methanol solution.
5. Mix the hexane solution containing TOP/TOPO-QDs with the ligand solution in methanol.
6. Seal the scintillation vial with a rubber stopper.
7. Switch the atmosphere to nitrogen using vacuum/nitrogen stopper with a needle.
8. Load the vial containing the mixture into the photoreactor and irradiate it for 30–40 min with stirring (*see* **Note 2**).

9. A colorful aggregate of QDs deposited on the vial walls results after UV irradiation.
10. Remove the hexane and methanol using a glass pipette.
11. Wash the precipitated QDs twice with methanol using centrifugation after each wash to remove the excess ligands along with the displaced TOP/TOPO.
12. Dry the QDs for 5–10 min under vacuum; only gentle drying is needed.
13. Add deionized water to the QD precipitate; a colorful homogeneous dispersion immediately results.
14. Filter the solution using 0.45 μm Millex-LCR syringe filter.
15. Transfer the filtrate to Amicon Ultra centrifugal membrane filter (Mw cutoff of approx. 50,000) and centrifuge at 1,840 × *g* for 5–10 min to separate the zwitterion-capped QDs from excess ligands and also from the TMAH base.
16. Repeat this filtration procedure two or three times. This will ensure removal of excess free ligands and allow reconcentration of the aqueous dispersion of QDs.
17. Collect absorption and emission spectra to check the integrity of the nanocrystals after photoligation and phase transfer. The concentration of the dispersions can be determined from the absorption data [32].

3.5 Characterization of the Prepared Ligands Using ^{1}H NMR and ESI-Mass Spectroscopy

The photoligation of the QDs with zwitterion ligands introduced above involves the synthesis of two sets of ligands: LA-ZW and LA-TEG-ZW. In the following paragraph, we provide the characterization of various ligands (two intermediate products and two final LA-based zwitterion ligands) using ^{1}H NMR and mass spectrometry.

- LA-*N*,*N*-dimethyl 1,3-propanediamine

  ^{1}H NMR (600 MHz, DMSO-d6): δ (ppm) 6.69 (s, 1H), 3.54–3.59 (m, 1H), 3.32–3.34 (m, 2 H), 3.09–3.20 (m, 2H), 2.43–2.48 (m, 1H), 2.37 (t, 2H, *J* = 6 Hz), 2.23 (s, 6H), 2.15 (t, 2H, *J* = 6 Hz), 1.88–1.93 (m, 1H), 1.67–1.74 (m, 1H), 1.52–1.61 (m, 5H), 1.41–1.52 (m, 2H).

  ESI-MS (*m*/*z*) calculated for $C_{13}H_{26}N_2OS_2$ $(M+H)^+$ 291.5; found 291.5.

  The typical yield of this reaction is ~70 %.

- LA-Zwitterion

  ^{1}H NMR (600 MHz, D_2O): δ (ppm) 3.68–3.72 (m, 1H), 3.45–3.48 (m, 2H), 3.32–3.36 (m, 2H), 3.28–3.30 (m, 2H), 3.16–3.25 (m, 2H), 3.11 (s, 6H), 2.97 (t, 2H, *J* = 6 Hz), 2.46–2.50 (m, 1H), 2.26 (t, 2H, *J* = 9 Hz), 2.18–2.22 (m, 2H), 1.96–2.03 (m, 2H), 1.73–1.79 (m, 1H),

1.58–1.67 (m, 4H), 1.39–1.44 (m, 2H). The ^{1}H NMR spectrum is provided in Fig. 2a.

ESI-MS (*m/z*) calculated for $C_{16}H_{32}N_2O_4S_3$ $(M+H)^+$ 413.2; found 413.2.

The typical yield of this reaction is ~90 %.

- LA-TEG-*N*,*N*-dimethyl aminobutyric acid

  ^{1}H NMR (600 MHz, $CDCl_3$): δ (ppm) 6.84 (s, 1H), 6.33 (s, 1H), 3.42–3.64 (m, 17H), 3.08–3.18 (m, 2H), 2.42–2.47 (m, 1H), 2.32 (t, 2H, *J*=9 Hz), 2.24 (t, 2H, *J*=9 Hz), 2.22 (s, 6H), 2.18 (t, 2H, *J*=9 Hz), 1.86 – 1.92 (m, 1H), 1.77–1.82 (m, 2H), 1.61–1.72 (m, 4H), 1.4–1.49 (m, 2H).

  ESI-MS (*m/z*) calculated for $C_{22}H_{43}N_3O_5S_2$ $(M+H)^+$ 494.7; found 494.7.

  The typical yield of this reaction is ~60 %.

- LA-TEG-Zwitterion

  ^{1}H NMR (600 MHz, D_2O): δ (ppm) 3.59–3.68 (m, 15H), 3.45–3.48 (m, 2H), 3.36–3.39 (m, 4H), 3.31–3.36 (m, 2H), 3.16–3.25 (m, 2H), 3.1 (s, 6H), 2.96 (t, 2H, *J*=6 Hz), 2.62–2.66 (m, 2H), 2.47–2.5 (m, 1H), 2.36 (t, 2H, *J*=6 Hz), 2.25 (t, 2H, *J*=6 Hz), 2.19–2.22 (m, 2H), 2.05–2.09 (m, 2H), 1.96–1.99 (m, 1H), 1.71–1.77 (m, 1H), 1.57–1.66 (m, 3H), 1.38–1.43 (m, 2H). The ^{1}HNMR spectrum is provided in Fig. 2b.

  ESI-MS (*m/z*) calculated for $C_{25}H_{49}N_3O_8S_3$ $(M+H)^+$ 616.3; found 616.3.

  The typical yield of this reaction is ~90 %.

3.6 Self-Assembly of Proteins onto the QDs

Self-assembly of the nanocrystals and His-tagged proteins and peptides has been explored by several groups over the past decade [12, 20, 33, 34]. The binding is driven by metal-histidine coordination and requires direct access of the imidazole groups of the histidines to the Zn-rich surface of the QDs. Though this conjugation strategy is effective and simple, it requires the use of ligands with minimal lateral extension (e.g., DHLA, *see* **Note 3**). DHLA, however, limits manipulation of the QDs and their conjugates primarily to alkaline solutions. Our ligand design, namely LA-zwitterion and LA-TEG-zwitterion, addresses such limitations by providing dispersions that are colloidally stable over a broad range of pH conditions as well as in the presence of cell culture media (Fig. 4). In addition, we found that polyhistidine-appended proteins such as MBP (MBP-His_n) can tightly self-assemble onto these zwitterion-capped QDs, with the conjugates maintaining their full biological activity (Fig. 5a) [24]. This his-conjugation model could be equally extended to mCherry (mCherry-His_n), antibody (antibody-His_n), or other protein

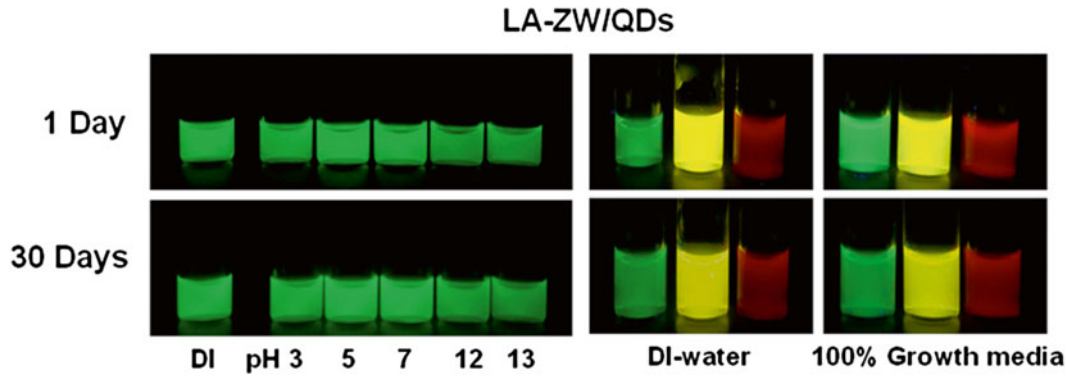

Fig. 4 Fluorescence images of QD dispersions (emission peak at $\lambda_{em} = 545$ nm) in phosphate buffer at different pHs, side by side with images of different size QDs (emission peak at $\lambda_{em} = 545$ nm, 574 nm, 624 nm) dispersed in RPMI growth media (100 %). Control samples in DI water are also shown; all the QD samples shown are photoligated with LA-ZW ligands

expressing a polystidine tag for self-assembly using such compact QDs [35, 36]. For instance, the activity of QD-MBP-His_n can be easily tested using affinity column chromatography, which relies on the competition between the binding of MBP onto amylose gel and the protein substrate maltose (*see* Fig. 5b, c). The protocol is described below:

3.7 Self-Assembly of QD-MBP-His_8 Conjugates and Amylose Assay

1. Mix 8.2 μL of MBP-His_8 (537 μM stock solution) with 90–100 μL of PBS (pH 7.5–8.0) in a microcentrifuge tube.
2. In a separate tube, dilute 50 μL of DHLA-ZW-QDs or DHLA-TEG-ZW-QD stock dispersion (7.3 μM) in PBS buffer (pH 7.5–8.0) to a total volume of 200 μL; these quantities correspond to a molar ratio of QDs to protein of 1:12. Other ratios can be used.
3. Add the MBP-His_8 solution to the tube containing QDs.
4. Gently mix and incubate the mixture at ~4 °C for 30–45 min.
5. Load 1.5–2 mL of amylose stock gel onto a 10 mL capacity column, and wash with 10 mL of buffer three times.
6. Load the incubated mixed solution of proteins with QDs on the top of the column and allow it to settle (by gravity) in the column.
7. Hold the UV light near the amylose column to visualize the immobilization of the conjugates onto the column (manifested as fluorescent band). This proves that formed conjugates maintain the MBP affinity to amylose.
8. Wash with PBS pH 7.3 (four times, 5 mL each). The colored band formed on the top of the column remains unaffected by the buffer washes, indicating binding of the QD-MBP conjugates to the amylose gel (*see* Fig. 5).

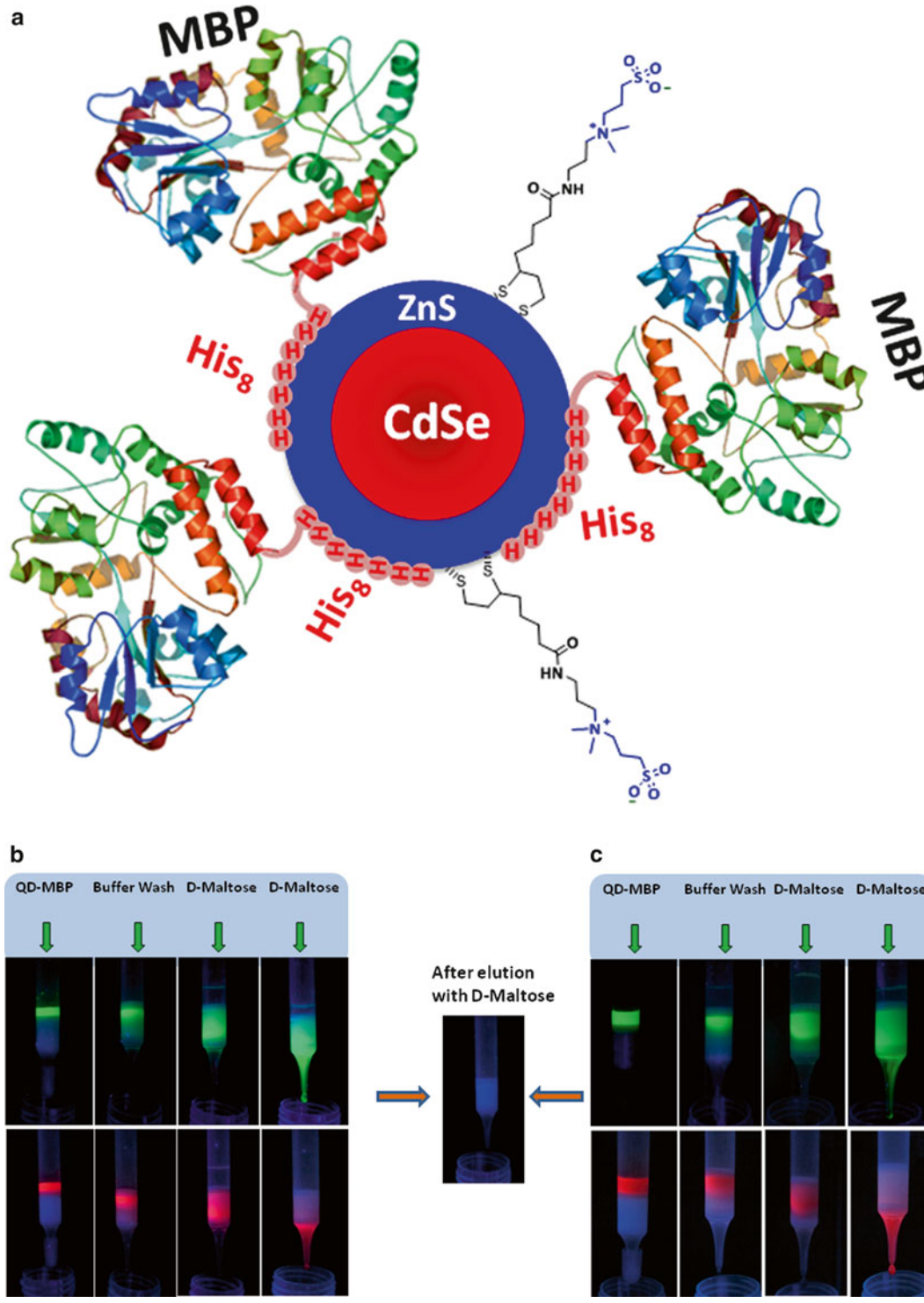

Fig. 5 (**a**) Schematic representation of a QD-MBP conjugate. The self-assembly is driven by the metal-affinity coordination between the polyhistidine tag appended on the MBP and the ZnS-rich surface of QDs. Affinity assay testing the biological activity of the QD-MBP-His conjugates. (**b**) Different size QDs (emission peak at $\lambda_{em} = 545$ nm, 624 nm) photoligated with LA-ZW are self-assembled with His-tagged MBP. (**c**) QDs (emission peak at $\lambda_{em} = 545$ nm, 624 nm) photoligated with LA-TEG-ZW form conjugates with His-tagged MBP. All the conjugates are first immobilized on the amylose column and washed with buffer multiple times; conjugates stay bound to the column. The conjugates are fully released from the column by adding 2–3 mL of 20 mM D-maltose solution

9. Add 5 mL of a 20 mM solution of D-(+)-maltose to the column.
10. Track the elution of the fluorescent band made of the QD-MBP conjugates and collect the materials in a microcentrifuge tube for further use. This indicates that the added maltose progressively displaces the QD conjugates, proving that the affinity of MBP to maltose is unaltered after self-assembly with the QDs (*see* **Notes 4–6**).

4 Notes

1. The intermediate compounds, LA-*N*,*N*-dimethyl 1,3-propanediamine and LA-TEG-*N*,*N*-dimethyl 1,3-propane diamine need to be stored in the presence of small amount of solvent. Overdrying of the two compounds mentioned above will result in insolubility in chloroform during the next step.
2. Depending on the quality of dots prepared and the amount of TOP/TOPO-QDs used, the required time for complete cap exchange via phase transfer slightly varies.
3. DHLA capped CdSe/ZnS QDs have been shown to conjugate with His-protein molecules at basic pH (<7.5) [12].
4. Due to the zwitterionic nature of the ligand, quantum dots are stable at pH 3–13.
5. The ability to carry out conjugation in acidic as well as basic conditions opens up the possibility to use such self-assembled QD-protein conjugates in various biological applications.
6. Mixed-surface conjugation can be combined with amylose column chromatography to purify the unbound proteins or other bio-molecules such as peptides from the conjugate.

Acknowledgements

We thank FSU and the National Science Foundation (NSF-CHE, # 1058957) for financial support. We also thank Tommaso Avellini, Anshika Kapur, Wentao Wang, Xin Ji, Fadi Aldeek, and Malak Safi for the helpful discussions and assistance.

References

1. Murray CB, Kagan CR, Bawendi MG (2000) Synthesis and characterization of monodisperse nanocrystals and close-packed nanocrystal assemblies. Annu Rev Mater Sci 30:545–610
2. Talapin DV, Lee JS, Kovalenko MV, Shevchenko EV (2010) Prospects of colloidal nanocrystals for electronic and optoelectronic applications. Chem Rev 110(1):389–458
3. Alivisatos AP (1996) Semiconductor clusters, nanocrystals, and quantum dots. Science 271(5251):933–937
4. Biju V, Itoh T, Ishikawa M (2010) Delivering quantum dots to cells: bioconjugated quantum dots for targeted and nonspecific extracellular and intracellular imaging. Chem Soc Rev 39(8):3031–3056

5. Murray CB, Norris DJ, Bawendi MG (1993) Synthesis and characterization of nearly monodisperse CdE (E = sulfur, selenium, tellurium) semiconductor nanocrystallites. J Am Chem Soc 115(19):8706–8715
6. Peng X, Schlamp MC, Kadavanich AV, Alivisatos AP (1997) Epitaxial growth of highly luminescent CdSe/CdS core/shell nanocrystals with photostability and electronic accessibility. J Am Chem Soc 119(30):7019–7029
7. Yu WW, Peng X (2002) Formation of high-quality CdS and other II-VI semiconductor nanocrystals in noncoordinating solvents: tunable reactivity of monomers. Angew Chem Int Ed 41(13):2368–2371
8. Hines MA, Guyot-Sionnest P (1996) Synthesis and characterization of strongly luminescing ZnS-Capped CdSe nanocrystals. J Phys Chem 100(2):468–471
9. Dabbousi BO, RodriguezViejo J, Mikulec FV et al (1997) (CdSe)ZnS core-shell quantum dots: synthesis and characterization of a size series of highly luminescent nanocrystallites. J Phys Chem B 101(46):9463–9475
10. Pinaud F, King D, Moore HP, Weiss S (2004) Bioactivation and cell targeting of semiconductor CdSe/ZnS nanocrystals with phytochelatin-related peptides. J Am Chem Soc 126(19):6115–6123
11. Liu WH, Choi HS, Zimmer JP et al (2007) Compact cysteine-coated CdSe(ZnCdS) quantum dots for in vivo applications. J Am Chem Soc 129(47):14530–14531
12. Mattoussi H, Mauro JM, Goldman ER et al (2000) Self-assembly of CdSe-ZnS quantum dot bioconjugates using an engineered recombinant protein. J Am Chem Soc 122(49):12142–12150
13. Nann T (2005) Phase-transfer of CdSe@ZnS quantum dots using amphiphilic hyperbranched polyethylenimine. Chem Commun 13:1735–1736
14. Chan WCW, Nie SM (1998) Quantum dot bioconjugates for ultrasensitive nonisotopic detection. Science 281(5385):2016–2018
15. Aldana J, Wang YA, Peng X (2001) Photochemical instability of CdSe nanocrystals coated by hydrophilic thiols. J Am Chem Soc 123(36):8844–8850
16. Susumu K, Uyeda HT, Medintz IL et al (2007) Enhancing the stability and biological functionalities of quantum dots via compact multifunctional ligands. J Am Chem Soc 129(45):13987–13996
17. Liu W, Howarth M, Greytak AB et al (2008) Compact biocompatible quantum dots functionalized for cellular imaging. J Am Chem Soc 130(4):1274–1284
18. Palui G, Na HB, Mattoussi H (2012) Poly(ethylene glycol)-based multidentate oligomers for biocompatible semiconductor and gold nanocrystals. Langmuir 28(5):2761–2772
19. Muro E, Pons T, Lequeux N et al (2010) Small and stable sulfobetaine zwitterionic quantum dots for functional live-cell imaging. J Am Chem Soc 132(13):4556–4557
20. Susumu K, Oh E, Delehanty JB et al (2011) Multifunctional compact zwitterionic ligands for preparing robust biocompatible semiconductor quantum dots and gold nanoparticles. J Am Chem Soc 133(24):9480–9496
21. Han HS, Martin JD, Lee J et al (2013) Spatial Charge configuration regulates nanoparticle transport and binding behavior in vivo. Angew Chem Int Ed 52(5):1414–1419
22. Park J, Nam J, Won N et al (2011) Compact and stable quantum dots with positive, negative, or zwitterionic surface: specific cell interactions and non-specific adsorptions by the surface charges. Adv Funct Mater 21(9): 1558–1566
23. Palui G, Avellini T, Zhan NQ et al (2012) Photoinduced phase transfer of luminescent quantum dots to polar and aqueous media. J Am Chem Soc 134(39):16370–16378
24. Zhan N, Palui G, Grise H et al (2013) Combining ligand design with photoligation to provide compact, colloidally stable, and easy to conjugate quantum dots. ACS Appl Mater Interfaces 5(8):2861–2869
25. Bucher G, Lu C, Sander W (2005) The photochemistry of lipoic acid: photoionization and observation of a triplet excited state of a disulfide. Chem Phys Chem 6(12):2607–2618
26. Susumu K, Uyeda HT, Medintz IL, Mattoussi H (2007) Design of biotin-functionalized luminescent quantum dots. J Biomed Biotechnol. doi:10.1155/2007/90651, Article ID 90651
27. Clapp AR, Goldman ER, Mattoussi H (2006) Capping of CdSe-ZnS quantum dots with DHLA and subsequent conjugation with proteins. Nat Protoc 1(3):1258–1266
28. Qu LH, Peng ZA, Peng XG (2001) Alternative routes toward high quality CdSe nanocrystals. Nano Lett 1(6):333–337
29. Talapin DV, Nelson JH, Shevchenko EV et al (2007) Seeded growth of highly luminescent CdSe/CdS nanoheterostructures with rod and tetrapod morphologies. Nano Lett 7(10): 2951–2959
30. Reiss P, Protiere M, Li L (2009) Core/shell semiconductor nanocrystals. Small 5(2): 154–168
31. Giovanelli E, Muro E, Sitbon G et al (2012) Highly enhanced affinity of multidentate versus bidentate zwitterionic ligands for long-term

quantum dot bioimaging. Langmuir 28(43): 15177–15184

32. Leatherdale CA, Woo WK, Mikulec FV, Bawendi MG (2002) On the absorption cross section of CdSe nanocrystal quantum dots. J Phys Chem B 106(31):7619–7622
33. Roullier V, Clarke S, You C et al (2009) High-affinity labeling and tracking of individual histidine-tagged proteins in live cells using Ni^{2+} tris-nitrilotriacetic acid quantum dot conjugates. Nano Lett 9(3):1228–1234
34. Kogot JM, England HJ, Strouse GF, Logan TM (2008) Single peptide assembly onto a 1.5 nm Au surface via a histidine tag. J Am Chem Soc 130(48):16156–16157
35. Medintz IL, Pons T, Susumu K et al (2009) Resonance energy transfer between luminescent quantum dots and diverse fluorescent protein acceptors. J Phys Chem C 113(43): 18552–18561
36. Goldman ER, Medintz IL, Whitley JL et al (2005) A hybrid quantum dot-antibody fragment fluorescence resonance energy transfer-based TNT sensor. J Am Chem Soc 127(18): 6744–6751

Chapter 3

Analysis of Quantum Dots and Their Conjugates by Capillary Electrophoresis with Detection of Laser-Induced Luminescence

Karel Klepárník, Vladimíra Datinská, Ivona Voráčová, and Marcela Lišková

Abstract

In many bioanalytical applications, important molecules such as DNA, proteins, and antibodies are routinely conjugated with fluorescent tags to reach an extraordinary sensitivity of analyses. Semiconductor nanoparticles, quantum dots, have already proved to be suitable components of highly luminescent tags, probes, and sensors with a broad applicability in analytical chemistry. Quantum dots provide high extinction coefficients together with a wide range of excitation wavelengths, size- and composition-tunable emissions, narrow and symmetric emission spectra, good quantum yields, relatively long size-dependent luminescence lifetime, and practically no photobleaching. Most of these properties are superior when compared with conventional organic fluorescent dyes. In this chapter, optimized procedures for the preparation of water-dispersed cadmium telluride (CdTe) quantum dots, conjugating reactions with antibodies, DNA, and macrocycles as well as their analyses by capillary electrophoresis are described. The potential of capillary electrophoresis for fast analyses of nanoparticles, their conjugates with antibodies, and immunocomplexes with targeted antigens is demonstrated on examples.

Key words Capillary electrophoresis, Quantum dots, Laser-induced fluorescence, Immunoassay, Bioconjugation

1 Introduction

Various applications of nanotechnologies in analytical chemistry have become increasingly frequent in the last decade [1–5]. Among the most successful applications is the implementation of highly luminescent quantum dots (QDs) in molecular diagnostics [2, 6–9]. Investigations of semiconductor nanocrystals performed during the past two decades revealed a wide range of unique optical, electronic, and chemical properties. The quantum confinement of the semiconductor structures is the cause of their size-dependent properties. This leads to unique electronic behavior of the quantum dots, which are neither bulk semiconductors, nor discrete molecules.

Adriana Fontes and Beate Saegesser Santos (eds.), *Quantum Dots: Applications in Biology*, Methods in Molecular Biology, vol. 1199, DOI 10.1007/978-1-4939-1280-3_3, © Springer Science+Business Media New York 2014

The most important manifestation of the QD electronic state is the sharp and symmetric emission spectrum, broad excitation spectrum, and size-dependent emission wavelength [10]. Additionally, QDs have a good chemical stability with practically no photobleaching [11–13]. The hydrophobic semiconductor central core can be modified by charged molecules, covalently attached to the particle via thiol groups [3]. These organic modifiers not only determine the particle hydrophilicity, but also serve as means to attaching ligands or conjugating biomolecules [7, 14].

QD bioconjugates can be used in a wide range of biological applications including immunoassays [15, 16], cellular labeling [9, 17, 18], single-molecule tracking, deep-tissue imaging [17], and efficient fluorescence resonance energy transfer donors [19]. For these purposes, QDs were conjugated covalently with antibodies [20, 21], proteins [22, 23], peptides [24], DNA [25], and enzymes [26, 27]. Other commonly used approaches for QD bioconjugations are electrostatic or hydrophobic attractions [16], avidin–biotin interaction [28], or direct interactions with the QD surface. Bifunctional linkage with universal coupling agents such as 1-ethyl-3-(3-dimethylaminopropyl)carbodiimide (EDC) or two-step procedure combining EDC with *N*-hydroxysulfosuccinimide (NHS) is also frequently used [29, 30]. The size distributions and structures of nanoparticles and their bioconjugates have been characterized by various methods, such as transmission electron microscopy (TEM), X-ray photoelectron spectroscopy, X-ray powder diffraction [10], and dynamic light scattering [26].

Since the water-dispersible nanoparticles typically carry positive or negative charges, electrophoretic methods play an important role in their characterization. The combination of high speed and high separation efficiency of capillary electrophoresis (CE) with high sensitivity of laser-induced fluorescence (LIF) detection together with the selectivity of the antibody-antigen binding is a unique way for identification of trace levels of target molecules in complex matrices [31]. Various techniques for high-throughput capillary immunofluorescence assays in pico or even zeptomolar concentrations have been developed [32]. Applications ranging from biomedical and environmental monitoring, toxicological assays, and disease diagnosis to drug testing have been described in literature [33–36].

A crucial point for achieving the desired analysis is the availability of high-quality immunoluminescence probes. The probes for highly efficient separations should meet several requirements including brightness, specificity, and chemical and spectral stability. The conjugates of luminophores with antibodies or other selectors should be also electrophoretically homogeneous; that is, they should not contribute significantly to the broadening of electrophoretic zones [36]. This is important for the separation and iden-

tification of an immunocomplex from the excess of an unreacted probe. The broadening and/or splitting of electrophoretic zones of conjugates can be caused by several reasons: (1) electrophoretic heterogeneity of substances, mainly by variation in the number of glycans in the molecules of antibodies, (2) random conjugation of an individual QD at different parts of antibody molecules, and (3) multiple labeling of an antibody by QDs.

The theory of electromigration of nanoparticles in free solution, in replaceable solutions of polymers and in sieving media in the state of gel, has recently been reviewed by Pyell [37]. In the same review, the results of applications of electrophoretic methods for the analytical separations of nanoparticles of various natures have also been analyzed. Capillary electrophoresis with laser-induced fluorescence detection (CE-LIF) has been used for characterization of the surface modifications of QDs and evaluation of the particle charge [21, 23, 38, 39]. A study on the separation of CdTe QDs with diameters of 1.9 and 4.5 nm in linear polyacrylamide (LPA) of 400 kDa and concentration range from 0 to 6 % was presented by Song et al. [39]. While the separation in 2 % solution of LPA was satisfactory, the solutions of hydroxypropylmethylcelluose and polyvinylpyrrolidone were shown to be unsuitable for the separation of QDs. In some cases, however, not only the addition of sieving polymer into the background electrolyte (BGE) but also a good choice of pH were essential to assure a good separation [38].

The objective of this chapter is to explain principles of QD separations by CE, character of their electromigration, and phenomena accompanying electrophoresis. A few examples will demonstrate preparations of semiconductor QDs and their conjugates as luminescent probes for high-sensitivity analyses of biologically important molecules by free solution CE with LIF detection. The potential of fast CE analyses in targeted analysis of DNA, proteins, and small molecules will be shown on applications.

2 Materials

2.1 Chemicals and Reagents

The following chemicals were used for the preparation of QDs and their conjugates.

1. Sodium borohydride ($NaBH_4$, 98.5 %).
2. Tellurium powder (Te^0, 99.8 %).
3. Cadmium chloride ($CdCl_2$, 99.99 %).
4. 3-Mercaptopropionic acid (MPA, 99 %).
5. Sodium sulfide (Na_2S, 97 %).
6. Zinc chloride ($ZnCl_2$, 98 %).

7. Isopropyl alcohol (99.7 %).
8. Linkers *N*-hydroxysulfosuccinimide sodium salt (sulfo-NHS, ≥98 %).
9. *N*-(3-Dimethylaminopropyl)-*N*′-ethylcarbodiimide hydrochloride (EDC, ≥99 %).
10. Albumin from chicken egg white lyophilized powder (≥98 %).
11. Monoclonal anti-chicken egg albumin (Ovalbumin) antibody produced in mouse (clone OVA-14, ascites fluid).
12. Oligonucleotide C6-NH_2-20 nt (Sigma-Aldrich).
13. Macrocyclic ligand 1,4,7-triacetyl-10-aminopenthyl-1,4,7,10-tetraazacyclododecane (MPI) is not commercially available. The compound was received as a gift to be tested for conjugation with QDs.

2.2 CE Materials and Chemicals

1. The capillary electrophoretic system with LIF detection was assembled in laboratory. The fluorescence detection was based on excitation by 488 nm Argon ion laser, Lasos Series 60 (Jena, Germany); emission was detected by a photomultiplier tube E849-35 (Shizouka, Japan) with long-pass blocker (500 nm) and band-pass filter (610 nm). The electrophoretic separations were performed in (1) bare fused-silica capillaries Polymicro Technologies (Phoenix, AZ) of an effective length of 15 and total length of 25 cm, internal diameter (i.d.) of 75 or 100 μm, and outer diameter (o.d.) of 367 μm or (2) polyvinylalcohol (PVA)-coated capillaries Alcor BioSeparations (Palo Alto, CA, USA) with an effective length of 15 and total length of 25 cm, i.d. of 100, and o.d. of 360 μm.
2. CE buffer components:
   (a) TRIS/TAPS buffer consisted of 0.05 M solution of Tris(hydroxymethyl)aminomethane (TRIS, 99.8 %) and 0.05 M N-[Tris(hydroxymethyl)methyl]-3-aminopropanesulfonic acid (TAPS, 99.5 %) giving pH 8.3.
   (b) Phosphate buffer consisted of 0.05 M solution of hydrogen and dihydrogen sodium phosphates (Na_2HPO_4/NaH_2PO_4, ≥99 %) giving pH 7.4.
3. Other chemicals were used for capillary conditioning: 0.1 M solution of sodium hydroxide (NaOH, 99.7 %) and 0.1 M solution of nitric acid (HNO_3, 65 %). Ultrapure water (18.2 MΩ/cm) was used for the preparation of all solutions. Samples were held in 0.2 mL microtubes PCR-tubes clear (Fisher Scientific). A 10^{-6} M solution of Coumarin (99 %) in water was used as a marker of electroosmotic flow.

3 Methods

3.1 Preparation of CdTe Water-Dispersed Quantum Dots

Water-dispersed CdTe quantum dots were prepared by a modified two-step reaction originally described elsewhere [40]. First, sodium hydrogen telluride (NaHTe) was prepared by the reaction of $NaBH_4$ with metal tellurium [41] in a vial shown in Fig. 1. This reaction is presented in Eq. 1:

$$4NaBH_4 + 2Te + 7H_2O \rightarrow 2NaHTe + Na_2B_4O_7 + 14H_2 \quad (1)$$

The second reaction between $CdCl_2$ and NaHTe (Eq. 2) was performed in the presence of thiolated ligands, e.g., MPA for the preparation of negatively charged carboxylated QDs:

$$CdCl_2 + NaHTe \xrightarrow{MPA} CdTe + NaCl + HCl \quad (2)$$

In Fig. 2, there is a high-resolution transmission electron microscopy (HRTEM) image of CdTe QDs. The atomic resolution confirms the face-centered cubic structure of the nanocrystal.

The scheme of the CdTe nanoparticle in Fig. 3 gives an idea of the QD composition.

3.1.1 Two-Step Synthesis Protocol

1. Mix 84.9 mg $NaBH_4$ and 127.0 mg Te powder in 2 mL of deionized degassed water inside a 5 mL vial. Cover the vial with a septum perforated by a needle to drain the generated hydrogen. *See* Fig. 1 for details (*see* **Note 1**).

Fig. 1 Reaction vial for preparation of NaHTe

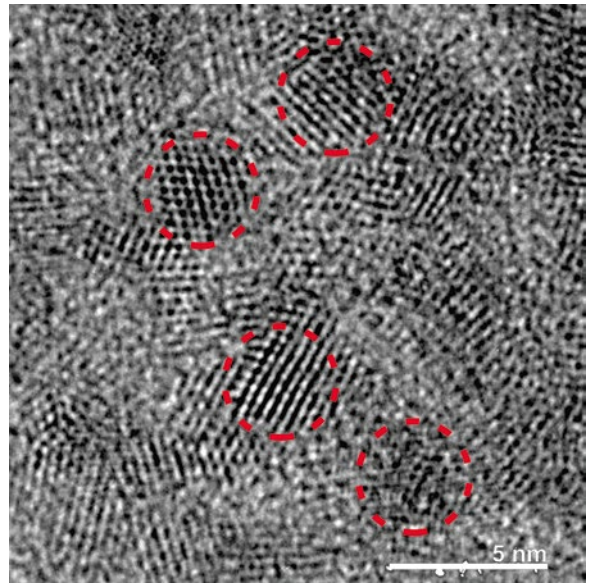

Fig. 2 High-resolution transmission electron microscopy image of 3.5 nm CdTe QDs

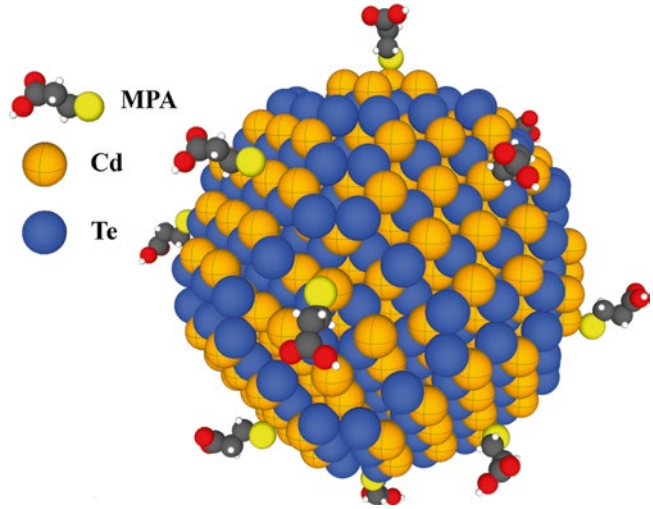

Fig. 3 Scheme of 3.5 nm CdTe QDs comprising 649 Cd and Te atoms (1:1) and 14 ligands of 3-mercaptopropionic acid (MPA) on the surface

2. Stir the reaction mixture inside the vial placed in a cool bath with ice cubes (0–5 °C) for approximately 6 h (*see* **Note 2**).
3. Decant the dark violet solution of NaHTe carefully with needle syringe through the septum and promptly inject into a reaction flask of degassed solution of 182.4 mg $CdCl_2$ and 209 μL MPA in 40 mL water (*see* **Notes 1** and **3**).

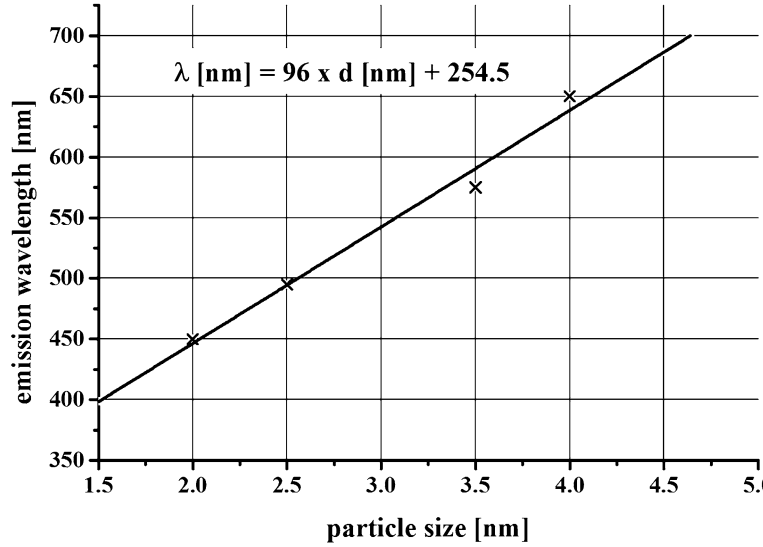

Fig. 4 Size dependence of CdTe QD luminescence emission maxima. Equation of linear regression of experimental data compiled from papers. The data taken from [10]

4. For the preparation of water-dispersed negatively charged nanocrystals, the second reaction between $CdCl_2$ and NaHTe must be performed in the presence of thiolated ligands, e.g., MPA for the preparation of carboxylated QDs. Dissolve MPA in the $CdCl_2$ solution prior to the NaHTe injection.
5. Adjust the pH to 9.5–10 (*see* **Note 4**) and heat the reaction mixture under the reflux condenser for periods of time from 12 to 48 h to reach the desired size of nanocrystals. The mean size of CdTe QD prepared by the described procedure increases with time in the range from 2 to 6 nm. The dependence of luminescence emission wavelength at its maximum intensity on QD size is shown in Fig. 4.

The luminescence properties of 3.5 nm CdTe QD are demonstrated in Fig. 5. Here, the dependences of emission and excitation wavelengths are shown.

3.2 Coating of CdTe QDs

To protect a toxic effect of Cd and Te metals on mammalian cells, coatings with inorganic salts, e.g., zinc sulfide (ZnS), are frequently used [42, 43]. Since the crystal structures of CdTe, cadmium selenide (CdSe), cadmium sulfide (CdS), and ZnS are the same, the coatings are formed as tight and stable epitaxial layers on the substrate crystal. However, the layer of CdS is recommended to precede the nontoxic layer of ZnS. Precipitation of crude QDs in organic solvents is necessary after each step of coating to clean the reaction products.

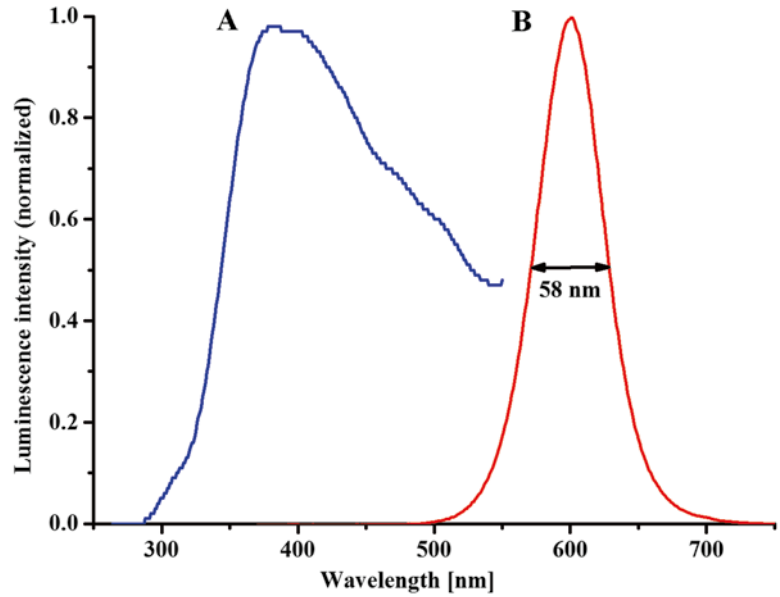

Fig. 5 Normalized luminescence excitation and emission spectra of 3.5 nm water-dispersed CdTe QDs. (**A**) Dependence of emission intensity at 610 nm on excitation wavelength. (**B**) Distribution of emission wavelengths of QD excited by 350 nm

3.2.1 Coating Protocol

1. Precipitation: To clean the synthesized CdTe QDs, use the isopropyl alcohol for their precipitation. Mix isopropyl alcohol with the crude reaction mixture of QDs in volume ratio of 3:1 (e.g., 1.5 mL isopropyl alcohol and 0.5 mL crude mixture of QDs). After centrifugation, decant a solvent excess and then dry QDs at vacuum concentrator at a temperature of 45 °C.
2. First coating (CdS): Disperse precipitated CdTe QDs in 10 mL of water with 2.3 mg $CdCl_2$, 0.8 mg Na_2S, and 38 μL MPA adjusted to pH of 9.5–10. Stir the mixture, heat to the boiling point, and reflux for 1 h.
3. Precipitation: Use the isopropyl alcohol for next precipitation of CdTe/CdS QDs (*see* procedure described in **step 1**).
4. Second coating (ZnS): Disperse CdTe/CdS QDs (product of coating) in 10 mL of water with 1.7 mg $ZnCl_2$, 0.8 mg Na_2S, and 38 μL of MPA adjusted to the pH of 9.5–10. Stir the mixture and reflux for 1 h.
5. Precipitation: Use the isopropyl alcohol for precipitation of CdTe/CdS/ZnS QDs (*see* procedure described in **step 1**).

3.3 Covalent Conjugation of QDs and Compounds with a Primary Amino Group

Conjugation of biologically relevant molecules via sulfo-NHS and EDC, the so-called zero-length cross-linkers, is the most popular and most often used technique nowadays. The conjugation protocol introduced here is based on the procedure described in the Hermanson's compendium [30], optimized for our substances [44].

The cross-linkers can be used for covalent bonding of QDs and molecules of interest (for example, molecule *A*) with primary amine ($-NH_2$) and carboxyl ($-COOH$) groups as shown in Eq. 3:

$$QD - COOH + A - NH_2 \rightarrow A - NHCO - QD + H_2O \qquad (3)$$

The method is very simple with a high reaction yield. QDs can be conjugated with primary amino-containing molecules, e.g., peptides, antigens, antibodies, oligonucleotides, macrocycles, saccharides, and DNA. In Fig. 6, there is a scheme of the conjugation reaction. In fact, it is a two-step process including two active intermediates, *O*-acylurea active intermediate and sulfo-NHS ester intermediate. While sulfo-NHS is optimized for water solutions, NHS is

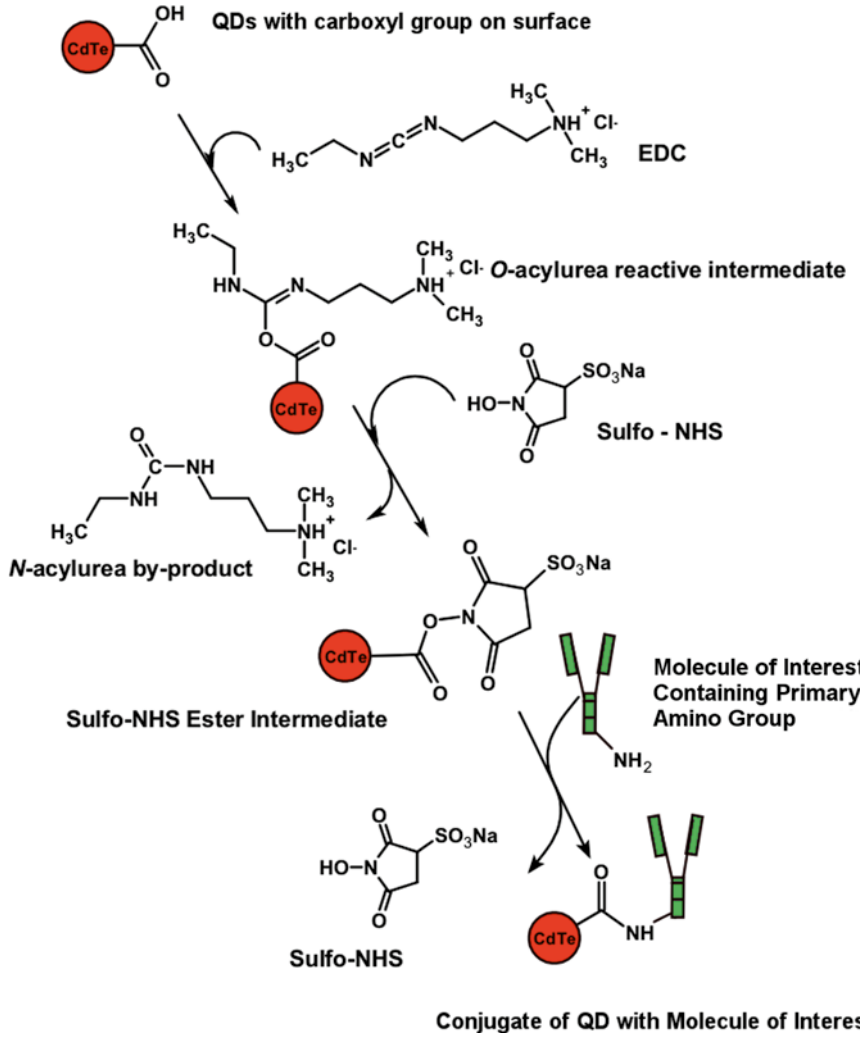

Fig. 6 Reaction scheme of conjugation via EDC and sulfo-NHS zero-length cross-linkers. QDs with carboxyl groups on the surface are covalently bonded with molecules of interest containing primary amino groups

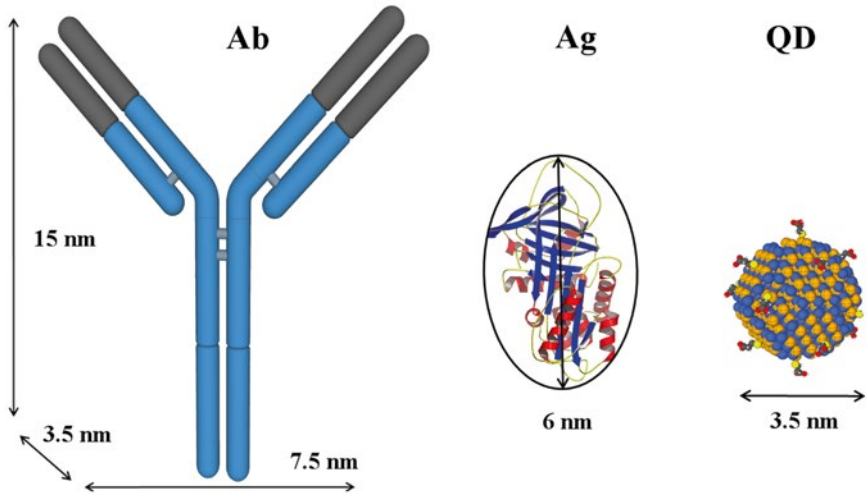

Fig. 7 Comparison of typical sizes of antibody Ab, antigen Ag, and QD

more convenient for applications in less polar media. As evident from the scheme, this conjugation reaction forms a new amide bond between reactants without any additional linker. The purpose of the sulfo-NHS linker stems from its ability to stabilize *O*-acylurea active intermediate of EDC. This stabilization prevents very fast hydrolysis of EDC to non-active *N*-acylurea in aqueous solutions.

In Fig. 7, there are compared sizes of typical antibodies, antigens, and QDs to give an idea of steric protection during conjugation. From steric point of view, a single antibody can adopt several QDs on different amino groups in the molecule. However, CE experiments show that the majority of conjugation reactions result in products where only a single antibody is coupled with a single QD. It is highly probable that also electrostatic repulsions play a role during conjugation reaction.

3.3.1 Protocol for QD Conjugation via EDC/ Sulfo-NHS

1. Disperse carboxylated QDs in 1 mL of ultrapure water or in a buffer of pH in the range between 7.0 and 10.5 (*see* **Note 5**) at room temperature to 10^{-5} M solution. Take an aliquot of 100 μL of suspension of QDs and give it into centrifuge microtube of a volume of 200 μL (*see* **Note 6**). Keep all suspensions of QDs in the dark. It is possible to reuse them in more reactions.
2. Weight out 1.5 mg EDC and 0.5 mg sulfo-NHS and add immediately as powder to the suspension of QDs (*see* **Note 7**).
3. Dissolve compound ***A*** (shown in Eq. 3) given for conjugation to concentration range of 1–10 mg/mL in ultrapure water or a buffer with pH from 7.0 to 10.5 and concentration from 50 to 100 mM (*see* **Note 8**).

4. Take aliquots of dissolved compound A and mix gently with activated suspension of QDs. Recommended molar ratios of QDs:sulfo-NHS:EDC:A = 1:2:8:1. Leave this mixture incubated at a room temperature for 1 h (*see* **Note 9**).
5. Stop conjugation reaction by addition of some amino-containing compounds, e.g., ammonia and ethylamine.

3.4 Capillary Electrophoresis of QDs and Their Conjugates

The basic assembly of typical CE instrumentation is shown in Fig. 8. Both ends of the capillary, where the separation takes place, are inserted into the cathode and anode electrode chambers filled with the same BGE. Electric voltage, usually from 1 to 30 kV, is controlled by electrodes made of platinum wire. Thus, the average electric field strength E is determined by inserted voltage U and total length of the capillary L_C. The migration time t of a species from the injection point to the detection window is given by the effective length of the capillary L_D electric field strength inside the capillary E and electrophoretic mobility of the specie μ, as shown in Eq. 4 [45]:

$$t = \frac{L_D L_C}{\mu U} \tag{4}$$

The electrophoretic mobility is defined as velocity at unit electric field strength. A very important accompanying phenomenon in CE is electroosmotic flow (EOF) [46]. The reason of this bulk flow of BGE through the separation capillary is a fixed charge

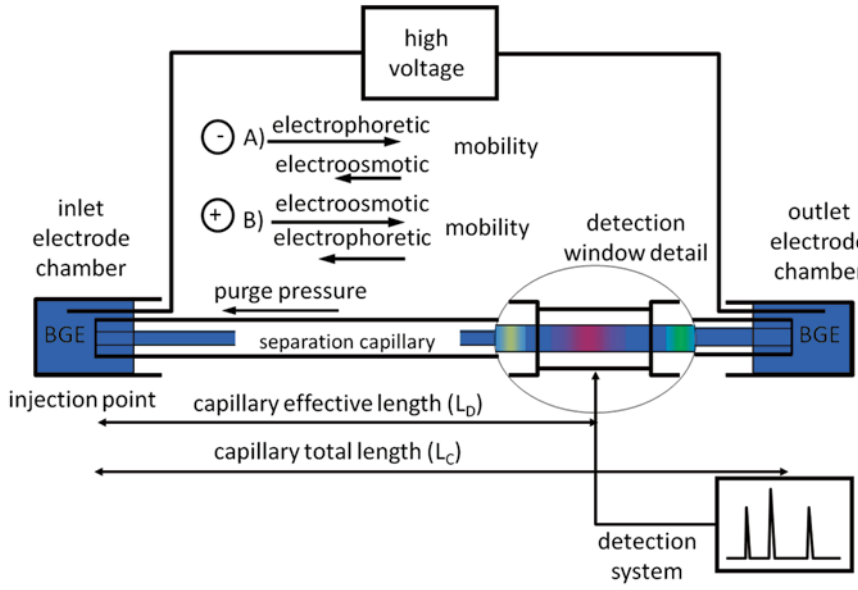

Fig. 8 Scheme of capillary electrophoresis. (**A**) Anions migrate to the detector at negative voltage. Opposite electroosmotic flow has only a minor effect on migration velocity. (**B**) Electroosmotic flow (in direction of cations) in bare fused-silica capillary has dominant effect. Anions are carried to the detector at positive voltage in order opposite to their electrophoretic mobilities

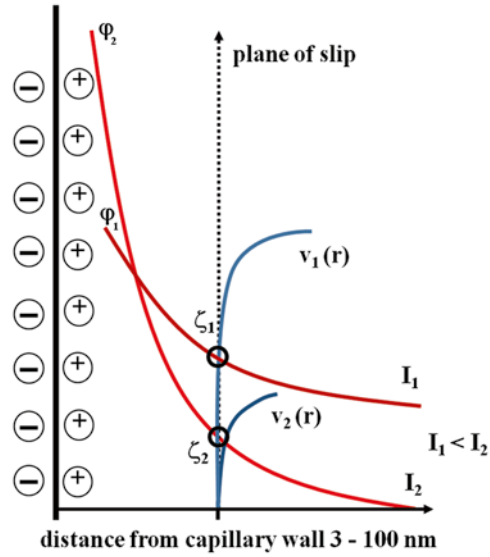

Fig. 9 Dependence of electroosmotic flow *v* on ionic strength *I* of background electrolyte. Zeta potential ζ, potential φ of electric double layer at plane of slip, is the driving force of electroosmotic flow in bare silica-fused capillary. Electric double layer is formed as a layer of counterions at negatively charged silanol groups on silica surface in solution of electrolytes. The higher is the concentration of electrolytes, the closer is the concentration layer of counterions to the silica surface. Compare courses of φ_1 and φ_2, v_1 and v_2, and values of ζ_1 and ζ_2

on the inner wall due to the dissociated silanol groups. The negatively charged silanol groups on silica surface induce formation of a layer of positively charged counterions in solutions of electrolytes (Fig. 9). In electric field, this positively charged layer is accelerated and induces EOF in the direction of migration of cations. In some occasions, at pH > 9, EOF can be faster than electromigration of analytes and can be used for transport of all species including the neutral ones to the detector. The mobility of EOF, transporting analytes from the injection end of the capillary to the detector at the positive voltage, can be determined using coumarin as a neutral marker in a broad range of pH values. Due to the strong EOF, the analytes are detected in reverse order, the ones with the lowest mobility first. The scheme of the effect of EOF at both polarities is shown in Fig. 8.

As demonstrated in Fig. 9, EOF increases with decreasing ionic strength *I* of electrolytes. This fact is associated with the formation of electric double layer and zeta potential $\boldsymbol{\zeta}$. Mobility of EOF is independent of capillary i.d. and is dependent on the permittivity ε, viscosity η, and zeta potential $\boldsymbol{\zeta}$, according to Eq. 5:

$$\mu_{\mathrm{EOF}} = \frac{\varepsilon\, \xi}{\eta} \tag{5}$$

Since the thickness of the electric double layer is only several tens of nanometers, the EOF velocity profile is very flat, and therefore does not contribute significantly to the dispersion of separated zones of analytes.

It is important to mention that the electromigration of a colloid particle in free electrolytes is a more complex phenomenon than the steady movement of a low-molecular-mass ion being in equilibrium between electrostatic and viscous drag forces. While the mobility μ of a spherical particle with a charge Q and radius r migrating through a continuum of viscosity η in an electric field strength E is given by simple relationship $\mu = Q/(6\pi r\eta)$, the mobilities of colloids depend on more parameters. To maintain electroneutrality, charges immobilized at a colloid particle surface induce formation of diffusion layer of counterions, similarly as explained in the case of silica-fused capillaries in Fig. 9. Since the counterions together with the surrounding liquid tend to move in the opposite direction to the particle, they exert another drag force on it. Moreover, in a strong electric field, the originally symmetrical cloud of counterions is distorted and induces electrostatic force acting against the migration of the particle. Thus, not only the particle size and charge but also the concentrations and mobilities of the background electrolyte ions affect its electrophoretic mobility. It is well known that the double-layer thickness decreases with increasing ion strength. The effect of counterions causes the decrease in mobility of colloids with increasing ionic strength of BGEs. Another important role of the electric double layer around the particles is their protection against an aggregation due to the repulsive forces between the counterions of the same sign. Thus, also the tendency to aggregate is higher in solutions of concentrated electrolytes as evidenced by the frequency of spikes in electropherograms.

The size separations of spherical particles in free electrolytes, i.e., without an addition of sieving media, are possible only under special conditions [37]. As has been shown by numerical analysis, the size-selective separations of particles are possible, if the particle diameter is comparable with the thickness of the electric double layer. In this case, when the particle is sufficiently charged, the double-layer polarization effect is responsible for the dependence of electrophoretic mobility on particle size [47]. Examples of size separations of nanoparticles in free electrolytes were recently summarized in a comprehensive review [37].

Implementation of LIF detection into the practice of CE enabled to increase detection sensitivity by several orders of magnitude. The relatively simple instrumentation of a laboratory-made LIF detector is shown in Fig. 10.

The epifluorescence arrangement of LIF detection is demonstrated in Fig. 11. Here, the sample is excited and fluorescence emission collected by the same microscope objective. This instrumentation is convenient for separations in short capillaries or

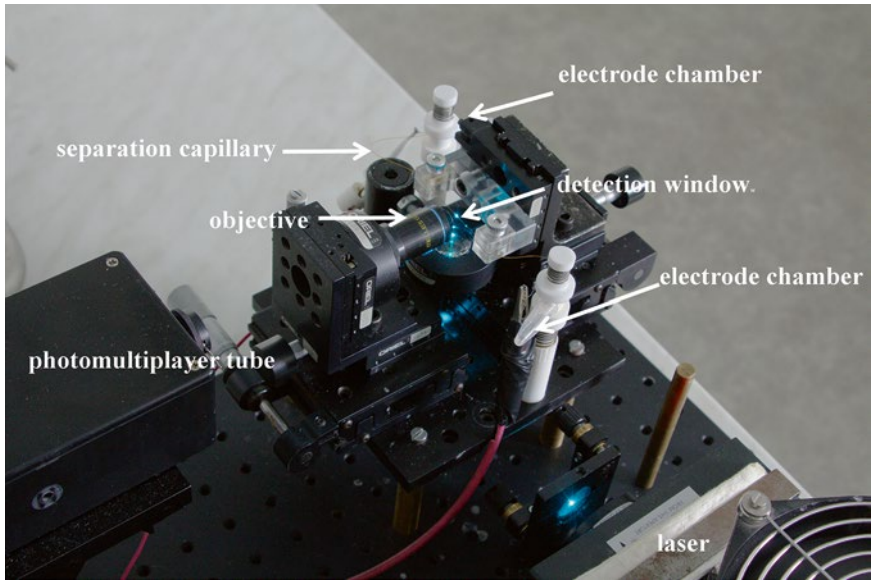

Fig. 10 Basic components of capillary electrophoresis with LIF detection

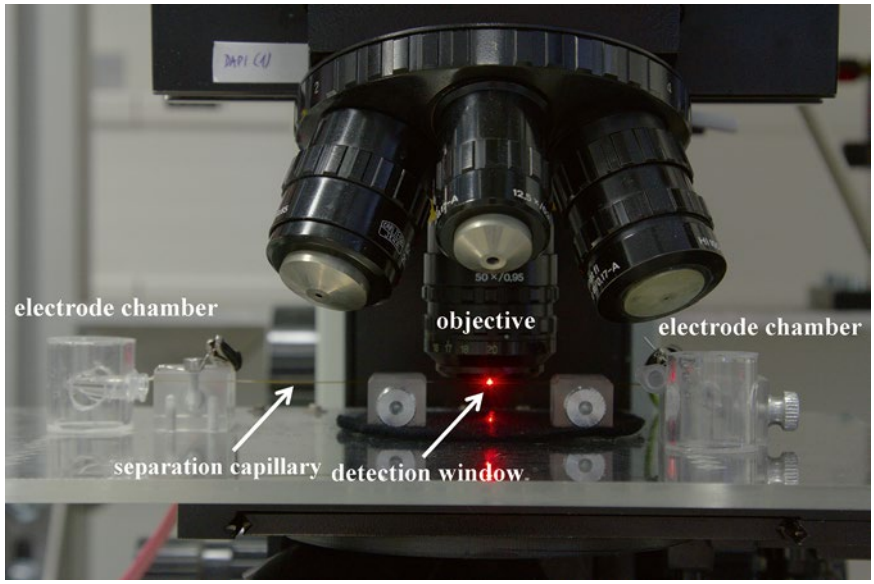

Fig. 11 Capillary electrophoresis with confocal variant of LIF detection. Analytes are excited and their luminescence emission collected by the same microscopy objective

microfluidic devices sitting just on the table of a fluorescence microscope. Inverted fluorescence microscopes give even more space for manipulations and control of the separation system.

3.4.1 Protocol for CE Instrumentation and Analysis

1. Follow the instructions of any commercial CE instrumentation with LIF detection.
2. QDs and their conjugates can easily be separated in free solution BGEs in bare or coated fused-silica capillaries. The capillaries must be prepared and inserted into cartridges according to the producer's instructions.
3. Rinse the capillaries consecutively with 0.1 M HNO_3 for 1 min (*see* **Note 10**), distilled water for 1 min, 0.1 M NaOH for 2 min, distilled water for 2 min, and finally by BGE for 3 min before the first usage in a series of measurements. Rinse capillaries with fresh solution of BGE before each run.
4. A convenient BGE for this type of analyses: 0.05 M solution of TRIS/TAPS, pH 8.3 (*see* **Note 11**).
5. Check all filters in LIF detection system to fit the excitation and emission parameters of an applied laser and used QDs.
6. Dissolve samples in BGE buffer or distilled water (*see* **Note 12**).
7. Use marker of EOF (e.g., coumarin, neutral in a broad range of pH) to check its value. Inject marker of EOF and sample separately to avoid a contamination of sample.
8. For forming immunocomplexes, add equimolar amount of antigens to antibodies. Incubate at 37 °C for 30 min.

3.5 Chosen Applications of QDs in CE Analysis

3.5.1 Conjugation of QDs with Macrocyclic Ligands

The macrocyclic ligands are known for their ability to form thermodynamically and kinetically stable complexes with metal ions. This ability is widely used in analytical chemistry. Metal complexes of macrocyclic ligands can be used as very efficient donors, acceptors, or quenchers of luminescence. Some applications take advantage of complexation equilibria for quantitative determinations. The reason for conjugation of QDs with macrocyclic ligands is synthesis of very sensitive luminescence sensors based on Förster resonance energy transfer. CE-LIF system was used to check the number of ligands conjugated with a single QD. A relatively small molecule of a macrocyclic ligand 1,4,7-triacetyl-10-aminopenthyl-1,4,7,10-tetraazacyclododecane (MPI) (*see* structure in Fig. 12) was chosen for the testing.

Various ratios of QD:MPI substance amounts were used for conjugation via EDC and sulfo-NHS. The results of analyses of crude reaction mixtures are demonstrated in Fig. 13.

The records indicate a consecutive saturation of MPA groups on the QD surface by macrocyclic ligands. Thus the maximum number of conjugated molecules should be as high as the number of MPA groups originally bonded on QD surface. Elsewhere, we have estimated this number to be 14 [48]. The dependence of conjugate mobility on ratio of MPI:QDs shows that from the ratio QDs:MPI = 1:20 the conjugate mobility is nearly constant. This corresponds with the estimate number of MPA molecules bonded to the surface.

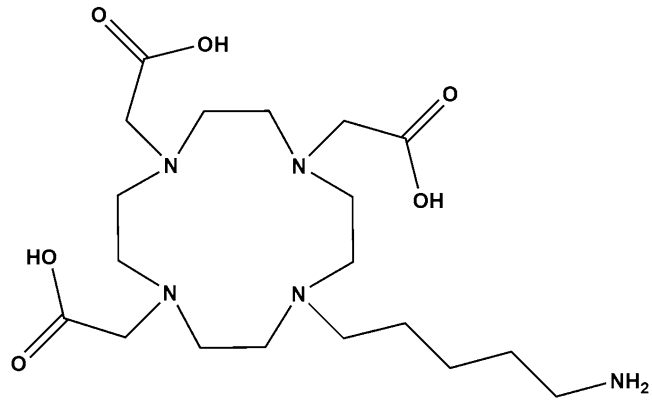

Fig. 12 Macrocyclic ligand 1,4,7-triacetyl-10-aminopenthyl-1,4,7,10-tetraazacyclododecane (MPI)

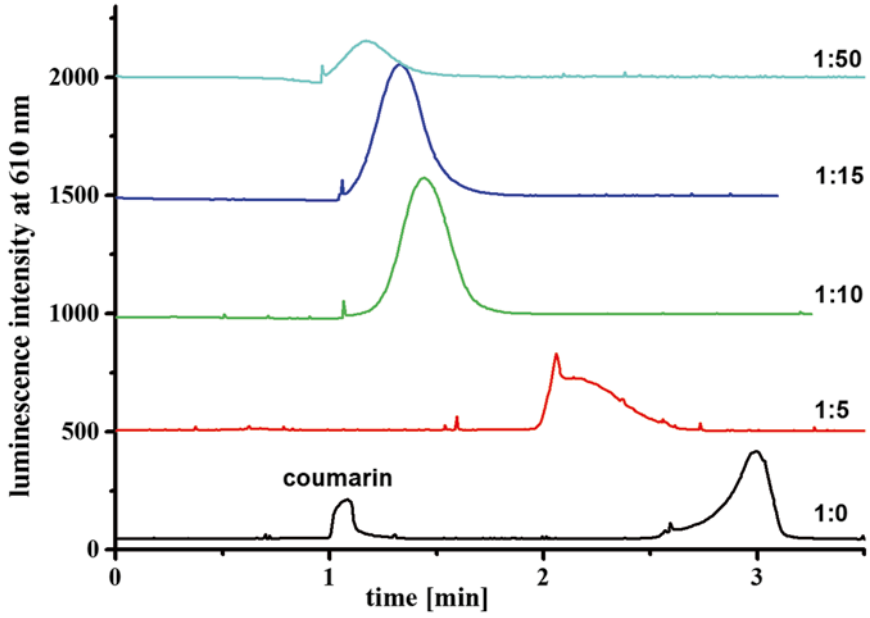

Fig. 13 Electromigration of conjugation products of CdTe QD with macrocycle MPI. Crude conjugation reaction mixtures at various ratios of QD:MPI amounts were injected directly into the capillary. Separation conditions: bare silica-fused capillary (i.d. 75 μm), effective/total length 14/24 cm, separation and injection voltage –6 kV, BGE 100 mM TRIS/TAPS at pH 8.3, excitation at 488 nm (Argon ion laser), detection at 610 nm. Neutral coumarin was used as EOF marker

3.5.2 DNA Sensor Based on Förster Resonance Energy Transfer

Förster resonance energy transfer (FRET) is a photophysical phenomenon through which an energy absorbed by a fluorophore (the energy donor) is transferred nonradiatively by dipole-dipole interactions to the second fluorophore (the energy acceptor) [49]. Thus, the excitation energy is transferred from donor to acceptor and emitted at a longer wavelength. The main advantage of implementation of QDs in FRET sensors is an extremely high extinction

coefficient and photostability [10]. The application of QDs as energy donors in FRET sensors is expected to provide their increased sensitivity.

A FRET sensor was designed for the mutation detection in cancer diagnostics [50]. Conjugation reaction between QDs and aminated oligonucleotides has been done via zero-length cross-linkers. A green QD conjugated with an oligonucleotide probe is chosen as the donor of energy and DNA sample labeled by rhodamine dye (ROX) plays the role of the acceptor. In Fig. 14, there are CE records of (1) CdTe QDs of a size of 3.2 nm passivated by inorganic salts (CdS, ZnS) with a maximum emission wavelength of 570 nm, (2) their conjugates with aminated ssDNA (20 nt), (3) PCR-amplified fragment of an investigated ssDNA (20 nt) labeled by rhodamine dye (ROX), and (4) product of hybridization between both labeled complementary ssDNA fragments forming the FRET construct with QD as a donor and ROX as an acceptor. The different migration times and narrow peaks indicate the potential of CE analyses in this type of mutation detections.

3.5.3 CE Immunoassay

Narrow-size distributions and favorable electrokinetic and optical properties of QDs make them excellent candidates as luminescence tags in immunoanalytical applications. The combination of high

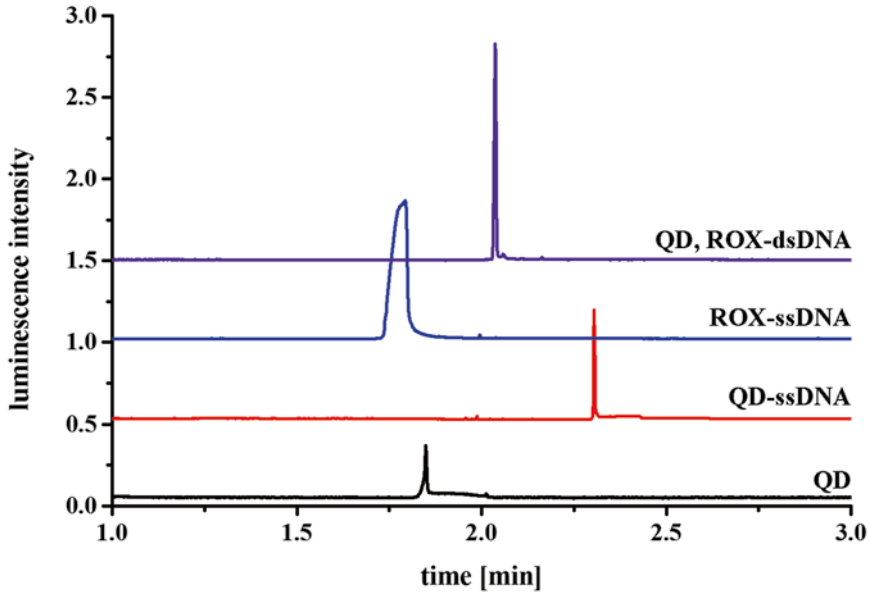

Fig. 14 Comparison of migration times of 3.2 nm CdTe/CdS/ZnS QDs (emission maximum 570 nm), conjugates with ssDNA fragments of 20 nt, complementary ssDNA labeled by rhodamine (ROX), and their dsDNA hybridizate. The presence of QD luminophore and ROX fluorophore on a single dsDNA molecule at a distance of 20 nt is a prerequisite of a Förster resonance energy transfer. Separation conditions: PVA-coated silica-fused capillary (i.d. 100 μm); effective/total length 15/25 cm; separation and injection voltage −10 kV; BGE 50 mM TRIS/TAPS, pH 8.65; excitation at 488 nm (Argon ion laser); detection at 610 nm

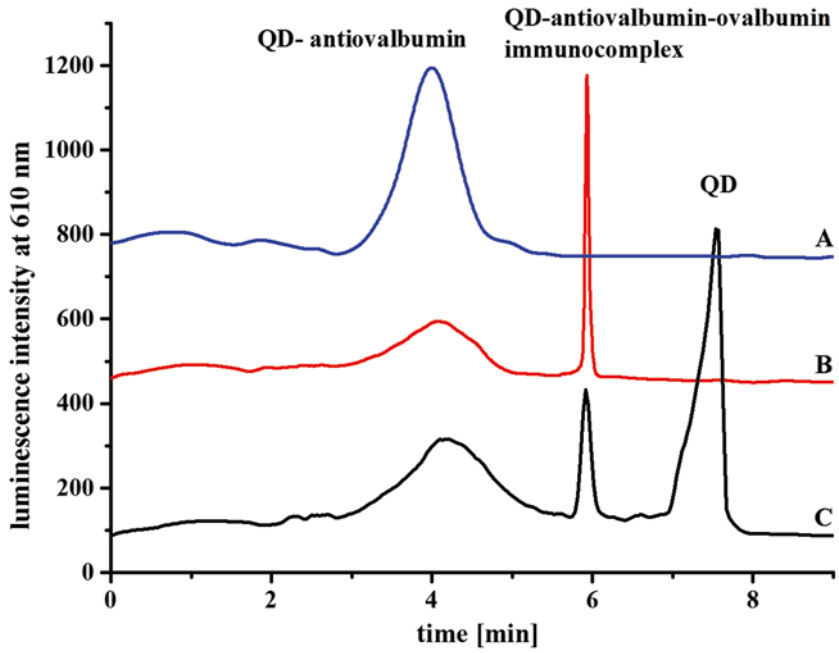

Fig. 15 Model capillary electrophoresis immunoassay. Separations of (**A**) crude reaction mixture after conjugation between CdTe QDs and antiovalbumin; (**B**) the same mixture after the addition of equimolar amount of ovalbumin, incubated at 37 °C for 30 min; (**C**) the same mixture with addition of free QDs. Separation conditions: bare silica-fused capillary (i.d. 75 μm), effective/total length 15/25 cm, separation and injection voltage −6 kV, BGE 100 mM TRIS/TAPS at pH 8.3, excitation at 488 nm (Argon ion laser), detection at 610 nm

selectivities of immunochemical reactions with the high analysis speed and high separation efficiency of CE attracts the attention of analytical chemists for the last two decades [32, 51]. It has already been demonstrated that the high-sensitivity LIF detection makes a CE immunofluorescence assay capable to identify trace levels of target molecules in complex biological matrices [33]. Detection limits in the picomolar or even zeptomolar concentration range of fluorescently labeled compounds were achieved. The optimized system for efficient QD luminescence immunoassay based on a separation method should provide a clear resolution of three zones of unreacted QDs, free conjugates of QD with an antibody or an antigen, and immunocomplex [48]. Such a separation is demonstrated in Fig. 15.

Here, the records present (A) the analysis of a crude conjugation reaction mixture of antiovalbumin with QD; (B) the separation of this conjugate from the respective immunocomplex after the addition of ovalbumin as antigen; and (C) the separation of the same mixture with the addition of free CdTe QDs. A single broad zone of conjugate without any traces of unreacted QDs (record A) is the evidence of a quantitative conjugation reaction under the chosen conditions. Record B shows the separation of the broad zone of conjugate and a narrow peak of immunocomplex.

The most important contribution to the width of the zones of antibodies is their structural variability. Antibodies are complex structures with variable regions. The variation in the number of sialic acids attached to the heavy chain (Fc region) of an antibody causes the heterogeneity not only in its size but also in p*I* value. In addition, the bivalent character of antibodies is the reason for the formation of both 1:2 and 1:1 antibody-antigen complexes. Another contribution to the polydispersity of a probe can be the nonspecific binding of the QDs at any primary amine group of a large antibody molecule. In some unfavorable instances, the antigen-binding sites of an antibody can even be blocked by attached QDs. All these facts can contribute significantly to the heterogeneity of the electrophoretic mobilities of immunoprobes, which negatively influences their separation resolution. One way of avoiding this problem is the use of only light chains cleaved off of the monoclonal antibodies as probes in CE immunoassays [41]. The peak of the immunocomplex (record B) is much narrower than that of the conjugate. This can be explained by the fact that only a limited number of the antibody molecules conjugated with QDs are suitable to form complex with the antigen. Then, free QDs were added to the sample B to prove an independent migration of all three substances. The complete separation of unconjugated QD, conjugate, and immunocomplex in record C confirms insignificant interactions of all three components. Moreover, the absence of free QDs in records A and B evidences a high reaction yield of the conjugation reaction.

4 Notes

1. It is important to mention that all manipulations with NaHTe must be done with media well degassed by nitrogen to prevent any contact with oxygen. Otherwise, the telluride is immediately oxidized and metal tellurium precipitates out of the solution.
2. An effective cooling of reaction mixture is needed, because sodium tetraborate ($Na_2B_4O_7$) precipitates at low temperature. Thus, the reaction equilibrium is continually shifted to the products.
3. A fast injection of NaHTe into a hot solution of $CdCl_2$ is necessary to keep the size distribution of nanocrystals as narrow as possible.
4. Bare QDs are not dispersible in water and must be prepared in organic solvents. A water dispersibility of QDs provides charged ligands, e.g., carboxyl or amine groups, covalently attached to their surfaces. Therefore, the positively or the negatively charged QDs are dispersed in acidic or alkaline pH, respectively. The pH values of QD suspensions must be kept carefully to protect their precipitation especially during syntheses.

5. To stabilize QDs and keep permanent charge on their surface use buffers in pH range from 7.0 to 10.5 instead of water. Phosphate or carbonate buffers were proved. Do not use buffers with primary amino groups! A permanent charge on QD surface at elevated pH is necessary not only to prevent their precipitation but also for initiation of conjugation reaction.
6. Low-binding protein microtubes, e.g., "PCR-tubes clear" (Life Science, Germany), are recommended to avoid adsorption of proteins on vial walls.
7. Prepare all solutions freshly for immediate use. Do not use the remaining solutions repeatedly since hydrolysis decreases conjugation activity of EDC/sulfo-NHS. Similarly, use a direct addition of cross-linker powder into the reaction mixture rather than their water solutions to prevent their hydrolysis.
8. Use phosphate or carbonate buffers at recommended pH to protect precipitation of reactants and to keep QDs, antibodies, antigens, etc. in a dissociated state.
9. In case of unstable compounds or vigorous reaction, leave reaction mixture to react overnight at 4 °C.
10. The rest of adsorbed QDs on inner capillary wall can be cleaned by rinsing with 0.1 M HNO_3.
11. It is recommended to change BGE buffer in electrode chambers after about ten consecutive CE runs.
12. Pure samples dissolved in distilled water are concentrated when entering capillary during electromigrational injection.

Acknowledgement

This work was financially supported by grant of the Grant Agency of the Czech Republic 203/11/2377.

References

1. Alivisatos AP (1996) Perspectives on the physical chemistry of semiconductor nanocrystals. J Phys Chem 100:13226–13239
2. Xu XY, Zhao Z, Qin LD, Wei W, Levine JE, Mirkin CA (2008) Fluorescence recovery assay for the detection of protein-DNA binding. Anal Chem 80:5616–5621
3. Eychmuller A, Rogach AL (2000) Chemistry and photophysics of thiol-stabilized II-VI semiconductor nanocrystals. Pure Appl Chem 72:179–188
4. Rogach AL, Franzl T, Klar TA, Feldmann J, Gaponik N, Lesnyak V, Shavel A, Eychmuller A, Rakovich YP, Donegan JF (2007) Aqueous synthesis of thiol-capped CdTe nanocrystals: state-of-the-art. J Phys Chem C 111: 14628–14637
5. Medintz IL, Uyeda HT, Goldman ER, Mattoussi H (2005) Quantum dot bioconjugates for imaging, labelling and sensing. Nat Mater 4:435–446
6. Fu AH, Gu WW, Larabell C, Alivisatos AP (2005) Semiconductor nanocrystals for biological imaging. Curr Opin Neurobiol 15:568–575
7. Burda C, Chen XB, Narayanan R, El-Sayed MA (2005) Chemistry and properties of nanocrystals of different shapes. Chem Rev 105:1025–1102

8. Medintz IL, Pons T, Delehanty JB, Susumu K, Brunel FM, Dawson PE, Mattoussi H (2008) Intracellular delivery of quantum dot-protein cargos mediated by cell penetrating peptides. Bioconjug Chem 19:1785–1795
9. Parak WJ, Boudreau R, Le Gros M, Gerion D, Zanchet D, Micheel CM, Williams SC, Alivisatos AP, Larabell C (2002) Cell motility and metastatic potential studies based on quantum dot imaging of phagokinetic tracks. Adv Mater 14:882–885
10. Rajh T, Micic OI, Nozik AJ (1993) Synthesis and characterization of surface-modified colloidal CdTe quantum dots. J Phys Chem 97:11999–12003
11. Ma J, Chen JY, Zhang Y, Wang PN, Guo J, Yang WL, Wang CC (2007) Photochemical instability of thiol-capped CdTe quantum dots in aqueous solution and living cells: process and mechanism. J Phys Chem B 111:12012–12016
12. Wang JH, Wang HQ, Zhang HL, Li XQ, Hua XF, Cao YC, Huang ZL, Zhao YD (2007) Purification of denatured bovine serum albumin coated CdTe quantum dots for sensitive detection of silver(I) ions. Anal Bioanal Chem 388:969–974
13. Ma J, Chen JY, Guo J, Wang CC, Yang WL, Cheung NH, Wang PN (2006) Improvement of the photostability of thiol-capped CdTe quantum dots in aqueous solutions and in living cells by surface treatment. Nanotechnology 17:5875–5881
14. Klostranec JM, Chan WCW (2006) Quantum dots in biological and biomedical research: recent progress and present challenges. Adv Mater 18:1953–1964
15. Feng H, Law W, Yu L, Li S (2007) Immunoassay by capillary electrophoresis with quantum dots. J Chromatogr A 1156:75–79
16. Goldman ER, Balighian ED, Kuno MK, Labrenz S, Tran PT, Anderson GP, Mauro JM, Mattoussi H (2002) Luminescent quantum dot-adaptor protein-antibody conjugates for use in fluoroimmunoassays. Phys Status Solidi B Basic Res 229:407–414
17. Huang XY, Li L, Qian HF, Dong CQ, Ren JC (2006) A resonance energy transfer between chemiluminescent donors and luminescent quantum-dots as acceptors (CRET). Angew Chem Int Ed Engl 45:5140–5143
18. Farias PMA, Santos BS, Menezes FD, Brasil AG, Lima LB, Silva DCN, Vieira AAS, Ferreira R, Fontes A, Almeida D, Barbosa LC, Cesar CL (2006) Monitoring activity of living cells marked with colloidal semiconductor quantum dots—art. no. 60880G. Imaging, Manipulation, and Analysis of Biomolecules, Cells, and Tissues IV 6088:114–121
19. Dennis AM, Bao G (2008) Quantum dot-fluorescent protein pairs as novel fluorescence resonance energy transfer probes. Nano Lett 8:1439–1445
20. Goldman ER, Anderson GP, Tran PT, Mattoussi H, Charles PT, Mauro JM (2002) Conjugation of luminescent quantum dots with antibodies using an engineered adaptor protein to provide new reagents for fluoroimmunoassays. Anal Chem 74:841–847
21. Pathak S, Davidson MC, Silva GA (2007) Characterization of the functional binding properties of antibody conjugated quantum dots. Nano Lett 7:1839–1845
22. Ding SY, Rumbles G, Jones M, Tucker MP, Nedeljkovic J, Simon MN, Wall JS, Himmel ME (2004) Bioconjugation of (CdSe)ZnS quantum dots using a genetically engineered multiple polyhistidine tagged cohesin/dockerin protein polymer. Macromol Mater Eng 289:622–628
23. Mamedova N, Kotov N, Rogach A, Studer J (2001) Albumin-CdTe nanoparticle bioconjugates: preparation, structure, and interunit energy transfer with antenna effect. Nano Lett 1:281–286
24. Shan YM, Wang LP, Shi YH, Zhang H, Li HM, Liu HZ, Yang B, Li TY, Fang XX, Li W (2008) NHS-mediated QDs-peptide/protein conjugation and its application for cell labeling. Talanta 75:1008–1014
25. Dwarakanath S, Bruno JG, Shastry A, Phillips T, John A, Kumar A, Stephenson LD (2004) Quantum dot-antibody and aptamer conjugates shift fluorescence upon binding bacteria. Biochem Biophys Res Commun 325:739–743
26. Ipe BI, Shukla A, Lu HC, Zou B, Rehage H, Niemeyer CM (2006) Dynamic light-scattering analysis of the electrostatic interaction of hexahistidine-tagged cytochrome P450 enzyme with semiconductor quantum dots. Chemphyschem 7:1112–1118
27. Ji XJ, Zheng JY, Xu JM, Rastogi VK, Cheng TC, DeFrank JJ, Leblanc RM (2005) (CdSe)ZnS quantum dots and organophosphorus hydrolase bioconjugate as biosensors for detection of paraoxon. J Phys Chem B 109:3793–3799
28. Lee J, Govorov AO, Dulka J, Kotov NA (2004) Bioconjugates of CdTe nanowires and Au nanoparticles: plasmon-exciton interactions, luminescence enhancement, and collective effects. Nano Lett 4:2323–2330
29. Pereira M, Lai EPC, Hollebone B (2007) Characterization of quantum dots using capillary zone electrophoresis. Electrophoresis 28: 2874–2881
30. Hermanson GT (1996) Bioconjugation techniques. Academic, San Diego

31. Kleparnik K, Bocek P (2010) Electrophoresis today and tomorrow: helping biologists' dreams come true. Bioessays 32:218–226
32. Heegaard NHH, Kennedy RT (2002) Antigen-antibody interactions in capillary electrophoresis. J Chromatogr B Analyt Technol Biomed Life Sci 768:93–103
33. Schultz NM, Kennedy RT (1993) Rapid immunoassays using capillary electrophoresis with fluorescence detection. Anal Chem 65:3161–3165
34. Schmalzing D, Buonocore S, Piggee C (2000) Capillary electrophoresis-based immunoassays. Electrophoresis 21:3919–3930
35. Yang WC, Schmerr MJ, Jackman R, Bodemer W, Yeung ES (2005) Capillary electrophoresis-based noncompetitive immunoassay for the prion protein using fluorescein-labeled protein a as a fluorescent probe. Anal Chem 77: 4489–4494
36. Shimura K, Karger BL (1994) Affinity probe capillary electrophoresis—analysis of recombinant human growth-hormone with a fluorescent-labeled antibody fragment. Anal Chem 66:9–15
37. Pyell U (2010) Characterization of nanoparticles by capillary electromigration separation techniques. Electrophoresis 31:814–831
38. Vicente G, Colon LA (2008) Separation of bioconjugated quantum dots using capillary electrophoresis. Anal Chem 80:1988–1994
39. Song XT, Li L, Chan HF, Fang NH, Ren JC (2006) Highly efficient size separation of CdTe quantum dots by capillary gel electrophoresis using polymer solution as sieving medium. Electrophoresis 27:1341–1346
40. Rogach AL, Katsikas L, Kornowski A, Su DS, Eychmuller A, Weller H (1996) Synthesis and characterization of thiol-stabilized CdTe nanocrystals. Ber Bunsen-Ges Phys Chem Chem Phys 100:1772–1778
41. Klayman DL, Griffin TS (1973) Reaction of selenium with sodium-borohydride in protic solvents—facile method for introduction of selenium into organic molecules. J Am Chem Soc 95:197–200
42. He Y, Lu HT, Sai LM, Su YY, Hu M, Fan CH, Huang W, Wang LH (2008) Microwave synthesis of water-dispersed CdTe/CdS/ZnS core-shell-shell quantum dots with excellent photostability and biocompatibility. Adv Mater 20:3416–3421
43. Su YY, He Y, Lu HT, Sai LM, Li QN, Li WX, Wang LH, Shen PP, Huang Q, Fan CH (2009) The cytotoxicity of cadmium based, aqueous phase—synthesized, quantum dots and its modulation by surface coating. Biomaterials 30:19–25
44. Liskova M, Voracova I, Kleparnik K, Hezinova V, Prikryl J, Foret F (2011) Conjugation reactions in the preparations of quantum dot-based immunoluminescent probes for analysis of proteins by capillary electrophoresis. Anal Bioanal Chem 400:369–379
45. Foret F, Krivankova L, Bocek P (1993) Capillary zone electrophoresis. Verlag Chemie, Weinheim
46. Kleparnik K, Bocek P (1991) Theoretical background for clinical and biomedical applications of electromigration techniques. J Chromatogr 569:3–42
47. Ohshima H (2001) Approximate analytic expression for the electrophoretic mobility of a spherical colloidal particle. J Colloid Interface Sci 239:587–590
48. Kleparnik K, Voracova I, Liskova M, Prikryl J, Hezinova V, Foret F (2011) Capillary electrophoresis immunoassays with conjugated quantum dots. Electrophoresis 32:1217–1223
49. Forster T (1946) Energiewanderung Und Fluoreszenz. Naturwissenschaften 33:166–175
50. Kleparnik K, Bocek P (2007) DNA diagnostics by capillary electrophoresis. Chem Rev 107:5279–5317
51. Heegaard NHH (2009) Affinity in electrophoresis. Electrophoresis 30:S229–S239

Chapter 4

Advanced Procedure for Oriented Conjugation of Full-Size Antibodies with Quantum Dots

Kristina Brazhnik, Igor Nabiev, and Alyona Sukhanova

Abstract

Ideal nanoparticle-based nanoprobes should contain on their surface homogeneously oriented highly active affinity molecules, e.g., antibodies (Abs), and should not exceed 15 nm in diameter. Direct conjugation of quantum dots (QDs) with Abs through cross-linking of QD amines with the sulfhydryl groups resulting from the reduction of the Ab disulfide bonds is a generally accepted technique. However, this procedure yields conjugates where Abs are oriented irregularly. This decreases the number of functionally active Abs on the nanoparticle surface, because some Ab recognition sites face inwards and cannot interact with the target moieties. Here, we describe an advanced procedure of Ab reduction, affinity purification, and QD-Ab conjugation with optimized critical steps. We have developed a method for partially reducing the Abs yielding highly functional 75 kDa heavy-light chain Ab fragments. Affinity purification of these Ab fragments followed by their tagging with QDs results in QD-Ab conjugates with largely improved functionality compared to those obtained according to the standard procedures. The new approach can be extended to conjugation of any type of Abs with different semiconductor, noble metal, or magnetic nanocrystals.

Key words Antibodies, Quantum dots, Oriented conjugation, Nanoprobe, Antibody reduction, Antibody functional fragments, Quantum dot-antibody conjugate

1 Introduction

Nanoprobes based on fluorescent nanocrystals or quantum dots (QDs) have recently become an attractive tool for bioimaging and detection of different biological processes, including disease diagnosis. Generally, these nanoprobes are composed of detection biomolecules specifically linked to QDs. Most common imaging techniques employ conjugates of QDs with monoclonal antibodies (mAbs) [1, 2]. However, these functionalized nanoprobes are large, which limits their intracellular and intratissular penetration [3]. In addition, the most critical issue in QD-based nanoprobe preparation is linking multiple Ab molecules to QDs in a way that keeps the Abs highly oriented and functionally active [4–9].

Adriana Fontes and Beate Saegesser Santos (eds.), *Quantum Dots: Applications in Biology*, Methods in Molecular Biology, vol. 1199, DOI 10.1007/978-1-4939-1280-3_4, © Springer Science+Business Media New York 2014

There are two general engineering techniques of linking Abs to QDs: direct cross-linking or indirect streptavidin-biotin interaction of streptavidin-coated QDs and biotinylated Abs. Indirect conjugation provides highly photoluminescent but very large nanoprobes with a hydrodynamic diameter often exceeding 40 nm [10]. Additionally, biotinylated Abs normally contain multiple biotinylated sites; therefore, the Ab orientation relative to the QD surface cannot be controlled properly [6]. The direct QD-Ab conjugation approach involves covalent cross-linking of amino or carboxylic groups introduced in the organic coating of the QD and sulfhydryl or amino groups of Abs [11].

The carbodiimide chemistry approach to covalent linking of the amino and carboxylic groups of Abs and QDs, respectively, is the most generally used technique for preparation of QD-based nanoprobes for in vitro cell labeling [12, 13] and for in vivo imaging [14, 15]. Although the resultant nanoprobes include full-size functional Abs, the random distribution of primary amines on the surface of Ab molecules makes the Ab orientation relative to the surface of QDs also random; hence, many of them are nonfunctional [6, 11].

In contrast to nanoprobes obtained using the carbodiimide chemistry approach, the nanoprobes engineered by cross-linking of the QD amino and Ab sulfhydryl groups are more effective due to a more uniform orientation of the Abs coupled with QDs via very few sulfhydryl groups uniformly located in the 3D structure of Ab molecules. In the ideal nanoprobe configuration, an Ab should be cleaved into two identical 75 kDa heavy-light chain fragments after the reduction of two disulfide bounds located in the hinge region (Fig. 1). All the resultant Ab fragments should be functional, because they contain intact antigen-binding sites (BSs). This direct conjugation of reduced Ab fragments with QDs also allows reducing the nanoprobe size, because there is no additional linker between the Ab fragments and the QD.

Although the approach based on the cross-linking of the QD amino and Ab sulfhydryl groups may provide advanced nanoprobes with an improved functionality, the advantages of this approach are not easy to use in practice. It has been demonstrated that the number of functional Abs in commercially available QD-Ab conjugates prepared according to this approach [9] is very low (0.076 ± 0.014 Abs per QD). Moreover, extended comparative studies of available conjugation methods have revealed a very important difference between the targeting capacities of the resultant conjugates [9, 16]. The intensity of the detected photoluminescence signal was found to be nearly 30 times higher for nanoprobes obtained through biotin-streptavidin interaction compared to those obtained by directly conjugating Abs with QDs [9]. The difference proved to be due to a very small number of functional Abs on the QD surface in the conjugates engineered

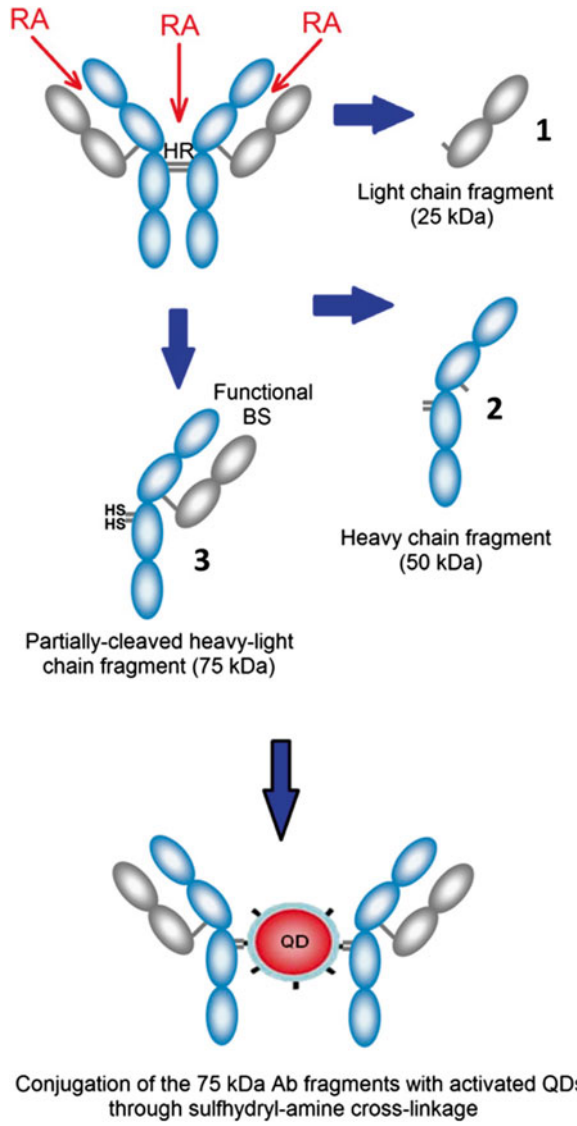

Fig. 1 Antibody reduction with reducing agents (RA) DTT or 2-MEA and strategy of conjugation of reduced Abs with the QDs. The Ab fragments which may be obtained after the disulfide bond cleavage and according to different reduction protocols are Ab light chain fragment (1), Ab heavy chain fragment (2), and partially cleaved Ab heavy-light chain fragment (3). For the product (3) the Ab-binding site (BS) which is composed of the different parts of the Ab heavy and light chains is intact and functionally active. The conjugation of the SMCC-activated QDs with Ab fragments (3) generates nanoprobes with highly improved functionality of ligand-specific recognition and binding (4). Reproduced from Mahmoud et al. (2011) [18] with permission from Elsevier

according to the commercial protocol of cross-linking of the QD amino and Ab sulfhydryl groups [14]. In fact, while the antigen-binding site of an Ab consists of parts of the heavy and light chains of the Ab, the existing Ab reduction procedure [17] leads to an almost complete reduction of Abs and release of separate heavy

chains (50 kDa) and light chains (25 kDa) (Fig. 1). The presence of separate heavy and light Ab chains on the QD surface strongly limits the number of functional capture molecules per nanoprobe and their capability of binding the target. This determines the low functionality of the existing QD-based nanoprobes and limits the sensitivity and specificity of antigen detection [9].

In an attempt to solve this problem, we have developed a method to finely control the conditions of the Ab reduction reaction in order to avoid complete separation of the light and heavy Ab chains, ensuring a high yield of functionally active 75 kDa heavy-light chain Ab fragments. Our advanced procedure for partial reduction of Abs using dithiothreitol (DTT) or 2-mercaptoethanolamine-HCl (2-MEA) provides a high output of functionally active 75 kDa Ab fragments. After affinity purification of these Ab fragments and their cross-linking with QDs, we have obtained QD-Ab nanoprobes with considerably improved functionality compared to the conjugates obtained using the standard protocols (Fig. 1).

The protocol described here includes the stages of antibody reduction with DTT or 2-MEA; affinity purification of the reduced 75 kDa Ab fragments; conjugation of antibody fragments with nanocrystals followed by quality analysis; and characterization and quality control of the resultant diagnostic nanoprobes [18].

2 Materials

All solutions should be prepared using ultrapure water with a resistivity of 18 MΩ cm at 25 °C.

2.1 Reagents and Buffers

1. Polyclonal goat anti-mouse antibody.
2. Water-soluble fluorescent colloidal CdSe/ZnS core/shell nanocrystals (QDs) containing amino groups on their surface (Qdot® 585 ITK™ amino (PEG) quantum dots, 8.6 μM solution in 50 mM borate, pH 8.3, Invitrogen) (*see* **Note 1**).
3. Dithiothreitol (DTT), 7.5 mM solution in water (*see* **Note 2**).
4. 2-Mercaptoethanolamine-HCl (2-MEA), 60 mM solution in water (*see* **Note 2**).
5. Succinimidyl 4-[*N*-maleimidomethyl]cyclohexane-1-carboxylate (SMCC), 10 mM solution in dimethyl sulfoxide (DMSO) (*see* **Note 2**).
6. 2-Mercaptoethanol (2-ME), 14.3 M.
7. Peripheral blood mononuclear cells (PBMC), which intensely express the CD4 antigen. These cells are freshly purified with the Ficoll gradient.

8. 10× Tris-Acetate-EDTA (ethylenediaminetetraacetic acid) buffer (TAE): 400 mM Tris acetate, pH 8.3, 10 mM EDTA.
9. 1.5 % agarose gel: Dissolve 1.5 g of agarose in 100 mL of 1× TAE by heating and boiling until complete dissolution.
10. Mouse anti-human CD4 monoclonal antibodies (clone BL4 supplied by Dr. Jean Brochier).
11. Rabbit anti-goat biotinylated Abs.
12. Streptavidin-horseradish peroxidase conjugates.
13. Protein electrophoresis and blotting reagents.
14. Polyvinyl difluoride (PVDF) membrane.
15. NHS-activated Sepharose 4 fast flow.
16. Phosphate buffer, pH 7.2: Mix 316 mL of 1 M monobasic sodium phosphate (NaH_2PO_4) and 684 mL of 1 M dibasic sodium phosphate (Na_2HPO_4) to obtain 1 L of a 1 M buffer solution. Filter the solution through a 0.22 μm filter.
17. Buffer for Ab reduction with DTT or 2-MEA: 20 mM phosphate buffer, pH 7.2, 150 mM sodium chloride (NaCl), 10 mM EDTA. Dilute 10 mL of 1 M phosphate buffer, pH 7.2, in 400 mL of water, add 15 mL of 5 M NaCl solution and 10 mL of 0.5 M EDTA solution, pH 8, adjust pH to 7.2, and bring the solution volume to 500 mL with water. Filter the solution through a 0.22 μm filter.
18. 1× PBS: Dissolve one tablet of phosphate-buffered saline (PBS) in 200 mL of deionized water to obtain 0.01 M phosphate buffer, pH 7.2 at 25 °C, containing 0.0027 M potassium chloride (KCl) and 0.137 M NaCl. Filter the solution through a 0.22 μm filter.
19. Washing buffer for affinity chromatography of Ab fragments: 100 mM phosphate buffer, pH 7.2, or 1× PBS, pH 7.2. Filter the buffer solution through a 0.22 μm filter.
20. Elution buffer for affinity chromatography of Ab fragments: 500 mM NaCl, 100 mM glycine-HCl, pH 2.7. Prepare 1 L of 200 mM glycine-HCl stock buffer: Dissolve 15.01 g of glycine in 800 mL of water, adjust pH to 2.7, and bring the total volume to 1 L. Prepare the working buffer: Mix 100 mL of 5 M NaCl solution with 400 mL of water and add 500 mL of 200 mM glycine-HCl. Filter the solution through a 0.22 μm filter.
21. Blocking buffer for affinity chromatography of Ab fragments: 5 M sodium hydroxide (NaOH), 10 mM EDTA. Carefully dissolve 20 g of NaOH in 80 mL of water by mixing on a magnetic stirrer. Supplement the solution with 2 mL of 0.5 M EDTA solution, pH 8, and adjust the total volume to 100 mL with water (*see* **Note 3**).

22. 5 % bovine serum albumin (BSA) in PBS: Dissolve 25 g of BSA in 500 mL of PBS, mix on a magnetic stirrer, and filter through a 0.22 μm filter.
23. 1 % bovine serum albumin (BSA) in PBS: Dissolve 5 g of BSA in 500 mL of PBS, mix on a magnetic stirrer, and filter through a 0.22 μm filter.
24. PBS with 0.05 % Tween 20: Mix 0.5 mL of Tween 20 and 1 L of PBS on a magnetic stirrer and filter through a 0.22 μm filter.

2.2 Special Equipment

1. Amicon Ultra-15 filter units with a 30 kDa cutoff (Millipore).
2. PD MiniTrap G-25 (GE Healthcare).
3. Superdex 200 Prep Grade exclusion column (GE Healthcare).
4. Protein G-Sepharose column (GE Healthcare).
5. Nanosep® concentration filters (VWR International S.A.S).
6. Eppendorf 5810R bench-top centrifuge (Eppendorf).
7. Eppendorf 5418 microcentrifuge (Eppendorf).
8. RM-2L Intelli-Mixer (Dutscher).
9. FACStar^{Plus} flow cytometer (Becton Dickinson).
10. ChemiDoc XRS imaging system (Bio-Rad).
11. TotalLab Quant software (TotalLab).
12. UV–VIS spectrophotometer (JASCO).

3 Methods

3.1 Reduction of Antibodies with Dithiothreitol (DTT)

Dilute 1 mg of goat anti-mouse Abs in 1 mL of a freshly prepared reduction buffer containing 0.075 mM DTT (*see* **Note 4**). Incubate the reaction mixture for 30 min at 37 °C, and then use PD MiniTrap G-25 desalting centrifugation columns to remove non-reacted DTT.

3.2 Reduction of Antibodies with 2-Mercapto-ethanolamine-HCl (2-MEA)

Dilute 200 μg of goat anti-mouse Abs (6.06 μM) in 220 μL of a freshly prepared reduction buffer containing 6 mM 2-MEA (*see* **Note 5**). Incubate the reaction mixture for 2 h at 37 °C, and then use PD MiniTrap G-25 desalting centrifugation columns to remove non-reacted 2-MEA.

3.3 Affinity Purification of Reduced Antibodies

To perform affinity chromatography of reduced Abs, purify mouse monoclonal antibody, for example, anti-CD4 monoclonal Abs from mouse ascites (clone BL4 supplied by Dr. Jean Brochier), on a protein G-Sepharose column. Immobilize 5 mg of purified anti-CD4 mouse Abs on an NHS-activated Sepharose column according to the protocol provided by the supplier. Apply each sample of

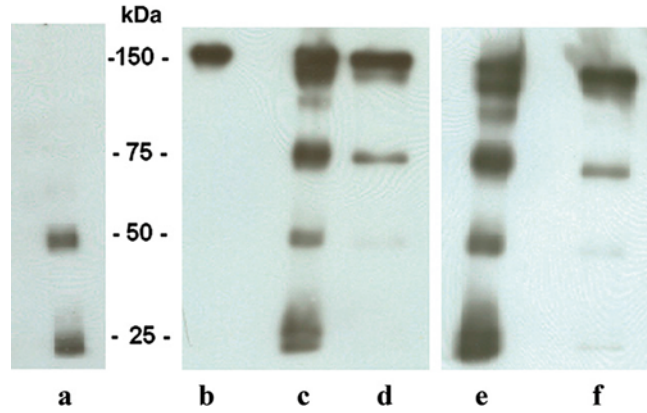

Fig. 2 Analysis of the goat anti-mouse Ab reduction and affinity purification using the Western blot assay. For the immunodetection, the rabbit anti-goat biotinylated Abs were first applied and further revealed with the streptavidin-horseradish peroxidase conjugates. *Lane a*: Ab reduction with 20 mM DTT; *lane b*: unreduced Ab; *lane c*: Ab reduction with 6 mM 2-MEA; *lane d*: Ab reduction with 6 mM 2-MEA followed by affinity purification; *lane e*: Ab reduction with 0.075 mM DTT; *lane f*: Ab reduction with 0.075 mM DTT followed by affinity purification. Reproduced from Mahmoud et al. (2011) [18] with permission from Elsevier

the anti-mouse Ab fragments reduced with DTT or 2-MEA onto the NHS-activated Sepharose column charged with mouse Abs to pass through by gravity flow. Repeat the procedure ten times for complete retention of functional Ab fragments. Wash the column with the washing buffer solution and elute functional anti-mouse Ab fragments with 10 mL of the elution buffer containing 500 mM NaCl and 100 mM glycine-HCl, pH 2.7. Add 80 µL of the blocking buffer containing 5 M NaOH and 10 mM EDTA to the purified Ab fragments immediately to equilibrate the pH and to avoid the reassociation between the Ab fragments. Concentrate the final samples using Amicon Ultra-15 centrifuge filter units with a molecular weight cutoff of 30 kDa (*see* **Notes 6** and **7** and Fig. 2).

3.4 Conjugation of Antibody Fragments with Nanocrystals

1. For the conjugation reaction, use 300 µg of purified Ab fragments per 125 µL of a 4 µM QD solution. For activation of the QD surface, dilute QD stock solution to obtain 125 µL of a 4 µM QD solution in a 100 mM phosphate buffer, pH 7.2. Add 14 µL of a 10 mM solution of SMCC in DMSO to the QD sample to obtain a final cross-linker concentration of 1 mM (*see* **Note 2**). Incubate the reaction mixture for 1 h at room temperature in the dark while stirring gently (40 rpm) on an RM-2L Intelli-Mixer. Immediately after incubation, purify the maleimide-activated QDs by applying the reaction mixture onto a PD MiniTrap G-25 desalting column.

2. Mix equal volumes (500 μL) of the solutions of maleimide-activated QDs and reduced Ab fragments (300 μg) to obtain 1 mL of a reaction mixture with a molar ratio of 1:4 (2 μM Ab fragments per 0.5 μM activated QDs) (*see* **Notes 2** and 7). Incubate the reaction mixture for 1 h at room temperature in the dark while stirring gently (40 rpm) on RM-2L Intelli-Mixer. Then, quench the conjugation reaction by adding 2-ME to a final concentration of 0.1 mM and incubating the mixture for 30 min at room temperature. Concentrate the resultant conjugates with ultrafiltration membranes (Nanosep 100MWCO filters; molecular weight cutoff 100 kDa) to obtain a final volume of 40 μL and purify them by gel-exclusion chromatography using homemade exclusion columns packed with Superdex 200 preparative gel filtration medium (composite matrix of dextran and agarose) and equilibrated with PBS, pH 7.2 (*see* **Note 8**).

3.5 Quality Analysis of Purified Quantum Dot-Antibody Conjugates

1. To determine the concentration of Abs in the samples of QD-Ab conjugates, use UV–VIS spectral analysis of sample absorbance at 280 nm.
2. Analyze the quality of purified conjugates using standard 1.5 % agarose gel electrophoresis. Free QDs and QD-Ab conjugates can be detected by photoluminescence emission in a ChemiDoc XRS system (Bio-Rad) with excitation at 302 nm under trans-illumination. In addition, stain the gels with Coomassie Blue to detect non-conjugated Ab fragments (Fig. 3).

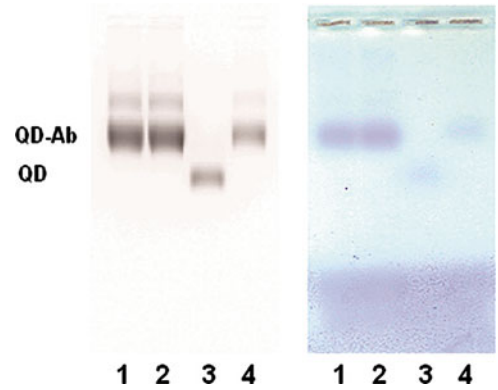

Fig. 3 Electrophoresis of QD-Ab conjugates after agarose gel purification revealed through PL emission under UV-lamp excitation (*left*) or through the Coomassie Blue staining (*right*). *Lane 1*: Nanoprobes with Ab fragments obtained through reduction with 6 mM of 2-MEA. *Lane 2*: Nanoprobes with Ab fragments obtained through reduction with 0.075 mM of DDT. *Lane 3*: Free QDs. *Lane 4*: Nanoprobes with Ab fragments obtained through reduction with 20 mM DTT according to the standard commercial protocol. Reproduced from Mahmoud et al. (2011) [18] with permission from Elsevier

3. In order to separate QD-Ab conjugates from non-conjugated material (free QDs and non-conjugated Ab fragments), carry out an additional purification step with preparative agarose gel electrophoresis. Load 30 μg of each conjugate sample on 1.5 % agarose gel and control the migration pattern of free QDs and conjugates by means of QD photoluminescence detection under UV-lamp illumination. After separation of QD-Ab conjugates from non-conjugated QDs, delicately incise the agarose gel to make a small well. Continue the electrophoresis procedure until the conjugates are concentrated inside the well and then aspirate the sample from the well. Wash and concentrate the resultant samples of QD-Ab conjugates with ultrafiltration membranes (Nanosep 100MWCO filters; molecular weight cutoff 100 kDa) in PBS at pH 7.2. Finally, quantify the Ab concentration in each of the conjugate samples using UV–VIS spectral analysis of sample absorbance at 280 nm (*see* **Note 9**).

3.6 Testing of the Functional Activity of Quantum Dot-Antibody Conjugates

The functionality, binding capacity, and specificity of the QD-Ab conjugates should be evaluated and compared using flow cytometry analysis (*see* **Note 10**).

1. Suspend PBMC by gently shaking for 5 min. Incubate 5×10^5 of PBMC with 1 μg of mouse anti-human CD4 Abs in PBS for 1 h at 4 °C. Wash the cells from unbound primary Abs three times with PBS containing 1 % of bovine serum albumin (BSA). Add the Ab-QD conjugates at the following dilutions in PBS: 1:10, 1:50, 1:100, 1:500, 1:1,000, 1:5,000, and 1:10,000. Incubate the cells with the conjugates for 1 h at 4 °C and thoroughly wash them with PBS containing 1 % of BSA.
2. Perform flow cytometry measurements of the stained cells. Use a 488 nm argon laser for excitation and measure the fluorescence intensity in the range of 564–586 nm. Collect at least 10,000 events for each sample. Use the geometric mean fluorescence (GMF) intensity channels to quantify the staining of each sample (Fig. 4).

3.7 Dot-Blot Determination of the Sensitivity Limit of Antigen Detection with the Quantum Dot-Antibody Conjugates

Load samples containing BL4 Abs in a quantity range from 100 ng to 0.1 ng (in PBS) on a PVDF membrane equilibrated with PBS. Block the membrane with 5 % BSA in PBS for 30 min at 37 °C. Wash the membrane three times with 0.05 % Tween in PBS and stain it with a 0.1 μg/mL solution of QD-Ab conjugates for 1 h of gentle shaking at room temperature. Analyze the photoluminescence emissions of the specifically bound QD-Ab conjugates with the ChemiDoc XRS system (Fig. 5).

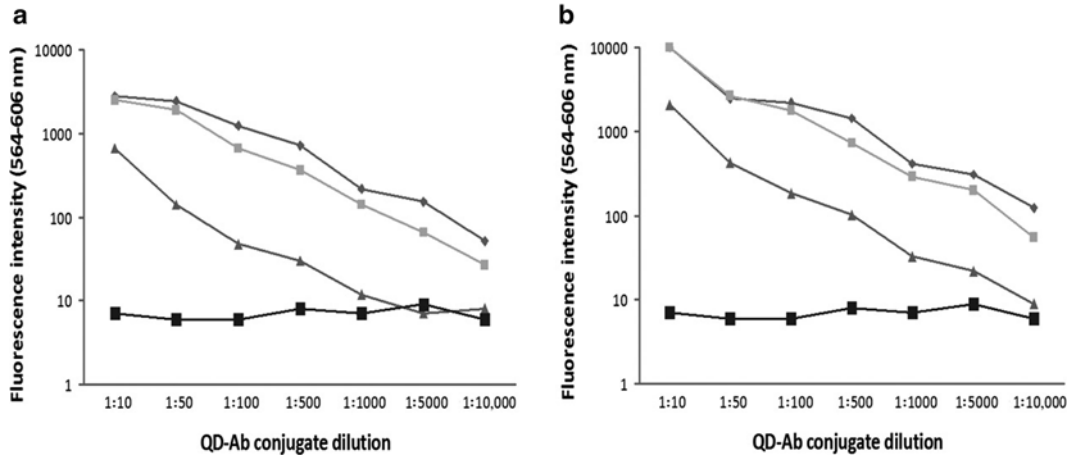

Fig. 4 Biolabeling of PBMC with QD-Ab conjugates analyzed by flow cytometry with FACSCalibur BD flow cytometer. Mouse anti-human CD4 Ab (clone BL4) was used as a primary Ab. Before dilutions, the initial concentrations of Abs for each nanoprobe were adjusted to be the same, 10 μg/mL. Fluorescence intensities of immune complexes of PBMC with QD-Ab before purification of QD-Ab conjugates (**a**) and after agarose gel purification of QD-Ab conjugates (**b**). QD-Ab conjugates were generated by Ab reduction with 6 mM 2-MEA (*line with filled diamond*), with 0.075 mM DTT (*line with filled square*) and with 20 mM DTT (*line with filled triangle*). Experiments with the non-conjugated QDs are presented as the controls on both the panels (*line with filled rectangle*). Reproduced from Mahmoud et al. (2011) [18] with permission from Elsevier

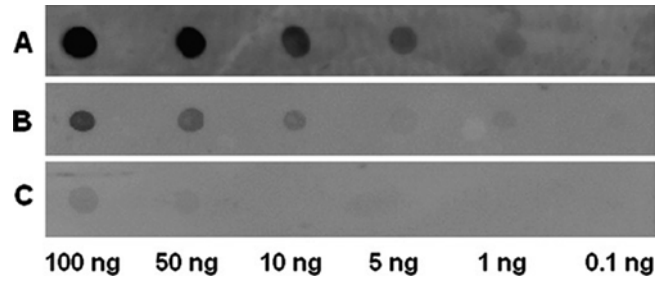

Fig. 5 Dot-blot assay for the detection of different amounts of the BL4 antibody used as an antigen with the QD-Ab conjugates. (**a**) Nanoprobes with Ab fragments obtained through reduction with 6 mM 2-MEA. (**b**) Nanoprobes with Ab fragments obtained through reduction with 0.075 mM DDT. (**c**) Nanoprobes with Ab fragments obtained through reduction with 20 mM DTT according to the standard procedure provided by the QD conjugate supplier. Reproduced from Mahmoud et al. (2011) [18] with permission from Elsevier

4 Notes

1. Colloidal CdSe/ZnS core/shell nanocrystals (QDs) may be home-synthesized and modified with a mixture of amino- and hydroxyl-modified polyethylene glycol (PEG) derivatives (a detailed procedure of nanocrystal synthesis and surface modification is described in Sukhanova et al. [19]).

2. Use a freshly prepared solution of DTT, 2-MEA, and the SMCC cross-linker.
3. Wear gloves and use a fume hood when handling NaOH.
4. Our data show that the Ab reduction with 0.075 mM DTT yields much more 75 kDa half-Ab fragments than the standard protocol of reduction with 20 mM DTT. These Ab fragments with a molecular weight of 75 kDa contain both heavy and light chains interconnected via non-reduced disulfide bonds (Fig. 1). Because the reduction of the Ab disulfide bonds with DTT is nonspecific and may not be limited by specifically selected bonds, some unidentified bands are still present in the electrophoretic pattern of the Abs reduced according to this technique even after optimization of the reaction conditions.
5. The yield of half-Abs obtained by Ab reduction with 6 mM 2-MEA was found to be the highest for the 2-MEA concentration range from 0.606 to 60.6 mM. This yield could not be further improved by variation of other reaction conditions, such as the temperature (from 20 to 37 °C) and reaction time (from 2 to 270 min).
6. To determine the profile of the functional Ab fragments, perform Western blot analysis with sequential application of rabbit anti-goat biotinylated Abs and streptavidin-horseradish peroxidase conjugate.
7. Use the sample of reduced Ab fragments for conjugation with QDs immediately after its affinity purification.
8. Elute conjugates with PBS, pH 7.2, and collect only the first colored fraction to limit the amount of non-conjugated material (free QDs and free Ab fragments).
9. The prepared conjugates should be kept at 4 °C.
10. Any specific receptor-bearing cells may be used for the functional flow cytometry test. In particular, when examining PBMC expressing the CD4 antigen [16], use mouse anti-human CD4 Abs (clone BL4) as primary binding Abs.

Acknowledgements

This study was partly supported by the Ministry of Education and Science of the Russian Federation (grant 11.G34.31.0050), by the European Commission through the FP7 Cooperation project NAMDIATREAM (grant NMP-2009-4.0-3-246479) and by the programs HYNNOV and Nano'Mat of the Champagne-Ardenne region, the DRRT Champagne-Ardenne, and the FEDER (France). I.N. acknowledges support of the Russian Science Foundation.

References

1. Jaiswal JK, Goldman ER, Mattoussi H et al (2004) Use of quantum dots for live cell imaging. Nat Methods 1:73–78
2. Xing Y, Rao J (2008) Quantum dot bioconjugates for in vitro diagnostics & in vivo imaging. Cancer Biomark 4:307–319
3. Parak WJ, Gerion D, Pellegrino T et al (2003) Biological applications of colloidal nanocrystals. Nanotechnology 14:R15–R27
4. Invitrogen. http://probes.invitrogen.com/media/pis/mp19010.pdf
5. Liu W, Howarth M, Greytak AB et al (2008) Compact biocompatible quantum dots functionalized for cellular imaging. J Am Chem Soc 130:1274–1284
6. Xing Y, Chaudry Q, Shen C et al (2007) Bioconjugated quantum dots for multiplexed and quantitative immunohistochemistry. Nat Protoc 2:1152–1165
7. Zaman MB, Baral TN, Jakubek ZJ et al (2011) Single-domain antibody bioconjugated near-IR quantum dots for targeted cellular imaging of pancreatic cancer. J Nanosci Nanotechnol 11:3757–3763
8. Zaman MB, Baral TN, Zhang J et al (2009) Single-domain antibody functionalized CdSe/ZnS quantum dots for cellular imaging of cancer cells. J Phys Chem C 113:496–499
9. Pathak S, Davidson MC, Silva GA (2007) Characterization of the functional binding properties of antibody conjugated quantum dots. Nano Lett 7:1839–1845
10. Clarke S, Pinaud F, Beutel O et al (2010) Covalent monofunctionalization of peptide-coated quantum dots for single-molecule assays. Nano Lett 10:2147–2154
11. Nabiev I, Sukhanova A, Artemyev M et al (2008) Colloidal nanoparticles in biotechnology. In: Elissari A (ed) Fluorescent Colloidal Particles as Detection Tools in Biotechnology Systems. Wiley, New York, pp. 133–168
12. Sukhanova A, Devy J, Venteo L et al (2004) Biocompatible fluorescent nanocrystals for immunolabeling of membrane proteins and cells. Anal Biochem 324:60–67
13. Sukhanova A, Venteo L, Devy J et al (2002) Highly stable fluorescent nanocrystals as a novel class of labels for immunohistochemical analysis of paraffin-embedded tissue sections. Lab Invest 82:1259–1261
14. Nie S, Xing Y, Kim GJ et al (2007) Nanotechnology applications in cancer. Annu Rev Biomed Eng 9:257–288
15. Smith AM, Ruan G, Rhyner MN et al (2006) Engineering luminescent quantum dots for in vivo molecular and cellular imaging. Ann Biomed Eng 34:3–14
16. Zajac A, Song D, Qian W et al (2007) Protein microarrays and quantum dot probes for early cancer detection. Colloids Surf B Biointerfaces 58:309–314
17. Hermanson G (2008) Bioconjugate techniques, 2nd edn. Academic, New York
18. Mahmoud W, Rousserie G, Reveil B et al (2011) Advanced procedures for labeling of antibodies with quantum dots. Anal Biochem 416:180–185
19. Sukhanova A, Even-Desrumeaux K, Kisserli A et al (2012) Oriented conjugates of single-domain antibodies and quantum dots: toward a new generation of ultrasmall diagnostic nanoprobes. Nanomedicine: NBM 8:516–525

Chapter 5

Quantum Dot–Antibody Conjugates via Carbodiimide-Mediated Coupling for Cellular Imaging

Daniel Alistair East, Michael Todd, and Ian James Bruce

Abstract

This chapter describes the processes of antibody (Ab) production, purification, conjugation to quantum dots (QDs), and the use of the conjugates produced in intracellular imaging of cell components and structures. Specifically, information is provided on the conjugation of carboxyl surface-terminated QDs to Abs via a one-step reaction using the water-soluble carbodiimide, 1-ethyl-3-(3-dimethylaminopropyl) carbodiimide (EDC). The chapter details the process of conjugate optimization in terms of its final fluorescence and biological activity. The method described should guarantee the production of QD–Ab conjugates, which outperform classic organic fluorophore–Ab conjugates in terms of both image definition produced and the longevity of the imaging agent.

Key words Quantum dot, Antibodies, Conjugation, Conjugate, Carbodiimide, EDC, Fluorescence, Imaging

1 Introduction

Biologists are often apprehensive about chemistry, particularly when it has no obvious or direct biological significance. This is despite the fact that much of their work is facilitated by commercial products/kits which rely on one type of chemistry or another. Such kits are frequently employed where things need to be linked together/conjugated to make composite structures, i.e., biological–biological (e.g., Abs or oligonucleotides to organic fluorophores) or biological–inorganic (e.g., Abs to microspheres or flat surfaces). A probable reason for this apprehension (from personal experience within the School of Biosciences at the University of Kent) is that many biologists lack a complete understanding of the chemical mechanisms involved in the processes undertaken and consequently what to do when it/they fail. This also means that it is difficult or impossible for them to optimize the conjugation process in an informed way. This chapter hopes to allay some of the possible apprehension about making QD–Ab conjugates using the

Adriana Fontes and Beate Saegesser Santos (eds.), *Quantum Dots: Applications in Biology*, Methods in Molecular Biology, vol. 1199, DOI 10.1007/978-1-4939-1280-3_5, © Springer Science+Business Media New York 2014

chemical approach described and deals specifically with the synthesis of conjugates using a simple and cheap method involving amine and carboxyl groups and the water-soluble carbodiimide, EDC. It describes in a step-by-step way not only the synthesis of conjugates but also their purification by ultrafiltration and their assay for biological activity and fluorescence. Following the protocols described, it is possible to generate QD–Ab conjugates with high levels of biological activity and low levels of non-specificity which possess long lifetimes in terms of fluorescence and that are capable of excellent cellular imaging. An example is given of one such application of conjugate in our laboratory using QD–anti-fission yeast tropomyosin Ab. *See* Fig. 1 for an overview of the process.

In biomedicine and biology, organic fluorophores have long been used as agents for imaging purposes, from cellular structures to individual molecules, either nonspecifically for general imaging of cells and tissues or as conjugates with specific bioligands for bioaffinity-based imaging [1]. In the latter case, this is most particularly when they are conjugated to antibodies or single-stranded nucleic acids. Organic fluorophores can be characterized as organic molecules that possess one or more π-bonds whose electrons, when exposed to light of a specific wavelength, are "promoted" to a higher energy level orbital and which "fall" back to the lower energy state when the illumination is removed. In "falling back" to the lower energy state, the energy difference is released as a photon. The wavelength(s) at which light is absorbed, energy transfer efficiency, and the wavelength at which light is reemitted depend on both specific fluorophore structure and its chemical environment [2]. An example of an organic fluorophore is fluorescein.

However, when comparing organic fluorophores and QDs, it is evident that QDs possess a number of benefits as agents for bioimaging [3–5]. They possess the significant advantage that they can be excited over a very wide range of wavelengths, meaning that special filter pairs currently used when working with organic fluorophores are unnecessary and that numerous different QDs can be excited simultaneously using a common light source. Practically, when comparing the two materials in cellular imaging applications, QDs yield brighter signals for longer periods of time with respect to organic fluorophores. A comprehensive list of examples relating to the preparation and use of QD conjugates in biological systems can be found in previous works [6].

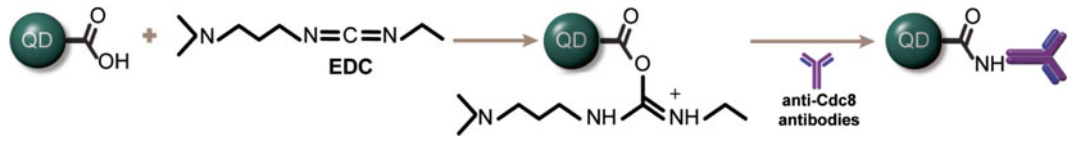

Fig. 1 Graphic of Ab–QD conjugation using carboxyl and amine groups in the presence of the water-soluble carbodiimide EDC

The surfaces of available QDs possess chemical structures that permit them to be conjugated to bioligands, such as proteins and nucleic acids. One such structure is streptavidin, which can be reacted with biotinylated ligands to produce conjugates [7–9]. While streptavidinated QDs are relatively expensive, the process of their conjugation to bioligands which have been biotinylated is relatively simple; the two materials simply need to be mixed together. Unfortunately, the high affinity of streptavidin for biotin makes the reaction difficult to control and usually results in fully saturated products/surfaces. This potentially renders the process of optimization of conjugate fluorescence and biological activity difficult or impossible. QDs with other types of surface functional groups also exist, e.g., those possessing carboxyl or amine groups. However, these tend to be employed much less frequently by biologists in making biomolecule–QD conjugates. Examples of QDs available on the market, along with a schematic of their structures, can be found elsewhere [10].

The alternative to the costly affinity-based conjugation strategy, typified by the interaction of streptavidin with biotin, is to use a classical and traditional chemical approach. Coupling in this fashion also makes it possible to take advantage of functional groups naturally present in/on a biomolecule, or which can be simply introduced during its production in synthetic form. Two classic examples of such groups are carboxyls and primary amines. This type of conjugation is cheap (relatively when compared with biotin–streptavidin) and can facilitate the variation of the QD surface density of conjugated ligand groups so as to optimize the materials in bio-applications. Specifically, we have employed carboxyl surface-modified QDs in reactions with the amino groups of Abs in the presence of EDC to produce QD–Ab conjugates that possessed high levels of biological activity and which were also highly fluorescent. Water is the preferred solvent system as it minimizes denaturation of the Ab which would otherwise occur in a nonpolar solvent environment. The coupling reaction mechanism was first described by Nakajima and Ikada in 1995 [11] and is shown in Fig. 2 with some explanatory notes. This scheme has recently been slightly amended for reactions involving the free base of EDC rather than the HCl salt [12]. While this is a commonly used strategy for carboxyl–amine couplings, it does not always work in the way either expected or desired, and perhaps this is the reason why it has been little used by biologists in producing QD–Ab conjugates to date. Briefly, in an aqueous environment, the formation of the QD–Ab conjugate using a carbodiimide can be considered to be a multistep process involving the activation of the QD surface carboxyl groups by their conjugation to the carbodiimide which is then displaced by the Ab to form the QD–Ab conjugate. The stoichiometry of the reaction overall is theoretically 1:1:1 (QD/carbodiimide/Ab), and generally, the carbodiimide is present in excess. Chemically, the process is as follows for EDC HCl [11] and very similar for the free base EDC [12].

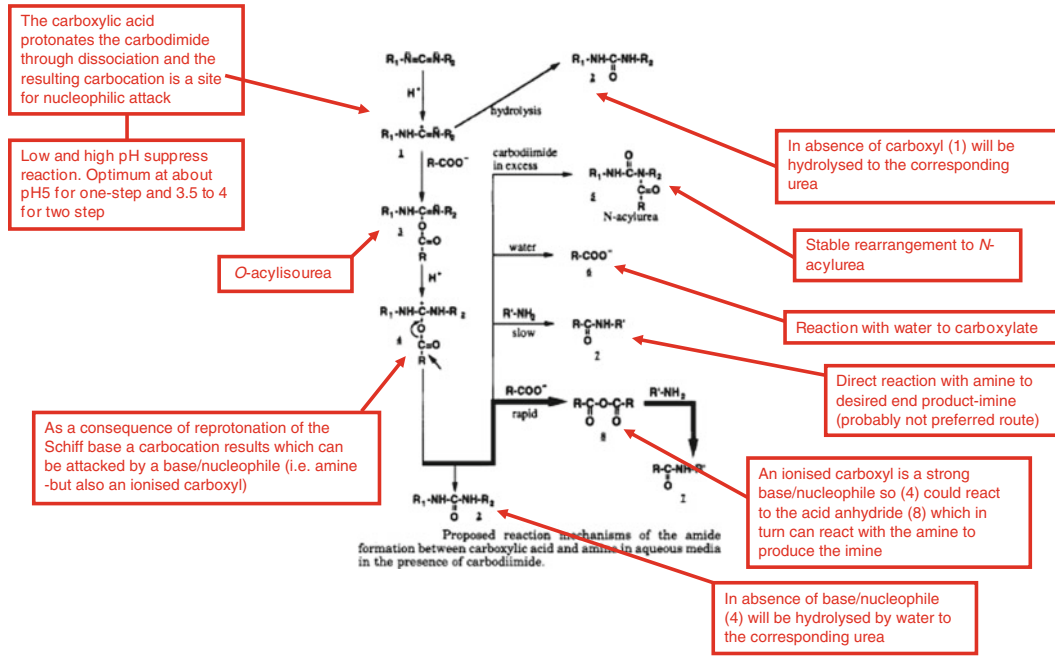
The carboxylic acid protonates the carbodimide through dissociation and the resulting carbocation is a site for nucleophilic attack
Low and high pH suppress reaction. Optimum at about pH5 for one-step and 3.5 to 4 for two step
O-acylisourea
As a consequence of reprotonation of the Schiff base a carbocation results which can be attacked by a base/nucleophile (i.e. amine -but also an ionised carboxyl)
In absence of carboxyl (1) will be hydrolysed to the corresponding urea
Stable rearrangement to N-acylurea
Reaction with water to carboxylate
Direct reaction with amine to desired end product-imine (probably not preferred route)
An ionised carboxyl is a strong base/nucleophile so (4) could react to the acid anhydride (8) which in turn can react with the amine to produce the imine
In absence of base/nucleophile (4) will be hydrolysed by water to the corresponding urea
hydrolysis
carbodiimide in excess
N-acylurea
water
slow
rapid
Proposed reaction mechanisms of the amide formation between carboxylic acid and amine in aqueous media in the presence of carbodiimide.

Fig. 2 EDC-mediated carboxyl–amine coupling (partially abstracted from reference [10])

In water, the carboxyl moieties present on the surface of the QDs disassociate into their conjugate base (-COO^-) and acid (H^+/H_3O^+) species; the degree of dissociation depends on the pH of the system and the specific carboxylic acid involved. The resulting protons can protonate the carbodiimide using the lone pair electrons present on the molecule's two central nitrogen atoms as indicated in Fig. 2. This leaves the central carbodiimide carbon atom electron deficient and consequently susceptible to nucleophilic attack by the nucleophilic QD carboxylate groups to form the QD-carbodiimide adduct. This is known as an acylisourea (which is also a Schiff base). At this stage, it is sometimes possible to separate out the adduct from the reaction mixture so as to remove contaminating/excess or unreacted reaction components before reacting it with the desired primary amine. In the case presented here, this approach is not adopted and a quantity of the Ab is then added to the reaction mixture containing the acylisourea. The antibody possesses an N-terminal primary amine group as well as amino acid side-chain primary amine groups which can potentially displace the carbodiimide moiety via nucleophilic substitution by attack on the electron-deficient carbon atom of the QD carboxyl group (Fig. 2). This completes the process of QD–Ab conjugate formation. Protons which are still present in the reaction environment from the disassociation of the QD surface carboxyl groups can also protonate the second central nitrogen

atom of the carbodiimide moiety of the acylisourea causing further polarization of the QD carboxyl carbon atom promoting its amine reactivity. Unfortunately, the Ab amine groups are not the only nucleophilic species in the reaction mix at this point; there will also be deprotonated QD surface carboxyl groups present, and consequently, these also possess the opportunity to react with the QD–carbodiimide adduct. These complexities and a whole host of other considerations require that for the reaction to work efficiently, it should preferably be optimized for each and every different carboxylic acid and amine to be conjugated. Figure 2 details the various possible outcomes from the reaction in terms of end products.

This chapter attempts to facilitate the use of the EDC in aqueous carboxyl–amine coupling in the conjugation of QDs with Abs. It describes the optimization process that can be used to facilitate the functionality of the products generated, the conjugates separation from unreacted reaction components, and the products' bioassay and fluorescence assay. The development of the protocols described here is discussed in detail in previous works [12, 13].

2 Materials

All solutions should be prepared using ultrapure water (sterilized deionized water, 18 mΩ/cm^3 at 25 °C) and analytical grade reagents and can be stored at room temperature unless indicated otherwise. Local waste disposal regulations should be adhered to when discarding used solutions and materials.

2.1 Antibody Affinity Purification

1. Pierce AminoLink® Plus Immobilization Kit (Thermo Fisher Scientific, Rockford, IL, USA).
2. Retort stand and clamp.
3. 1.5 mL microcentrifuge tubes.
4. Microvolume cuvettes.
5. UV spectrophotometer.

2.2 SDS-PAGE of Purified Antibody

1. Resolving buffer: 1.5 M 2-Amino-2-hydroxymethyl-propane-1,3-diol (Tris), pH 8.8. Weigh 18.17 g of Tris and transfer to a glass beaker. Add water to a volume of 80 mL. Mix and adjust pH with HCl (*see* **Note 1**). Make up to 100 mL with water. Store at room temperature (RT).
2. Stacking gel buffer: 1.0 M Tris, pH 6.9. Weigh 60.60 g Tris–Base and prepare a 100 mL solution as in previous step. Store at RT.
3. 30 % Acrylamide/bisacrylamide solution, 29:1.
4. Ammonium persulfate: 10 % solution in deionized water (*see* **Note 2**).

5. *N*,*N*,*N*′,*N*′-Tetramethylethylenediamine (TEMED). Store at 4 °C.
6. Isopropanol.
7. 6× SDS-PAGE loading buffer: 375 mM Tris–HCl, pH 6.8, 6 % SDS, 48 % glycerol, 9 % 2-mercaptoethanol, and 0.03 % bromophenol blue.
8. Mini-PROTEAN® 3 Gel electrophoresis system (Bio-Rad, Hercules, CA, USA).
9. Protein molecular weight marker. We used Kaleidoscope™ prestained standards (Bio-Rad, Hercules, CA, USA).
10. Coomassie stain: 0.1 % Coomassie brilliant blue, 50 % methanol, 10 % acetic acid.
11. Destain solution: 50 % methanol, 10 % acetic acid.
12. Plastic trays for staining/destaining.

2.3 Antibody–QD Conjugation

1. Carboxyl-functionalized QDs. We used eFluor 490NC nanocrystals (eBioscience, San Diego, USA).
2. 1-Ethyl-3-(3-dimethylaminopropyl)carbodiimide.
3. 10× Phosphate buffered saline (PBS): 1.37 M NaCl, 100 mM Na_2HPO_4, 18 mM KH_2PO_4, pH 7.4.
4. Tris–HCl, 1 M, pH 7.5.
5. Purified antibody (from Subheading 2.1).

2.4 Ultrafiltration of Antibody–QD Conjugates

1. Vivaspin 500 centrifugal concentrator cartridges 100,000 MWCO (Sartorius GmbH, Gottingen, Germany).
2. 0.1 M Potassium hydroxide (KOH).
3. 1× PBS Buffer: 137 mM NaCl, 2.7 mM KCl, 10 mM Na_2HPO_4, 1.8 mM KH_2PO_4, pH 7.4.

2.5 Antibody–QD Conjugate Assay (Sandwich and Fluorescence)

1. 384 well microtiter plates.
2. Fluorescence spectrophotometer.
3. Protein transfer membrane. We used Hybond-P PVDF membrane from GE Healthcare UK (Little Chalfont, UK).
4. Anti-rabbit alkaline phosphatase-conjugated secondary antibody.
5. 3 % nonfat powdered milk in PBS (*see* **Note 3**).
6. PBST: 0.1 % Tween 20 in PBS.
7. Development buffer: 0.1 M NaCl, 0.1 M Tris, 5 mM $MgCl_2$, pH 9.6.
8. BCIP/NBT-Purple Liquid Substrate (Sigma-Aldrich, Poole, UK). Store at 4 °C.
9. Flat bed scanner.
10. ImageJ software (http://rsb.info.nih.gov/ij/).

2.6 Intracellular Immunofluorescence

1. PEM Buffer: 0.1 M piperazine-N,N′-bis[2-ethanesulfonic acid] (PIPES), 1 mM $MgCl_2$, 1 mM $MgSO_4$, pH 6.9.
2. 1 M NaOH.
3. 30 % Paraformaldehyde solution in PEM (*see* **Note 4**).
4. Sorbitol.
5. Triton X-100.
6. Zymolase.
7. PBS.
8. PEMBAL buffer: 0.1 M PIPES, 1 mM $MgCl_2$, 1 mM $MgSO_4$ + 1 % w/v BSA, 0.1 % w/v NaN_3, 100 mM lysine hydrochloride, pH 6.9. Store at 4 °C.
9. Glass slides and coverslips.

3 Methods

Carry out all procedures at room temperature unless otherwise specified.

3.1 Ab Affinity Purification

In our experiments, the production of anti-Cdc8 Abs was commissioned commercially and involved immunizing a specific pathogen-free rabbit with purified full-length recombinant Cdc8 protein in TiterMax® Gold adjuvant (TiterMax USA, Inc., Norcross, USA). Serum was collected at 1-month intervals 1 week after an antigen boost [14] and Abs were supplied in serum. Consequently, the removal of contaminating serum proteins was required before Abs could be used in conjugation reactions. If you are using an Ab which is already purified, this affinity purification step may be omitted and you can proceed directly to the conjugation and conjugate assay sections of the method.

Purification of Abs can be performed using an AminoLink® Plus Immobilization Kit (see Subheading 2) following the detailed instructions supplied by the manufacturer, and we have always used the gravity-flow method. Our exceptions to the manufacturer's instructions are listed below:

1. Follow the procedure for coupling the antigen to the column using pH 7.2 coupling buffer.
2. Elute the bound antibody as 1 mL aliquots into 1.5 mL sterile microcentrifuge tubes containing 50 µL of neutralization buffer using 8 mL of elution buffer (*see* **Note 5**).

3.2 Ab Assay

When assaying the eluted fractions from Subheading 3.1 for Ab, UV spectroscopy is a quick and simple preliminary method to check for the presence of protein. Once protein has been detected, and before those fractions containing it are pooled, a sample of

each fraction should be analyzed by SDS-PAGE to check for protein bands of the appropriate size relating to Ab.

3.2.1 Spectroscopy

Add 50 μL of neutralization buffer to 1 mL of elution buffer in a quartz or plastic UV transparent cuvette and "zero" the spectrophotometer at λ_{280nm} using the solution. We do this in a 1 cm path length cuvette.

1. Measure the optical density at 280 nm (OD_{280}) of each eluted fraction and record the value. Plot a graph of fraction number against OD_{280} and a peak in the plot will identify which fractions contain protein (Fig. 3a).

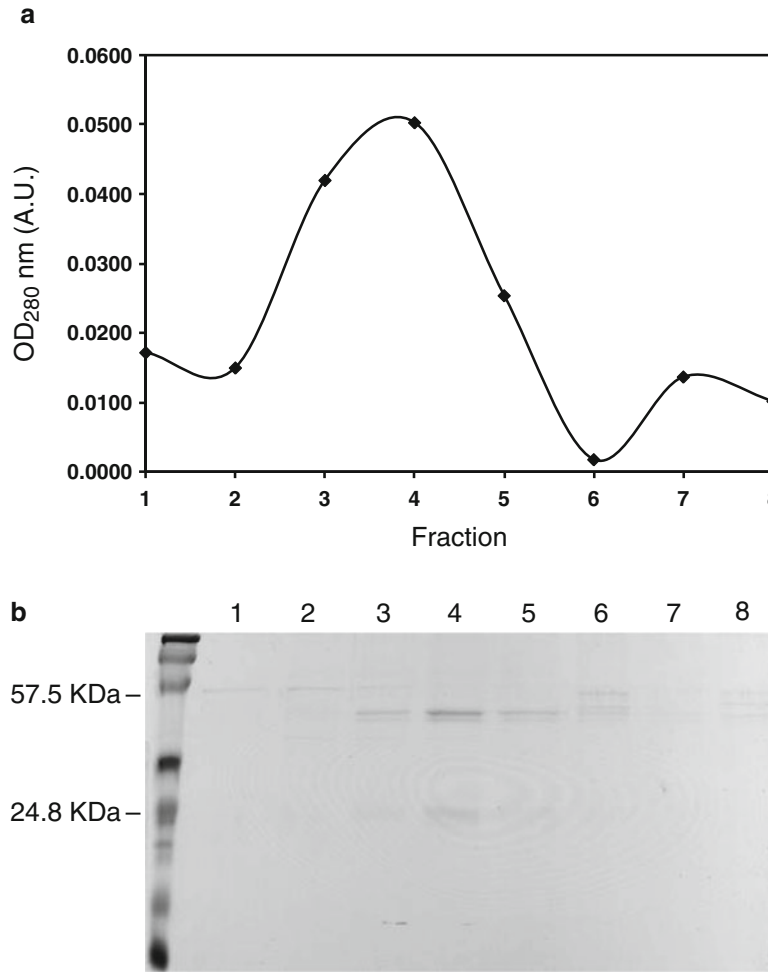

Fig. 3 Spectrophotometric and SDS-PAGE analysis of eluted fractions: (**a**) Plot of absorbance at 280 nm of 1 mL column fractions during anti-Cdc8 antibody affinity purification and (**b**) SDS-PAGE of fractions 1–8 (from **a**) after affinity purification with molecular weight marker (*far left*). The majority of the purified antibody can be observed in fractions 3–5

3.2.2 SDS-PAGE

1. The presence of Ab in the protein fractions identified above can be established via polyacrylamide gel electrophoresis. Mix 1.125 mL of resolving buffer with 1.8 mL of acrylamide solution and 1.48 mL water in a sterile 50 mL Falcon tube®. Add 45 μL of 10 % w/v SDS, 45 μL of 10 % w/v ammonium persulfate with 2.5 μL of TEMED and mix well (avoid the formation of bubbles). Rapidly but smoothly pour the solution (4 mL) into a 7.25 cm × 10 cm × 1.0 mm Mini-PROTEAN® 3 Gel electrophoresis system gel cassette and allow to polymerize leaving space for addition of a stacking gel. Gently overlay with isopropanol (*see* **Note 6**).
2. Prepare the stacking gel by mixing 312.5 μL of resolving buffer, 425 μL of acrylamide solution, and 1.7 mL water in a sterile 50 mL Falcon tube®. Add 25 μL of 10 % w/v SDS, 25 μL of 10 % w/v ammonium persulfate, and 2.5 μL of TEMED and mix gently (avoid the formation of bubbles). Remove the isopropanol from the gel, replace with stacking gel solution, and immediately insert a 10-well gel comb (avoid the formation of bubbles).
3. Add 4 μL of 6× SDS-PAGE loading buffer to 20 μL of each eluted fraction in a 1.5 mL sterile microcentrifuge tube. Heat the samples at 95 °C for 5 min, cool rapidly on ice, and centrifuge briefly at 10,000 × *g* to pull down any condensation that has formed on the lid and walls of the tube.
4. Load 5 μL of prestained standard to the first well of the gel. Load the entire volume of each sample to successive lanes of the gel making a note of the order in which they are added. Electrophorese the gel at constant voltage (120 V) until the dye front reaches 1 cm from the base of the gel.
5. For gel staining and band visualization: gently pry the gel cassette open using a spatula, carefully remove the gel (*see* **Note 7**), immerse in Coomassie stain, and leave for 1 h with gentle agitation. Subsequently, transfer the gel to a tray containing destain solution for 1 h (*see* **Note 8**).
6. Transfer the destained gel to a tray containing sterile deionized water and view gel bands. It may be necessary to place the gel on a light box to do this. There should be two bands observed in protein fractions if Ab is present: one at approximately 55 kDa (representing IgG heavy chains) and one at approximately 25 kDa (representing IgG light chains). *See* Fig. 3b.
7. Once the presence of Ab has been confirmed, pool the Ab-containing fractions and assay the resulting solution as described in Subheading 3.1. Calculate antibody concentration using Beer's law and the extinction coefficient of IgG: 210,000 M^{-1} cm^{-1}.

3.3 QD–Ab Conjugation

Conjugation of Ab and QD is achieved via a one-step water-soluble carbodiimide-mediated approach using EDC. A two-step approach is effectively impossible to use with this procedure as the reaction

intermediate, i.e., the acylisourea, is too difficult to separate from the other reaction component, i.e., excess carbodiimide.

1. Pipette 120 picomoles of QDs into a 1.5 mL sterile microcentrifuge tube and 600 nanomoles of EDC. Incubate for 5 min at room temperature.
2. Add 6 picomoles of purified Ab and 10 μL of 10× PBS. Adjust to a final volume of 100 μL with sterile deionized water.
3. Incubate the reaction, protected from light (*see* **Note 9**) for 1.5 h with end-over-end mixing.
4. Add 5 μL of 1 M Tris–HCl pH 7.5 and incubate for 15 min with end-over-end mixing to quench EDC-activated, but non-Ab-conjugated, QD surface groups.

3.4 Purification of QD–Ab Conjugate: Ultrafiltration and Fluorescence Assay

The QD–Ab conjugate is separated from unwanted/excess reaction components by ultrafiltration in a Vivaspin 500 filter unit with a size cutoff limit of 100,000 Da.

1. Prerinse the filter unit with 200 μL (×3) of 0.1 mM KOH by centrifugation at 6,000 × *g* for 5 min.
2. Wash the filter unit three times with 200 μL of deionized water by centrifugation at 6,000 × *g* for 5 min.
3. Add the entire QD–Ab reaction mixture (from Subheading 3.3) to the unit and centrifuge for between 2 and 5 min until the volume retained above the filter membrane (retentate) is approximately 25 μL.
4. Wash the retentate with 200 μL (×3) of sterile deionized water by centrifuging at 6,000 × *g* for 2–5 min.
5. Remove the washed retentate from the unit (*see* **Note 10**) and adjust to a final volume of 100 μL with sterile PBS.
6. Carefully pipette the conjugate into the wells of a sterile 384-well microtiter plate. Include a well that contains PBS alone as a reference for zero/baseline measurement. Record fluorescence at λ_{max}excitation 468 nm and λ_{max}emission 495 nm. Remove the conjugate from the well, taking care to recover the whole volume. Store at 4 °C until use.

3.5 Assay of QD–Ab Conjugates for Biological Activity: Membrane Sandwich Assay

The QD–Ab conjugate can be assayed for its biological activity using a membrane-based immuno-sandwich assay approach. In this process, an anti-rabbit secondary antibody conjugated to alkaline phosphatase is used to detect and quantify QD–Ab conjugate bound to a polyvinylidene fluoride (PVDF) membrane. The binding of the secondary antibody is detected via a colorimetric approach [12, 13].

1. Prepare a series of antibody (in our case, anti-Cdc8) standard solutions at concentrations of 1.23×10^{-2}, 6.15×10^{-3}, 2.46×10^{-3}, 1.23×10^{-3}, and 6.15×10^{-4} nanomoles in a total

of 300 μL of PBS (sufficient to construct a standard curve with three replicates for each point).

2. Cut a strip of PVDF membrane (*see* **Note 12**) large enough to accommodate spotting 100 μL samples of the conjugates and standards (15 cm × 7 cm should be sufficient). Activate the membrane by immersing it briefly in methanol and place on a stiff flat surface such as a shallow plastic tray and allow excess methanol to evaporate in air.
3. Pipette each standard (in triplicate) and conjugate (100 μL) onto the membrane so as to form single spots. Take care to allow sufficient spacing between each application so as not to cause overlapping of spots and allow to dry (*see* **Note 13**). Flow-through samples can also be spotted so as to monitor flow-through Ab concentration.
4. Incubate the membrane in a plastic tray with anti-rabbit alkaline phosphatase-conjugated secondary antibody (1 in 10,000 dilution) in 3 % w/v dried milk solution for 1 h with gentle agitation. Subsequently wash the membrane (×3) in sterile PBST for 5 min.
5. Develop the membrane by incubating in development buffer for 2 min. Remove the excess buffer from the membrane by gently blotting with a sheet of absorbent tissue and transfer it to a clean plastic tray. Add enough BCIP/NBT-Purple Liquid Substrate to cover the membrane and incubate for 10 min.
6. Stop the reaction by washing the membrane in sterile deionized water for 1 min (×3), gently place on absorbent tissue, and allow to fully dry. An example of a developed membrane is presented in Fig. 4a.
7. Scan the dried membrane using a flatbed scanner connected to a PC at 300 dpi gray scale and analyze the intensity of the spots using ImageJ software®. A standard curve should be plotted using the intensity value obtained for the known antibody standard solutions (Fig. 4b) against which unknown values can be compared. Antibody concentrations in samples can be calculated using the slope of the trend line.

3.6 Optimization of Conjugation Reaction (to Be Carried Out if Subheading 3.3 Does Not Yield Conjugates Which Are Satisfactory in Terms of Fluorescence and Biological Activity)

The optimum QD–Ab conjugate should demonstrate a high level of fluorescence and biological activity, viz., Ab content. Although the protocol described above should result in an optimal product, it cannot be completely guaranteed. Consequently, it may occasionally be necessary to optimize the conjugation reaction. If so, follow the method described below and for more details, *see* previous works [12, 13].

1. Prepare and perform a series of conjugation reactions (*see* **Note 11**) following the protocol described in Subheadings 3.3 and 3.4 with EDC-to-QD ratios of 40,000:1, 5,000:1, and 1,000:1 and QD-to-Ab ratios of 10:1, 10:0.5, and 10:0.1. A series of control

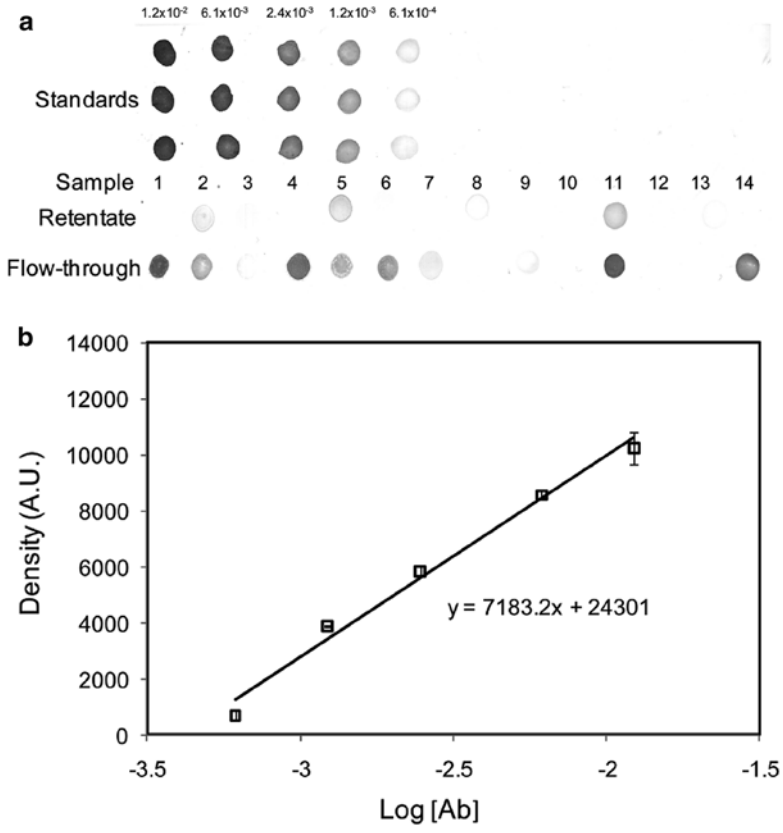

Sample	EDC:QD	EDC:QD		QD:Ab	QD:Ab
1	40000:1	4800 nmol:120 pmol		10:1	120 pmol:12 pmol
2	5000:1	600 nmol:120 pmol		10:1	120 pnmol:12 pmol
3	1000:1	120 nmol:120 pmol		10:1	120 pmol:12 pmol
4	40000:1	4800 nmol:120 pmol		10:0.5	120 pmol:6 pmol
5	5000:1	600 nmol:120 pmol		10:0.5	120 pmol:6 pmol
6	1000:1	120 nmol:120 pmol		10:0.5	120 pmol:6 pmol
7	40000:1	4800 nmol:120 pmol		10:0.1	120 pmol:1.2 pmol
8	5000:1	600 nmol:120 pmol		10:0.1	120 pmol:1.2 pmol
9	1000:1	120 nmol:120 pmol		10:0.1	120 pmol:1.2 pmol
10	5000:1	600 nmol:120 pmol		10:0	120 pmol:0
11	0:1	0:120 pmol		10:1	120 pmol:12 pmol
12	0:1	0:120 pmol		10:0	120 pmol:0
13	0:1	0:120 pmol		10:0	120 pmol:0
14	0:0	0:0		0:1	0:12 pmol

Fig. 4 Assaying conjugate biological activity: (**a**) An example of a PVDF membrane spotted with known amounts of anti-Cdc8 antibody standard solutions and retentate and flow-through of 14 samples produced during QD–Ab conjugation optimization experiments (*see* table for reaction conditions) after color development. (**b**) The average color density values for anti-Cdc8 standards obtained from (**a**) were plotted against concentration to produce a standard concentration curve. The Ab concentration of the QD–Ab conjugation reactions was calculated using the gradient of the trend line (adapted from East et al. 2010 [12], with permission from the American Chemical Society)

reactions omitting QD, EDC, and Ab in various combinations can also be included. For more details, *see* previous works [12, 13].

3.7 Immunofluorescence Imaging of Cdc8 in Schizosaccharomyces pombe

In our experiments, we used QD–Ab conjugates to image tropomyosin (Cdc8) in the fission yeast *S. pombe* [13]. Consequently, this part of the method may need to be adapted to individual users' needs or changed completely. However, the protocol adopted in our laboratory for using QD–Ab conjugates in imaging is very similar to that already used by us when employing organic fluorophore–Ab conjugates. Consequently, a useful starting point for applying QD–Ab conjugates in intracellular imaging is likely to be adoption of whatever protocol may be in use currently in the laboratory with more "classical materials" and subsequent optimization as appropriate.

1. Add 10 mL of mid-log *S. pombe* culture in EMM (Edinburgh Minimal Medium) [15] to a conical flask and place on an orbital shaker set to rotate at 100 rpm.
2. Add 1.25 mL of 30 % v/v paraformaldehyde solution to the cells and incubate for 30 min and continue agitation.
3. Harvest the fixed cells by centrifugation at 1,000 × *g* for 2 min at room temperature and discard the supernatant. Wash the pellet by resuspension in 1 mL of PEM, transfer to a sterile 1.5 mL microcentrifuge tube and centrifuge at 1,000 × *g* for 2 min at room temperature, remove the supernatant, and resuspend the pellet in 1 mL PEM. Repeat this process a total of three times (*see* **Note 14**). Finally, resuspend the pellet in 1 mL of PEM containing 1 M sorbitol and 1.2 mg of zymolase and incubate for 30 min to 1 h at 37 °C (*see* **Note 15**).
4. Pellet the cells by centrifugation at 1,000 × *g* for 2 min and resuspend in 1 mL of PEM containing 1 M sorbitol and 1 % v/v Triton for 30 s, and then wash three times in PEM as described above.
5. Resuspend the cell pellet in the purified QD–Ab conjugate (100 μL) and incubate overnight with end-over-end mixing protected from light. Wash the cells twice in 200 μL PBS then resuspend in 100 μL of PBS.
6. Pipette 10 μL of cell suspension onto a glass coverslip, spread around the surface using the tip of the pipette, and allow the suspension to dry. Place a small drop of glycerol onto a glass slide and carefully place the coverslip, cell-side down onto the glycerol. Seal the coverslip to the slide by painting around the edges with clear nail varnish and allow to dry before imaging. Imaging was performed as described in previous works [12, 13]. Store slides at 4 °C protected from light. Example images obtained using this method compared to those with traditional fluorophores are presented in Fig. 5.

a

	EDC:QD	QD:Ab	R Fluor	R [Ab]	R % TOTAL
1	40000:1	10:1	17.09	0.00E+00	0.00
2	5000:1	10:1	146.94	3.34E-04	7.53
3	1000:1	10:1	210.15	1.23E-04	0.96
4	40000:1	10:0.5	9.62	0.00E+00	0.00
5	5000:1	10:0.5	183.90	3.88E-04	11.83
6	1000:1	10:0.5	211.06	3.88E-05	0.04
7	40000:1	10:0.1	10.69	0.00E+00	0.00
8	5000:1	10:0.1	147.09	1.85E-04	1.73
9	1000:1	10:0.1	258.57	3.89E-05	0.12
10	5000:1	10:0	66.35	0.00E+00	0.00
11	0:1	10:1	291.00	4.11E-04	8.52
12	0:1	10:0	299.43	0.00E+00	0.00
13	0:1	10:0	804.31	0.00E+00	0.00
14	0:0	0:1	4.73	0.00E+00	0.00

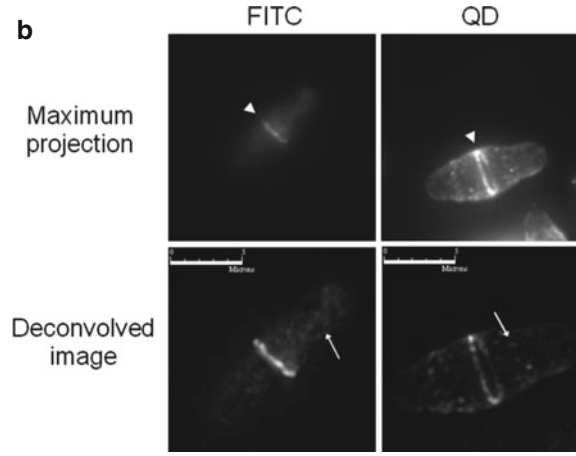

Fig. 5 QD–Ab conjugate optimization and use in imaging: (**a**) Fluorescence values are displayed as arbitrary fluorescence units. The concentration of IgG present in both retentate and flow-through determined colorimetrically is displayed in nanomoles and is also expressed as a percentage of the total IgG added to the reaction. Optimum conditions are indicated by the *green* highlight; control reactions are highlighted in *gray*. The reaction highlighted in *yellow* was not subjected to filtration. (**b**) *S. pombe* cells labeled using a QD–antiCdc8 Ab and a primary/FITC labeled secondary antibody sandwich. The *top two panels* show a maximum projection of 21 images taken at separate focal planes, using identical exposure settings. The contractile actomyosin ring is indicated with *arrow heads*. The *bottom panels* show the same cells after digital deconvolution by imaging software. Cdc8-decorated actin filaments are indicated with *fine arrows* (adapted from East et al. 2010 [12], with permission from the American Chemical Society) (Color figure online)

4 Notes

1. It will take a large volume of HCl to adjust the pH of 1.5 M Tris. This volume can be reduced by using concentrated HCl (10 M or similar). When close to the desired pH, it is advisable to use a lower concentration (1 M) to avoid dropping below the required pH value.
2. The 10 % w/v APS solution can be aliquoted and frozen until required. This avoids repeated freezing/thawing of the solution and the smaller storage quantities can be quickly thawed prior to gel casting. Each gel requires a volume of 70 μL.
3. Vortex the solution to dissolve the majority of the milk powder, then allow at least 30 min with rolling or end-over-end mixing at room temperature to ensure all of the powder is dissolved. Undissolved milk powder particles can cause background staining when developing membranes.
4. Always use fresh formaldehyde solution. Weigh 3 g of paraformaldehyde solution into a 50 mL Falcon tube® inside a fume hood (paraformaldehyde is toxic). Add approximately 7 mL of PEM to the tube, gently mix, and place in a water bath at 50 °C. Add 1 M NaOH dropwise from a Pasteur pipette placing the tube in the water bath for 1 min between drops until the solution begins to clear. Continue to incubate at 50 °C until the paraformaldehyde has completely dissolved. Allow the solution to cool to room temperature and centrifuge at $1{,}000 \times g$ for 5 min to remove the small remaining amounts of undissolved paraformaldehyde.
5. Arrange the elution tubes next to each other in a microcentrifuge tube rack (pre-labeled) with the column clamped (using a retort stand) approximately 1 cm above the tubes. This allows for quick switching between tubes and no ambiguity about identity of the collected fractions. The flow rate is relatively slow and should provide enough time to change tubes between drops.
6. Addition of isopropanol helps to level the gel and prevent it from drying out during polymerization. It is advisable to allow 1 h for each part of the gel (resolving and stacking) to fully polymerize. Gels can be stored at 4 °C after casting by wrapping in moist paper towels followed by aluminum foil/Clingfilm and can be kept for at least a week.
7. The stacking gel may be removed at this stage by gently separating it from the resolving gel using the edge of a glass plate. Gently spraying sterile deionized water underneath the gel from the nozzle of a squeeze bottle will help loosen it from the plate.

8. It may be necessary to change the destained solution periodically to maintain the rate of destaining.
9. Wrap the tubes tightly in aluminum foil.
10. A proportion of unconjugated QD will usually bind to the filter membrane and may be visible (a yellow color when using eFluor 490NC). Consequently, this will not pass into the flow-through.
11. Both EDC and IgG can quench QDs' fluorescence; therefore, a balance between conjugate fluorescence and antibody possession/biological activity must be achieved.
12. Membranes should never be handled with bare hands. Wear gloves or use forceps.
13. It will take a long time for the samples to dry at room temperature. The drying process can be accelerated by placing the membrane at 37 °C or even 60 °C. Care should be taken to prevent droplets running or contacting each other when carrying the membrane to the incubator.
14. A wash in this protocol involves resuspending the cell pellet in the desired wash buffer then centrifuging at 1,000 × *g* for 2 min to separate the cells from the dirty wash buffer, which is then discarded. During each washing step a small amount of cells will be lost. In a fixed angle rotor performing half the wash centrifugation (i.e. 1 min) with the tube in one orientation then rotating it through 180 °C before performing the second half of the spin will pull the cells into a tighter pellet that is easier to see and therefore avoid when aspirating the supernatant.
15. Zymolase hydrolyzes a yeast cell-wall component allowing conjugate to pass into the cells. Incubation for longer than 1 h can digest too much of the cell wall and damage cell morphology and ultrastructure.

References

1. Johnson ID (ed) (2010) The Molecular Probes® handbook—a guide to fluorescent probes and labeling technologies, 11th edn. Life Technologies™ Corporation, Carlsbad, CA
2. Valeur B, Berberan-Santos MN (2012) Molecular fluorescence: principles and applications. Wiley-VCH Verlag GmbH & Co. KGaA, Weinheim, Germany
3. Bruchez M Jr, Moronne M, Gin P, Weiss S, Alivisatos AP (1998) Semiconductor nanocrystals as fluorescent biological labels. Science 281:2013–2016
4. Parak WJ, Gerion D, Pellegrino T, Zanchet D, Micheel C, Williams SC, Boudreau R, Le Gros MA, Larabell CA, Alivisatos AP (2003) Biological applications of colloidal nanocrystals. Nanotechnology 14(7):R15–R27
5. Alivisatos AP, Gu W, Larabell C (2005) Quantum dots as cellular probes. Annu Rev Biomed Eng 7:55–76
6. http://www.invitrogen.com/site/us/en/home/brands/Molecular-Probes/Key-Molecular-Probes-Products/Qdot/Qdot_Citations.html and others at http://www.invitrogen.com

7. Giepmans BN, Deerinck TJ, Smarr BL, Jones Y, Ellisman M (2005) Correlated light and electron microscopic imaging of multiple endogenous proteins using quantum dots. Nat Methods 2:743–749
8. Kingeter LM, Schaefer BC (2009) Expanding the multicolor capabilities of basic confocal microscopes by employing red and near-infrared quantum dot conjugates. BMC Biotechnol. doi:10.1186/1472-6750-9-49
9. Li R, Dai H, Wheeler TM, Sayeeduddin M, Scardino PT, Frolov A, Ayala GE (2009) Prognostic value of Akt-1 in human prostate cancer: a computerized quantitative assessment with quantum dot technology. Clin Cancer Res 15:3568–3573
10. http://www.ebioscience.com and http://www.invitrogen.com
11. Nakajima N, Ikada Y (1995) Mechanism of amide formation by carbodiimide for bioconjugation in aqueous media. Bioconjug Chem 6:123–130
12. East DA, Mulvihill DP, Todd M, Bruce IJ (2011) QD-antibody conjugates via carbodiimide-mediated coupling; a detailed study of the variables involved and a possible new mechanism for the coupling reaction under basic aqueous conditions. Langmuir 27:1388–13896
13. East DA (2010) PhD thesis. University of Kent, Canterbury, UK
14. Skoumpla K, Coulton AT, Lehman W, Geeves MA, Mulvihill DP (2007) Acetylation regulates tropomyosin function in the fission yeast *Schizosaccharomyces pombe*. J Cell Sci 120: 1635–1645
15. Moreno S, Klar A, Nurse P (1991) Molecular genetic analysis of fission yeast *Schizosaccharomyces pombe*. Method Enzymol 194:795–823

Chapter 6

Measuring the Hydrodynamic Radius of Quantum Dots by Fluorescence Correlation Spectroscopy

André A. de Thomaz, Diogo B. Almeida, and Carlos L. Cesar

Abstract

Fluorescence Correlation Spectroscopy (FCS) is an optical technique that allows the measurement of the diffusion coefficient of molecules in a diluted sample. From the diffusion coefficient it is possible to calculate the hydrodynamic radius of the molecules. For colloidal quantum dots (QDs) the hydrodynamic radius is valuable information to study interactions with other molecules or other QDs. In this chapter we describe the main aspects of the technique and how to use it to calculate the hydrodynamic radius of quantum dots (QDs).

Key words Fluorescence correlation spectroscopy, Hydrodynamic radius measurement, Quantum dots, Microscopy, Diffusion coefficient

1 Introduction

The Fluorescence Correlation Spectroscopy (FCS) technique was developed in 1972 by Magde, Elson, and Webb [1] and relies on the analysis of the fluctuation of the fluorescence intensity. It was first used to monitor, noninvasively, the diffusion and dynamics of DNA–drugs interactions. We notice the technique was developed much earlier than the first appearance of the commercial laser scanning confocal microscopy [2].

Only molecules in the focal volume of a confocal microscope, as shown in Fig. 1, can have their fluorescence detected in a photon counting mode. As a molecule diffuses away, through Brownian motion, from the focal volume its contribution vanishes. When we look at the fluorescence detected photons we observe the intensity trace curve as shown in Fig. 2. From this curve we can obtain the autocorrelation curve performing the following mathematical operation:

$$G(\tau) = \frac{<\delta F(t)\delta F(t+\tau)>}{<F(t)>^2} \quad (1)$$

Adriana Fontes and Beate Saegesser Santos (eds.), *Quantum Dots: Applications in Biology*, Methods in Molecular Biology, vol. 1199, DOI 10.1007/978-1-4939-1280-3_6, © Springer Science+Business Media New York 2014

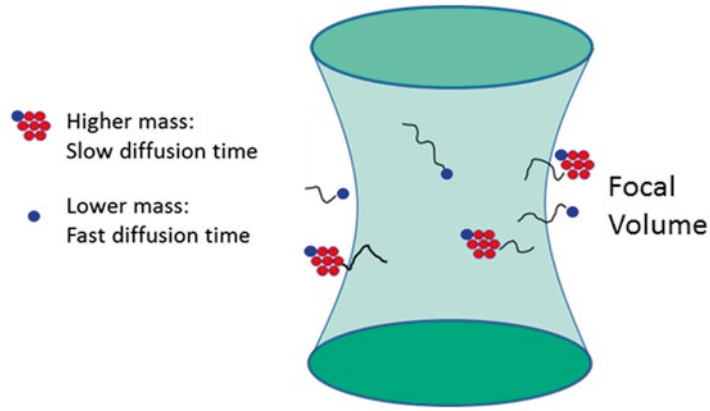

Fig. 1 FCS scheme illustrating the diffusion of molecules with different masses diffusing through the focal volume

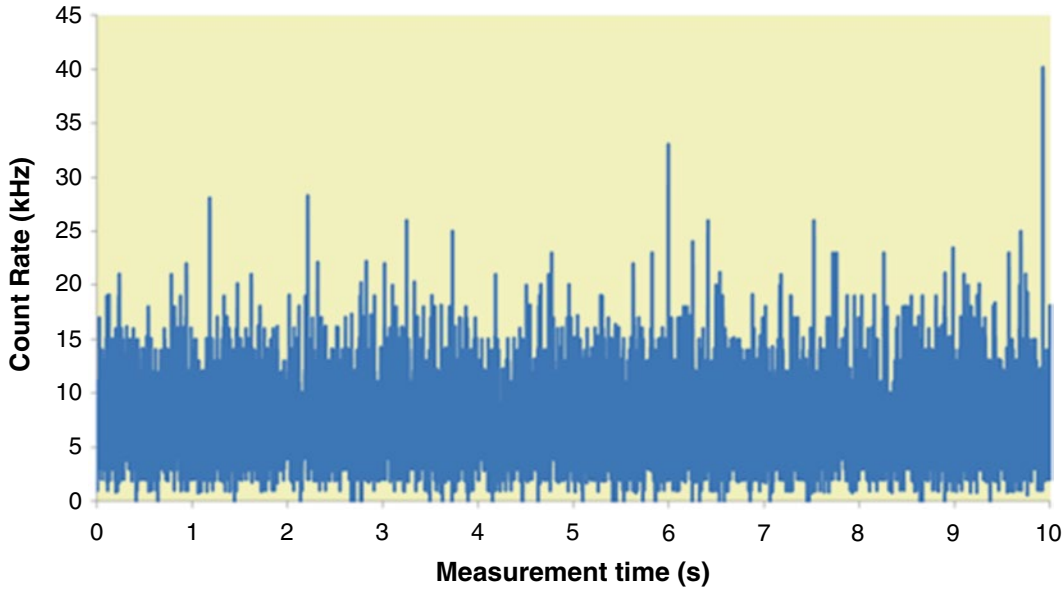

Fig. 2 Intensity of the fluorescence signal detected as function of time

where $\delta F(t) = F(t) - \langle F(t) \rangle$ is the fluorescence fluctuation, <> is a time average, and τ a time delay.

Figure 3 shows a typical autocorrelation curve. The beginning of the correlation curve (lag times in the range 1×10^{-6} s) is dominated by fluctuations in the fluorescence signal caused by rotational movement of the fluorophores and singlet-triplet transitions. After this range of lag time the correlation curve is dominated by fluctuations caused by diffusion of the molecules through the focal volume. This slow diffusion decay is the one which brings information about the molecule size and mass, because the characteristic time extracted from the correlation is related to the diffusion time

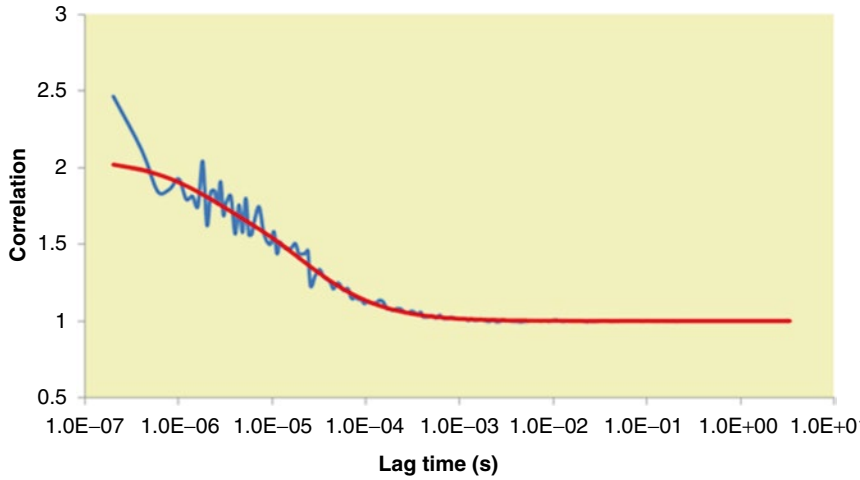

Fig. 3 Typical correlation curve with fitting

of the molecule through the focal volume. These diffusion times are dependent on the solution temperature and viscosity and also on the hydrodynamic radius of each emitting molecule. Large molecules, with large hydrodynamic radius and high mass, will travel slower than molecules with smaller radius and mass through the focal volume. A fitting of the autocorrelation trace allows us to extract the diffusion time and, then, to calculate the hydrodynamic radius and molecular mass.

In a way, FCS is like if we have a mass spectrometer (with far less accuracy) that can measure nondestructively in real time and spatially confined the presence of certain molecules. This technique allows following chemical reactions and their constants of equilibrium in time in a very small volume in a noninvasive way, or following the concentration of different molecules in time, or, finally, as a local viscosity sensor of the solution. Moreover, the number of molecules detected, or the sensitivity of the technique, is incredible small, in the nanomolar (nM) concentration range. The average number of molecules in the focal volume at a time is around 1–10, which is practically undetectable by any other non-optical techniques.

Actually, FCS requires a small number of molecules in the excitation/detection focal volume. This is because the fluctuations with low concentration are much intense when the concentration is high. One molecule leaving the focal volume filled with 5 molecules causes a relative fluctuation much higher than the same molecule leaving a focal volume filled with 100 molecules. That is, the fluctuations due to diffusion of only a few molecules in focal volume are intense compared with the average fluorescence signal [3]. On the other hand, when the number of molecules is too high the relative fluctuation is irrelevant. Therefore, to obtain a good

autocorrelation curve it is important to keep only few molecules in the detection volume. This can be accomplished by two ways: (1) by decreasing the focal volume or (2) by using very high dilution, or a combination of both strategies. In any case, the detection system must be able to detect emissions from single molecule.

Although FCS appeared before the commercialization of laser scanning confocal microscopes, the small focal volume achieved using the pinhole in the confocal system greatly enhanced the capability of the technique and allowed an exponential growth of the number of publications with this technique. Besides that, the photomultipliers sensitivity increased quite a lot and single-molecule detection became much more common [4, 5].

In the confocal configuration a high numerical objective is used to focus the laser beam, at the diffraction limit, and a pinhole is used to obtain focal volumes of the order of attoliters. A solution with a concentration of tenths of nanomolar would result in around 10 molecules in this focal volume. With this small number of molecules small fluctuations are easily detected.

Equation 2 is the theoretical fluctuation autocorrelation curve obtained with the model of molecules suffering Brownian motion and free to move in three dimensions through a focal volume of a Gaussian beam profile of lasers [3, 6]:

$$G(\tau) = \frac{1}{N} \frac{1}{\left(1 + \tau / \tau_D\right)} \frac{1}{\sqrt{\left(1 + \tau / k^2 \tau_D\right)}} \tag{2}$$

Three parameters can be extracted from the autocorrelation curve fitting. The value of $G(0)$ is inversely proportional to the average of fluorescent molecules inside the focal volume. Knowing the size of the focal volume the concentration can be calculated. The other parameter is the diffusion time τ_D and the last parameter, k^2, is the ratio between ω_z and ω_x, the axial and lateral radius of the focal volume $k = \omega_z / \omega_x$.

If the diffusing particle is spherical we can associate a hydrodynamic radius which can be calculated from the Stokes–Einstein equation:

$$D = \frac{k_B T}{6\pi\eta R} \Rightarrow R = \frac{k_B T}{6\pi\eta D} \tag{3}$$

where k_B is the Boltzmann constant, T is the absolute temperature, η is the medium viscosity, and D is the diffusion coefficient. However, it is common that the diffusion coefficient D of the particles studied is not known. It is possible to express Eq. 3 in terms of better known quantities substituting the diffusion coefficient defined by:

$$\tau_D = \frac{\omega_x^2}{4D} \tag{4}$$

In terms of these parameters the hydrodynamic radius is given by:

$$R = \frac{4k_B T \tau_D}{6\pi\eta\omega_x^2} \tag{5}$$

Now the diffusion time τ_D is extracted from the FCS curve, the temperature and viscosity must be known, and the only parameter difficult to measure is the lateral radius ω_x of the focal volume. To obtain this parameter a calibration of the system with a known fluorescent molecule is necessary. Using a molecule with a known diffusion coefficient and using the diffusion time measured by the correlation curve it is possible to calculate ω_x from Eq. 4.

2 Materials

1. Dye with a known coefficient diffusion; examples are Rhodamine B, Rhodamine 6G, and Fluorescein.
2. Ultra pure water.
3. QDs dispersed in water.
4. Glass slides or coverslips.

3 Methods

3.1 Calibration of Lateral Radius of the Focal Volume

1. Dissolve the dye in ultra pure water to get a concentration in the order of nanomolar.
2. Place a drop of this solution, 50 μL is enough, on top of the glass slide on the microscope (use a coverslip if the microscope is inverted).
3. If using an inverted microscope follow the scheme of Fig. 4 to focus the laser inside the droplet.

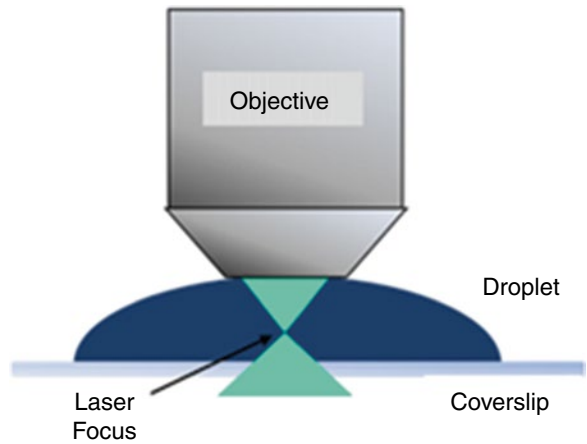

Fig. 4 Focusing scheme in an upright microscopy

4. Focus the laser using a high NA objective. Preferably use a water immersion objective to avoid index refraction mismatch.
5. Acquire the fluorescence intensity curve (*see* **Note 1**).
6. Calculate the correlation curve from the acquired intensity curve (some systems do that automatically).
7. Fit the curve using Eq. 2 and calculate the diffusion time τ_D.
8. Using Eq. 4 to calculate the lateral radius of the focal volume ω_x.

3.2 Calculation of the Hydrodynamic Radius of Quantum Dots

1. Dilute the QDs suspension until it is in the order of nanomolar.
2. Use the same procedure of calibration sample to place the drop of QDs solution.
3. Focus the laser using a high NA objective. Preferably use a water immersion objective to avoid index refraction mismatch.
4. Acquire the fluorescence intensity curve. Select a low laser power to avoid blinking effects in the measurement (*see* **Note 2**).
5. Calculate the correlation curve from the acquired intensity curve (some systems do that automatically).
6. Fit the curve using Eq. 2 and calculate the diffusion time τ_D.
7. Use the lateral radius ω_x, diffusion time of QD, and Eq. 5 to calculate the hydrodynamics radius R of the QD.

4 Notes

1. Use low laser power also for the calibration measurements to avoid saturation effects. If the molecule presents singlet-triplet transitions use this correlation function to fit the data

$$G(\tau) = \left(\frac{1 - T + Te^{-\frac{\tau}{\tau_{\text{triplet}}}}}{1 - T} \right) \frac{1}{N} \frac{1}{\left(1 + \tau/\tau_D\right)} \frac{1}{\sqrt{\left(1 + \tau/k^2\tau_D\right)}} \tag{6}$$

   where τ_{triplet} is the relaxation time of triplet state.
2. Quantum dots are known to exhibit blinking process [7, 8]. Low laser power is necessary to avoid this phenomenon.

References

1. Magde D, Webb WW, Elson E (1972) Thermodynamic fluctuations in a reacting system—measurement by fluorescence correlation spectroscopy. Phys Rev Lett 29(11):705–708
2. Amos WB, White JG (2003) How the confocal laser scanning microscope entered biological research. Biol Cell 95(6):335–342
3. Schwille P (2001) Fluorescence correlation spectroscopy and its potential for intracellular applications. Cell Biochem Biophys 34(3): 383–408
4. Rigler R, Mets U (1993) Diffusion of single molecules through a Gaussian laser beam. SPIE Proc 1921:239–248
5. Rigler R, Mets U, Widengren J et al (1993) Fluorescence correlation spectroscopy with high count rate and low-background—analysis of translational diffusion. Eur Biophys J 22(3): 169–175
6. Krichevsky O, Bonnet G (2002) Fluorescence correlation spectroscopy: the technique and its applications. Rep Prog Phys 65(2):251–297
7. Doose S, Tsay JM, Pinaud F, Weiss S (2005) Comparison of photophysical and colloidal properties of biocompatible semiconductor nanocrystals using fluorescence correlation spectroscopy. Anal Chem 77(7):2235–2242
8. Heuff RF, Swift JL, Cramb DT (2007) Fluorescence correlation spectroscopy using quantum dots: advances, challenges and opportunities. Phys Chem Chem Phys 9(16): 1870–1880

Chapter 7

Quantum Dots Fluorescence Quantum Yield Measured by Thermal Lens Spectroscopy

Carlos Estupiñán-López, Christian Tolentino Dominguez, Paulo E. Cabral Filho, Adriana Fontes, and Renato E. de Araujo

Abstract

An essential parameter to evaluate the light emission properties of fluorophores is the fluorescence quantum yield, which quantify the conversion efficiency of absorbed photons to emitted photons. We detail here an alternative nonfluorescent method to determine the absolute fluorescence quantum yield of quantum dots (QDs). The method is based in the so-called Thermal Lens Spectroscopy (TLS) technique, which consists on the evaluation of refractive index gradient thermally induced in the fluorescent material by the absorption of light. Aqueous dispersion carboxyl-coated cadmium telluride (CdTe) QDs samples were used to demonstrate the Thermal Lens Spectroscopy technical procedure.

Key words Quantum dots, Fluorescence, Quantum yield, Thermal lens, Optical properties

1 Introduction

During the last two decades, thanks to the progress in wet chemistry, highly luminescent semiconductor nanocrystals or quantum dots (QDs) have been achieved [1, 2], then, in order to evaluate the application and validation of new fluorophores for applications in life and material science, a complete spectroscopic characterization is requires. In this sense, an essential parameter in the comparison and in the determination of the optical quality of QDs is the fluorescence quantum yield or quantum efficiency (Φ_f) [3–5]. For example, the optical properties of QDs are dependent of its size and physicochemical properties [6], and therefore a realistic knowledge of Φ_f allows optimize the synthesis parameters of these functional fluorophores. The fluorescence quantum efficiency is defined as the ratio of the number of emitted photons divided by the number of absorbed photons occurring into luminescent materials. From Φ_f it is possible to determine the analytical sensitivity from the fluorophore side using the expression

Adriana Fontes and Beate Saegesser Santos (eds.), *Quantum Dots: Applications in Biology*, Methods in Molecular Biology, vol. 1199, DOI 10.1007/978-1-4939-1280-3_7, © Springer Science+Business Media New York 2014

$B = \Phi_f \times \varepsilon(\lambda_{ex})$, where B is the fluorophore's brightness and $\varepsilon(\lambda_{ex})$ is the molar absorption coefficient at the excitation wavelength. Φ_f also is important for the calculation of the efficiencies of fluorescence resonance energy transfer (FRET) processes [7].

Different techniques have been used to measure this quantity, depending on whether the fluorophore is in solution or in solid phase. These techniques can be classified into absolute and relative method [8–10]. Earlier quantum yields measurements based mostly in fluorometric methods were wrong mainly due to lack of care on the experimental conditions and suffered from the low resolution of the measuring instruments, as review by Demas and Crosby [8]. In that context, Thermal Lens Spectroscopy (TLS) emerges as a technique that presents more accurate results for Φ_f measurements when compared with methods that directly explore relative and absolute fluorescence analysis [8–12], which require an accurate measure of total light emitted by the sample or involve a careful comparison between the emission of the unknown and standard sample [9, 13–16]. Lens Spectroscopy was introduced by Gordon et al. [17] and by Leite et al. [18] in 1960s, and since then it has been established as a powerful tool for material characterization. In recent years, TLS technique has been used to evaluate fluorescence quantum yield, diffusivity, and thermal conductivity of liquid and transparent solid media showing precision and high sensitivity [19, 20], for scattering samples other techniques are recommended (*see* **Note 1**).

The TL method is based on the principle of energy conservation. So if P_{in} and P_{out} are the incident and transmitted power of excitation beam, respectively, then the absorbed power P_{abs} is the sum of the luminescence emission power P_L and the thermal power transformed to heat P_{th}, consequently

$$P_{in} = P_{out} + P_L + P_{th} = P_{out} + P_{abs} \tag{1}$$

Defining the transmission ratio $T = P_{out}/P_{in}$ and the absorbance $A = 1 - T$. The absorbed power is given by

$$AP_{in} = P_{abs} \tag{2}$$

In order to measure Φ_f using the TLS technique, a modulated Gaussian laser beam is focused onto a host containing fluorophores and the transmitted light, at the center of the beam profile, is detected in the far-field. By absorption of the excitation laser beam, the fluorophores at ground energy state are promoted to excited states, from which they decay by radiative and nonradiative processes. The latter process relies on the transference of heat to the host, heating it, and thus leading to a time-dependent transverse spatial profile of the temperature $\Delta T(r, t)$ in the sample, creating a refractive index gradient (dn/dT) normal to the beam axis.

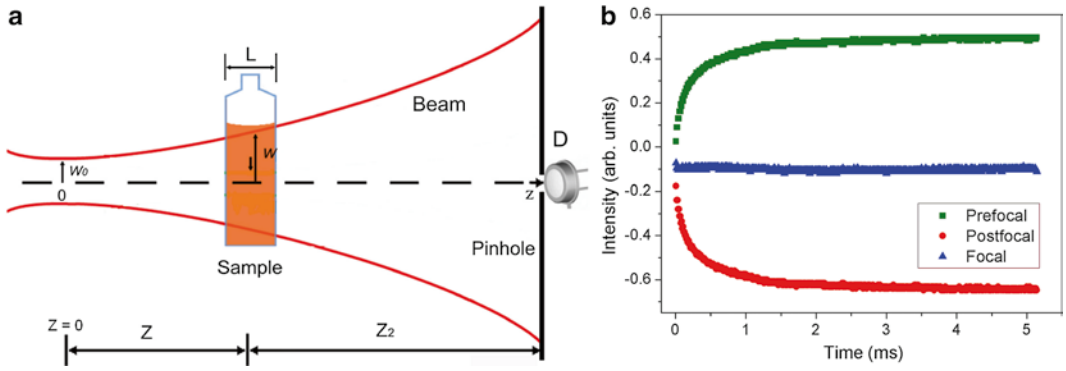

Fig. 1 (**a**) Scheme of the geometric position of the excitation beam for quantum yield measurement using TLS, D is a photodetector, w_0 the beam waist, and L the sample thickness. (**b**) TLS signal evolution for sample at the prefocal, focal, and postfocal position

It produces a lens-like object, the so-called thermal lens effect [20]. The thermal lens evolution as a function of time can be evaluated by monitoring the light intensity measured by the far-field photodetector (Fig. 1a). A typical signature of the TLS signal, measured with an oscilloscope, is presented in Fig. 1b, with the sample at positions $z \approx -z_R$ (prefocal), $z = 0$ (focal), and $z \approx z_R$ (postfocal). Here z_R is the Rayleigh length (*see* **Note 2**).

The analytical expression for the time dependence of the light beam reaching the detector is shown in Eq. 3 [21].

$$I = I_0 \left[1 - \frac{\theta}{2} \tan^{-1} \left(\frac{2V}{\left[9 + V^2 \right] \left(t_c / 2t \right) + 3 + V^2} \right) \right]^2 \tag{3}$$

where I_0 is the intensity of the beam at $t = 0$. V is given by:

$$V = z / z_R + \left(z_R / z_2 \right) \left[1 + \left(z / z_R \right)^2 \right] \tag{4}$$

Where the focus of the excitation beam is considered the origin of z-axis ($z = 0$). The parameters z and z_2 represent the sample and the photodetector positions (Fig. 1a), respectively. t_c is the characteristic heat diffusion time given by $t_c = w_{ex}/4D$, with $D = (k/\rho)\ C_P$ as the thermal diffusivity, ρ is the volumetric density, and C_P is the specific heat of sample and w_{ex} is the excitation beam radius measured at the sample position. Typical values for these parameters can be found in the literature for different solvents (Table 1). The parameter θ is the thermal phase shift.

The thermal phase shift can be obtained by fitting the experimental result with Eq. 3. Moreover the thermal phase shift, θ, can be associated to the fraction of absorbed light energy transformed

Table 1
Physical parameters for some solvents

Sample	$-dn/dT \times 10^{-4}$ (K^{-1})	C_P (kJ/kg K)	κ (W/m K)	ρ (kg/m^3)
Water	0.8 [21]	4.18 [25]	0.609 [24]	995.7 [22]
Ethanol	3.9 [21]	2.46 [26]	0.171 [24]	785.1 [23]
Methanol	3.9 [21]	2.53 [27]	0.202 [24]	786.5 [23]

in thermal energy, also called the absolute nonradiative quantum efficiency, φ, as shows Eq. 5 [11, 28].

$$\theta = -\frac{\varphi P_{abs}}{\kappa \lambda_{ex}} \frac{dn}{dT}, \tag{5}$$

where λ_{ex} is the excitation beam wavelength, κ is the thermal conductivity of solvent, dn/dT is the thermo-optic coefficient of solvent and P_{abs} is the absorbed power from excitation beam, given by $P_{abs} = P_{in}(1 - e^{-\alpha L})$, where P_{in} is the excitation power, α is the linear optical absorption coefficient at the excitation wavelength, and L is the thickness of sample. In the TL experiment P_{abs} can be calculated directly measuring P_{in} and P_{out} e using Eq. 1 (*see* **Note 3**). Typical values for κ and dn/dT are shown in Table 1.

For nonfluorescent materials, $\varphi = 1$ and for fluorescent materials $\varphi < 1$. Fluorescence quantum yield and the absolute nonradiative quantum efficiency are related by Eq. 6.

$$\varphi = 1 - \Phi_f \frac{\lambda_{ex}}{\langle \lambda_{em} \rangle} \tag{6}$$

Where $\langle \lambda_{em} \rangle = \int \lambda_{em} dN(\lambda_{em}) / \int dN(\lambda_{em})$ is the average emission wavelength and $dN(\lambda_{em})$ is the number of photons emitted per second in an incremental wavelength centered at λ_{em}. Therefore, fluorescence quantum yield can be determined by monitoring the thermal lens evolution in the sample. Figure 2 shows the theoretical fit of Eqs. 3 and 4 adjust to postfocal TL signal obtained for CdTe QDs aqueous suspension, synthesized using the method reported in the literature [29, 30].

From the fit adjustment, the thermal phase shift (θ) was calculated, and using Eqs. 5 and 6, the fluorescence quantum yield of CdTe QDs was determined. In Table 2 the calculated quantum yield for two CdTe QDs samples are shown.

It is important to be aware that reabsorption processes due to the superposition between the absorption spectra and emission spectra in more concentrated samples can change the measured Φ_f value (*see* **Note 4**). Excitation wavelength, sample pH, thermal conductivity of solvent are also relevant parameters for the fluorescence quantum yield determination.

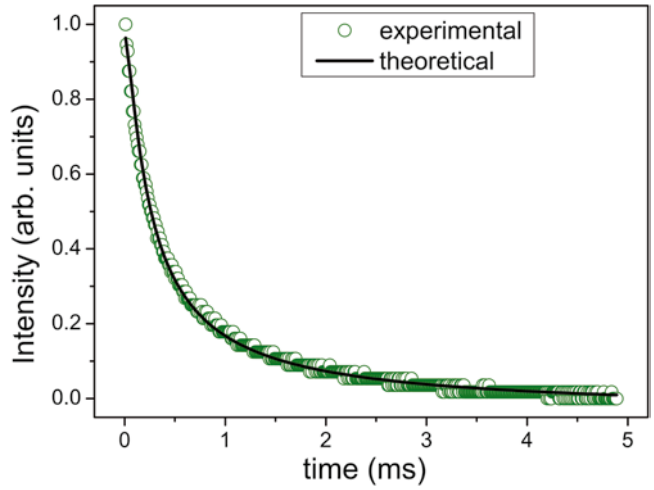

Fig. 2 Theoretical fit of Eq. 1 adjusted to postfocal TL signal of a CdTe QDs sample excited with $\lambda_{ex} = 532$ nm

Table 2
Mean values for fluorescence quantum yield (<Φ_f>) of CdTe QDs measured using TLS. Other important values are also listed

Sample	Absorbance	P_{in}[a] (mW)	P_{out}[b] (mW)	<λ_{em}> (nm)	<Φ_f> (%)	σ[c] (%)
S1	0.68	11.7	9.9	547.7	71.1	4.5
S2	0.07	11.8	10.9	538.6	89.0	3.5

[a] P_{in} is the laser power before the sample
[b] P_{out} is the laser power after the sample
[c] σ is the standard deviation

2 Materials

Typical TLS experimental setup/materials to measure fluorescence quantum yield is shown in Fig. 3.

1. UV–Vis spectrophotometer for absorbance measurements (e.g., spectrophotometer model Evolution 600 B, Thermo Scientific, Inc.).
2. Spectrometer for emission spectra acquisitions (e.g., spectrometer model HR4000, Ocean Optics, Inc.).
3. Continuous wave (CW) laser, power > 15 mW. Example: Frequency-doubled (532 nm, cw) Nd:YAG laser (Compass 215M-20; Coherent, Inc.).
4. Spherical lenses, L_1 and L_2 (telescope), forming a telescope to expand the laser beam (*see* **Note 5**).

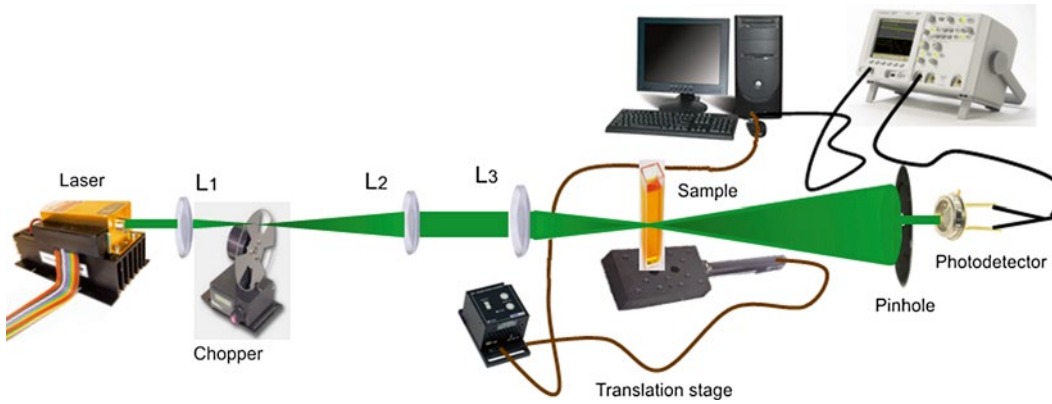

Fig. 3 Experimental scheme to measure the fluorescence quantum yield of CdTe QDs. L_1, L_2, and L_3 are spherical lens

5. Variable frequency Chopper to modulate the laser beam, controlling the excitation time on the sample. Example: Modulation with duty cycle = 0.05 and rotation frequency = 50 Hz.
6. Convergent lens, L_3, to focus the beam onto the sample. Example: 10 cm focal lens.
7. Manual or motorized linear translation stage, use to better place the sample within the Rayleigh length of laser beam.
8. Pinhole, placed in a far field (>80 cm) from the sample, allowing the transmission only of the central part of the beam. The diameter of the pinhole should ~1 % of the beam diameter.
9. Silicon photodiode placed after of the pinhole (*see* **Note 6**).
10. Digital oscilloscope.
11. A quartz cuvette, with thickness smaller than the Rayleigh length after lens L_3. Example: 1 mm thick cuvette for 1.5 mm Rayleigh length (*see* **Note 6**).
12. QDs suspensions with absorption lower than 0.1 at the laser wavelength of the experiment (*see* **Note 4**).

3 Methods

1. Measure the absorbance and emission spectra of sample using a spectrophotometer and a photoluminescence spectrometer, respectively. In the absorbance measurements may be necessary dilute the sample and use a cuvette of 1 cm of optical length (*see* **Note 4**).
2. Place the sample at the prefocal or postfocal position ($z \approx -z_R$ or z_R). At those positions, one can observe the highest change in the oscilloscope signal (Fig. 1b).

3. Observe the time evolution of the detected signal shown in the oscilloscope. If necessary, minimize the rise time of signal (*see* **Note 7**).
4. Record the time evolution of the detected signal sometimes to confirm that the shape and intensity of the TL signal remains constant over the time (*see* **Note 8**).
5. Fit the experimental curve using Eqs. 3 and 4, and calculate the thermal phase shift value, θ.
6. Use Eq. 5 and the obtained value of θ to determine the absolute nonradiative quantum efficiency, φ. To perform this procedure the excitation wavelength, the thermal conductivity of solvent, and the thermo-optic coefficient of solvent should be known.
7. Use Eq. 6 and the obtained value of φ to determine the sample fluorescence quantum yield. To perform this procedure the average emission wavelength should be calculated.
8. Use the equation $\langle \lambda_{em} \rangle = \int \lambda_{em} \mathrm{d}N(\lambda_{em}) / \int \mathrm{d}N(\lambda_{em})$ to calculate the average emission wavelength integrating over all emission spectrum.

4 Notes

1. TLS is only convenient to measure the quantum efficiency of transparent samples. For scattering samples, we suggest use the integrating sphere method.
2. Obtain the Rayleigh length from using the expression $z_R = \pi w_0^2 / \lambda_{ex}$, where λ_{ex} is the excitation wavelength and $w_0 = f\lambda_{ex} / (w_i \pi)$ with w_0 being the minimum laser beam waist and w_i is the beam waist before L_3 and f is the focal length of L_3. Both w_0 and w_i can be measured using the knife-edge technique [31].
3. When measure P_{in} and P_{out} using an optical power meter having a photodiode sensor, ensure to select the correct wavelength (laser excitation wavelength). Note that to obtain the correct values of P_{in} and P_{out}, the power loss due to reflection in the faces of cuvette must be discounted (~4 % per face). After using the Eq. 1, P_{abs} can be calculated as $P_{abs} = P_{in} - P_{out}$.
4. After to fill the cuvette with the QDs solution, wait for some minutes to stabilize the sample, measure the absorption and emission spectra at least twice at intervals of 5 min to confirm that spectra intensities remain constant over time. Spectral changes suggest aggregation and reabsorption processes; in this case, dilute the sample and repeat the procedure.
5. Make sure that Rayleigh length is larger than the cuvette length, because it is necessary ensure that laser beam cross

section remains at least constant throughout the cuvette. Occasionally, it is necessary to expand the beam laser to obtain the condition $z_R > L$. If necessary, substitute the lens L_1 and L_2 by other lens having different focal lengths until obtaining the required condition.

6. Use an appropriate photodiode to detect the TL signal. Example: If the excitation laser emitted at 532 nm, you can use a photodiode model BPW21R with maximum spectral response at 565 nm.
7. In order to obtain the real TL signal, ensure that the Chopper is at focal point of lens L_1 and verified that rise time of TL signal in the oscilloscope is < 40 μs. Move the Chopper parallel to beam laser trajectory until to minimize this value.
8. The TL signal in the oscilloscope must be recorded at least 5 times; consequently an equal number of θ values will be obtained. The better value of Φ_f is obtained considering the average value over all the data values.

Acknowledgments

This study was supported by CAPES, the Center of Excellence of Nanophotonics and Biophotonics (PRONEX/FACEPE/CNPq), FACEPE, and INCT Fotônica (CNPq).

References

1. Murray CB, Norris DJ, Bawendi MG (1993) Synthesis and characterization of nearly monodisperse CdE (E = S, Se, Te) semiconductor nanocrystallites. J Am Chem Soc 115: 8706–8715
2. Rosenthal SJ, McBridea J, Pennycook SJ, Feldman LC (2007) Synthesis, surface studies, composition and structural characterization of CdSe, core/shell and biologically active nanocrystals. Surf Sci Rep 62:111–157
3. Qu L, Peng X (2002) Control of photoluminescence properties of CdSe nanocrystals in growth. J Am Chem Soc 124:2049–2055
4. Deka S, Quarta A, Lupo MG, Falqui A, Boninelli S, Giannini C, Morello G, de Giorgi M, Lanzani G, Spinella C, Cingolani R, Pellegrino T, Manna L (2009) CdSe/CdS/ZnS double shell nanorods with high photoluminescence efficiency and their exploitation as bio-labeling probes. J Am Chem Soc 131: 2948–2958
5. Donega CM, Hickey SG, Wuister SF, Vanmaekelbergh D, Meijerink A (2003) Single-step synthesis to control the photoluminescence quantum yield and size dispersion of CdSe nanocrystals. J Phys Chem B 107:489–496
6. Laverdant J, de Marcillac WD, Barthou C, Chinh VD, Schwob C, Coolen L, Benalloul P, Nga PT, Maître A (2011) Experimental determination of the fluorescence quantum yield of semiconductor nanocrystals. Materials 4: 1182–1193
7. Sapsford KE, Berti L, Medintz IL (2006) Materials for fluorescence resonance energy transfer analysis: beyond traditional donor-acceptor combinations. Angew Chem Int Ed 45:4562–4588
8. Demas JN, Crosby GA (1971) The measurement of fluorescence quantum yields. A review. J Phys Chem 75:991–1024
9. Würth C, Grabolle M, Pauli J, Spieles M, Resch-Genger U (2012) Comparison of methods and achievable uncertainties for the relative and absolute measurement of fluorescence quantum yields. Anal Chem 83:3431–3439

10. Cruz RA, Pilla V, Catunda T (2010) Quantum yield excitation spectrum (UV-visible) of CdSe/ZnS core-shell quantum dots by thermal lens spectrometry. J Appl Phys 107:083504
11. Kurian A, George NA, Paul B, Nampoori VPN, Vallabhan CPG (2002) Studies on fluorescence efficiency and photodegradation of Rhodamine 6G doped PMMA using a dual beam thermal lens technique. Laser Chem 20:99–110
12. Hu C, Whinnery JR (1973) New thermooptical measurement method and a comparison with other methods. Appl Opt 12:72–79
13. Brannon JH, Magde DJ (1978) Absolute quantum yield determination by thermal blooming. Fluorescein. J Phys Chem 82: 705–709
14. Suzuki K, Kobayashi A, Kaneko S, Takehira K, Yoshihara T, Ishida H, Shiina Y, Oishi S, Tobita S (2009) Reevaluation of absolute luminescence quantum yields of standard solutions using a spectrometer with an integrating sphere and a back-thinned CCD detector. Phys Chem Chem Phys 11:9850–9860
15. Würth C, González MG, Niessner R, Panne U, Haisch C, Genger UR (2012) Determination of the absolute fluorescence quantum yield of rhodamine 6G with optical and photoacoustic methods—providing the basis for fluorescence quantum yield standards. Talanta 90:30–37
16. Brouwer AM (2011) Standards for fluorescence quantum yield measurements in solution (IUPAC technical report). Pure Appl Chem 83:2213–2228
17. Gordon JP, Leite RCC, Moore RS, Porto SPS, Whinnery JR (1965) Long transient effects in lasers with inserted liquid samples. J Appl Phys 36:3–8
18. Leite RCC, Moore RS, Whinnery JR (1964) Low absorption measurement by mean of the thermal lens effect using a He:Ne laser. Appl Phys Lett 5:141–143
19. Snook DR, Lowe RD (1995) Thermal lens spectroscopy. A review. Analyst 120: 2051–2068
20. Estupiñán-López C, Dominguez CT, de Araujo RE (2013) Eclipsing thermal lens spectroscopy for fluorescence quantum yield measurement. Opt Express 21:18592–18601
21. Sheldon SJ, Knight LV, Thorme JM (1982) Laser-induced thermal lens effect: a new theoretical model. Appl Opt 21:1663–1668
22. http://www.engineeringtoolbox.com/water-density-specific-weight-d_595.html. Accessed 07 Jan 2014
23. http://www.engineeringtoolbox.com/liquids-densities-d_743.html. Accessed 07 Jan 2014
24. http://www.engineeringtoolbox.com/thermal-conductivity-liquids-d_1260.html. Accessed 07 Jan 2014
25. http://www.engineeringtoolbox.com/water-thermal-properties-d_162.html. Accessed 07 Jan 2014
26. http://www2.ucdsb.on.ca/tiss/stretton/database/Specific_Heat_Capacity_Table.html. Accessed 07 Jan 2014
27. http://thermo.sdsu.edu/testcenter/testhome/Test/solve/basics/tables/tablesComb/hhv.html. Accessed 07 Jan 2014
28. Shen J, Love RD, Snook RD (1992) A model for cw laser induced mode-mismatched dual-beam thermal lens spectrometry. Chem Phys 165:385–396
29. Santos BS, Farias PMA, Fontes A (2008) Semiconductor quantum dots for biological applications. In: Henini M (ed) Handbook of self assembled semiconductor nanostructures novel devices in photonics and electronics. Elsevier, The Netherlands, pp 771–798
30. Menezes FD, Brasil AG Jr, Moreira WL, Barbosa LC, Cesar CL, Ferreira RC, de Farias PMA, Santos BS (2005) CdTe core shell quantum dots for photonic applications. Microelectr J 36:989–991
31. de Araújo MA, Silva R, de Lima E, Pereira DP, de Oliveira PC (2009) Measurement of Gaussian laser beam radius using the knife-edge technique: improvement on data analysis. Appl Opt 48:393–396

Chapter 8

Semiquantitative Fluorescence Method for Bioconjugation Analysis

Aluízio G. Brasil Jr., Kilmara H.G. Carvalho, Elisa S. Leite, Adriana Fontes, and Beate Saegesser Santos

Abstract

Quantum dots (QDs) have been used as fluorescent probes in biological and medical fields such as bioimaging, bioanalytical, and immunofluorescence assays. For these applications, it is important to characterize the QD–protein bioconjugates. This chapter provides details on a versatile method to confirm quantum dot–protein conjugation including the required materials and instrumentation in order to perform the step-by-step semiquantitative analysis of the bioconjugation efficiency by using fluorescence plate readings. Although the protocols to confirm the QD–protein attachment shown here were developed for CdTe QDs coated with specific ligands and proteins, the principles are the same for other QDs–protein bioconjugates.

Key words Quantum dot, Fluorescence plate reader, Bioconjugate, CdTe, Protein

1 Introduction

One of the key problems for successfully using the quantum dots as new optical probes in biological systems [1–3] is to guarantee the quality and efficiency of the conjugation processes to proteins and other specific biomolecules and ultimately the interaction of the ensemble with the biological systems. A poor conjugation leads to unsuccessful applications. For this reason the characterization and evaluation of the QDs' bioconjugation is necessary, independently of the physicochemical conjugation approaches applied.

In the last decades different methods to characterize QDs bioconjugates have been reported in the literature [4–9]. Sapsford et al. [4] classified in a recent review the bioconjugation characterization approaches for various nanomaterials different kind of techniques: separation, scattering, microscopy, and spectroscopy. However, lack of standardization for interpreting the results, the use of expensive equipment, and/or laborious methodologies represent common disadvantages to current methods.

Adriana Fontes and Beate Saegesser Santos (eds.), *Quantum Dots: Applications in Biology*, Methods in Molecular Biology, vol. 1199, DOI 10.1007/978-1-4939-1280-3_8, © Springer Science+Business Media New York 2014

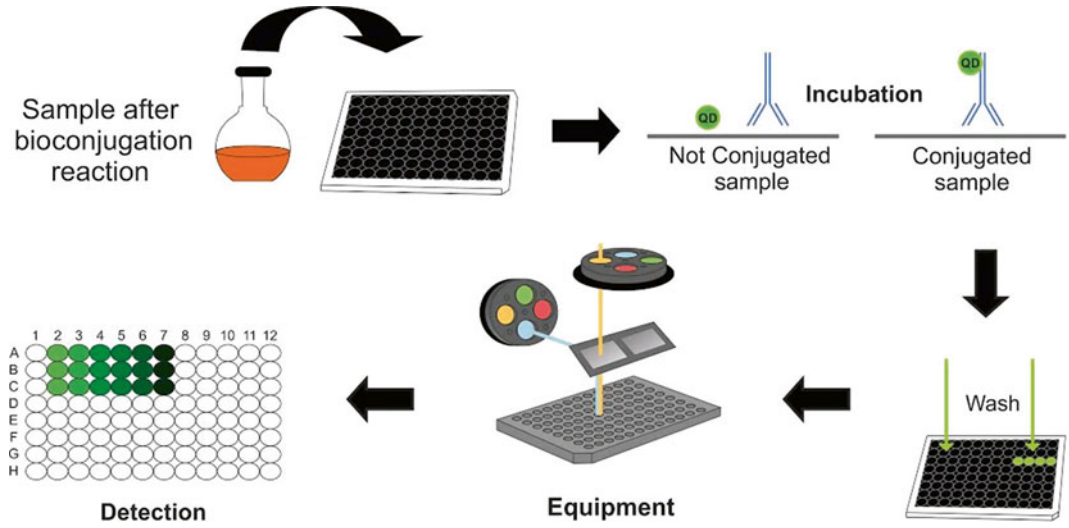

Fig. 1 Experimental procedure used in the Fluorescence Plate Reader method for QDs–protein covalent binding bioconjugates. The scheme shows the interaction process between the microplates with different samples: the two controls used in the experiment present no considerable fluorescence signal and QDs–protein bioconjugates present fluorescence indicating conjugation

For example, among the most cited methods, electrophoresis is a laborious technique and can be applied only for qualitative analyses of charged specimens. Moreover, if the conjugated molecule has low or medium molecular weight, electrophoresis is no longer feasible [5, 8, 9]. Another cited method, the dynamic light scattering (DLS) can qualitatively analyze the success of the bioconjugation based on the average sizes of the systems prior and after the conjugation processes but present a poor resolution. Additionally, it analyzes just one sample at a time and can resolve particle populations within the same sample only if they differ in size at least by a factor of three [4, 6]. The fluorescence correlation spectroscopy (FCS) [7] although is more sensitive than DLS for discriminating similar sizes, needs a confocal microscopy, an expensive equipment which is not common in laboratories. Moreover, the FCS cannot give much information about the efficiency of the bioconjugation process. Therefore, new and complementary methods are always welcome to evaluate bioconjugation process.

Here, an alternative method for investigating QDs–protein bioconjugates provides a simple attempt to resolve some of these difficulties described (Fig. 1). We propose the use of Fluorescence Plate Reader as a complementary approach to distinguish QDs and proteins from QDs–proteins based on the QDs' native fluorescence and on the different intensities showed by the bioconjugates and control samples [10]. The protein part of the bioconjugates attaches itself through hydrophobic interactions to the polymer based plate. The equipment detects the fluorescence output of the

bioconjugates and also a small fraction of stray light which must be estimated for each analysis, resulting a relative intensity. The relative fluorescence intensity (*RelativeFL*), which evaluates the increase of the bioconjugates' fluorescence over the controls, can be calculated by applying Eq. 1.

$$RelativeFL(\%) = \frac{(BioconjugateFL - ControlFL)}{ControlFL} \times 100\%, \quad (1)$$

where *BioconjugateFL* is the fluorescence intensity of the QDs–biomolecule samples and *ControlFL* is the average signal detected for the controls. We recommend at least two controls: the first one consists of isolated colloidal QDs and the second control consists of the protein molecules.

If *BioconjugateFL* (the signal intensity of the QDs–biomolecule samples) is at least twice the value of *ControlFL* (the average controls values), this is considered an indication of conjugation. The higher the signal the more satisfactory and efficient is the process (*see* **Note 1**). On the other hand, if the *BioconjugateFL* is of the same order of the control signals, the conjugation is considered unsuccessful (*see* **Note 1**). In other words, the result is considered positive if *RelativeFL* is equal or higher than 100 % and is considered negative if *RelativeFL* is lower than 100 %. This criterion of 100 % was chosen by empirical experimental observation after exhaustive test reproduction of this bioconjugation method with different QD and biomolecule systems.

This alternative method is fast, simple, sensitive, and practical. Moreover, it is not limited by the charge or the size of the bioconjugates. Besides, it has the advantage to be able to evaluate and discriminate semiquantitatively a great number of different types of bioconjugates simultaneously, depending on the number of the wells in the microplate [10].

This chapter provides the basic procedures and detailed information on how to determine the efficiency of the conjugation reaction process of QDs–protein bioconjugates. The protocols described here employ cadmium telluride water-based QDs, albumin and immunoglobulin, but the procedures can be adapted to analyze bioconjugates prepared with different QDs and proteins.

2 Materials

2.1 CdTe QDs Synthesis (See Note 2)

1. Thioglycolic acid (TGA), $HSCH_2CO_2H_{(l)}$.
2. Cysteamine (CTM), $HSCH_2CH_2NH_{2(s)}$.
3. Cadmium Perchlorate, $Cd(ClO_4)_{2(s)}$.
4. Metallic tellurium, $Te^{o}_{(s)}$.
5. Sodium borohydride, $NaBH_{4(s)}$.
6. Ultrapure water.

2.2 Bioconjugation

1. 1-Ethyl-3-[3-dimethylaminopropyl] carbodiimide hydrochloride (EDC).
2. *N*-hydroxysulfosuccinimide (Sulfo-NHS).
3. 2-[morpholino] ethanesulfonic acid (MES).
4. Bovine Serum Albumin (BSA) (*see* **Note 3**).
5. Thioglycolic acid-coated cadmium telluride QDs (TGA-coated CdTe QDs).
6. Sulfosuccinimidyl 4-[*N*-maleimidomethyl] cyclohexane-1-carboxylate (Sulfo-SMCC) (*see* **Note 4**).
7. Tris (2-carboxyethyl) phosphine (TCEP).
8. Human Immunoglobulin G (IgG).
9. Cysteamine-coated cadmium telluride (CTM-coated CdTe).
10. Phosphate buffer solution (PBS).

2.3 Bioconjugate Analysis

1. Fluorescence microplate reader. For example, we used Model Wallac Victor² (Perkin Elmer).
2. Black microplates. For example, we used polystyrene black microplates.
3. Phosphate buffer solution (PBS).
4. Negative controls (*see* **Note 5**).

3 Methods

3.1 General Procedure for CdTe QDs Synthesis

Aqueous colloidal dispersion of CdTe QDs could be synthesized by adapting a previously reported method [11]. Briefly, QDs can be prepared by the addition of Te^{2-} in a $Cd(ClO_4)_2$ solution of pH > 10 in the presence of TGA as stabilizing agent in a 2:1:4.2 ratio of Cd:Te:TGA and a pH in the range of 5.6–5.9 in the presence of CTM as stabilizing agent in a 2:0.2:2.4 ratio of Cd:Te:CTM. The Te^{2-} aqueous solution should be prepared using metallic tellurium and $NaBH_4$, at a high pH and both under argon saturated inert atmosphere. We recommend to proceed the reaction in this way, under constant stirring and heating at 80 °C for at least 1 h. The time interval of the synthesis will depend on the expected size (and emission profile) of the QDs.

3.2 Bioconjugation Procedure

Covalent binding is among the most widely used techniques for bioconjugation. Here we outline the procedures for the conjugation of TGA-coated CdTe QDs with BSA protein using EDC and Sulfo-NHS as coupling reagents and of CTM-coated CdTe QDs with IgG using Sulfo-SMCC as coupling reagent [8, 9].

It is necessary to employ QDs which show fluorescence in wavelength region different from the biomolecule's autofluorescence avoiding spectral overlap. This allows the analysis of QDs–protein

bioconjugates based on the fluorescence intensities of samples placed in a fluorescence plate reader. In the sequence, we present examples of conjugation protocols that apply the proposed method, first to BSA and then for IgG. For this protocol, the bioconjugates used were carboxyl-coated CdTe QDs with BSA and amine-coated CdTe QDs with IgG obtained by using EDC/Sulfo-NHS and Sulfo-SMCC coupling agents, respectively.

It is important to mention that a robust QD should be acquired or synthesized to maintain the original optical properties after the bioconjugation procedure (*see* **Note 6**).

3.2.1 QD Conjugation by Covalent Binding to BSA

1. Add 20 nmol of TGA-coated CdTe QDs to the activation buffer at 0.1 M MES at pH 6.0.
2. Add 0.4 mg EDC and 1.1 mg Sulfo-NHS to buffered quantum dot.
3. Allow the reaction to proceed for 15 min at room temperature.
4. Then, add 1.4 μL of 2-mercaptoethanol (20 mM) to quench the EDC.
5. Add 1 mL of BSA at 1 mg/mL to activate quantum dot.
6. Allow the protein and quantum dot to react for at least 2 h at room temperature.
7. Prepare the microplate reader and measure the fluorescence intensity of the samples (*see* Subheading 3.3).

3.2.2 QD Conjugation by Covalent Binding to IgG

1. Raise the pH of CTM-coated CdTe QDs up to 7.0–7.2.
2. Then, add 3 mg of Sulfo-SMCC in 6.2 nmol of CTM-coated CdTe QDs for their chemical activation.
3. Incubate reaction mixture for 60 min at room temperature.
4. Remove excess crosslinker employing an ultracentrifugation device with a cut off of 20 MWCO (*see* **Note 7**).
5. In another vial, add 40 μL of IgG at 1 mg/mL in PBS buffer and employ a final concentration of 10–20 mM TCEP (*see* **Note 8**).
6. Allow the IgG and TCEP to react during 30 min at room temperature for disulfide reduction.
7. Combine and mix the maleimide-activated QDs and IgG-SH (reduced) and incubate for 60 min at 25 °C.
8. Prepare the microplate and measure the samples' fluorescence intensity (*see* Subheading 3.3).

3.3 Procedure for Immobilized Bioconjugates and Analysis

1. Add 200 μL in each well of all samples (controls and bioconjugates) at least in triplicate (*see* **Note 9**).
2. Protect the wells from external environment.
3. Incubate the microplate at room temperature for at least 1 h, gently rotating the microplate at an angle to ensure coverage of the internal well surface, during this period.

Table 1
Results of fluorescence intensity from detection of free and bioconjugated QDs systems by covalent binding in a Fluorescence Microplate Reader

Systems	Fluorescence intensity (a. u.)[a]	Relative fluorescence intensity (%)
Control 1 (BSA)	299	–
Control 2 (QDs)	260	–
Average control	280	–
QDs–BSA 2 h	560	100 %
QDs–BSA 4 h	1,483	430 %
Control 1 (IgG)	268	–
Control 2 (QDs)	295	–
Average control	281	–
QDs–IgG 2 h	2,252	701 %

[a]Acquisition performed with the F485 excitation and F535 emission filters to BSA and F355 excitation and F595 emission filters to IgG, acquisition time of 1 s and normal slits. QDs used for BSA was TGA capped CdTe and for IgG was CTM capped CdTe

4. Add 200 μL of PBS solution at pH 7.4 as the wash buffer in each well.
5. Wash the wells at least three times, gently rotating the microplate and wait 2 min, then discard the wells's samples (*see* **Note 10**).
6. Measure the fluorescence intensity of the samples (controls and QDs–protein samples) in a Microplate Fluorescence Reader (*see* **Notes 11–13**).
7. The analysis of some data of the presented characterization procedure is showed in Table 1.

4 Notes

1. Values for the *RelativeFL* show quantitative reproducibility (with standard errors smaller than 10 %) when the same samples of bioconjugates where used, evidencing the effectiveness of this detection method [10].
2. A wide range of high quality QDs are now available from commercial sources and may be used to avoid the synthesis step.
3. The BSA's fluorescence is related to tryptophan residues which provide major contribution to the intrinsic fluorescence of this protein near 340 nm [12, 13].
4. Amine-containing QDs may be usually activated with sulfo-SMCC which contains sulfhydryl-reactive maleimides for conjugation with thiol-containing proteins or other molecules [9].

5. It is important to use controls in the analysis to compare their fluorescence signal with the QD–biomolecules conjugates fluorescence. The negative controls suggested are the isolated colloidal QDs and the protein molecules.
6. The CdTe QDs' preparation procedure does not always comprehends a passivation with another semiconductor material shell. The QDs prepared in the present example were kept in closed vials for at least 60 days. This time is necessary for the emission intensity to increase and reach a plateau, due to the slow hydrolysis of the alkyl-thiol molecules and subsequent formation of a CdS shell on the particles. This is not necessary for the commercially acquired QDs.
7. It is important to remove the excess of crosslinker, which can be performed by employing a desalting column or other gel filtration column. The excess of crosslinker which does not interact with QDs can react with biomolecules producing protein dimmers.
8. In most situations, TCEP concentrations < 10–20 mM are compatible with maleimide reaction chemistry and provides sufficient molar excess to effectively reduce protein disulfide bonds with reduced risk of protein denaturation. TCEP does not have to be removed from solutions before performing reactions involving maleimide labeling or cross-linking reagents.
9. Proteins have usually affinity for polystyrene, which is one of the most used plastic in microplates employed for protein immobilization in immunoassays [14–16] but for those which do not show a good adsorption to this material another alternatives may be tested: (1) to try other types of polymeric plates and (2) to coat the polystyrene plate with a complementary protein or other biomolecules which show a greater affinity to the polymer and may associate to the tested bioconjugate.
10. Isolated QD samples do not efficiently link to the polymer because they do not have enough specific groups required for a strong interaction. So, after washing the microplate with a buffer solution such as PBS, the QDs should be removed and no fluorescence signal will be detected.
11. Adjust the parameters such as excitation and emission filters, acquisition time, intensity lamp and slits for excitation and emission, based on the QDs applied.
12. The biomolecules alone usually do not present fluorescence in the same wavelength region of the QDs employed. So in the case of a well-succeeded QD–protein bioconjugation, the Fluorescence Plate Reader will give a fluorescence signal indicating that QDs are bound to the proteins attached to the well surface.
13. The low signals for the controls are due to stray light coming from the excitation source and being scattered by the wells.

Acknowledgments

The authors are grateful to Coordenação de Aperfeiçoamento de Pessoal de Nível Superior (CAPES), Conselho Nacional de Desenvolvimento Científico e Tecnológico (CNPq), and Fundação de Amparo à Ciência e Tecnologia do Estado de Pernambuco (FACEPE) for financial support and student fellowships. We are also grateful to the National Institute of Science in Photonics (INFo) for financial resources. The authors also wish to thank Pedro Barroca and Beatriz S. Santos for the schematic drawing.

References

1. Medintz IL, Uyeda HT, Goldman ER, Mattoussi H (2005) Quantum dot bioconjugates for imaging, labelling and sensing. Nat Mater 4:435–446
2. Michalet X, Pinaud FF, Bentolia LA, Tsay JM, Doose S, Li JJ, Sundaresan G, Wu AM, Gambhir SS, Weiss S (2005) Quantum dots for live cells, in vivo imaging, and diagnostics. Science 307:538–544
3. Santos BS, Farias PMA, Fontes A (2008) Semiconductor quantum dots for biological applications. In: Henini M (ed) Handbook of self-assembled semiconductor nanostructures novel devices in photonics and electronics, vol 1. Elsevier, Amsterdam, pp 771–798
4. Sapsford KE, Tyner KM, Dair BJ, Deschamps JR, Medintz IL (2011) Analyzing nanomaterial bioconjugates: a review of current and emerging purification and characterization techniques. Anal Chem 83(12):4453–4488
5. Huang X, Weng J, Sang F, Song X, Cao C, Ren J (2006) Characterization of quantum dot bioconjugates by capillary electrophoresis with laser-induced fluorescent detection. J Chromatogr A 1113:251–254
6. Al-Jamal WT, Al-Jamal KT, Cakebread A, Halket JM, Kostarelos K (2009) Blood circulation and tissue biodistribution of lipid–quantum dot (L-QD) hybrid vesicles intravenously administered in mice. Bioconjug Chem 20: 1696–1702
7. Shao L, Dong C, Sang F, Qian H, Ren J (2008) Studies on interaction of CdTe quantum dots with bovine serum albumin using fluorescence correlation spectroscopy. J Fluoresc 19:151–157
8. Mattousi H, Mauro JM, Goldman ER, Anderson GP, Sundar VC, Mikulec FV, Bawendi MG (2000) Self-assembly of CdSe–ZnS quantum dots bioconjugates using an engineered recombinant protein. J Am Chem Soc 122:12142–12150
9. Hermanson GT (2008) Bioconjugate techniques, vol 2. Elsevier, Amsterdam, p 215
10. Carvalho KHG, Brasil AG Jr, Cabral Filho PE, Tenório DPLA, de Siqueira ACA, Leite ES, Fontes A, Santos BS (2014) Fluorescence plate reader for quantum dot-protein bioconjugation analysis. J Nanosci Nanotechnol 14: 3320–3327
11. Santos BS, Farias PMA, Menezes FD, Brasil Júnior AG, Ferreira R, Motta MA, Castro Neto AG, Vieira AAS, Silva DCN, Fontes A, Cesar CL (2007) Highly fluorescent semiconductor core–shell CdTe–CdS nanocrystals for monitoring living yeast cells activity. Appl Phys A 89(4):957–961
12. Mamedova NN, Kotov NA, Rogach AL, Studer J (2001) Protein-CdTe nanoparticle conjugates: preparation, structure and interunit energy transfer. Nano Lett 1(6):281–286
13. Wu D, Wei Q, Li Y, Du B, Xu G (2005) Quenching of the intrinsic fluorescence of bovine serum albumin by phenylfluorone-Mo(VI) complex as a probe. Int J Biol Macromol 37:69–72
14. Pesce AJ, Ford DJ, Gaizutis M, Pollak VE (1977) Binding of protein to polystyrene in solid-phase immunoassays. Biochim Biophys Acta 492(2):399–407
15. Cantarero LA, Butler JE, Osborne JW (1980) The adsorptive characteristics of proteins for polystyrene and their significance in solid-phase immunoassays. Anal Biochem 105(1): 375–382
16. Fair BD, Jamieson AM (1980) Studies of protein adsorption on polystyrene latex surfaces. J Colloid Interface Sci 77(2):525–534

Part III

Quantum Dots for Live Cells and Tissues Applications

Chapter 9

Assembly, Characterization, and Delivery of Quantum Dot Labeled Biotinylated Lipid Particles

Valeria Sigot

Abstract

Lipid nanoparticles composed of mixtures of PEGylated-lipids; cationic and neutral lipids prepared by detergent dialysis can encapsulate biological active molecules and show considerable potential as systemic therapeutic agents. Addition of biotinylated lipids to this formulation allows surface modification of these particles with a suitable ligand or probe conjugated to streptavidin for specific cell targeting. Monitoring long circulating particles and cellular uptake requires stable and bright fluorescent probes. Quantum dots (QDs) constitute a relatively new class of fluorescent probes that overcome the limitations of organic fluorophores in biological imaging applications. Here, a protocol for the encapsulation of QD_{655} (red) in biotinylated lipid particles (BLPs) prepared by a detergent dialysis technique is presented followed by characterization of the loaded liposomal vehicles. Then, a protocol for BLPs surface modification via biotin-streptavidin linkage with preformed complexes of ligand-QD_{525} (green) for specific cell targeting of the nanoparticle is detailed. Conditions for cell binding and uptake of two colors QD labeled BLPs as well as basic microscopic settings for confocal live cell imaging are described.

Key words Biotinylated lipid particles, Quantum dots, Epidermal growth factor, Targeted delivery, Detergent dialysis, Confocal fluorescence microscopy

1 Introduction

Liposomal carriers have become major tools for introducing not only a variety of nucleic acids but also proteins, peptides, and nanoparticles into cells in vitro and in vivo [1]. Lipid composition as well as the method of preparation will determine the average size of the carrier as well as the permeability through biological membranes, and thus the efficiency of uptake by cells [2, 3]. An important issue is the targeting of the carriers to specific cell types for which the delivery approach is intended. The role of receptors as molecular target has opened new opportunities for cellular or intracellular targeting using liposomal systems appended with appropriate ligands [4].

Adriana Fontes and Beate Saegesser Santos (eds.), *Quantum Dots: Applications in Biology*, Methods in Molecular Biology, vol. 1199, DOI 10.1007/978-1-4939-1280-3_9, © Springer Science+Business Media New York 2014

Continuous cell imaging has been substantially improved with the introduction of fluorescent probes such as quantum dots (QDs), colloidal nanocrystals composed of cadmium selenide (CdSe) or cadmium telluride (CdTe) core enclosed within a zinc sulfide (ZnS) passivation shell [5, 6]. The main advantages of QDs over organic fluorophores are the greater photostability and the excitation wavelengths range that extends above 500 nm. The latter feature reduces cell phototoxicity, essential for long-term fluorescence imaging. Whereas absorption spectra are broad, emission spectra are narrow without the extension to the red characteristic of organic dyes. This feature allows for simultaneous detection of multiple color QDs upon illumination with a single light source [7].

We report here the preparation and characterization of BLPs, loaded with QD_{655} and surface-modified with preformed complexes of EGF-QD_{525} (EGF, Epidermal Growth Factor) mediated by biotin-streptavidin linkage. The receptor specificity of biotinylated EGF tagged with streptavidin coated QDs, has been extensively investigated in the laboratory, where this protocol was developed. EGF-QDs preformed complexes are biochemically competent ligands for erbB1, the EGF receptor [8]. BLPs were formulated containing up to 3 % of PEGylated-lipids to stabilize the lipid bilayer, and 2.7 % of fusogenic lipid in order to facilitate endosomal escape of loaded cargo into the cytoplasm. PEG (polyethylene glycol) content above 5 % may interfere for instance with the endocytic mechanism of uptake by either lowering the binding affinity to cell receptors or by preventing the intermembrane contact between liposomal surface and endosomal membranes, required to release the cargo in the cytoplasm [9]. In the present protocol QDs loaded BLPs were prepared using a detergent dialysis technique [10, 11] modified for the encapsulation of 10 nm carboxyl-QD_{655} (red) as an approach for delivering these fluorescent nanoparticles into cells.

QD_{655} loaded BLPs were purified by ultracentrifugation in discontinuous sucrose gradient and then characterized according to size, QDs encapsulation efficiency, and biotin incorporation.

Surface labeling and targeting of BLP-QD_{655} were achieved by coupling preformed complexes of biotin-EGF with a second color of Streptavidin coated QD_{525} (green) (Fig. 1) providing a monitoring tool for the specificity of BLPs uptake and cargo release in live cells by confocal laser scan microscopy (CLSM). The two-color particles, hereafter referred to as EGF-QD_{525}-BLP-QD_{655} were targeted to A431 cells, a human epidermoid carcinoma cell line that overexpresses the EGF receptor. The rationale behind this two-color labeling strategy is that only QD_{525} and QD_{655} that are colocalized would indicate the intracellular distribution of the targeted BLPs whereas time dependent loss of colocalization would suggest endosomal escape of QD_{655}.

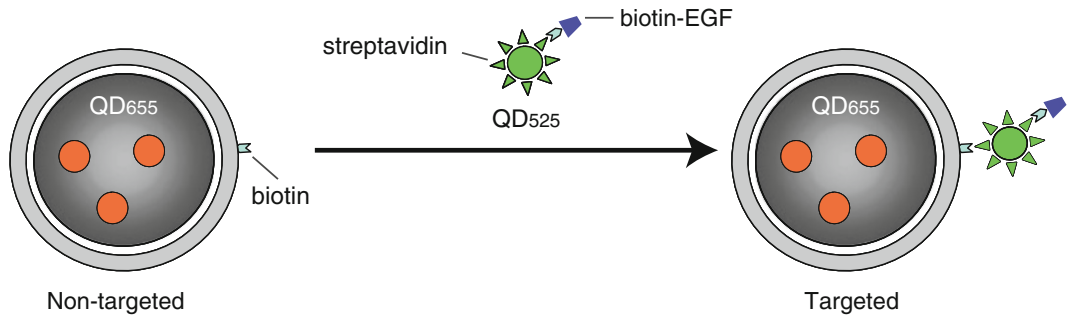

Fig. 1 Scheme depicting the targeting and dual color labeling strategy of BLPs with encapsulated QD_{655}. Preformed complexes of EGF-QD_{525} are conjugated to biotin molecules on the BLP surface. Specific uptake is evidenced as colocalized dots by confocal fluorescence microscopy. *Red fluorescence* indicates unspecific binding of non-targeted BLP-QD_{655}. Reproduced from Sigot et al. (2010) [15], with permission from American Chemical Society

2 Materials

Prepare all solutions using sterile ultrapure water and analytical grade reagents. Manipulate lipids dissolved in chloroform under a fume hood until they are desiccated and transfer volumes employing appropriate Hamilton syringes, avoiding plastic lab-ware. Protect lipid solutions; BLPs and fluorophores should be protected from direct light and maintain refrigerated.

2.1 Buffers

1. Tyrode's buffer without glucose: 135 mM NaCl, 10 mM KCl, 0.4 mM $MgCl_2$, 1 mM $CaCl_2$, 10 mM of (2-hydroxyethyl)-1-piperazine ethanesulfonic acid (HEPES), pH 7.2. Autoclave before use and store at room temperature (20–25 °C).
2. Tyrode's plus: add sterile solutions of 20 mM glucose and 0.2 % of bovine serum albumin (BSA) just before use.
3. HEPES buffered saline (HBS): 10 mM HEPES, 150 mM NaCl, pH 7.4. Sterilized by filtration through a 0.22 μm-pore-size membrane.

2.2 Preparation of QDs Loaded and Targeted BLPs

Synthetic Lipids (Avanti Polar Lipids, Alabaster, AL, USA) were used as lyophilized powders or dissolved in chloroform and stored under argon in a desiccator at −20 °C.

1. DOPE: 1,2-Dioleoyl-sn-Glycero-3-Phosphoethanolamine (neutral lipid).
2. DOTAP: 1,2-Dioleoyloxy-3-trimethylammoniumpropane chloride (cationic lipid).
3. PEG-750-Cer-C8: N-Octanoyl-Sphingosine-1-[Succinyl (Methoxy (Polyethylene Glycol) 750)] (fusogenic lipid).

4. Biotin-PEG-DSPE: 1,2-Distearoyl-sn-Glycero-3-Phosphoethanolamine-N [Biotinyl (Polyethylene Glycol) 2000] (Ammonium Salt) (biotinylated lipid).
5. Chloroform (HPLC quality).
6. OGP: 1-o-n-octyl-β-D-glucopyranoside (detergent for dialysis).
7. ITK-carboxyl QD_{655} (CdSe core and ZnS shell) with maximum fluorescence emission peak at 655 nm. Hereafter referred to as QD_{655}.
8. Streptavidin-coated QD_{525}, maximum fluorescence emission peak at 525 nm, hereafter referred to as QD_{525}. Due to narrow emission spectra, alternative two non-overlapping QDs colors can be used.
9. Biotin-EGF (or appropriate biotinylated ligand).
10. Dialysis Cassette, Slide-A-Lyzer of 10 kDa cut-off for 0.5–3 mL sample (Pierce, Rockford, IL, USA).
11. SM-2 Biobeads with adsorbent capacity ~117 mg OGP/g beads (Bio-Rad, Hercules, CA, USA).

2.3 Preparing Discontinuous Sucrose Gradient

1. Prepare 20 % sucrose solution in HBS and filter-sterilize through a 0.22 μm pore size filter. Stock solutions of 20 % sucrose can be stored in frozen aliquots at –20 °C (*see* **Note 1**).
2. 2.5 % sucrose solution in HBS.
3. 10 % sucrose solution in HBS.
4. 2.5 mL thin-wall centrifuge tubes (*see* **Note 2**).

2.4 Measuring Biotin Incorporation in BLPs

1. Stock solution of 1 μM biocytin in sterile distilled water.
2. Freshly prepared mix containing 50 nM Alexa Fluor® 488-Streptavidin conjugates and 125 μM of 4-Hydroxyazobenzene-2-carboxylic acid (HABA) in HBS.

2.5 Cell Culture and Microscopy

1. Sterile Glass bottom cell culture chambers suitable for fluorescence microscopy.
2. Coverslips, acid washed and sterilized.
3. Cell culture medium and antibiotics appropriate for the particular cell line.

3 Methods

3.1 Preparation of BLPs with Encapsulated Quantum Dots

1. Prepare BLPs formulation by mixing 8.4 μmols DOPE, 0.6 μmols DOTAP, 0.024 μmols Biotin-PEG-DSPE, and 0.25 μmols of PEG-750-Cer-C8 in 2 mL glass vials (Fig. 2) (*see* **Note 3**).

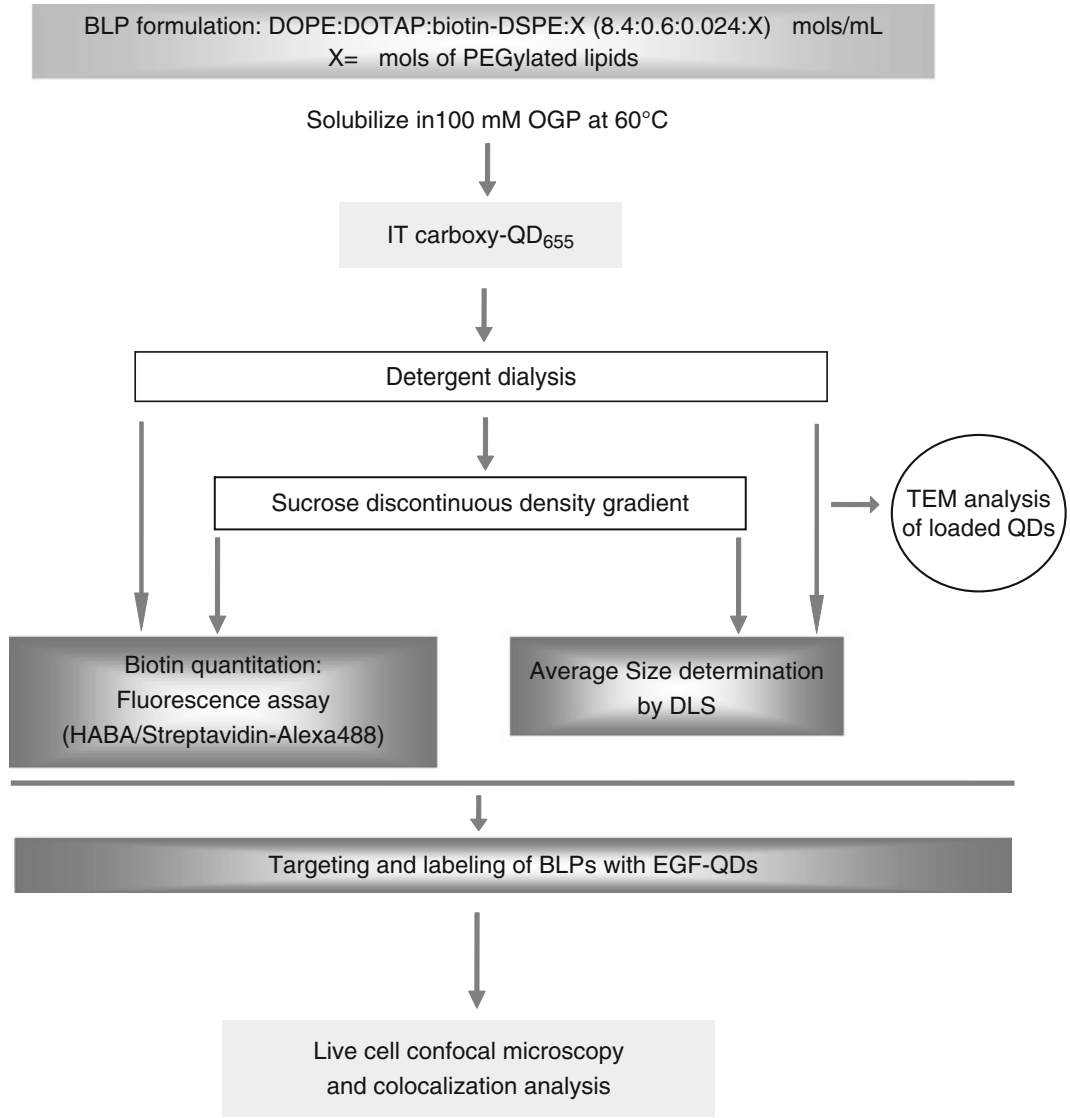
BLP formulation: DOPE:DOTAP:biotin-DSPE:X (8.4:0.6:0.024:X) mols/mL
X= mols of PEGylated lipids
Solubilize in100 mM OGP at 60°C
IT carboxy-QD655
Detergent dialysis
Sucrose discontinuous density gradient
TEM analysis of loaded QDs
Biotin quantitation: Fluorescence assay (HABA/Streptavidin-Alexa488)
Average Size determination by DLS
Targeting and labeling of BLPs with EGF-QDs
Live cell confocal microscopy and colocalization analysis

Fig. 2 Flow diagram of BLPs preparation, characterization, and targeting

2. Dry the solution with a stream of argon under a fume hood and remove residual chloroform under vacuum overnight.
3. Solubilize the opaque dry lipid film by adding 0.5 mL of 100 mM OGP in HBS with continuous stirring at 60 °C. Let the transparent lipid mix cool to room temperature (20–25 °C).
4. Prepare 0.5 mL of a 50 nM ITK-carboxyl QD_{655} in HBS (*see* **Note 4**) and add to the solubilized lipid–detergent mixture at room temperature (20–25 °C), mix well with micropipette and transfer the final 1 mL volume into the Dialysis Cassette.

In this step, and for any lipid variation in the original formulation, prepare a control of BLPs without QDs to check for vesicle formation during detergent dialysis.

5. Dialyze lipids-detergent-QDs solution and control formulation without QDs against 1 L HBS for 3 h (*see* **Note 5**).
6. Change buffer (1 L of HBS) and continue dialysis in a cold room (4–8 °C).
7. Carry out the last buffer change (third) adding polystyrene SM-2 Biobeads in the HBS buffer to minimize residual OGP content.
8. Recover the solution (~1 mL) from the dialysis cassette; this should not change at the end of dialysis. Keep on ice protected from light or in refrigerator while preparing the discontinuous sucrose density gradient (*see* **Note 6**).

3.2 Ultracentrifugation in Discontinuous Sucrose Density Gradient

In order to separate QDs loaded BLPs from less dense empty BLPs and free non-encapsulated QDs, load the samples obtained after the detergent dialysis on top of a discontinuous sucrose density gradient and perform ultracentrifugation as described:

1. Cool the ultracentrifuge with swinging buckets to 10 °C and set speed to 160,000 × *g*.
2. Prepare a discontinuous sucrose gradient in 2.5 mL ultraclear thin-wall centrifuge tubes by carefully applying with a tip or syringe, layers of 0.5 mL sterile sucrose solutions in HBS [12]. Two centrifuge tubes are required for loading the 1 mL sample recovered after detergent dialysis.
3. Add first 0.5 mL of 2.5 % w/v sucrose solution, under this fraction pipette 0.5 mL of 10 % sucrose fraction and under this, the 20 % sucrose (*see* **Note 7**). Carefully equilibrate the ultracentrifuge tubes by weight before adding dialysate containing the BLPs.
4. Add carefully 0.5 mL of the dialysate on top of the gradient by touching the internal wall of the tube over the 2.5 % sucrose band and place the ultracentrifuges tubes in the rotor with swinging buckets with the help of forceps. Carry out ultracentrifugation for 5 h at 10 °C.
5. After ultracentrifugation put the tubes in a transparent holder and briefly illuminate with UV light to excite QD_{655} fluorescence. Three well-defined fluorescent bands should be observed (Fig. 3, panel a). Mark with an indelible pen the QDs containing fractions.
6. Back in the bench, carefully recover sucrose fraction I (*see* **Note 8**) then, recover the broader, turbid, and less intense fluorescent band underneath (fraction II) enriched in BLP-QD_{655} and finally the pellet with free non-encapsulated QD_{655} (fraction III).

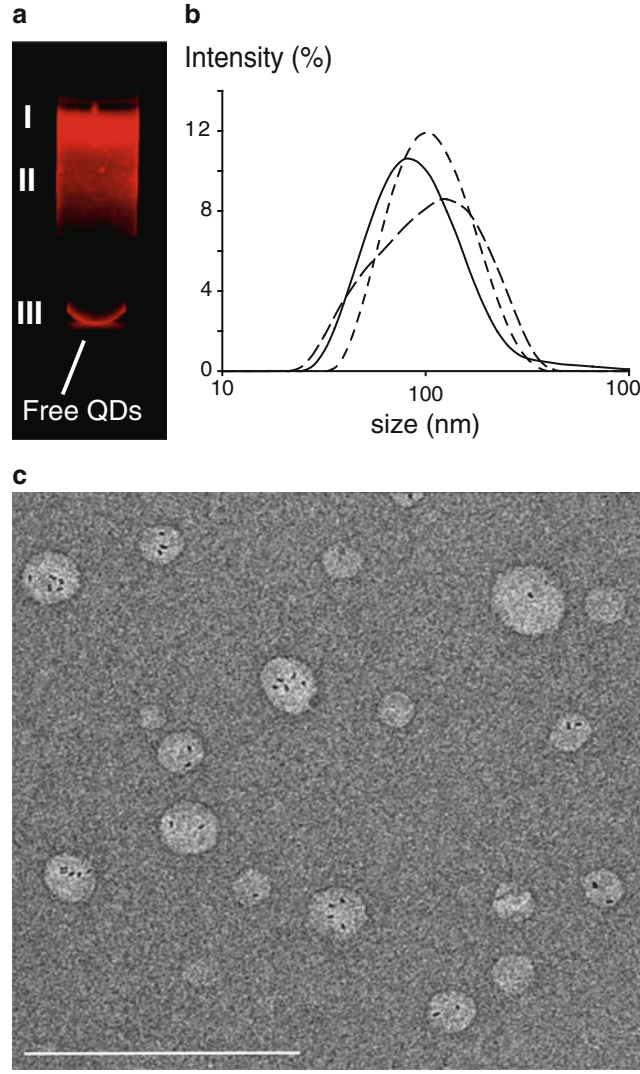

Fig. 3 Size characterization of BLP-QD_{655} after purification in discontinuous sucrose density gradient. (**a**) BLP-QD_{655} recovered in fluorescent fraction II, whereas free QDs appeared mainly in the pellet (fraction III). (**b**) Size distribution of three independent BLP-QD_{655} preparations measured in fraction II by DLS (**c**) TEM analysis of QD_{655} encapsulated in BLPs. Scale bar 500 nm. Reproduced from Sigot et al. (2010) [15], with permission from American Chemical Society

7. Take an aliquot of fraction II of the gradient and analyze for particle size, biotin incorporation, and QDs encapsulation efficiency (*see* **Note 9**).
8. Sterilize the BLP-QD_{655} samples through 0.22 μm filter, separate an aliquot for further characterization of the particles (Subheadings 3.3–3.5) and continue working under the laminar flow hood for BLPs surface labeling and cell targeting (Subheadings 3.6–3.9) (*see* **Note 10**).

3.3 BLPs-QDs Size Analysis

1. Measure average hydrodynamic diameter (Fig. 3, panel b) of recovered BLP-QD_{655} as well as control BLPs without QDs by Dynamic Light Scattering (DLS) (*see* **Note 11**).
2. Select an operating protocol for spherical particles; applying 12–15 runs per measurement, depending on the instrument number of runs is automatically selected according to the concentration of particles in the sample.
3. Perform three measurements on each sample and use the obtained intensity correlation data to calculate size distribution and average hydrodynamic diameter of the obtained BLPs. This can be achieved using the CONTIN algorithm [13] to fit the autocorrelation data, this mathematical approach is recommended for hetero- and polydisperse systems (*see* **Notes 12** and **13**).

3.4 QD_{655} Encapsulation Efficiency

Transmission Electron Microscopy (TEM) analysis of sucrose fraction II reveals an average of 2–5 QDs encapsulated in BLPs ranging from 100 to 130 nm in size (Fig. 3, panel c). Particle dimensions estimated from TEM are in agreement with the mean hydrodynamic diameter of ~110 nm as determined by DLS in the same fraction (Fig. 3, panel b).

3.5 Biotin Incorporation into BLPs

Biotin content was quantified using a fluorometric assay with nanomolar sensitivity based on Foster resonance energy transfer (FRET) [14]. Briefly, in the absence of biotin, HABA quenches the fluorescence emission of the Alexa Fluor® 488 dye via FRET. When biotin or a biotinylated molecule is added, HABA is displaced from the biotin binding sites resulting in an increase in the donor fluorescence intensity proportional to the amount of biotin present in the sample. Biotin concentration allows an estimation of biotinylated lipid recovery relative to the molar amounts of biotinylated lipid initially added to the formulation; and has to be checked for each liposomal preparation after detergent dialysis and after purification from sucrose gradient.

1. Prepare a standard curve (eight points in duplicate) of biocytin, a water-soluble biotin analogue, to give final concentrations between 0–200 nM.
2. Prepare before use, Mix-1 containing 25 nM Streptavidin-Alexa Fluor® 488 and 125 μM HABA in HBS.
3. Add 5 μL of standards or BLPs samples to 45 μL of Mix-1 in cuvettes suitable for fluorescence measurements. Excite Alexa Fluor® 488 with $\lambda = 485$ nm and collect spectra between 500 and 700 nm (*see* **Note 14**).
4. Plot fluorescence intensity at the emission maximum (519 nm) as a function of biocytin concentration (nM) and fit the data to a sigmoid curve to obtain the corresponding values for the unknown samples (Fig. 4) (*see* **Note 15**).

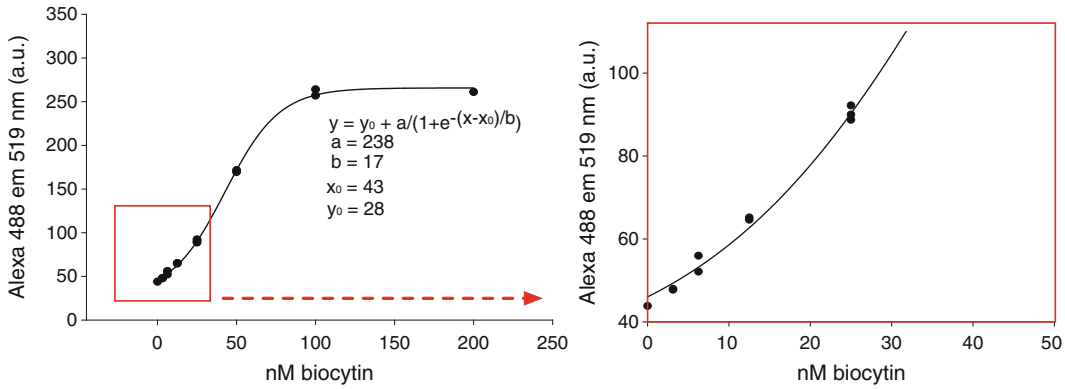

Fig. 4 Fluorometric assay for biotin quantitation. Biocytin standard curve concentrations range between 0 and 200 nM. Excitation of Alexa488 at 485 nm and emission collected from 500 to 700 nm. The data illustrate a ~6-fold increase in fluorescence signal upon complete displacement of HABA. The detection limit achieved was approximately 3 nM biocytin

3.6 Preparation of Ligand-Biotin-Streptavidin-QDs Complexes

The employed formulation of the streptavidin conjugated QDs contained an average of 6–8 covalently linked streptavidin molecules per QD molecule (*see* **Note 16**). Coupling Biotin-EGF to Streptavidin-QD_{525} at a ratio of 4:1 leaves free streptavidin in QDs for subsequent coupling to BLPs (*see* Subheading 3.7).

1. Dilute biotin-EGF (or biotinylated ligand of interest) to 400 nM in HBS + 0.2 % BSA.
2. Dilute Streptavidin-QD_{525} to 100 nM in HBS + 0.2 % BSA.
3. Mix equal volumes of Streptavidin-QD_{525} and biotinylated ligand with a micropipette.
4. Incubate at 4 °C for at least 30 min with gentle agitation or rotation before coupling to BLPs. This mix should be used within 5 days to prevent deterioration of the peptidic ligand.

3.7 Surface Modification of BLP-QD_{655} with Preformed Complexes of EGF-QD_{525}

1. Adjust biotin concentration of BLPs-QD_{655} to 1 μM and separate two aliquots of 150 μL.
2. Add 100 μL of preformed complexes of EGF-QD_{525} to 150 μL BLPs-QD_{655} and incubate for at least 2 h at 15 °C with continuous shaking (*see* **Note 17**).
3. In parallel, add 100 μL of HBS + 0.2 % BSA to 150 μL BLPs-QD_{655} and incubate for at least 2 h at 15 °C with continuous shaking.

3.8 Cell Targeting of EGF-QD_{525}-BLP-QD_{655} Particles

1. Plate cells in culture dishes containing sterile glass coverslips or in glass bottom culture chambers suitable for fluorescence confocal microscopy.
2. Grow A431 cells or the selected cells expressing the receptor of interest in complete culture medium with antibiotics at the appropriate densities 1 or 2 days prior to the experiment.

3. Prior to the incubation with BLPs starve cells in serum free medium for 16 h to reduce signaling induced by EGF present in the serum.
4. Set the time lapse acquisition parameters in a confocal microscope (*see* Subheading 3.9).
5. Wash cells once with Tyrode's plus and maintain in this buffer for the experiment.
6. Dilute EGF-QD_{525}-BLP-QD_{655} in Tyrode buffer plus to obtain final concentration of 4 nM EGF.
7. Follow identical dilutions for the non-targeted BLPs-QD_{655} as performed with the targeted particles and use this solution as control to test for unspecific uptake.
8. Pre-incubate starved A431 cells with 200 μL of targeted EGF-QD_{525}-BLP-QD_{655} or non-targeted BLP-QD_{655} at 15 °C for 5 min to concentrate BLPs on the cells surface, at this temperature EGF receptor mediated endocytosis can be reversibly blocked.
9. Place the cell chamber on the microscope stage pre-equilibrated to 37 °C.
10. After initial binding (within 5 min) at 37 °C, take a snapshot; carefully remove excess of BLPs solution, BLPs in suspension will contribute to background fluorescence.
11. Add 500 μL of warm Tyrode's plus buffer and start a time lapse imaging acquiring every 5 min during 30 min or until endocytic uptake of the BLPs is evident (*see* **Note 18**).

When employing a different biotinylated ligand specific receptor targeting should be tested in the presence of soluble excess ligand and/or using cells devoid of the receptor of interest [15] and optimal concentrations of ligands has to be checked according to the binding constant for stimulated uptake of specific receptors. Residual free preformed complexes (EGF-QD_{525}) were expected to bind to EGF receptors (Fig. 5).

3.9 Simultaneous Detection of Two Different Colors of QDs and Colocalization Analysis

1. Begin acquisition of a time series with single or multiple focal planes (z-stack). Typically, a 63× or 40× 1.2 numerical aperture (NA) water immersion objective is recommended.
2. Simultaneous excitation of QD_{525} and QD_{655} can be achieved at 488 nm employing an imaging system with two detectors, e.g., Zeiss LSM 510 META, with appropriate filters (in this case, 520/20 band-pass and 585 long-pass, respectively (*see* **Note 19**)).
3. For visual analysis of BLPs internalization, subtract background from each channel and to every single focal plane of a z-stack at each time point. Then, reconstruct the 3D image and merge both channels to look for colocalization.

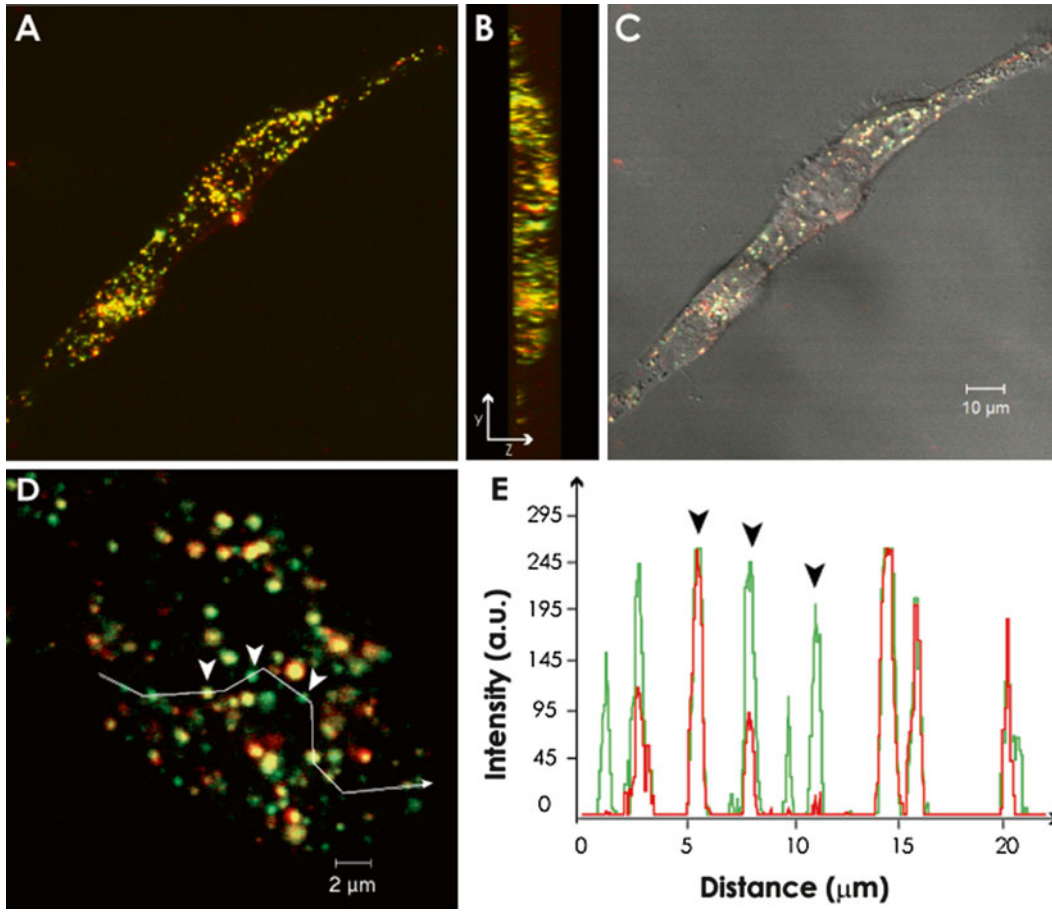

Fig. 5 Intracellular fate of EGF Receptor targeted and QDs labeled BLP. (**a**) 3D reconstruction of two A431 cells with internalized BLP after 10 min pulse incubation and 1 h chase at 37 °C. (**b**) *y–z* plane showing colocalized QDs inside cells and underneath the cell membrane. (**c**) Overlay of image (**a**) with DIC image. (**d**) Line-profile across endosomal vesicles. (**e**) Fluorescence intensity along the line-profile in (**d**) revealing different intensity levels for colocalized QDs as well as size variations among vesicles. Internalized two-color QDs labeled and targeted BLP were distinguished from independently internalized green EGF-QD_{525} complexes (*arrowheads* in panels *d* and *e*). Scale bar 2 µm. Reproduced from Sigot et al. (2010) [15], with permission from American Chemical Society

Select z-stack at $t = 0$ min, when BLPs are bound but not internalized and then select z-stacks after 5, 10, 15, 20, and 30 min (end point) imaging at room temperature (20–25 °C). Additionally, 2D representations of 3D cells can be created from maximum intensity projections of several slices in the z-dimension, excluding the top and bottom planes of all cells in the microscopic field.

4. Analyze colocalization of both QDs in background-corrected images of single focal intracellular planes (not projections) by presenting a plate of three images, two corresponding to the

red (loaded QD_{655}) and green (surface tagged QD_{525}) channels, and a third image where the channels are merged and the overlapping pixels displayed in yellow (Fig. 5).

5. Quantitate colocalization of QD_{525} and QD_{655} by calculating Manders' overlap coefficients [16] (*see* **Note 20**).

4 Notes

1. Thaw 20 % sterile sucrose solution in the refrigerator and mix well until the solution appears homogeneous before proceeding with subsequent dilutions. Is preferable to prepare multiple aliquots of the stock and use one for each gradient to prevent bacterial contamination.
2. For this purpose we employed Beckman ultraclear thin-wall centrifuge tubes in TL-100 Beckman ultracentrifuge and rotor TLS 55 with swinging buckets.
3. If lipids are obtained as lyophilized powders, dissolve first each lipid in chloroform and transfer volumes with Hamilton syringe or glass pipettes, avoid plastic tips during this step, contaminants could be extracted by chloroform and micropipette can be damaged as well.
4. Commercially obtained QDs solution should be homogeneous and free of aggregates. Number of streptavidins conjugated to QDs has to be check for each lot number of the product from the selected supplier.
5. Visible turbidity should be detected within the first hour of dialysis, indicating the formation of self-assembled lipid–QDs particles. The particles should remain in solution without forming aggregates. Empty self-assembled BLPs are smaller ~50–70 nm size and their true presence has to be checked by DLS.
6. BLP-QD_{655} cannot be frozen due to irreversibly QDs fluorescence quenching and destabilization of BLPs bilayer and should be stored refrigerated (4–8 °C), for storage periods longer than a week, BLPs solution should be filter-sterilized through 0.22 μm pore size. However, this step results in considerable sample loss.
7. Use a syringe with long needle to load the solutions at the bottom of the tubes. Clear lines between the layers should be seen, indicating that minimal mixing has occurred.
8. Sucrose fraction I, may contain QD loaded BLPs but it is enriched in free lipids and empty vesicles and is not further employed.
9. Sucrose does not interfere with DLS measurements, biotin quantitation, or subsequent BLPs labeling. However, is

susceptible of bacterial contamination. Alternatively, samples can be dialyzed against 2 L of sterile HBS to minimize sucrose content before particle analysis.

10. Significant sample loss occurs during filtering. In our experience, using sterile solutions and labware during BLPs preparation and working under a laminar flow during cell targeting allowed us to perform BLPs binding and uptake experiments for up to 24 h in the presence of antibiotics with occasional contamination.
11. DLS measurements were performed with ZetaSizer Nano from Malvern Instruments. Samples were diluted in phosphate buffered saline (PBS) and measurements performed at room temperature (20–25 °C). The PBS used to dilute the samples was previously filtered through 0.02 μm pore size to eliminate potential interfering impurities.
12. The mean hydrodynamic diameter of a population of particles calculated by Dynamic light scattering involves the determination of how the intensity of the light scattered by a solution of moving particles varies with time. This variation is correlated with the speed at which particles move, which can be characterized by their diffusion coefficients [17]. The average hydrodynamic diameter of particles is obtained from the diffusion coefficients.
13. The average hydrodynamic diameter represents only an intensity-based average value and does not give any information on the prevailing size distribution. For this reason, the polydispersity index (pdi) is also stated to give information about the actual distortion of a monomodal distribution. The pdi can have values between 0 and 1 and is equivalent to the variance σ^2 of the size distribution. BLPs preparations with pdi <0.25 were considered as monodisperse solutions and further characterized.
14. It is convenient to test several dilutions in duplicate of BLPs to obtain an accurate biotin concentration, high concentration of BLPs particles may also interfere in biotin quantitation due light scattering.
15. In the conditions assayed a ~6-fold increase in fluorescence signal upon complete displacement of HABA was observed with a detection limit of approximately 3 nM biocytin. Standard colorimetric HABA assay can be performed for samples containing above 10 μM biotin.
16. Previous control experiments are necessary to establish that streptavidin-QDs does not interfere with the normal biological function of the selected biotin-ligand [18].
17. Although increasing the number of EGF ligands per particle should in principle improve the binding to cells and increase the

number of internalized particles, larger size of the carrier would probably interfere with the receptor-mediated endocytosis [19].

18. A431 cells are maintained healthy in Tyrode's plus for up to 30 min at 37 °C. However, for longer incubations Tyrode's buffer should be replaced by phenol free culture medium and imaging performed under oxygen-controlled atmosphere. The labeled and targeted BLPs can be continuously monitored using confocal microscopy during cell binding and uptake for periods longer than 1 h without significant photobleaching highlighting the convenience of QDs as labeling probes for long-term imaging of dynamic processes. However, cell phototoxicity cannot be overlooked.
19. Within the given settings, channel cross-talk was negligible as determined using single-labeled samples.
20. Manders' coefficients are proportional to the fraction of fluorescence of the colocalizing fluorophores in each channel of the composite image, i.e., relative to the total fluorescence in that channel. These coefficients are more appropriate when signal intensities in the two image channels have significant different levels.

Acknowledgements

This work was financially supported by the Max Planck Society, the DFG Research Center for Molecular Physiology of the Brain (CMPB)—Excellence Cluster EXC 171—FZT103 "Microscopy at the Nanometer Range," and the EU sixth framework (FP6) project FLUOROMAG, LHSB-CT-2006-037465.

References

1. Fenske DB, Cullis PR (2008) Liposomal nanomedicines. Expert Opin Drug Deliv 5(1): 25–44
2. Musacchio T, Torchilin VP (2011) Recent developments in lipid-based pharmaceutical nanocarriers. Front Biosci 16:1388–1412
3. Li W, Szoka FC Jr (2007) Lipid-based nanoparticles for nucleic acid delivery. Pharm Res 24(3):438–449
4. Vyas SP, Singh A, Sihorkar V (2001) Ligand-receptor-mediated drug delivery: an emerging paradigm in cellular drug targeting. Crit Rev Ther Drug Carrier Syst 18(1):1–76
5. Pellegrino T, Parak WJ, Boudreau R et al (2003) Quantum-dot-based cell motility assay. Differentiation 71:542–548
6. Qi L, Gao X (2008) Emerging application of quantum dots for drug delivery and therapy. Expert Opin Drug Deliv 5(3):263–267
7. Smith AM, Gao X, Nie S (2004) Quantum dot nanocrystals for in vivo molecular and cellular imaging. Photochem Photobiol 80(3):377–385
8. Lidke DS, Nagy P, Heintzmann R et al (2004) Quantum dot ligands provide new insights into erbB/HER receptor-mediated signal transduction. Nat Biotechnol 22(2):198–203
9. Song LY, Ahkong QF, Rong Q et al (2002) Characterization of the inhibitory effect of PEG-lipid conjugates on the intracellular delivery of plasmid and antisense DNA mediated by cationic lipid liposomes. Biochim Biophys Acta 1558(1):1–13

10. Wheeler JJ, Palmer L, Ossanlou M et al (1999) Stabilized plasmid-lipid particles: construction and characterization. Gene Ther 6(2):271–281
11. Hofland HE, Shephard L, Sullivan SM (1996) Formation of stable cationic lipid/DNA complexes for gene transfer. Proc Natl Acad Sci U S A 93(14):7305–7309
12. Mok KW, Lam AM, Cullis PR (1999) Stabilized plasmid-lipid particles: factors influencing plasmid entrapment and transfection properties. Biochim Biophys Acta 1419(2): 137–150
13. Provencher SW (1982) CONTIN: a general purpose constrained regularization program for inverting noisy linear algebraic and integral equations. Comp Phys Commun 27:229–242
14. Batchelor RH, Sarkez A, Cox WG et al (2007) Fluorometric assay for quantitation of biotin covalently attached to proteins and nucleic acids. Biotechniques 43(4):503–507
15. Sigot V, Arndt-Jovin DJ, Jovin TM (2010) Targeted cellular delivery of quantum dots loaded on and in biotinylated liposomes. Bioconjug Chem 21(8):1465–1472
16. Manders EEM, Verbeek FJ, Aten JA (1993) Measurement of co-localization of objects in dual-color confocal images. J Microsc 169: 375–382
17. Pecora R, Aragon SR (1974) Theory of light scattering from hollow spheres. Chem Phys Lipids 13(1):1–10
18. Lidke DS, Nagy P, Jovin TM et al (2007) Biotin-ligand complexes with streptavidin quantum dots for in vivo cell labeling of membrane receptors. Methods Mol Biol 374:69–79
19. Rejman J, Oberle V, Zuhorn IS et al (2004) Size-dependent internalization of particles via the pathways of clathrin- and caveolae-mediated endocytosis. Biochem J 377(Pt1): 159–169

Chapter 10

Oriented Conjugation of Single-Domain Antibodies and Quantum Dots

Kristina Brazhnik, Igor Nabiev, and Alyona Sukhanova

Abstract

Nanoparticle-based biodetection routinely employs monoclonal antibodies (mAbs) for targeting. However, the large size of mAbs limits the number of ligands per nanoparticle and severely restricts the bioavailability and distribution of these probes in a sample. Furthermore, conventional conjugation techniques provide nanoprobes with irregular orientation of mAbs on the nanoparticle surface and often provoke mAb unfolding. Here, we describe a protocol for engineering a new generation of ultrasmall diagnostic nanoprobes through oriented conjugation of semiconductor quantum dots (QDs) with 13 kDa single-domain antibodies (sdAbs) derived from llama immunoglobulin G (IgG). The sdAbs are conjugated with QDs in a highly oriented manner via an additional cysteine residue specifically integrated into the sdAb C-terminus. The resultant nanoprobes are <12 nm in diameter, ten times smaller in volume compared to the known alternatives. They have been proved highly efficient in flow cytometry and immunuhistochemical diagnostics. This approach can be easily extended to other semiconductor and plasmonic nanoparticles.

Key words Single-domain antibody (sdAb), Semiconductor quantum dot (QD), Nanoparticle, Highly oriented conjugates, Diagnostic nanoprobes

1 Introduction

The common approach to bioimaging, detection, and diagnosis with nanoparticles is based on the specificity and avidity of monoclonal antibodies (mAbs) [1, 2]. Although several mAb–nanoparticle conjugates have been used for biomarker labeling, these functionalized nanoprobes are large, which restricts the number of linked ligands, interferes with intratumoral distribution of nanoprobes, and limits their intracellular and intratissular penetration [3].

Furthermore, most conventional strategies for Ab covalent binding to nanoparticles yield nanoprobes with irregular orientation of Abs on the nanoparticle surface [4–8] and often provoke Ab unfolding [9]. Smaller antibody fragments conjugated with nanoparticles in a highly oriented manner may become an attractive alternative as components of the smallest possible targeted nanoprobes.

Adriana Fontes and Beate Saegesser Santos (eds.), *Quantum Dots: Applications in Biology*, Methods in Molecular Biology, vol. 1199, DOI 10.1007/978-1-4939-1280-3_10, © Springer Science+Business Media New York 2014

With a molecular weight of only 13 kDa, single-domain antibodies (sdAbs) engineered from heavy-chain antibodies of camelids (VHH fragment or variable heavy-chain antibody fragment) are the smallest functionally active Ab fragments capable of binding antigens with affinities comparable to those of conventional antibodies [10, 11]. In addition, sdAbs are not prone to aggregation, exist as monomers, and diffuse much better into tissues than full-size IgGs [12]. Their small size allows them to label finer and more remote segments of organs and bind with the corresponding antigens more accurately compared to conventional mAbs [13, 14]. The sdAbs can be produced inexpensively using *Escherichia coli* or yeast cultures. To fully exploit the advantages of these unique ultrasmall capture molecules, they should be conjugated with the nanoparticles in a highly oriented manner.

Here, we describe a well-tested protocol for engineering a new generation of ultrasmall, stable, specific diagnostic nanoprobes based on sdAbs linked to QDs in a highly oriented manner (Fig. 1) [13, 14]. We present a method for preparing diagnostic nanoparticles <12 nm in diameter (ten times smaller in volume than that obtainable with alternative techniques) and demonstrate their high efficiency in flow cytometry and immunohistochemical diagnostic platforms.

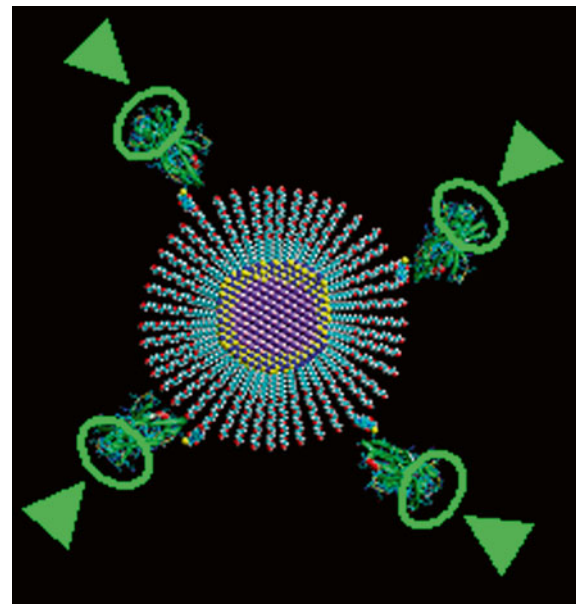

Fig. 1 An ultrasmall nanoprobe engineered from a CdSe-ZnS QD and sdAbs by oriented conjugation. The QD is conjugated with single-domain antibodies (sdAbs) via a single Cys residue specifically integrated into the sdAb C-terminus. The antigen-binding domain of each sdAb (*green circles*) is exposed to the outside and remains functionally active (*green arrows*). *The anatomy of QDs:* Se, *orange*; Cd, *violet*; S, *yellow*; Zn, *dark-blue*; C, *light-blue*; O, *red*; H, *white. The anatomy of Abs*: β-structures, *green bands*; α-helix, *red cylinders*. Adapted from Sukhanova et al. (2012) [13] with permission from Elsevier

The protocol is so designed that it can be easily extended to other types of semiconductor or noble metal plasmonic or magnetic nanoparticles of different shapes, such as nanodots, nanorods, and nanowires.

It is even possible to obtain multivalent nanoprobes, where small, functionally active fragments of different Abs against different antigens are bound to the same nanoparticle in the same orientation [15]. In this way, more than one cellular target can be identified with a single multivalent probe [16].

The protocol described here includes stages of nanocrystal water solubilization, purification, functionalization, and quality control and conjugation of sdAb-Cys recombinant antibodies with hydroxy- or amino-modified colloidal nanocrystals followed by characterization and quality control of the resultant diagnostic nanoprobes.

The efficiency of this protocol was proved by the use of the engineered diagnostic nanoprobes in flow cytometry detection of cells expressing a rare biomarker and detection of immunohistochemistry biomarkers in clinical biopsies, where the probes have ensured clear discrimination between pathological and healthy areas [13, 14]. The sdAb–QD conjugates stain all antigenic sites revealed by "gold standard" anatomopathological diagnostic methods, whereas the conventional fluorescence-based medical diagnostic protocol leaves many antigenic sites undetected.

2 Materials

2.1 Components for Nanocrystal Water Solubilization and Surface Modification

All solutions should be prepared using ultrapure water with a resistivity of 18 MΩ cm at 25 °C.

1. Colloidal hydrophobic CdSe/ZnS core/shell nanocrystals (QDs) were synthesized as described earlier [17].
2. DL-Cysteine solution: Dissolve 10 mg of DL-cysteine hydrochloride hydrate in 1 mL of methanol (*see* **Note 1**).
3. Polyethylene glycol (PEG) derivatives solutions: Dissolve 75 mg of SH- and OH-modified polyethylene glycol (HS-C11-EG6, ProChimia Surfaces) or 50 mg of SH- and NH_2-modified (HS-C11-EG6-NH2, ProChimia Surfaces) in 0.5 mL of water (*see* **Note 2**).

2.2 Components for Conjugation of Single-Domain Antibodies Modified with Cysteine Residue with Surface-Modified Colloidal Nanocrystals

1. Engineered Single-domain antibodies containing single exposed cysteine residue (sdAb-Cys) are prepared as described earlier [13].
2. Phosphate buffer, pH 7.0: Mix 423 mL of 1 M monobasic sodium phosphate (NaH_2PO_4) and 577 mL of 1 M dibasic sodium phosphate (Na_2HPO_4) to obtain 1 L of a 1 M buffer stock solution.
3. Phosphate buffer solution, pH 7.2: Mix 316 mL of 1 M NaH_2PO_4 and 684 mL of 1 M Na_2HPO_4 to obtain 1 L of a 1 M buffer solution.

4. Tris(2-carboxyethyl) phosphine (TCEP·HCl): Dissolve 28.67 mg of TCEP·HCl in 0.5 mL of 50 mM phosphate buffer, pH 7.0, to obtain 200 mM stock solution (20×). Dilute an aliquot of the TCEP stock solution (20×) to obtain 10 mM working solution of TCEP.
5. Sulfosuccinimidyl 4-(*N*-maleimidomethyl)-cyclohexane-1-carboxylate (Sulfo-SMCC), a water-soluble heterobifunctional cross-linker (*see* **Note 3**).
6. *N*-(p-Maleimidophenyl)isocyanate (PMPI), a heterobifunctional cross-linker soluble in dimethyl sulfoxide (DMSO) (*see* **Note 4**).
7. Sodium borate buffer, pH 8.5: Empty the contents of one foil envelope of a BupH (Dry-Blend Packs of borate buffer, Thermo Scientific) into a beaker, add ultrapure water, and stir to dissolve. When dissolved in 500 mL of water, each pack yields 50 mM borate, pH 8.5.
8. Homemade column packed with Sephadex G-25 resin.
9. Homemade column packed with Superdex 200 resin.

2.3 Components for Functional Tests: Cell Labeling and Immunohistochemistry with sdAb–QD Diagnostic Nanoprobes

1. MC38 colon carcinoma cells.
2. MC38CEA colon carcinoma cells expressing carcinoembryonic antigen (CEA).
3. 1× PBS: Dissolve one tablet of phosphate-buffered saline (PBS) in 200 mL of deionized water to obtain 0.01 M phosphate buffer, pH 7.4 at 25 °C, containing 0.0027 M potassium chloride (KCl) and 0.137 M sodium chloride (NaCl).
4. 1 % bovine serum albumin (BSA) in PBS: Dissolve 5 g of BSA in 500 mL of PBS, mix on a magnetic stirrer, and filter through a 0.22 μm filter.
5. Human appendix tissue samples from retrospective incision biopsy specimens (obtained from the Department of Pathology of University Hospital Robert Debré, Reims, France).
6. Citrate buffer solution: 2 % w/v citric acid and 8 % w/v sodium citrate (*see* **Note 5**).
7. 2 % BSA in PBS with 0.05 % Tween 20: Add 10 g of BSA to 500 mL of PBS containing 0.05 % Tween 20, stir on a magnetic stirrer, and filter through a 0.22 μm filter.
8. Anti-CEA monoclonal antibody, clone TF 3H8-1 (Ventana Medical Systems).
9. Polyclonal goat anti-mouse immunoglobulin conjugated with fluorescein isothiocyanate.
10. Biotinylated sheep anti-mouse polyclonal immunoglobulin.
11. REAL™ System kit (peroxidase/DAB) (Dako).
12. PBS with 0.05 % Tween 20: Mix 0.5 mL of Tween 20 and 1 L of PBS on a magnetic stirrer.

2.4 Special Equipment

1. Varian Cary 50 Conc. UV/Vis spectrophotometer (Agilent Technologies).
2. Varian Cary Eclipse spectrofluorimeter (Agilent Technologies).
3. Zetasizer Nano ZS (Malvern Instruments).
4. Bransonic ultrasonic cleaner, Branson 2510EMT (Sigma).
5. Eppendorf 5810R bench-top centrifuge (Eppendorf).
6. Eppendorf 5418 microcentrifuge (Eppendorf).
7. Eppendorf Concentrator Plus complete system (Eppendorf).
8. RM-2L Intelli-Mixer (Dutscher).
9. FACStar^{Plus} flow cytometer (Becton Dickinson).
10. Guava^{R} EasyCyte™ Plus flow cytometer (Guava Technologies).
11. Inverted fluorescent microscope (Carl Zeiss).
12. PD MiniTrap G-25 (GE Healthcare).
13. Amicon Ultra-15 filter units with a 10 kDa cutoff (VWR).
14. Disposable polypropylene columns (2–10 mL) (Pierce).
15. Nalgene filter units with a capacity of 500 mL, MF75 series (VWR).

3 Methods

3.1 Water Solubilization of Nanocrystals

1. Dissolve 10 mg of QDs in 1 mL of chloroform. Add 1 mL of methanol and wash by centrifugation for 5 min at 16,500 × *g*. Repeat the washing two times and dissolve the pellet in 1 mL of chloroform. Add 200 μL of 10 mg/mL solution of DL-cysteine (DL-Cys) in methanol dropwise to 1 mL of the solution of QDs in chloroform until the solution becomes cloudy (*see* **Notes 6** and **7**).
2. Sediment the QDs by centrifugation at 16,500 × *g*, wash them three times with methanol to remove the excess DL-Cys that has not reacted, and dry them under vacuum during 2 min.
3. Dissolve the dry powder of QDs in 1 mL of water by adding 1 M solution of sodium hydroxide (NaOH) dropwise (*see* **Note 8**). Sonicate the solution and filter it through 0.22 μm filters (*see* **Note 9**). The resultant water-soluble QDs exhibit bright orange photoluminescence with an emission maximum at 570 nm and quantum yield close to 40 % at room temperature (*see* **Note 10**).

3.2 Functionalization and Purification of Nanocrystals

1. To replace DL-Cys from the surface of QDs with thiol-modified PEG derivatives containing hydroxyl or amino end groups, add 156 μL of a 150 mg/mL hydroxy-PEG-SH solution in pure water or a mixture of 25 μL of a 100 mg/mL amino-PEG-SH solution and 140 μL of a 150 mg/mL hydroxy-

PEG-SH solution to 1 mL of a 10 mg/mL pure-water solution of the preparations of QDs coated with DL-Cys (*see* **Notes 2** and **10**).

2. Incubate the samples overnight at 4 °C, pre-purify them by centrifugation with the use of Amicon Ultra-15 filter units (10 kDa cutoff), and finally purify them from excess ligands by gel-exclusion chromatography on Sephadex-25 homemade columns (*see* **Note 11**).

3.3 Quality Control of Nanocrystals

The QD samples can be characterized using the dynamic light scattering (DLS) and electrophoresis techniques by means of a Zetasizer Nano ZS device (Malvern Instruments). Pass the samples through a 0.1 μm filter and measure the particle size distribution at 25 °C in a low-volume quartz batch cuvette (Malvern Instruments). Calculate the particle hydrodynamic size from the diffusion times using the Stokes-Einstein equation. Repeat measurements at least three times for each sample and at each value of intensity of scattering measurement (ten runs per measurement) and calculate the hydrodynamic diameter of the sample using the CONTIN algorithm (Fig. 2). Record the absorbance spectra and measure the photoluminescence at $\lambda_{ex} = 400$ nm (*see* **Note 11**).

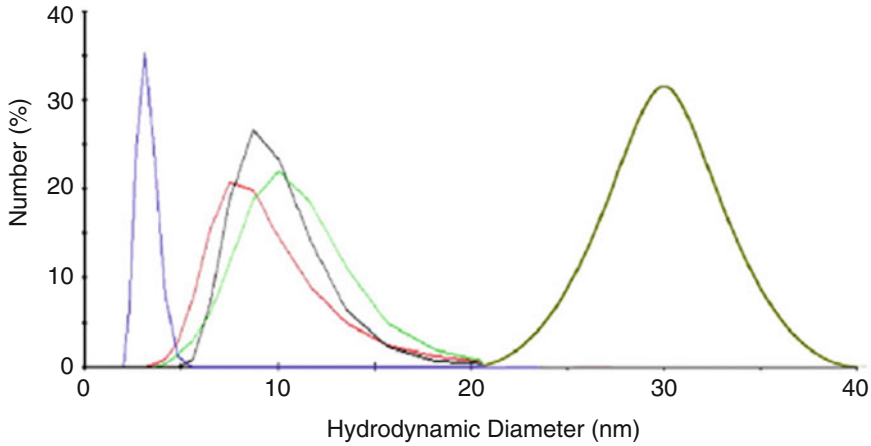

Sample	Hydrodynamic diameter (nm)
QDs	8.84 ± 2.9
sdAb	3.2 ± 0.52
Conjugates sdAbs-QD	11.9 ± 2.9
IgG	11.4 ± 2.5
Conjugates IgG-QD	30.3 ± 3.2

Fig. 2 Comparative dynamic light scattering measurements of sdAbs, QDs, sdAb–QD conjugate, and commercial mAb-QD conjugate purchased from Invitrogen. Reproduced from Sukhanova et al. (2012) [13] with permission from Elsevier

3.4 Reduction of the Intermolecular Disulfide Bonds in Single-Domain Antibody Dimers

1. Prepare a 10 mM working solution of TCEP in 50 mM phosphate buffer, pH 7.0, immediately before use. Dilute a sdAb sample to obtain a 100 μM solution in 50 mM phosphate buffer, pH 7.0.
2. Add a tenfold molar excess of TCEP, incubate the mixture for 30 min at room temperature, then use PD MiniTrap G-25 desalting centrifugation columns to remove the TCEP product, and concentrate the sdAb-SH (*see* **Note 12**).

3.5 Conjugation of sdAb-Cys with PEG-Modified Colloidal Nanocrystals

This step can be performed using option in Subheading 3.5.1 or option in Subheading 3.5.2, depending on the active functional groups on the surface of QDs (Fig. 3).

3.5.1 Conjugation of sdAb-SH with Amino-Modified QDs Using the Sulfosuccinimidyl 4-(N-Maleimidomethyl)-Cyclohexane-1-Carboxylate (Sulfo-SMCC) Reaction (Fig. 3a)

1. Dilute the aqueous solution of QDs containing 10 % of amino-PEG and 90 % of hydroxy-PEG on their surface to obtain 0.5 mL of a 4 mg/mL QD solution in 100 mM phosphate buffer, pH 7.2.
2. Add a 100-fold molar excess of Sulfo-SMCC to the QD preparation. Incubate the reaction mixture for 1 h at room temperature in the dark while stirring gently (40 rpm) on an RM-2L Intelli-Mixer. Immediately purify the maleimide-activated QDs

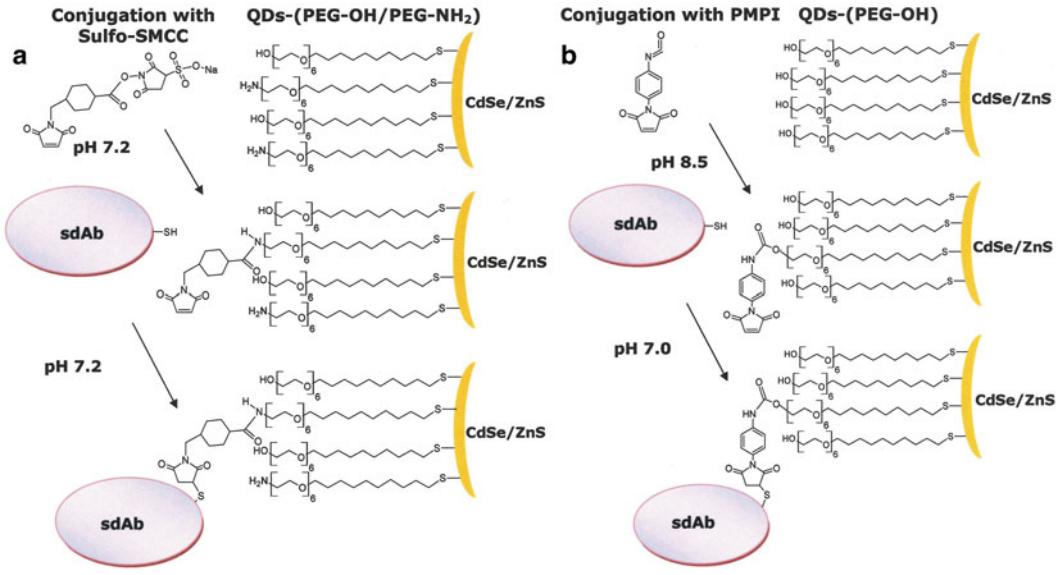

Fig. 3 Schematic presentation of the use of (**a**) sulfo-SMCC conjugation reaction or (**b**) the PMPI conjugation reaction for production of oriented sdAb–QD conjugates by linking, respectively, NH_2 or OH groups on the QD surface with SH groups of sdAbs. Both conjugations involve the SH group of the single Cys residue specifically integrated in the C-terminus of sdAbs that is available for conjugation. The procedures yield conjugates with an average of four copies of homogeneously oriented sdAbs per QD. Reproduced from Sukhanova et al. (2012) [13] with permission from Elsevier

by applying the reaction mixture onto a homemade column packed with Sephadex G-25 resin equilibrated with 100 mM phosphate buffer, pH 7.2.

3. Mix the maleimide-activated QDs with sdAb-SH to obtain a molar ratio of 1:10 (*see* **Notes 3** and **12**). Incubate the reaction mixture for 2 h at room temperature in the dark while stirring gently (40 rpm) on an RM-2L Intelli-Mixer. Finally, purify sdAb–QD conjugates by gel-exclusion chromatography on a homemade Superdex 200 resin column equilibrated with 100 mM phosphate buffer, pH 7.2 (*see* **Note 13**).

3.5.2 Conjugation of sdAb-SH with Hydroxyl-Modified QDs Using the N-(p-Maleimidophenyl) Isocyanate (PMPI) Reaction (Fig. 3b)

1. Dilute the solution of QDs containing only hydroxyl groups on their surface to obtain 0.5 mL of a 2 mg/mL QD solution in 50 mM sodium borate buffer, pH 8.5.
2. Add a 50-fold molar excess of PMPI to the sample. Incubate the reaction mixture for 30 min at room temperature in the dark while stirring gently (40 rpm) on an RM-2L Intelli-Mixer. Immediately purify maleimide-activated QDs by applying the reaction mixture onto a homemade column packed with Sephadex G-25 resin and equilibrated with 50 mM phosphate buffer, pH 7.0.
3. Mix purified maleimide-activated QDs with sdAb-SH to obtain a molar ratio of 1:10 (*see* **Notes 4** and **12**). Incubate the mixture for 2 h at room temperature in the dark while stirring gently (40 rpm) on an RM-2L Intelli-Mixer. Finally, purify the sdAb–QD conjugates by gel-exclusion chromatography on a homemade Superdex 200 resin column equilibrated with 50 mM phosphate buffer, pH 7.0 (*see* **Note 13**).

3.6 Characterization and Quality Control of the Resultant sdAb–QD Diagnostic Nanoprobes

3.6.1 Labeling Cells with sdAb–QD Conjugates and Flow Cytometry Measurements (Fig. 4)

1. Suspend MC38 and MC38CEA cells by gently shaking for 5 min. Wash 3×10^5 cells and incubate them for 30 min at 4 °C in the dark with 50 µL of different dilutions of sdAb–QD conjugates in PBS or human serum. Wash two times with PBS containing 1 % of BSA. Begin the next step immediately.
2. Perform flow cytometry measurements of the stained cells. Use a 488 nm argon laser for excitation and measure the fluorescence intensity in the range of 564–586 nm. Collect at least 5,000 events for each sample. Use the geometric mean fluorescence (GMF) intensity channels to quantify the staining of each sample.

3.6.2 Immunohistochemistry and Fluorescence Immunostaining with sdAb-QD Conjugates (Fig. 5)

1. Deparaffinize 5 µm paraffin sections in xylene, rehydrate them through ethanol (100, 96, and 70 %), and finally bring them to water. Incubate the slides for 60 min in a citrate buffer solution (2 % citric acid and 8 % sodium citrate) at 95 °C and then for 20 min at room temperature in the same buffer. Incubate the slides with 3 % hydrogen peroxide and 20 % methanol to quench the endogenous peroxidase activity and then wash

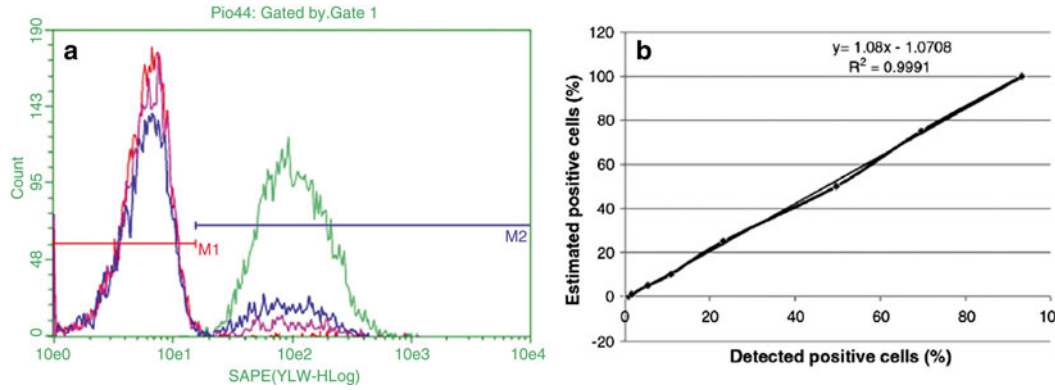

Fig. 4 Discrimination of CEA-positive (MC38CEA) and CEA-negative (MC38) cells in their mixture using sdAb–QD conjugates. (**a**) Distribution of the intensity of staining with sdAb–QD conjugates in a mixture of MC38CEA and MC38 cells. The MF intensity of MC38 cells (M1) is 5.7; the MF intensity of MC38CEA cells (M2) is 95.7 (*red*, 100 % of MC38; *pink*, 90 % of MC38 + 10 % of MC38CEA; *blue*, 75 % of MC38 + 25 % of MC38CEA; *green*, 100 % of MC38CEA). (**b**) The calibration curve for quantitative detection of MC38CEA cells in mixtures of MC38CEA and MC38 cells. Reproduced from Sukhanova et al. (2012) [13] with permission from Elsevier

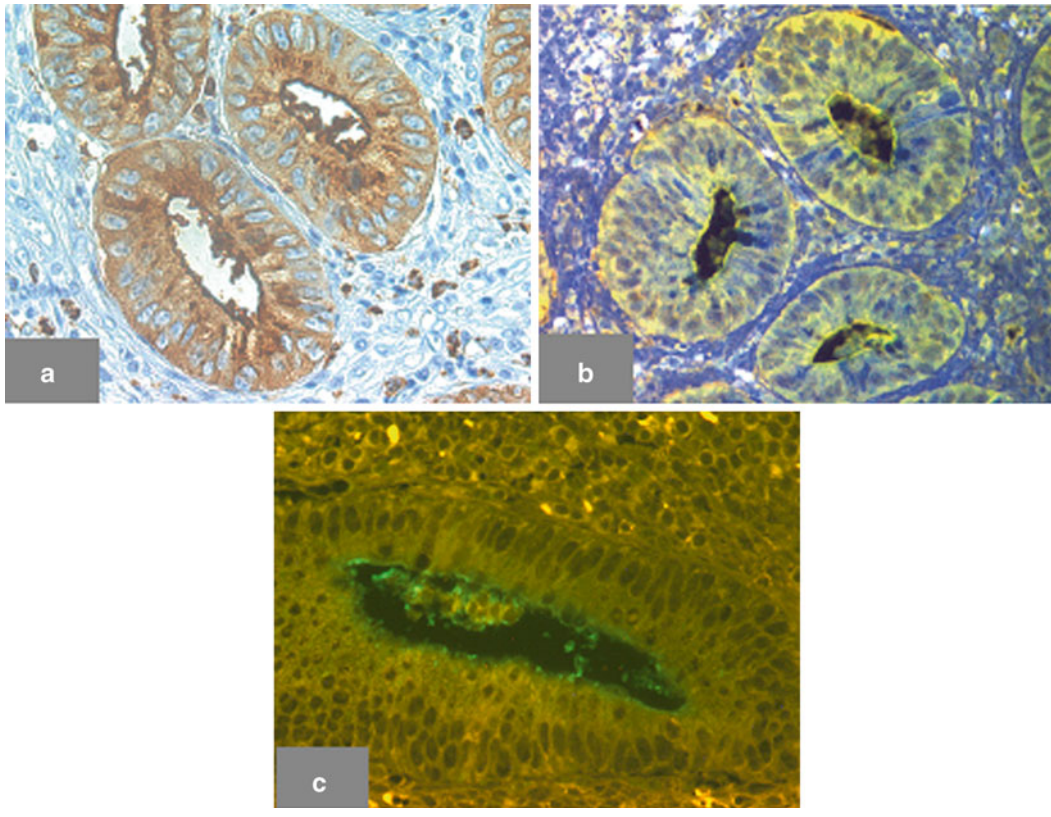

Fig. 5 Comparative histochemical immunostaining of patient's appendix epithelial crypts using the sdAb–QD and conventional techniques. (**a**) CEA (*brown*) revealed with the use of anti-CEA IgG and DAB chromogen (light microscopy). (**b**) CEA (*yellow*) revealed with the use of anti-CEA sdAb covalently linked to QD570 (epi-fluorescence microscopy). (**c**) CEA (*green*) revealed with the use of mouse anti-CEA IgG and anti-mouse IgG-FITC (epi-fluorescence microscopy). Reproduced from Sukhanova. et al. (2012) [13] with permission from Elsevier

them with water. Block nonspecific binding by a 20-min incubation of the tissue sections in a 2 % solution of BSA in PBS containing 0.05 % Tween 20.

2. Stain the tissue section with a 1.5×10^{-8} M solution of anti-CEA sdAb–QD conjugates for 1 h in a humidified chamber at room temperature. Wash three times with PBS. Observe fluorescence emission under a fluorescence microscope using UV (350–400 nm) excitation and 450 nm (long pass) emission filters.
3. For the control test, apply a 1.6×10^{-9} M solution of anti-CEA monoclonal antibody (clone TF3H8) to the tissue section for 1 h in a humidified chamber at room temperature. Wash it three times with PBS. Stain the tissue with polyclonal goat anti-mouse IgG conjugated with FITC for 1 h at room temperature. After washing three times with PBS, mount the slides with the mounting medium and view them under a fluorescence microscope using a 420–490 nm excitation filter and a 520 nm (long pass) emission filter.
4. For the "gold standard" immunohistochemical control labeling of the tissue section, incubate the slides with anti-CEA monoclonal antibody (clone TF 3H8-1, 6×10^{-9} M) for 1 h in a humidified chamber at room temperature. Wash the slides with PBS and incubate them with biotinylated sheep anti-mouse polyclonal IgG in PBS at room temperature for 1 h; develop the slides using a REAL™ System kit (peroxidase/DAB). After washing with PBS-Tween, view the slides under an optical microscope.

4 Notes

1. Use the solution of DL-cysteine in methanol immediately after preparation.
2. Use PEG derivatives solutions immediately after preparation.
3. Use a freshly prepared solution of the Sulfo-SMCC cross-linker.
4. Use a freshly prepared solution of the PMPI cross-linker.
5. Wear gloves and use a fume hood when handling sodium citrate.
6. Add the methanol solution of DL-Cys to the chloroform solution of QDs slowly, dropwise, controlling the aggregation state of the mixture.
7. In case the addition of the specified volume of the DL-Cys solution to the QD solution does not change the aggregation state of the mixture, add more 10 mg/mL DL-Cys solution until the mixture becomes cloudy.
8. Wear gloves and use a fume hood when handling concentrated NaOH.

9. In case the Cys-modified QD solution does not pass through 0.22 μm Ultrafree microcentrifuge filters, centrifuge the QD solutions for 10 min at 8,600 × *g* before filtering to remove the possible QD aggregations. Use the supernatant for further manipulations.
10. Cys-modified QDs are unstable and tend to lose the hydrophilic cysteine shell and aggregate. The solutions can be stored for no more than 3–7 days at 4 °C before functionalization with PEG derivatives.
11. PEG-functionalized QDs can be stored at 4 °C for up to 2 months before conjugation with antibodies. Do not freeze the samples, because this will cause irreversible aggregation.
12. Use the sample of reduced sdAb-SH for conjugation with QDs immediately.
13. The prepared conjugates can be kept at 4 °C.

Acknowledgements

This study was partly supported by the Ministry of Education and Science of the Russian Federation (grant 11.G34.31.0050), by the European Commission through the FP7 Cooperation project NAMDIATREAM (grant NMP-2009-4.0-3-246479) and by the programs HYNNOV and Nano'Mat of the Champagne-Ardenne region, the DRRT Champagne-Ardenne, and the FEDER (France). I.N. acknowledges support of the Russian Science Foundation.

References

1. Jaiswal JK, Goldman ER, Mattoussi H et al (2004) Use of quantum dots for live cell imaging. Nat Methods 1:73–78
2. Xing Y, Rao J (2008) Quantum dot bioconjugates for in vitro diagnostics & in vivo imaging. Cancer Biomark 4:307–319
3. Parak WJ, Gerion D, Pellegrino T et al (2003) Biological applications of colloidal nanocrystals. Nanotechnology 14:R15–R27
4. Invitrogen. http://probes.invitrogen.com/media/pis/mp19010.pdf
5. Liu W, Howarth M, Greytak AB et al (2008) Compact biocompatible quantum dots functionalized for cellular imaging. J Am Chem Soc 130:1274–1284
6. Xing Y, Chaudry Q, Shen C et al (2007) Bioconjugated quantum dots for multiplexed and quantitative immunohistochemistry. Nat Protoc 2:1152–1165
7. Zaman MB, Baral TN, Jakubek ZJ et al (2011) Single-domain antibody bioconjugated near-IR quantum dots for targeted cellular imaging of pancreatic cancer. J Nanosci Nanotechnol 11:3757–3763
8. Zaman MB, Baral TN, Zhang J et al (2009) Single-domain antibody functionalized CdSe/ZnS quantum dots for cellular imaging of cancer cells. J Phys Chem C 113:496–499
9. Pathak S, Davidson MC, Silva GA (2007) Characterization of the functional binding properties of antibody conjugated quantum dots. Nano Lett 7:1839–1845
10. Saerens D, Kinne J, Bosmans E et al (2004) Single domain antibodies derived from dromedary lymph node and peripheral blood lymphocytes sensing conformational variants of prostate-specific antigen. J Biol Chem 279: 51965–51972

11. Behar G, Chames P, Teulon I et al (2009) Llama single-domain antibodies directed against nonconventional epitopes of tumor-associated carcinoembryonic antigen absent from nonspecific cross-reacting antigen. FEBS J 276:3881–3893
12. Perruchini C, Pecorari F, Bourgeois JP et al (2009) Llama VHH antibody fragments against GFAP: better diffusion in fixed tissues than classical monoclonal antibodies. Acta Neuropathol 118:685–695
13. Sukhanova A, Even-Desrumeaux K, Kisserli A et al (2012) Oriented conjugates of single-domain antibodies and quantum dots: toward a new generation of ultrasmall diagnostic nanoprobes. Nanomedicine: NBM 8:516–525
14. Sukhanova A, Even-Desrumeauxc K, Millot J-M et al (2012) Oriented conjugates of monoclonal and single-domain antibodies with quantum dots for flow cytometry and immunohistochemistry diagnostic applications. Proc SPIE 8232, Colloidal Nanocrystals for Biomedical Applications VII:82320T-1-82320T-9
15. Kumar S, Aaron J, Sokolov K (2008) Directional conjugation of antibodies to nanoparticles for synthesis of multiplexed optical contrast agents with both delivery and targeting moieties. Nat Protoc 3: 314–320
16. Holliger P, Hudson PJ (2005) Engineered antibody fragments and the rise of single domains. Nat Biotechnol 23:1126–1136
17. Sukhanova A, Devy J, Venteo L et al (2004) Biocompatible fluorescent nanocrystals for immunolabeling of membrane proteins and cells. Anal Biochem 324:60–67

Chapter 11

Functional Integration of Quantum Dot Labeled Mesenchymal Stem Cells in a Cardiac Microenvironment

Maria C. Collins, Philip R. Gunst, and Barbara J. Muller-Borer

Abstract

Bone marrow derived multipotent mesenchymal stem cells (MSCs) have the potential to differentiate into bone, cartilage, fat, and muscle cells and are being investigated for their utility in cell-based therapies. Stem cell transplantation therapy represents a novel and innovative approach with the promise to restore function to diseased or damaged heart muscle. Transplanted MSCs are expected to engraft, differentiate, and remodel in response to the surrounding cardiac microenvironment significantly changing the therapeutic approach for heart disease. Quantum Dots (QDs) offer an alternative to organic dyes and fluorescent proteins to label and track cells in vitro and in vivo. Here, we describe in vitro QD labeling of MSCs, MSC integration in a cardiomyocyte co-culture microenvironment, and a fluorescent recovery after photobleaching (FRAP) technique to assess functional cell–cell communication. FRAP techniques establish an optical record of dynamic cellular interactions with high spatial and temporal resolution and can be used to successfully evaluate dynamic changes in cellular coupling in multicellular preparations.

Key words Mesenchymal stem cells, Co-culture, Quantum dots, Cell labeling, Cell tracking, Nanotechnology, Live cell imaging, Confocal fluorescent microscopy, Fluorescent recovery after photobleaching

1 Introduction

Quantum dots (QDs) are fluorescent semiconductor nanoparticles, used in in vitro and in vivo bioimaging [1, 2]. Reported advantages of QDs include a narrow band emission and broadband excitation with a high quantum yield, photostability, luminescence, and resistance to chemical and metabolic degradation [1, 3, 4]. These properties make QDs amenable to multicolor imaging applications and the tracking of live cells [5]. The procedures described use commercially available CdSe/ZnS QDs to label and track MSCs in vitro in a cardiac microenvironment for up to 7 days. A cardiac microenvironment is generated by dissociating neonatal rat hearts and establishing cardiomyocyte primary cultures on laminin-coated cover slides. The primary cultures are maintained

Adriana Fontes and Beate Saegesser Santos (eds.), *Quantum Dots: Applications in Biology*, Methods in Molecular Biology, vol. 1199, DOI 10.1007/978-1-4939-1280-3_11, © Springer Science+Business Media New York 2014

for 48 h before adding the QD labeled MSCs [6–8] and the co-cultures are maintained for up to 14 days in culture. QD labeled MSCs are tracked in an in vitro cardiomyocyte co-culture and functional gap junction mediated cell-to-cell communication between the cardiomyocytes and MSCs is evaluated using a fluorescent dye diffusion assay, FRAP, with laser scanning confocal microscopy.

Confocal FRAP provides an optical record of cellular interaction with high spatial and temporal resolution. FRAP measurements in co-cultures are independent of cellular geometry and tissue architecture and assume that fluorescence recovery is the result of two-dimensional (2-D) diffusion in an infinite plane. Using confocal fluorescent microscopy an optical plane of specified thickness is defined for a region of interest (ROI) within the cell culture, i.e., all measured fluorescence recovery is from a 2-D area of nominal thickness. In addition, the surrounding cells in culture provide a continuous supply of fluoroprobe, which redistributes between adjacent cells through permeable gap junctions. FRAP uses an intense light pulse to photobleach fluoroprobe molecules in one area and fluorescence recovery is mediated via fluoroprobe diffusion from surrounding unbleached areas. Monitoring the redistribution of a fluoroprobe as a function of time results in a single exponential recovery curve, yielding a rate constant for dye transport. FRAP techniques have evolved to provide spatial and temporal fluorescence recovery measurements in cell pairs and small groups of cells [8, 9].

2 Materials

Prepare general laboratory materials, supplies, and equipment necessary for culturing MSCs, cardiomyocytes, and co-cultures, QD labeling and secondary fluorescent labels for live cell imaging. Have the following additional materials available:

1. 37 °C water bath or warmer.
2. Laboratory centrifuge.
3. Plate rotator.
4. 15 mL and 50 mL sterile conical tubes.
5. 1.5 mL sterile microcentrifuge tubes.
6. T-75 flask.
7. Sterile pipettes.
8. Stainless steel surgical scissors.
9. Microsurgical scissors.
10. Sterile disposable scalpels.
11. Forceps.

12. Sterile gauze.
13. 60 mm culture dish.
14. Betasept.
15. 70 % ethanol.
16. Confocal laser scanning fluorescent microscope with time series image acquisition software control.

2.1 Cell Culture Materials

Prepare and store reagents/buffers as directed. Perform all cell culture under a biological hood using sterile cell culture procedures.

1. 1× phosphate buffered saline (1× PBS).
2. Medium 199 (M199).
3. Fetal Bovine Serum (FBS).
4. Penicillin/Streptomycin antibiotic/Amphotericin-B (Pen/Strep/Amphotericin-B).
5. Dulbecco's Minimal Essential Medium with phenol (DMEM).
6. Phenol-Free DMEM.
7. Anhydrous dimethylsulfoxide (DMSO).
8. Laminin-coated coverslips. Use 25 mm round glass coverslips (#1.5) with a thickness of 170 nm, or coverglass bottom 35 mm petri dish designed for high-resolution imaging (*see* **Note 1**). Dilute laminin in sterile 1× PBS, to a 10 μg/mL concentration. Thinly coat each coverslip or coverglass bottom petri dish with 1 mL laminin solution and incubate at 37 °C for 2 h. Wash each coverslip three times with sterile 1× PBS. Place under UV lights for a minimum of 1 h to sterilize.

2.2 Quantum Dots

1. We used commercially available Q-dot® nanocrystals to label MSCs. The Q-dot® nanocrystals in the Q-Tracker® 605 Cell Labeling kit (Life Technologies—Invitrogen, Carlsbad, CA, USA) had an excitation range of 405–565 nm and emission maxima of 605 nm (*see* **Note 2**).
2. Complete Media: Dulbecco's Minimal Essential Medium (DMEM) with 16.5 % FBS, Pen/Strep/Amphotericin-B. To prepare Complete Media add 100 mL FBS and 5 mL of Pen/Strep/Amphotericin-B to 500 mL bottle of DMEM. Store Complete Media at 4 °C.

2.3 Cardiomyocyte Isolation

1. We used a cell isolation system for rat neonatal heart tissue (Worthington Biochemical Corporation, Lakewood, NJ, USA). Kit includes Hanks Buffered Saline Solution (HBSS), trypsin, trypsin inhibitor, collagenase, 70 μm cell conical tube filters, L-15 powdered media.
2. One liter sterile cell culture grade water.

2.4 Solutions for Secondary Labeling of Live Cell Cultures

1. FBS-FREE Complete Media: To prepare FBS-FREE Complete Media, add 5 mL Pen/Strep/Amphotericin-B to 500 mL bottle of DMEM. Gently mix by swirling bottle. Date, label, and store at 4 °C. Media should be used within 1 month (*see* **Note 3**).
2. 1 mmol/L Calcein AM: Resuspend 50 μg Calcein AM in 50 μL DMSO. Vortex vial to dissolve. Prepare just prior to labeling live cell cultures. Date unused, dissolved calcein AM and store in desiccant, protected from direct light exposure, at 20 °C for up to 6 months (*see* **Note 4**).
3. 1 μmol/L Calcein AM in FBS-FREE Complete Media for intracellular labeling of live cell cultures: In a 15 mL conical tube, add 2 μL of 1 mmol/L Calcein AM resuspended in DMSO to 2 mL of FBS-FREE Complete Media. This is enough volume to cover and label one 25 mm round glass coverslip in a 35 mm petri dish or coverglass bottom 35 mm petri dish. Prepare media with fluoroprobe just prior to labeling live cell cultures. Protect from direct light exposure (*see* **Note 5**).
4. Phenol-Free Complete Media for imaging live cell cultures: Prepare Complete Media as in Subheading 2.2, **item 2**, using phenol-free DMEM. Store at 4 °C for 1 month (*see* **Note 6**).

3 Methods

Sterilize all instruments in autoclave and lay out the sterile field under the biological hood to create a workspace.

3.1 MSC Isolation

Rat MSCs can be purchased frozen or isolated following the Caplan procedure described below [10].

1. Sacrifice one Sprague–Dawley rat at 6–8 weeks in accordance with accepted institutional guidelines for the ethical care and treatment of experimental animals.
2. Wipe each leg with Betasept followed by 70 % ethanol. Collect the femur and tibia of each rat leg using sterile scissors, forceps, and gauze. Separate the two bones from each other.
3. Clean the bones of all tissue and place the bones in a sterile Petri dish. Wash each bone with 70 % ethanol and let dry. Cut the two ends of each bone with sterile scissors.
4. Using 10 mL of DMEM media and a sterile syringe and needle, hold the bone with sterile forceps and insert the needle with syringe and wash the cells from the bone marrow into a 50 mL conical tube. Use a separate conical tube for each leg.
5. Pipette the cells from each of the conical tubes into a T-75 flask. Place the flasks in a cell culture incubator at 37 °C and 5 % CO_2 for 24 h to allow the MSCs to attach to the bottom of the flask.

6. Change the media after 24 h and thereafter every 3 days.
7. Observe the cultured MSCs under phase microscope daily to assess confluency and verify cell morphology (*see* **Note 7**).
8. Grow cells for 1 week or ~80 % confluency and split into two flasks. Grow cells again until 80 % confluency. Harvest and freeze cells in aliquots of 500,000 cells in 10 % DMSO and complete media. Store in liquid nitrogen for future use.

3.2 Cardiomyocyte Isolation

Cardiomyocyte isolation procedures provided by Worthington Biochemical Corporation were followed with modifications. This is a 2 day process. Unless otherwise stated, all steps are performed under a biological hood and all items are to be sterile.

1. Isolate the hearts of 10 one-day-old Sprague–Dawley rats in accordance with accepted institutional guidelines for the ethical care and treatment of experimental animals. Quickly place the hearts in a 50 mL conical tube with 30 mL of HBSS on ice.
2. After all hearts have been harvested, obtain an ice pack from the freezer and place a 60 mm culture dish on top of the ice pack.
3. Reconstitute trypsin by adding 2 mL cold HBSS to the trypsin vial. Keep on ice.
4. Swirl the 50 mL conical tube with HBSS to rinse the blood from the heart tissue. Pour off the rinse and add 10 mL of cold HBSS to the heart tissue. Carefully swirl the 50 mL conical tube again to rinse the blood from the heart tissue. Pour off the rinse fluid.
5. Transfer heart tissue to the cold 60 mm culture dish on the ice pack and mince the hearts thoroughly with sterile disposable scalpels.
6. Add 9 mL of cold HBSS and 1.5 mL of the reconstituted trypsin to the 60 mm culture dish, swirling to mix well. Cover and place entire 60 mm culture dish in the refrigerator overnight. Tissue digestion requires 16–20 h.
7. Reconstitute one envelope of powdered L-15 media in 1 L of sterile cell culture grade water. Wash out the envelope to remove all the powdered media.
8. Turn on water bath and environmental shaker incubator and allow both to warm to 37 °C.
9. Pipette 25 mL of L-15 media and 50 mL of M199 medium supplemented with 10 % FBS and 1 % Pen/Strep/Amphotericin-B into separate 50 mL conical tubes. Warm to room temperature, 22 °C.
10. Remove 60 mm culture dish with heart tissue from the refrigerator and transfer entire tissue suspension to a 50 mL conical tube using a wide mouth pipette.

11. Reconstitute trypsin inhibitor with 1 mL HBSS and add to 50 mL conical tube with heart tissue. Shake by hand for 30 s.
12. Warm the 50 mL conical tube with hearts and trypsin inhibitor in the 37 °C water bath (about 5 min).
13. Reconstitute 1 vial of collagenase with 5 mL of L-15 media. Slowly add vial of collagenase solution to 50 mL conical tube with heart tissue, cap the tube tightly, and place at a 30° angle in the environmental shaker incubator at 37 °C for 45 min at a very slow rotational speed (50 rpm) (*see* **Note 8**).
14. Triturate the heart tissue in the 50 mL conical tube 4× with a normal mouthed pipette under the biological hood. Allow tissue to settle 3–4 min.
15. Place a 70 μm filter over a new 50 mL conical tube and wet the screen with 1 mL L-15 media. Filter only the supernatant, i.e., the media above the settled tissue, into the new conical tube being careful not to disturb the settled heart tissue.
16. Add 5 mL of L-15 media to the heart tissue in the first conical tube, and again triturate 4× with a normal mouthed pipette. Strain the entire tissue suspension into the new conical tube. Rinse the filter with 2 mL of L-15 media (*see* **Note 9**).
17. Swirl cells gently, then spin down at 600 rpm (between 50 and $100 \times g$) for 5 min. Remove supernatant, and resuspend in 10 mL of M199 medium supplemented with 10 % FBS and 1 % Pen/Strep/Amphotericin-B (*see* **Note 10**).
18. Transfer the cell suspension into a sterile 75 cm^2 flask and place in incubator for 45 min. Remove the cell suspension from the flask and transfer into another 75 cm^2 flask. Place in incubator for 45 min (*see* **Note 11**).
19. Transfer the cell suspension from the flask to a new 15 mL conical tube and spin down at 600 rpm (between 50 and $100 \times g$) for 5 min. Discard supernatant.
20. Count cardiomyocytes before plating (*see* **Note 12**).
21. Plate the cardiomyocytes in 35 mm petri dishes containing the laminin-coated 25 mm, #1.5 glass coverslips, at 1×10^6 cells per dish in 2 mL M199 medium supplemented with 10 % FBS and 1 % Pen/Strep/Amphotericin-B.
22. Maintain cardiomyocyte cultures at 37 °C, 5 % CO_2 in a cell culture incubator for 48 h before the QD labeled MSCs are added to establish co-cultures.

3.3 MSC Preparation

The following procedure applies to mesenchymal stem cells (MSCs) stored in DMSO in liquid nitrogen (*see* **Note 13**). Stem cells stored in liquid nitrogen should be thawed quickly and diluted with media to reduce damage from DMSO. Most of the stem cells live through the thawing process but some do not. Counting the

stem cells before plating will provide an indication of how many cells survived the freezing/thawing process. This procedure also removes the liquid DMSO that is used to freeze the cells. This procedure must be performed under a biological hood using sterile cell culture procedures.

1. Warm Complete Media to 37 °C in water bath.
2. Remove cryotube with MSCs from liquid nitrogen and thaw quickly at 37 °C. Hold the cryotube with gloved hands in the water bath. Thaw MSCs until the pellet begins to move. This will take 30 s to 1 min.
3. Transfer the thawed MSCs to a 50 mL conical tube that contains 1 mL of pre-warmed Complete Media and mix gently with pipette by gently aspirating and dispensing volume in conical tube three to four times.
4. Place the conical tube with cell suspension in a centrifuge and spin the cells to pellet at 1,500 rpm (about $450 \times g$) for 5 min.
5. Remove the media above the cell pellet and resuspend the cell pellet in 2 mL of Complete Media. Mix gently to remove any cell clumps by gently aspirating and dispensing volume in conical tube three to four times.
6. Count MSCs before plating (*see* **Note 14**).
7. Remove 1×10^6 cells and place in sterile 50 mL conical tube and centrifuge cells to pellet at 1,500 rpm (about $450 \times g$) for 5 min.

3.4 QD Labeling of MSCs and Co-culture

1. Following directions provided by the manufacturer premix 1 μL each of the Qtracker proprietary labeling reagents in a 1.5 mL microcentrifuge tubes (10 nmol/L final concentration). Incubate QD labeling media in microcentrifuge tube for 5 min at 21 °C.
2. Add 0.2 mL of Complete Media to QD labeling media and vortex for 30 s.
3. Add the 0.2 mL QD labeling solution to the cell pellet containing 1×10^6 MSCs, previously prepared and described in **step 7** of Subheading 3.3.
4. Incubate MSCs in QD labeling solution for 1 h at 37 °C, 5 % CO_2 in cell culture incubator.
5. Remove unincorporated QDs by washing MSCs with Complete Media. To wash MSCs add 1 mL of Complete Media to the MSCs. Centrifuge at 1,500 rpm (about $450 \times g$) for 5 min. Discard supernatant, i.e., the media above the cell pellet. Repeat wash sequence.
6. Resuspend washed MSCs in 1 mL of Complete Media.

7. To prepare cardiomyocyte co-cultures, add QD labeled MSCs to cardiomyocyte cultures plated for 48 h as described in Subheading 3.2. Add QD labeled MSCs at a ratio of 1/100 (MSCs to cardiomyocytes) and maintain at 37 °C, 5 % CO_2 in a cell culture incubator for up to 14 days. Change M199 medium supplemented with 10 % FBS and 1 % Pen/Strep/Amphotericin-B every 2 days.

3.5 Fluorescent Recovery After Photobleaching

Here we describe a procedure using the fluorescent dye diffusion assay FRAP with laser scanning confocal microscopy to evaluate quantitative intercellular cytosolic communication via gap junctions between MSCs and cardiomyocytes. The procedure outlined is for MSCs and cardiomyocytes plated on glass coverslips. Adapt technique if co-cultures are plated in glass coverslip bottom petri dishes.

1. Co-cultures should be confluent or semi-confluent before FRAP study. Cells need to be touching; however the culture should not be overgrown.
2. Prepare solutions for secondary labeling of live cell cultures: FBS-FREE Complete Media, FBS-FREE Complete Media with 1 μmol/L Calcein AM and Phenol-Free Complete Media as described in Subheading 2.4.
3. Wash one co-culture on coverslip with FBS-FREE Complete Media. To wash, use a pipette to aspirate the media from the co-culture, then add FBS-FREE Complete Media. Repeat wash sequence.
4. Remove media and add 1–2 mL of 1 μmol/L Calcein AM in FBS-FREE Complete Media to co-culture (*see* **Note 5**).
5. Cover with aluminum foil and incubate at 37 °C, 5 % CO_2 in a cell culture incubator for 30 min (*see* **Note 15**).
6. Remove co-culture from incubator and wash co-culture twice with Phenol-Free Complete Media. Use a pipette to aspirate the media from the co-culture, then add 2 mL Phenol-Free Complete Media. Repeat wash sequence twice.
7. Add 1–2 mL Phenol-Free Complete Media to co-culture and return to cell culture incubator for 10 min.
8. To prepare co-culture for imaging, place coverslip in a coverslip chamber with Phenol-Free Complete Media. If using glass bottom petri dishes add Phenol-Free Complete Media to co-culture and place directly on the stage of a laser scanning confocal fluorescence microscope (*see* **Notes 16** and **17**).
9. Select a high magnification objective with a numerical aperture close to 1 (*see* **Note 18**).
10. Use a 488 nm excitation wavelength to illuminate the QDs (*see* **Note 19**). Locate a QD labeled MSC that is touching at

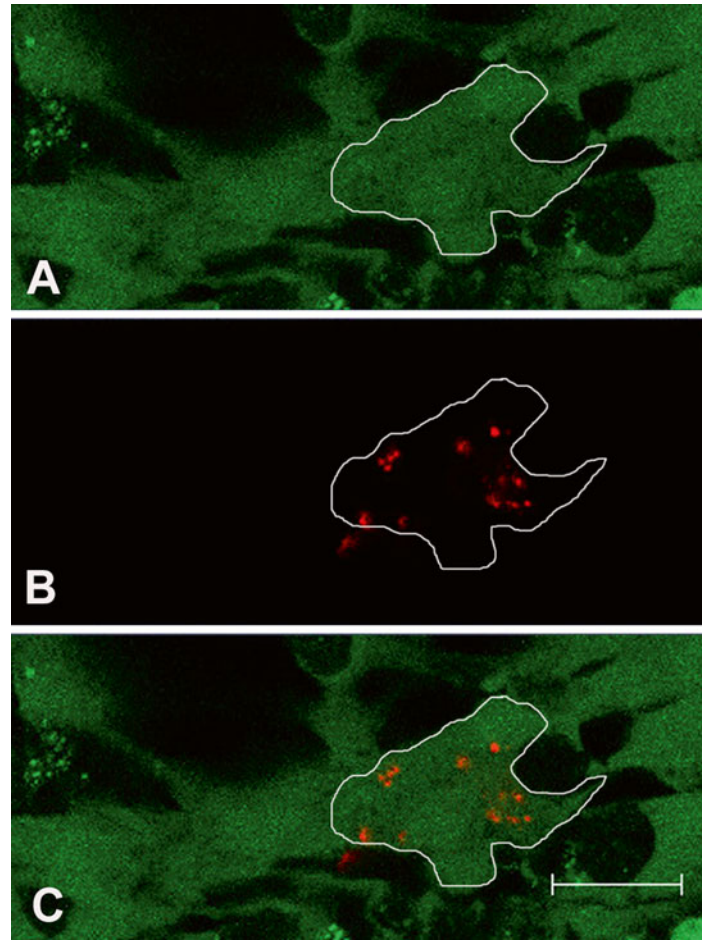

Fig. 1 High resolution confocal optical image of QD labeled MSC cardiomyocyte co-culture at 7 days. A 1-μm optical section shows QD labeled MSC (*outlined in figure*) is adjacent to and surrounded by cardiomyocytes. All cells were labeled with the cytosolic fluoroprobe calcein AM. An argon ion laser with an excitation wavelength of 488 nm was used. Emission wavelengths were collected simultaneously through a 515 ± 15 nm band pass filter (**a**) and 590 nm long pass filter (**b**). The overlay image is shown in (**c**). Images illustrate spatial characteristics of the co-culture, documenting cell orientation, QD MSC location, and cellular environment. The images were acquired with a Zeiss 510 laser scanning confocal fluorescent microscope equipped with a 40×/1.3 Numerical Aperture (NA) oil immersion objective. Scale bar = 20 μm

least one cardiomyocyte in the field of view. QD labeled MSCs are identified by punctate red fluorescent cellular inclusions as shown in Fig. 1 (*see* **Note 20**).

11. Image the region of interest (ROI), both QD and calcein emission wavelengths, and save reference image. The 488 nm excitation wavelength can be used to simultaneously collect

emission wavelengths through a 580 nm long-pass filter (emission wavelength for QDs) and 515 ± 15 nm band pass filter (emission wavelength for calcein or fluoroprobes with green wavelength emission spectra) as shown in Fig. 1 (*see* **Note 21**).

12. Using the software controls, select and outline the QD labeled MSC in the ROI.
13. Set up a time series to bleach and image the selected QD labeled MSC. The laser is used as the excitation and bleaching source. A short laser pulse (less than 5 s) of high intensity (100 % laser power) is used to bleach the calcein molecules within the QD labeled MSC. Within a few milliseconds post-bleach, record images at predefined time intervals to document fluorescence redistribution in the ROI cell (*see* **Note 22**).
14. Initiate the bleach and image acquisition sequence. At the end of the bleach-recovery sequence save the image series (*see* **Note 23**).
15. You can perform 6–8 FRAP sequences per coverslip (see **Note 16**).
16. A representative image of a 7-day co-culture is shown in Fig. 2, illustrating the FRAP protocol and fluorescence recovery in the QD labeled MSC. The graph in Fig. 2 shows the average fluorescence recovery over 8 min measured in QD labeled MSC adjacent to cardiomyocytes. Monitoring the fluorescence emission intensity of calcein in the QD labeled MSC as a function of time results in a single exponential recovery curve, yielding a rate constant for the fluoroprobe transport, a measure of gap junction permeability [9]. Fluorescence recovery time is comparable to published results from similar stem cell-cardiomyocyte co-culture models [7].

4 Notes

1. Select glass coverslips #1.5 with a thickness of 170 nm, designed for high resolution imaging. The focal plane of the images will be shifted if the coverslip is too thin (<170 nm) or too thick (>170 nm), decreasing image resolution. Do not use plastic coverslips. Plastic coverslips are autofluorescent and will prevent high resolution imaging of the MSCs and QDs. Cells are plated on 25 mm round #1.5 glass coverslips placed in petri dishes. For live cell imaging place the coverslip in a coverslip chamber with media before imaging.
2. A Q-Tracker® 605 Cell Labeling kit was used with QDs composed of a cadmium selenium core and an inner zinc sulfide shell with a custom peptide bound to the QD's outer shell. The peptide allowed the QDs to be endocytosed into the

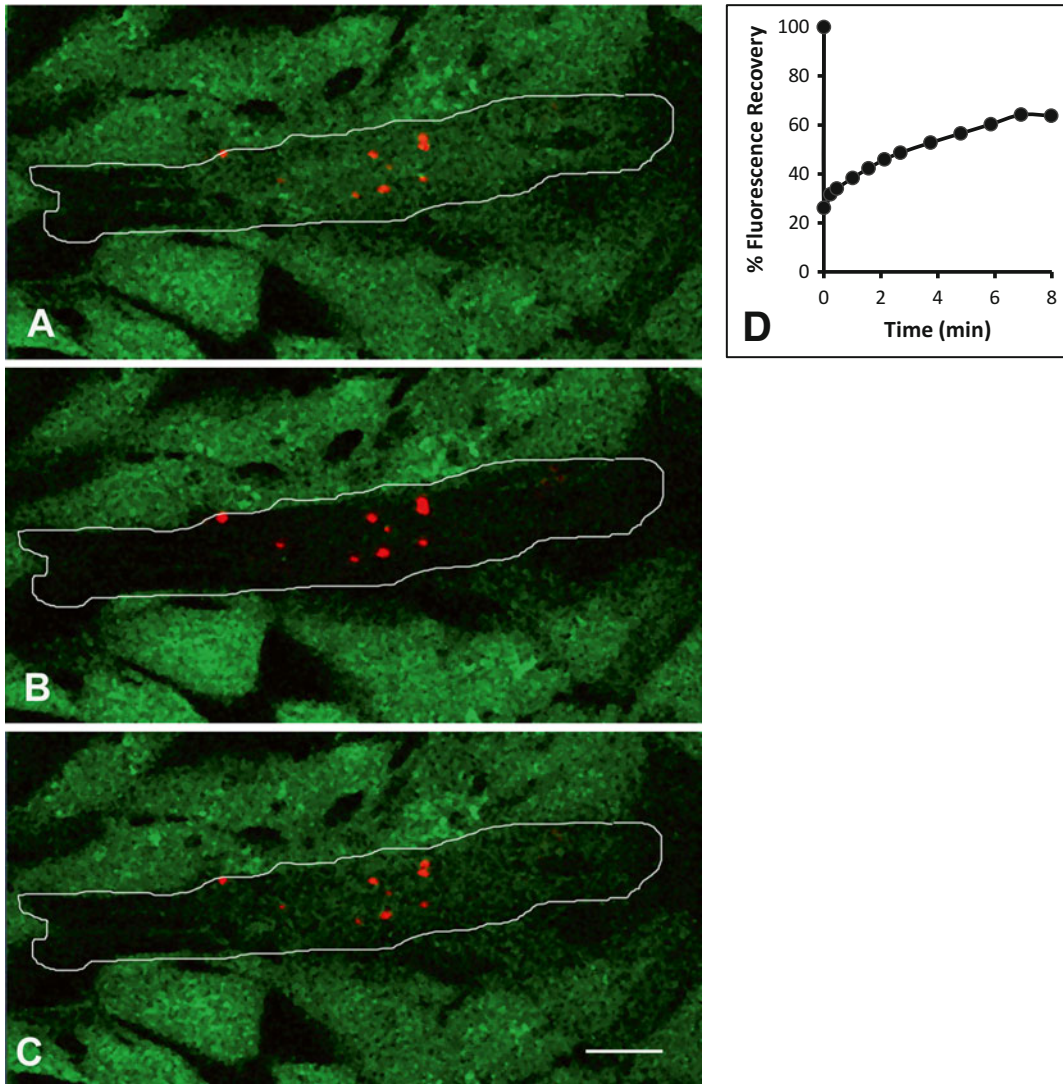

Fig. 2 FRAP assay demonstrates functional cell–cell communication between MSCs and cardiomyocytes. FRAP sequence demonstrates cell–cell communication between QD labeled MSCs (*outlined*) co-cultured with cardiomyocytes. All cells were intracellularly labeled with calcein AM. (**a**) Image of co-culture, with QD labeled MSC (*outlined*) surrounded by cardiomyocytes, before photobleach sequence. (**b**) Image of co-culture acquired with 4 ms after calcein AM in QD labeled MSC was photobleached with high intensity 488 nm laser pulse (100 % laser power). Note that QDs are still visible in MSC. (**c**) Image of co-culture, acquired 8 min after photobleaching, demonstrating FRAP as a result of calcein diffusion from neighboring cardiomyocytes into the QD labeled MSCs (scale bar = 20 μm). (**d**) Fluorescence recovery in QD labeled MSC with FRAP assay demonstrates cell–cell communication between MSC and cardiomyocytes at 7 days in co-culture. Fluorescent calcein recovery after photobleach was measured in MSC adjacent to cardiomyocytes. Measurements were recorded at 21 °C

MSC interior and exist in periplasmic vesicles [1, 2]. QDs were approximately 10–15 nm in diameter with spectral characteristics of 488 nm wavelength excitation and 605 nm wavelength peak emission.

3. Prepare Complete Media without FBS to facilitate calcein AM intracellular labeling. It is important to wash the co-cultures with the FBS-free media to remove any residual FBS in the cell culture before adding the fluoroprobe. The FBS-free Complete Media should only be used during incubation with the fluoroprobe.
4. If possible purchase and resuspend small aliquots of fluorescent dyes. Resuspended calcein AM can be thawed and refrozen several times without affecting cell labeling efficiency. Resuspend calcein AM just prior to cell loading. Keep resuspended calcein AM covered and protected from light exposure.
5. The intracellular fluoroprobe calcein is bright and photostable in co-cultures for several hours. We have used calcein at concentrations ranging from 500 nmol/L to 1 μmol/L with success. Label co-cultures only as necessary and preferably just before imaging. We have observed calcein being taken up by intracellular organelles and/or leaking out of the cells several hours after labeling.
6. Prepare phenol-free Complete Media to use for live MSC imaging. The color of the phenol will introduce noise into the images acquired at wavelengths greater than 600 nm (i.e., images acquired in the red spectrum).
7. Bone marrow derived MSCs are a heterogeneous population of progenitor cells. MSCs will enlarge and elongate as they proliferate and grow in culture.
8. To insure thorough mixing and prevent leakage of the cell solution, orient the tube's cap at 30° above the horizontal in the rocker/incubator.
9. When filtering MSCs the filter may become clogged with cells. Replace and use a new filter if necessary.
10. When aspirating supernatant from conical tubes be careful not to aspirate the cell pellet.
11. To isolate a pure cardiomyocyte population we use a two-step preplating process. For each step the adherent cells are not of interest and cardiomyocytes will remain in suspension.
12. Remove 20 μL of cell suspension and add to 80 μL 1× PBS. Add 100 μL of Trypan Blue to the cell suspension and obtain a total cell count using a hemocytometer. Be careful not to count red blood cells (very small, toroidal shape). This will give you a 10× dilution.

13. This procedure has been used with passage 2 and passage 3 MSCs. Results may differ with MSCs at later passages. This procedure was not evaluated on freshly isolated MSCs.
14. Count cells using a hemocytometer, remove 30 μL of cells in media and place in a 1.5 mL microfuge tube. Add 30 μL of trypan blue and mix well. Load the hemocytometer with 10 μL and count live cells only, excluding all blue cells from count.
15. When working with live cells labeled with fluoroprobes keep light exposure to a minimum to reduce photobleaching.
16. When imaging live cell cultures an onstage incubator attachment with atmosphere and temperature control is beneficial to provide a stable environment for the cell cultures. If an onstage incubator system is not available replace the media covering the co-cultures with fresh media every 30 min. A heated stage set to 37 °C may also be used.
17. Use an inverted microscope for live cell imaging. Gently clean the bottom of coverslip (cell free side) with lens paper and lens cleaning solution before placing on microscope stage.
18. For live MSCs a 63×/1.2 Numerical Aperture (NA) water immersion objective should be used. A 40× objective also provides good images. We observed no enhancement of images with a 100× objective.
19. The optimum wavelength to excite QDs is 405 nm but QDs can also be excited at 488 nm.
20. QD labeled MSCs are identified by punctate red fluorescent cellular inclusions. Acquiring a series of 1 μm thick optical images through the cell culture (three-dimensional Zstack) will allow you to evaluate QD location within the cells and location of QD labeled MSC in cardiac microenvironment. Image analysis software is available with Zeiss microscopes and ImageJ software (http://rsb.info.nih.gov/ij) is a free download.
21. A fluorescence image of the QD and calcein labeled co-culture should be acquired at the beginning and end of each FRAP protocol to reference fluoroprobe stability and cell viability. The QD fluorescence is acquired and is necessary to identify MSC location for the bleach protocol.
22. A short (5–10 ms), high intensity laser pulse (100 % laser power) will bleach the calcein molecules causing a drop in fluorescence. The high intensity laser pulse should not affect the fluorescence emissions of the QDs. The decrease in calcein fluorescence should be at least 50 % of the initial fluorescence intensity. Within a few milliseconds after the end of the bleach pulse, start recording postbleach images at predefined time intervals to document fluorescence redistribution in the

bleached QD labeled MSC. Rate constants for dye diffusion are calculated to quantitate cell–cell coupling.

23. The QD labeled MSCs will demonstrate fluorescence recovery after photobleaching as a result of calcein diffusion from neighboring cardiomyocytes into the QD labeled MSCs. We have observed fluorescence recovery for MSC cardiomyocyte co-cultures recorded at room temperature (22 °C) to average 8–10 min. Lack of fluorescence recovery suggests no gap junction mediated functional cell–cell coupling between adjacent cells. This can be evaluated by adding a gap junction blocker to the experimental protocol.

References

1. Jaiswal J, Mattoussi H, Mauro J, Simon S (2003) Long-term multiple color imaging of live cells using quantum dot bioconjugates. Nat Biotechnol 21:47–51
2. Larson D, Zipfel W, Williams R, Clark S, Bruchez M, Wise F, Webb W (2004) Water-Soluble quantum dots for multiphoton fluorescence imaging in vivo. Science 300: 1434–1436
3. Chan W, Maxwell D, Gao X, Bailey R, Han M (2002) Luminescent quantum dots for multiplexed biological detection and imaging. Curr Opin Biotechnol 13:40–46
4. Alvisiatos A (2004) The use of nanocrystals in biological detection. Nat Biotechnol 22: 47–52
5. Zheng J, Ghazani A, Song Q, Mardvani S, Chan W, Wang C (2006) Cellular imaging and surface marker labeling of hematopoietic cells using quantum dot bioconjugates. Lab Hematol 12:4–8
6. Muller-Borer B, Esch G, Aldina R, Woon W, Fox R, Bursac N, Hiller S, Maeda N, Shepherd N, Jin JP, Hutson M, Anderson P, Kirby ML, Malouf NN (2012) Calcium dependent CAMTA1 in adult stem cell commitment to a myocardial lineage. PLoS One 7:e38454
7. Muller-Borer BJ, Cascio WE, Esch GL, Kim HS, Coleman WB, Grisham JW, Anderson PA, Malouf NN (2007) Mechanisms controlling the acquisition of a cardiac phenotype by liver stem cells. Proc Natl Acad Sci U S A 104: 3877–3882
8. Muller-Borer BJ, Cascio WE, Anderson PA, Snowwaert JN, Frye JR, Desai N, Esch GL, Brackham JA, Bagnell CR, Coleman WB, Grisham JW, Malouf NN (2004) Adult-derived liver stem cells acquire a cardiomyocyte structural and functional phenotype ex vivo. Am J Pathol 165:135–145
9. Wade MH, Trosko JE, Schindler M (1986) A fluorescence photobleaching assay of gap junction mediated communication between human cells. Science 232:525–528
10. Caplan AI (1991) Mesenchymal stem cells. J Orthop Res 9:641–650

Chapter 12

In Vitro Approaches to Assessing the Toxicity of Quantum Dots

Ryan S. McMahan, Vivian Lee, William C. Parks, Terrance J. Kavanagh, and David L. Eaton

Abstract

Advances in nanotechnology have produced a new class of fluorescent nanoparticles known as quantum dots (Qdots). Compared with organic dyes and fluorescent proteins, Qdots offer several unique advantages in terms of spectral range, brightness, and photostability. Relative to other imaging modalities, optical imaging with Qdots is highly sensitive, quantitative, and capable of multiplexing. Thus, Qdots are being developed for a wide range of applications, including biomedical imaging. Qdot production has also emerged in a number of industrial applications, such as optoelectronic devices and photovoltaic cells. This widespread development and use of Qdots has outpaced research progress on their potential cytotoxicity, engendering major concerns surrounding occupational, environmental, and diagnostic exposures. Given the extensive physicochemical heterogeneity of Qdots (size, charge, chemical composition, solubility, etc.), high-throughput in vitro cytotoxicity assays represent a feasible means of determining effects of multiple variables and can inform design of lower-throughput in vivo cytotoxicity studies. Here, we describe the application of two commonly used assays, lactate dehydrogenase (LDH) and 3-(4,5-dimethylthiazol-2-yl)-5-(3-carboxymethoxyphenyl)-2-(4-sulfophenyl)-2H-tetrazolium (MTS), for detection of Qdot-induced cytotoxicity.

Key words Quantum dots, Nanomaterials, Cytotoxicity, In vitro, Cell culture, LDH, MTS, MTT

1 Introduction

Semiconductor quantum dots (Qdots) are novel nanoparticles (~2–100 nm) that have recently received significant attention because their unique photochemical and photophysical properties hold promise for a number of commercial applications including optoelectronics, counterfeiting inks, photovoltaics, and biomedical imaging. Qdots have recently become broadly available to the scientific community through several commercial sources, and many researchers are using Qdots as fluorescence imaging probes because their spectral properties are superior to traditional organic fluorophores [1–5]. Qdots are synthesized with a heavy metal core, typically composed of cadmium selenide (CdSe) or cadmium telluride (CdTe).

Adriana Fontes and Beate Saegesser Santos (eds.), *Quantum Dots: Applications in Biology*, Methods in Molecular Biology, vol. 1199, DOI 10.1007/978-1-4939-1280-3_12, © Springer Science+Business Media New York 2014

Another semiconductor, such as ZnS (zinc sulfide), is usually grown over the core to reduce toxicity and improve biocompatibility. Many groups have further modified Qdots with secondary coatings such as mercaptopropionic acid or polyethylene glycol (PEG), which can prevent aggregation, maintain photoluminescent properties, and provide a platform for other ligands.

Public health concerns have been expressed regarding the biocompatibility and toxicity of Qdots, and this has been primarily focused on their potential to degrade in vivo, thus releasing cadmium, selenium, or other toxic metals [6–9]. In addition, many studies of nanoparticle toxicity have focused on their ability to induce oxidative stress and/or free radical-based cellular injury [10–15], and some Qdots have been shown to cause oxidative stress in vivo in an invertebrate model [16]. In recent reviews of Qdot toxicity [7, 8, 17], the adverse effects of Qdots were attributed not only to release of heavy metal constituents, but to many factors, including electronic structure, free radical generation, and in some cases the material used to cap or modify the Qdot core [18, 19] (ZnS, mercaptoacetic acid, etc.). These surface modifications may themselves be problematic and might lead to undesirable effects such as thrombosis [20], or off target accumulation by reticuloendothelial cells (primarily macrophages and dendritic cells) in the liver, spleen, and lymph nodes [8, 21]. Because so many factors influence Qdot toxicity, including cell type, in vitro assays offer a practical means to test multiple modifications and doses in a high-throughput manner. In addition, Yong et al. have highlighted the importance of in vitro assays for predetermining biocompatibility and putative cytotoxicity of Qdots prior to in vivo testing and validation [22].

The MTS assay is one of the most commonly used methods to assess cell viability and cytotoxicity. This colorimetric assay measures the activity of cellular enzymes in reduction of MTS or other related tetrazolium salts, such as MTT (3-(4,5-dimethylthiazol-2-yl)-2,5-diphenyltetrazolium bromide) to formazan, which produces a purple color. Reduction of MTS requires nicotinamide adenine dinucleotide phosphate (NADPH) dependent oxidoreductive enzymes that are located in the cytosol. Thus, under defined conditions, the amount of purple color produced is directly proportional to the number of active mitochondria and viable cells present. In this chapter, we describe how this common assay can be modified to assess cytotoxicity induced by Qdots in cultured cells.

Measuring release of lactate dehydrogenase (LDH) is also a commonly used method to assess cell membrane integrity and cell viability. LDH is a stable cytosolic enzyme that functions to catalyze the interconversion of lactate and pyruvate concomitantly with the oxidation and reduction of nicotinamide adenine dinucleotide (NADH and NAD^+). LDH plays an important role in carbohydrate metabolism, and at least one of its five isoforms is expressed in most

tissues and cells. Upon loss of membrane integrity following tissue death, LDH is released into serum or in the case of cultured cells, into the media. In this chapter, we describe how this commonly used method can be applied to Qdot-treated cells in culture. It should be noted that the assays in this chapter measure cytotoxicity and not genotoxicity, a distinct term that refers to the ability to cause DNA damage. Genotoxicology, which can be evaluated with assays such as the Ames test, comet assay, and micronucleus assay, is increasingly recognized as another important area of study for assessing the public health risk of nanomaterials [23, 24]. Indeed, a number of recent publications have demonstrated that specific types of quantum dots can induce DNA damage [25–28].

2 Materials

2.1 Cell Culture

1. Adherent cell line of choice.
2. Media: Use standard media for cell type of interest. Store at 4 °C and warm to room temperature or 37 °C before culturing cells.
3. Serum for standard media for cell type of interest (e.g., fetal bovine serum): Heat-inactivate serum for 30 min at 56 °C before addition to media (*see* **Note 1**).
4. Sterile 96-well tissue culture treated plates (flat bottom with lid).
5. Sterile-top pre-sterilized vacuum-driven disposable bottle top filter.
6. Trypan blue solution 0.4 %.
7. Hemocytometer.

2.2 Qdot Preparation

1. Quantum dots.
2. Vortex.
3. 0.20–0.22 μm pore filter (syringe or vacuum-driven bottle top).

2.3 MTS Assay

1. Promega CellTiter 96® AQueous One Solution Cell Proliferation Assay (MTS) kit.
2. Orbital shaker.
3. Microplate reader.
4. Swinging bucket rotor with microplate capacity.
5. 200 μL multichannel pipette.
6. 96-well microplate.

2.4 LDH Assay

1. Promega CytoTox96® Non-Radioactive Cytotoxicity Assay kit.
2. Sterile 1× PBS (*see* **Note 2**).
3. Tissue culture-grade bovine serum albumin (BSA).

3 Methods

All preparation and handling of Qdots and suspensions/media containing Qdots should be performed in a biosafety cabinet while wearing appropriate personal protective equipment to minimize risk of inhalation or skin exposure (*see* **Note 3**). Cells should be cultured in sterile, tissue culture-treated plates in a standard, high-efficiency particulate absorption (HEPA)-filtered tissue culture incubator at 37 °C with 5 % CO_2, or according to standard culturing conditions for the cell type.

3.1 Seeding Cells

1. Prepare fresh media for the cell type of interest, using only sterile, endotoxin-free reagents. Before addition to the media, heat-inactivate serum for 30 min at 56 °C to eliminate background enzymatic activity (*see* **Note 1**).
2. Seed cells at a density of 50,000 cells/cm^2 or according to standard culturing conditions for the cell type.
3. Before performing experiments with Qdots, monitor cell growth, viability, and generation. Determine baseline cell viability by Trypan blue exclusion.
4. Plate cells onto multi-well, tissue culture-treated plates and attempt to distribute evenly within each well (Fig. 1). Ninety six-well plates are recommended for ease of use with the MTS

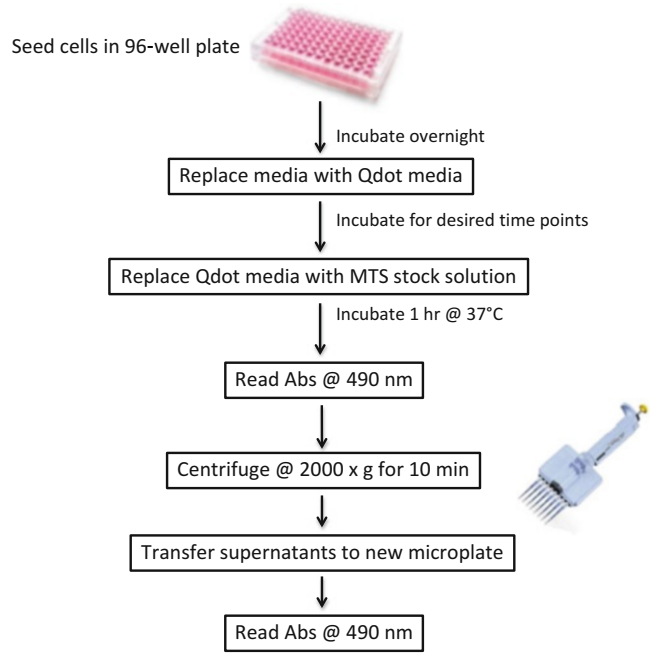
Seed cells in 96-well plate
Incubate overnight
Replace media with Qdot media
Incubate for desired time points
Replace Qdot media with MTS stock solution
Incubate 1 hr @ 37°C
Read Abs @ 490 nm
Centrifuge @ 2000 x g for 10 min
Transfer supernatants to new microplate
Read Abs @ 490 nm

Fig. 1 Workflow of MTS assay for determining Qdot effects on mitochondria activity and cell viability

and LDH assays. Carefully transfer the plates to the incubator to avoid clumping of cells in the center or periphery of the wells. Incubate for 24 h to allow the cells to adhere.

3.2 Preparation of Qdots

1. Vortex the stock suspension of Qdots at high speed for 2–3 min to homogenize the mixture and reduce aggregation. Proceed immediately to the next step.
2. Immediately after vortexing, pipet the Qdot stock suspension for dilution in fresh media to the highest dose that will be used for the experiment (*see* **Note 4**).
3. Sterile-filter the Qdot-containing media through a 0.20–0.22 μm-pore filter attached to a sterile syringe (*see* **Note 5**). For volumes > 50 mL, use a disposable sterile filter system. This filtration will further break up or remove Qdot aggregates.
4. Prepare suspensions of Qdot media for each dose to be tested in the experiment. Invert the tubes several times immediately before pipetting to ensure that the Qdots remain well mixed.
5. Aspirate regular media from each well and gently add fresh media containing Qdots. For negative controls, add fresh media without Qdots. Each treatment should be performed in triplicate or quadruplicate wells.

3.3 MTS Assay

To reduce Qdot interference with the MTS assay, we have modified the protocol from the Promega CellTiter 96® AQueous One Solution Cell Proliferation Assay (MTS) kit.

1. Thaw the Cell Titer 96® AQueous One Solution Reagent from an aliquoted source immediately prior to use. Make a stock solution by combining cell culture medium (100 μL per well per number of wells) and MTS reagent (20 μL per well × number of wells). Remove the original cell culture supernatant (containing the Qdots) from the wells and replace with 120 μL of the stock solution containing MTS reagent directly to each well (Fig. 1).
2. Incubate the 96-well plates for 60 min at 37 °C in a humidified, 5 % CO_2 atmosphere to allow full color development.
3. After incubation, shake the plate for 5 s in the plate reader or a shaker before formazan absorbance is measured at 490 nm by using a microplate reader (e.g., Bio-Tek, Winooski, VT). Save the raw data for reference. After reading the plate, centrifuge the same plate at 2,000 × *g* for 10 min to spin down the Qdot particles in the wells, then transfer 100 μL supernatant using a multichannel pipette (one row at a time) from each well to a new microplate.
4. Spin the new plate at 1,000 × *g* for 3 min to remove bubbles in the wells (*see* **Note 6**). Read the new plate at 490 nm; the data

will be used for data analysis. The amount of colored product formed is proportional to the number of live cells in culture without Qdot interference.

5. Data analysis: Data are expressed as % cell viability. Use mean absorbance at 490 nm of non-exposed cells (control cells) as the reference value for calculating 100 % cellular viability. If x = mean value for control cells then the % cellular viability for samples (s) is calculated using the following equation: $s = (\text{mean value of sample}/x) \times 100$.

3.4 LDH Assay

To reduce Qdot interference with the LDH assay, we have modified the protocol from the Promega CytoTox96® Non-Radioactive Cytotoxicity Assay kit. Perform all experimental and control reactions in triplicate or quadruplicate wells.

1. Prepare medium with 10× Lysis Solution (from Promega CytoTox96® Non-Radioactive Cytotoxicity Assay kit) for the maximal cell death wells: 10 µL Lysis Solution (9 % Triton X-100) per 100 µL culture medium (*see* **Note 7**). Replace the regular culture medium in these wells with lysis medium 45 min before Qdot treatment endpoint (Fig. 2).
2. Prepare positive control: Add 2 µL LDH positive control to 10 mL sterile PBS with 1 % BSA. This solution should be made fresh for each assay and kept on ice.

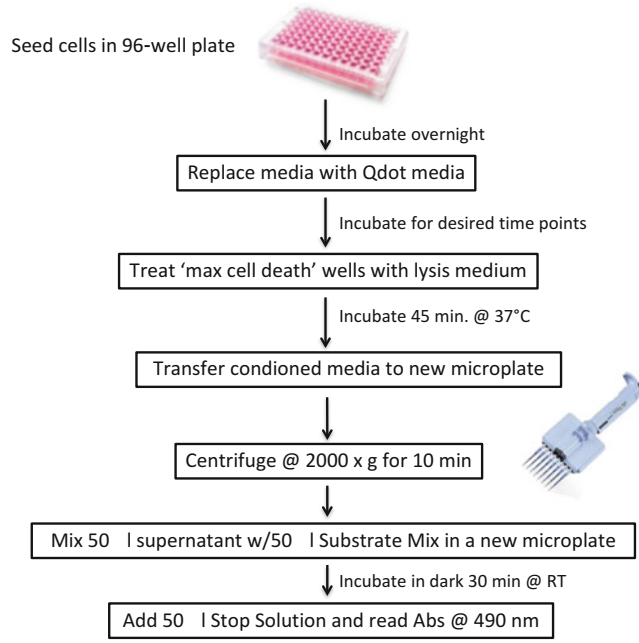
Seed cells in 96-well plate
Incubate overnight
Replace media with Qdot media
Incubate for desired time points
Treat 'max cell death' wells with lysis medium
Incubate 45 min. @ 37°C
Transfer condioned media to new microplate
Centrifuge @ 2000 x g for 10 min
Mix 50 l supernatant w/50 l Substrate Mix in a new microplate
Incubate in dark 30 min @ RT
Add 50 l Stop Solution and read Abs @ 490 nm

Fig. 2 Workflow of LDH assay for determining Qdot effects on cell membrane integrity and cell viability

3. Prepare volume control solution (10 μL Lysis Solution in 100 μL culture medium per well). This control will correct for changes in media volume, specifically the reduced serum present in the maximal death wells.
4. Collect supernatants after Qdot treatment from the original 96-well plate and transfer to a new 96-well microplate using a multichannel pipette. Centrifuge at 2,000 × *g* for 10 min to pellet the cell debris and Qdots from the supernatant.
5. After centrifugation, transfer 50 μL of the supernatant from the wells to a new 96-well microplate. Supernatants from untreated (negative control) and maximal death wells should be included on the same microplate as those from Qdot-treated cells. To correct for any residual LDH activity in the media serum or interference by phenol red, add 50 μL of regular culture medium to a set of wells to be used for blanks/normalization. Add 50 μL of the LDH positive control solution to a set of wells for a positive control to ensure that LDH activity is detectable.
6. Thaw Assay Buffer and reconstitute 1 vial of Substrate Mix by adding 12 mL Assay Buffer and mixing by pipet.
7. Add 50 μL of reconstituted Substrate Mix to each well and incubate at room temperature in dark for 30 min.
8. Add 50 μL of Stop Solution (1 M acetic acid) to each well. Centrifuge at 1,000 × *g* for 3 min to remove bubbles (*see* **Note 6**).
9. Record absorbance at 490 nm on microplate reader.
10. Subtract blank absorbance from all samples except the maximal death wells.
11. Subtract the volume control absorbance from the maximal death wells.
12. Calculate % cell death using the following formula: % cytotoxicity = (experimental OD_{490}–untreated OD_{490})/max death $OD_{490} \times 100$, where OD_{490} is optical density or absorbance at 490 nm.

4 Notes

1. Use of serum-free media or low-protein serum alternatives is not recommended as it can cause many Qdot preparations to aggregate and prevent passage through a sterile filter (unpublished data). Resistance encountered during plunging with a syringe filter is indicative of such aggregation. For experiments that require an absence of serum, it is recommended that Qdot particle size in the experimental media be empirically determined in advance of cytotoxicity assays.

2. The following PBS formulation is recommended: 0.2 g/L KCl, 8.0 g/L NaCl, 0.2 g/L KH_2PO_4, and 1.15 g/L Na_2HPO_4, dissolved in dH_2O and filter-sterilized.
3. Cells or media exposed to Qdots should be disposed as hazardous waste and handled according to institutional guidelines.
4. Qdot dose should be determined empirically as Qdot uptake and subsequent effects vary significantly depending on cell type and physicochemical properties of the Qdots. In most primary cells, 10–80 nM doses of polymer-coated CdSe ZnS Qdots are generally not cytotoxic.
5. To account for loss of media during sterile filtration, prepare Qdot media in a volume at least 15 % in excess of the total required volume for the experiment.
6. Remaining bubbles may be manually popped with a sterile small-gauge needle.
7. Freeze–thaw lysis may be used as an alternative to Lysis Solution, in which case volume correction controls are not necessary.

References

1. Azzazy HME, Mansour MMH, Kazmierczak SC (2007) From diagnostics to therapy: prospects of quantum dots. Clin Biochem 40:917–927
2. Jakobs S, Subramaniam V, Schönle A, Jovin TM, Hell SW (2000) EFGP and DsRed expressing cultures of Escherichia coli imaged by confocal, two-photon and fluorescence lifetime microscopy. FEBS Lett 479:131–135
3. Pepperkok R, Squire A, Geley S, Bastiaens PI (1999) Simultaneous detection of multiple green fluorescent proteins in live cells by fluorescence lifetime imaging microscopy. Curr Biol 9:269–272
4. Gao X et al (2005) In vivo molecular and cellular imaging with quantum dots. Curr Opin Biotechnol 16:63–72
5. Ghasemi Y, Peymani P, Afifi S (2009) Quantum dot: magic nanoparticle for imaging, detection and targeting. Acta Biomed 80:156–165
6. Derfus AM, Chan WCW, Bhatia SN (2004) Probing the cytotoxicity of semiconductor quantum dots. Nano Lett 4:11–18
7. Rzigalinski BA, Strobl JS (2009) Cadmium-containing nanoparticles: perspectives on pharmacology and toxicology of quantum dots. Toxicol Appl Pharmacol 238:280–288
8. Pelley JL, Daar AS, Saner MA (2009) State of academic knowledge on toxicity and biological fate of quantum dots. Toxicol Sci 112:276–296
9. Chen N et al (2012) The cytotoxicity of cadmium-based quantum dots. Biomaterials 33:1238–1244
10. Green M, Howman E (2005) Semiconductor quantum dots and free radical induced DNA nicking. Chem Commun 7:121–123
11. Ipe BI, Lehnig M, Niemeyer CM (2005) On the generation of free radical species from quantum dots. Small 1:706–709
12. Cho SJ et al (2007) Long-term exposure to CdTe quantum dots causes functional impairments in live cells. Langmuir 23:1974–1980
13. Madl AK, Pinkerton KE (2009) Health effects of inhaled engineered and incidental nanoparticles. Crit Rev Toxicol 39:629–658
14. Xia T, Li N, Nel AE (2009) Potential health impact of nanoparticles. Annu Rev Public Health 30:137–150
15. Nel A, Xia T, Mädler L, Li N (2006) Toxic potential of materials at the nanolevel. Science 311:622–627
16. Gagne F et al (2008) Ecotoxicity of CdTe quantum dots to freshwater mussels: impacts on immune system, oxidative stress and genotoxicity. Aquat Toxicol 86:333–340
17. Bottrill M, Green M (2011) Some aspects of quantum dot toxicity. Chem Commun (Camb) 47:7039–7050
18. Clift MJ et al (2011) Quantum dot cytotoxicity in vitro: an investigation into the cytotoxic

effects of a series of different surface chemistries and their core/shell materials. Nanotoxicology 5:664–674

19. Hoshino A, Hanada S, Yamamoto K (2011) Toxicity of nanocrystal quantum dots: the relevance of surface modifications. Arch Toxicol 85:707–720
20. Geys J et al (2008) Acute toxicity and prothrombotic effects of quantum dots: impact of surface charge. Environ Health Perspect 116:1607–1613
21. Dobrovolskaia MA, McNeil SE (2007) Immunological properties of engineered nanomaterials. Nat Nanotechnol 2:469–478
22. Yong KT et al (2013) Nanotoxicity assessment of quantum dots: from cellular to primate studies. Chem Soc Rev 42:1236–1250
23. Singh N et al (2009) NanoGenotoxicology: the DNA damaging potential of engineered nanomaterials. Biomaterials 30:3891–3914
24. Doak SH, Manshian B, Jenkins GJ, Singh N (2012) In vitro genotoxicity testing strategy for nanomaterials and the adaptation of current OECD guidelines. Mutat Res 745: 104–111
25. Aye M et al (2013) Genotoxic and mutagenic effects of lipid-coated CdSe/ZnS quantum dots. Mutat Res 750:129–138
26. Galeone A et al (2012) In vivo assessment of CdSe-ZnS quantum dots: coating dependent bioaccumulation and genotoxicity. Nanoscale 4:6401–6407
27. Tang W et al (2012) The cadmium-mercaptoacetic acid complex contributes to the genotoxicity of mercaptoacetic acid-coated CdSe-core quantum dots. Int J Nanomedicine 7:2631–2640
28. Khalil WK, Girgis E, Emam AN, Mohamed MB, Rao KV (2011) Genotoxicity evaluation of nanomaterials: DNA damage, micronuclei, and 8-hydroxy-2-deoxyguanosine induced by magnetic doped CdSe quantum dots in male mice. Chem Res Toxicol 24: 640–650

Chapter 13

Basics for the Preparation of Quantum Dots and Their Interactions with Living Cells

Xiue Jiang, Jing Bai, and Tiantian Wang

Abstract

A study of the interactions between nanoparticles and living cells is invaluable in understanding the nano-biological effect and the mechanism of cellular endocytosis. Here we describe two methods for the preparation of semiconductor quantum dots with different physiochemical properties. Furthermore, we describe how to study the interaction of the two quantum dots with living HeLa cells and red blood cells with confocal microscopy.

Key words Semiconductor quantum dots, Confocal microscopy, Living HeLa cells, Red blood cells, Nano–cell interaction

1 Introduction

The use of engineered nanoparticles in medical, cosmetic, or food products has been rapidly expanding, which inevitably increases the chance of human exposure to nanoparticles. Nanoparticles can enter the human body by inhalation, ingestion, and dermal exposure [1]. Their small size enables them to penetrate physiological barriers and invade in living organisms, which is useful to nanomedicine, such as diagnose and drug delivery [2, 3], but may also lead to adverse health effects [4, 5]. Therefore, a deep understanding of the interactions of nanoparticles with living cells and organisms is indispensable for their safe and beneficial use while avoiding possible biological hazards.

Upon nanoparticle exposure, cells incorporate them either by endocytosis, i.e., active going with vesicle formation, or by passive penetration, generally driven by concentration gradient [6–11]. Fluorescence particles provide us the chance to visualize the uptake process and intracellular tracking of cargo combining confocal microscopy. Owing to their narrow emission spectra, size-tunable photoluminescence, high molar extinction coefficients, high fluorescence quantum yields, and exceptional brightness and

Adriana Fontes and Beate Saegesser Santos (eds.), *Quantum Dots: Applications in Biology*, Methods in Molecular Biology, vol. 1199, DOI 10.1007/978-1-4939-1280-3_13, © Springer Science+Business Media New York 2014

photostability, colloidal semiconductor quantum dots (QDs) are good candidates used to in situ investigate the interactions of nanoparticles with living cells for a long time. A key challenge for application of QDs in biology is to create a polar surface on the nonpolar core/shell nanocrystals to make them dispersed in biological buffer or medium. Water-dispersed, thiolated molecules are among the most commonly used ligands for this purpose [12].

Here we describe two methods for preparation of QDs [13, 14]. One is a facile one-pot synthesis of mercaptosuccinic acid-capped CdTe QDs (MSA-QDs) and the other is for CdSe/ZnS core/shell QDs capped with the small, zwitterionic thiol ligand d-penicillamine (DPA-QDs) prepared by chemical exchange. Then, we also describe how to grow living HeLa cells and how to manipulate the red blood cells [13–15]. Meanwhile, we describe how to study the interaction of QDs with living cells by optical microscopy. These detailed practical procedures will provide basic knowledge for a researcher in the field of nano–cell interaction.

2 Materials

Prepare all solutions using ultrapure water (prepared by purifying deionized water to attain a sensitivity of 18 MΩ cm at 25 °C) and analytical grade reagents. Prepare all reagents at room temperature (25 °C) and store at 4 °C (unless indicated otherwise). Diligently follow all waste disposal regulations when disposing waste materials. Materials related to the cell cultures were all prepared in superclean bench.

2.1 QD Preparation Components

2.1.1 Preparation Components for CdTe

1. 0.04 M Cadmium chloride ($CdCl_2$) solution: Weigh 70 mg of $CdCl_2$ in pan paper and transfer to a 15 mL centrifugal tube. Then add 9.55 mL of water to dissolve the solid (*see* **Note 1**).
2. 0.01 M Sodium telluride (Na_2TeO_3) solution: Weigh 10 mg of Na_2TeO_3 power in pan paper and transfer to a 7 mL centrifugal tube. Then add 4.51 mL of water to dissolve the solid (*see* **Note 1**).

2.1.2 Preparation Components for CdSe/ZnS QDs

1. The injection solution 1 (selenium solution): Weigh 0.064 g of selenium and transfer to a 7 mL centrifugal tube. Then add trioctylphosphine (TOP) to a volume of 4 mL. Mix and dissolve under the ultrasound.
2. Cadmium oxide (CdO) hexadealamine (HAD) trioctylphosphine oxide (TOPO). Store at 4 °C.
3. The injection solution 2 (0.05 M Zn injection solution): Weigh 0.079 g of zinc distearate and ultrasound dissolve with the mixture of 1 mL oleic acid (OA) plus 1.5 mL oleyl amine (OLA).

The injection of 0.05 M sulphur (S) solution: Weigh 0.004 g of sulphur, and dissolve with 2.5 mL of oleyl amine (OLA).

4. DPA solution: Weigh 40 mg D-penicillamine (DPA) and transfer to a 20 mL centrifugal tube containing about 15 mL of 2-propanol, and adjust pH to 12.5 with tetramethylammonium hydroxide pentahydrate (TMAHP).
5. The Tris buffer solution: 5 mM Tris–HCl, pH 10. Weigh 0.0606 g Tris(hydroxymethyl)aminomethane (Tris) and add water to a volume of 50 mL. Mix and adjust pH to 10 with chloride acid (HCl). Make up to 100 mL with water. Store at 4 °C.

2.2 Materials for Cell Culture

1. Phosphate buffer solution (PBS): PBS was prepared by weighing 144 mg of Potassium phosphate monobasic (KH_2PO_4), 9 g of sodium chloride (NaCl), and 795 mg of heptahydrated sodium phosphate ($Na_2HPO_4{\cdot}7H_2O$) and transferring them to 1 L deionized water in a glass beaker. The pH value should be adjusted to 7.4 by 0.1 M HCl and 0.1 M sodium hydroxide (NaOH). Then the PBS was filtered with 0.22 μm filtration membrane and was further sterilized in autoclave at 121 °C for 20 min. The sterilized PBS was stored at 4 °C.
2. Cell culture medium: 500 mL of Dulbecco's modified Eagle medium was supplemented with 50 mL of fetal bovine serum (FBS), 5 mL of l-glutamine, and 5 mL of penicillin/streptomycin and stored at 4 °C (*see* **Note 2**).
3. Versen solution: 8 g of NaCl was mixed with 0.2 g of potassium chloride (KCl), 2.57 g of Na_2HPO_4, 0.29 g of KH_2PO_4, and 0.5 g of ethylenediaminetetraacetic acid (EDTA), then was dissolved to 1 L with ultrapure water, and autoclaved at 121 °C for 20 min.
4. Trypsin/Versen solution: 20 mL of Trypsin (2.5 %) (Biochrom Ltd.) was mixed with 180 mL of Versen solution, and 200 mL of Trypsin/Versen solution was stored at −20 °C.
5. Human blood samples are freshly collected from multiple healthy adult volunteers in local hospital.

3 Methods

3.1 Synthesis of Mercaptosuccinic Acid-Capped CdTe QDs

1. Mix 4 mL of 0.04 M $CdCl_2$ solution with 50 mL water in a one-necked flask, and add 100 mg of trisodium citrate dehydrate, 1 mL of 0.01 M Na_2TeO_3 solution, and 50 mg of mercaptosuccinic acid (MSA) orderly with stirring. In 5 min, add 100 mg of sodium borohydride ($NaBH_4$) slowly (*see* **Note 3**).
2. In 20 min, when the color of the solution changes to yellow, attach the flask to a condenser and reflux at 100 °C under open-air conditions (*see* **Note 4**).

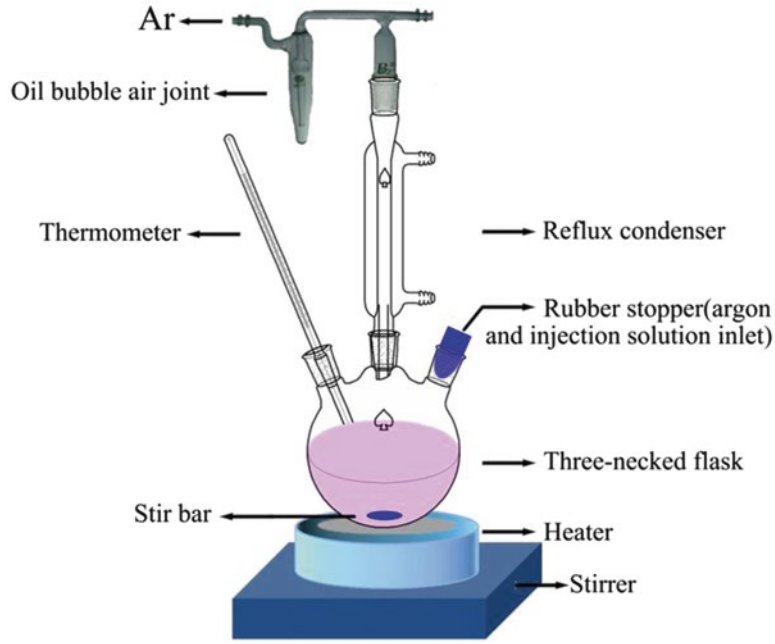

Fig. 1 The schematic drawing of the synthesis of CdSe QD core

3. After refluxing about 90 min, green fluorescence of the mixture will appear under UV light, and with the reflux proceeding, the emission will change from green to yellow, and then orange and red.
4. After the reaction, the mixture was cooled to room temperature. Mix the MSA-QD suspension with ethanol at a volume ratio of 1:3 (QD:ethanol) and separate them by centrifugation at 6,640 × *g* for 20 min. Discard the supernatant liquid and dry the particles in vacuum drying chamber (*see* **Note 5**).

3.2 Synthesis of CdSe Quantum Dots

1. Building reaction device from bottom to up at room temperature, according to Fig. 1: On the magnetic stirrer put three-necked flask under heating, consecutively connected rubber stopper (argon and injection inlet), reflux condenser and thermometer from left to right, and then connected oil bubble air joint above condenser (controlling argon flow rates).
2. Add a mixture of 0.1028 g of CdO and 1.2 g of stearic acid into distillation flask (mixture 1) together with magnetic stirring bar, put the distillation flask into the setup again, and put the thermometer, and argon in the right position (*see* **Note 6**, Fig. 1).
3. Observe the color of the mixture 1, till a clear solution is obtained (190–210 °C). Under magnetic stirring add 3.35 g,

8.66 mmol of TOPO, and 1.65 g, 6.8 mmol of HAD, and increase the temperature to 300 °C (*see* **Note 7**).

4. When the temperature was increased to 300 °C, stop to heat. Inject the solution 1 quickly into this hot solution, and then take 1–2 mL and add to 20 mL cool toluene (one series with three aliquots: toluene 1, toluene 2, toluene 3) (*see* **Note 8**).

3.3 Synthesis of CdSe-ZnS Core–Shell QDs

1. After synthesis for one series including three small aliquots, mix 10 mL of aliquots and 20 mL of acetone for centrifugation for 40 min at 6,640 × *g*. Discard acetone, and redissolve the solid in 5 mL of chloroform, ultrasonic to disperse CdSe QDs completely.
2. Measure absorption spectrum to determine the mean size of CdSe core (see Table 1) and calculate the chemicals for capping process. Take optical density (*O.D.*) value at 350 nm and calculate concentration of QDs, [QDs], using $O.D. = C(\text{abs}) \times [\text{QDs}]$; $C(\text{abs})$ is the absorption cross section for QDs using formula $C(\text{abs}) = (5.501 \times 10^5)\ a^3/\text{cm}$, where a is the QD radius in cm; from [QDs], you get the number of particles (*see* **Note 9**).
3. The amount of Zn and S precursors needed for capping CdSe of a given size was calculated by the required increase in volume: $4\pi/3(r_c + n \cdot r_m)^3 - 4\pi/3[r_c + (n-1) \cdot r]^3$, where r_c is the CdSe core radius, r_m is the thickness of one of the monolayers of ZnS

Table 1
The relationship of the maximum adsorption peak position and the mean size of CdSe QDs

	A[X]	B[Y]
1	UV–vis wavelength/nm	QD size/nm
2	484	2.1
3	488	2.1
4	516	2.4
5	526	2.6
6	534	2.7
7	542	2.9
8	550	3.1
9	560	3.3
10	566	3.4
11	570	3.5
12	576	3.6

(one monolayer has 0.31 nm), and *n* is the desired number of monolayers (ML). The necessary number of moles of Zn and S was calculated from this volume using the density of ZnS (3.98 g/cm^3). For example, your CdSe is 2.6 nm and shell thickness is 3 ML, so 0.93 nm from every side. Total diameter is 4.46 nm, and then you can calculate the required increase in volume of ZnS (*see* **Note 10**).

4. After calculation, the injection solution 2 was prepared. The corresponding amount of uncapped CdSe was mixed with 6 mL of OLA, heating until chloroform disappears (70–80 °C); reflux the mixture and heat to 150–170 °C (*see* **Note 11**).
5. Add the sulphur solution with 1 mL injector, very slowly stir for more than 15 min. Take out aliquot and check with UV–vis (*see* **Note 12**).
6. Add the injection of solution 2, and stir for 15 min again.
7. Repeat **steps 6** and **7** three times.
8. Stop the reaction, take out the core/shell QD solution (about 5 mL), mix with acetone or MetOH, and then centrifugate for 40 min (6,640 × *g*).
9. Discard the supernatant solution, and redissolve the solid in chloroform.

3.4 Ligand Exchange of CdSe-ZnS Core/Shell QDs

1. The flask was purged with N_2, then 0.25 mg of OLA-coated CdSe/ZnS QDs and DPA solution were added, and the reaction mixture was left stirring at 60–70 °C for 15 min (*see* **Note 13**).
2. After the end of the reaction, the mixture was cooled to room temperature. The exchanged hydrophilic DPA-capped QDs were precipitated with ethyl acetate (V/V = 1:3) and the solution was centrifuged at 6,640 × *g* for 45 min. The supernatant was discarded and the pellet was redissolved in 5 mM Tris buffer solution. This procedure was repeated at least three times.

3.5 Interaction of MSA-QDs with HeLa Cells

1. HeLa cells were routinely cultured in cell culture medium in 25 cm^2 culture bottle in a humidified incubator at 37 °C, 5 % CO_2.
2. Check cells on the microscope for checking the growth (*see* **Note 14**).
3. Remove the medium from bottle with pipette.
4. Add 5–6 mL PBS to the culture bottle.
5. Rock culture bottle back and forth shortly, and remove the PBS.
6. Add 1 mL of trypsin Versen and rock back and forth (*see* **Note 15**).
7. Incubate the cell culture bottle in the incubator for approximately 5 min at 37 °C, 5 % CO_2.

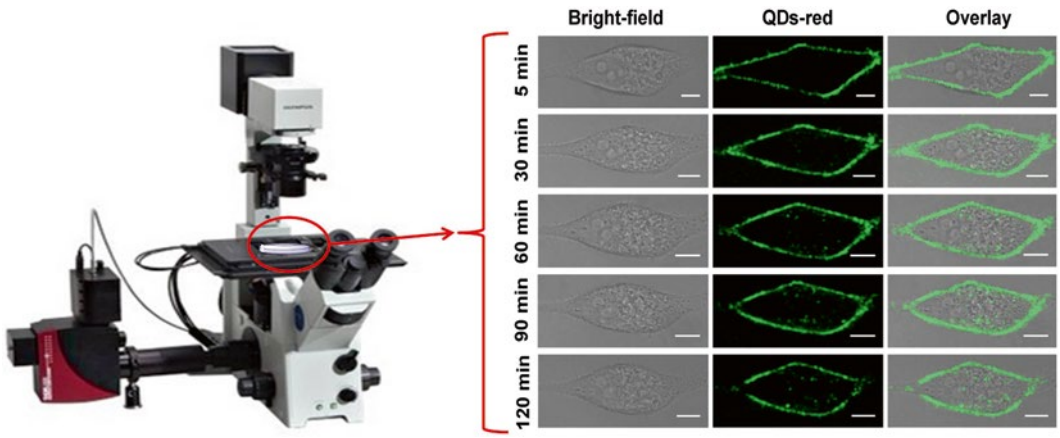

Fig. 2 Scheme of time-dependent QD uptake observed by confocal microscopy. Reproduced from Wang and Jiang [13] with permission from American Chemical Society

8. In the meantime, prepare new bottles (fill with 9.5 mL medium).
9. Take bottle out of the incubator and check if cells are detached with microscopy. If not, incubate further or shake slightly. When cells are detached, rinse them with 4 mL medium (*see* **Note 16**).
10. Take 0.5 mL of 4 mL medium and put them into each of the prepared new bottles for routine culture.
11. Take 50 μL cell solution into 1 mL cell culture medium and seed them in a 35 mm tissue culture dish. The dish is cultured in a humidified incubator at 37 °C, 5 % CO_2, overnight.
12. Add the culture dish onto the microscope stage to focus the cells.
13. Discard the culture media and wash the cells three times with PBS. For nanoparticle uptake experiments, cells are incubated with 800 μL of MSA-QDs at a concentration of 8 μg/mL in PBS. Nanoparticles are excited with an argon ion laser at 488 nm and observed through 505–568 nm emission band-pass filter. The cells were imaged over 2 h at selected times using a confocal laser scanning fluorescence microscope and every image should be averaged 16 times to reduce the background interference (*see* **Note 17**, Fig. 2).

3.6 Interaction of DPA-QDs with Red Blood Cells

1. Centrifuge the whole blood at 266 × *g* for 3 min and discard the top layer of cells to remove the plasma, buffy coat. Then the packed cells should be washed five times with sterile PBS by centrifugation.
2. Mix 50 μL of packed cells that have been washed five times with 5 mL PBS, and dilute 300 μL of the stocked solution into 1 mL PBS, followed by centrifugation and discarding the

supernatant. Then dilute the pellet to 150 μL with DPA-QDs at a concentration of 10 nM in PBS. The mixture is kept in a humidified incubator at 37 °C and 5 % CO_2 for 1 h (or 4 h).

3. After incubation with DPA-QDs for 1 h (or 4 h), the cells are separated by centrifugation at 266 × *g* for 3 min and washed three times with PBS. Then dilute the cells into 300 μL PBS and introduce 100 μL of the cell solution into the channel of a sandwich sample cell. After 20 min for the cells to adhere to the surface of the bottom glass slide, the channel was rinsed with fresh portions of buffer to remove nonadhering cells.
4. The cells were imaged using a confocal laser scanning fluorescence microscope. Nanoparticles were excited at 488 nm and observed through a 550–650 nm emission band-pass filter.

4 Notes

1. The preparations of the stock solutions are not so rigid. It is alright only if the ratio is correct.
2. All supplemented chemicals should be filtered with 0.22 μm filtration membrane.
3. The adding of sodium borohydride will produce a yellow solution. So this progress must be slow.
4. The refluxing progress should be mild and the temperature is not very strict. Just keeping a few of small bubbles is OK. If the refluxing is intense, the QDs will grow quickly and the mean sizes of particles are not well distributed.
5. Before mixing the QD suspension with ethanol, the centrifugal tube should be weighed, and after dried in vacuum drying chamber, the centrifugal tube with particles should be weighed again. So the quantity of the particles is known as the difference value. The QDs can be stocked in a determined mass concentration.
6. The CdO must be weighed with the stearic acid. If the separate CdO was poured into flask, CdO can be stuck to the sidewall. Before adding a stir bar, put mixture into flask. Switch on the magnetic stirrer after solid melting. This will prevent fluttering of mixture in the flask.
7. When opening argon, it would be important a small flux, only one or two bubbles from the oil within 10 s.
8. Quickly inject selenium solution into hot solution. Take 1–2 mL, add to 20 mL cool toluene 1, and then take 1–2 mL cool toluene 1 and put into 20 mL cool toluene 2. This helps to form a smaller CdSe core and easily cover ZnS shell.

9. The method of calculating the number of particles:
For example, peak $A = 527$ nm, $d = 2.6$ nm, and $A_{abs} = 0.63$:

$$O.D. = C(\text{abs}) \times [\text{QDs}] = 7.37 \times 10^4 \times [\text{QDs}] = 0.63$$
$$[\text{QDs}] = 8.55 \times 10^{-6}\,\text{M}$$

$$N = 8.55 \times 10^{-6}\,\text{M} \times 6.02 \times 10^{23} = 5.15\,\text{x}\,10^{18} / \text{L} = 5.15 \times 10^{15} / \text{mL}$$

In 5 mL
$N = 5.15 \times 10^{15} / \text{mL} \times 5 = 2.575 \times 10^{16}$

10. Calculating the required increase in volume of ZnS, for 0.05 M injection solution:

1 ML:

V shell per particle: $V_1 = 4\pi/3(r_c + n \cdot r_m)^3 - 4\pi/3[r_c + (n-1) \cdot r_m]^3 = 4\pi/3\ (1.3 \times 10^{-7} + 1.031 \times 10^{-7})^3 - 4\pi/3\ (1.3 \times 10^{-7})^3 = 8.25 \times 10^{-21}\,\text{cm}^3$

V shell total: $V_{1T} = V_1 N = 8.25 \times 10^{-21} \times 2.575 \times 10^{16} = 2.13 \times 10^{-4}\,\text{cm}^3$

Density (ρ) of ZnS 3.98 g/cm^3, and mass of ZnS $M_w = 97$ g/mol:

$$n(\text{ZnS}) = V_{1T} \times \rho / M_w = 2.13 \times 10^{-4}\,\text{cm}^3 \times 3.98\,\text{g} / \text{cm}^3 / 97 = 8.72 \times 10^{-6}\,\text{mol}$$
$$n(\text{Zn}) = 8.72 \times 10^{-6}\,\text{mol}$$
$$n(\text{S}) = 8.72 \times 10^{-6}\,\text{mol}$$

For 0.05 M injection solution:

$$V_{1\text{Zn}} = V_{1\text{S}} = 8.72 \times 10^{-6}\,\text{mol} / 0.05\,\text{mol} / \text{L} = 0.174\,\text{mL}$$

2 ML:

V shell per particle: $V_2 = 4\pi/3(r_c + n \cdot r_m)^3 - 4\pi/3[r_c + (n-1) \cdot r_m]^3 = 4\pi/3\ (1.3 \times 10^{-7} + 2 \times 0.31 \times 10^{-7})^3 - 4\pi/3\ (1.61 \times 10^{-7})^3 = 1.21 \times 10^{-20}\,\text{cm}^3$

V shell total: $V_{2T} = V_2 N = 1.21 \times 10^{-20} \times 2.575 \times 10^{16} = 3.12 \times 10^{-4}\,\text{cm}^3$

Density (ρ) of ZnS 3.98 g/cm^3, and mass of ZnS $M_w = 97$ g/mol:

$$n(\text{ZnS}) = V_{2T} \times \rho / M_w = 3.12 \times 10^{-4}\,\text{cm}^3 \times 3.98\,\text{g} / \text{cm}^3 / 97 = 1.28 \times 10^{-5}\,\text{mol}$$
$$n(\text{Zn}) = 1.28 \times 10^{-5}\,\text{mol}$$
$$n(\text{S}) = 1.28 \times 10^{-5}\,\text{mol}$$

For 0.05 M injection solution:

$$V_{2\mathrm{Zn}} = V_{2\mathrm{S}} = 1.28 \times 10^{-5}\,\mathrm{mol} / 0.05\,\mathrm{mol} / \mathrm{L} = 0.256\,\mathrm{mL}$$

3 ML:

V shell per particle: $V_3 = 4\pi/3(r_c + n \cdot r_m)^3 - 4\pi/3[r_c + (n-1) \cdot r_m]^3 = 4\pi/3(1.3 \times 10^{-7} + 3 \times 0.31 \times 10^{-7})^3 - 4\pi/3(1.92 \times 10^{-7})^3 = 1.68 \times 10^{-20}\mathrm{cm}^3$

V shell total: $V_{3\mathrm{T}} = V_1 N = 8.25 \times 10^{-21} \times 2.575 \times 10^{16} = 4.31 \times 10^{-4}\mathrm{cm}^3$

Density of (ρ) ZnS 3.98 g/cm^3, and mass of ZnS $M_w = 97$ g/mol:

$$n(\mathrm{ZnS}) = V_{3\mathrm{T}} \times \rho / M_w = 4.31 \times 10^{-4}\,\mathrm{cm}^3 \times 3.98\,\mathrm{g} / \mathrm{cm}^3 / 97 = 1.77 \times 10^{-5}\,\mathrm{mol}$$
$$n(\mathrm{Zn}) = 1.77 \times 10^{-5}\,\mathrm{mol}$$
$$n(\mathrm{S}) = 1.77 \times 10^{-5}\,\mathrm{mol}$$

For 0.05 M injection solution:

$$V_{3\mathrm{Zn}} = V_{3\mathrm{S}} = 1.77 \times 10^{-5}\,\mathrm{mol} / 0.05\mathrm{mol} / \mathrm{L} = 0.354\,\mathrm{mL}$$

11. The heating was continued until 130 °C, and the gas peak disappears with smoke appearing, indicating that chloroform evaporated completely. Then the mixture was refluxed and heated to 150–170 °C. Take a little amount of QDs out, dissolve in chloroform, and measure with UV–vis spectrometer to check the characteristics of QDs.
12. Add S solution firstly, and then add Zn solution.
13. The method of calculating the concentration of CdSe-ZnS core/shell: Measure UV–vis spectrum of CdSe/ZnS, take *O.D.* value at 350 nm, and calculate the absorption cross section $C(\mathrm{abs})$ for QDs using the formula $C(\mathrm{abs}) = (5.501 \times 10^{15})\ a^3$/cm, where a is the QDs radius in cm (the expected value, core + shell, you have it in your calculations for capping). Calculate concentration of QDs, [QDs], using $O.D. = C(\mathrm{abs}) \times$ [QDs]; from [QDs], you get the number of particles. You calculate the mass of one particle from the volumes of core and shell (you have them in the calculations for capping), and bulk densities for CdSe and ZnS. Then you calculate the volume of particles as sphere, $4/3\pi\ (r_c)^3$ in cm^3, multiply this by the density of CdSe-ZnS 5.81 g/cm^3, and get mass in grams. Multiply this mass on one particle by the number of particles, and get the mass in 1 mL QD solution.
14. Cells are best passaged when they are growing logarithmically, at 70–80 % confluency.

15. Avoid trypsinizing the cells you are carrying forward too often, since this selects for trypsin-resistant cells and causes the passage count to increase too quickly. Cells should be carried for a maximum of 25 passages (from original stocks). Always do your experiments in a 20-passage window.
16. Cells should be mixed sufficiently.
17. The wavelength of the excitation laser and emission band-pass filter should be selected according to the fluorescence property of the QDs.

Acknowledgments

This work was financially supported by Youth Foundation of China (21105097) and the President Funds of the Chinese Academy of Sciences and Natural Science Foundation of Jilin Province (201215092).

References

1. Love SA, Maurer-Jones MA, Thompson JW et al (2012) Assessing nanoparticle toxicity. Annu Rev Anal Chem 5:181–205
2. Maesaki S (2002) Drug delivery system of anti-fungal and parasitic agents. Curr Pharm Des 8:433–440
3. Lewin M, Carlesso N, Tung CH et al (2000) Tat peptide-derivatized magnetic nanoparticles allow in vivo tracking and recovery of progenitor cells. Nat Biotechnol 18:410–414
4. Andre N, Lutz M, Darrell V et al (2009) Understanding biophysicochemical interactions at the nano-bio interface. Nat Mater 8: 543–557
5. Rocker C, Potzl M, Zhang F et al (2009) A quantitative fluorescence study of protein monolayer formation on colloidal nanoparticles. Nat Nanotechnol 4:577–580
6. Jiang X, Dausend J, Hafner M et al (2010) Specific effects of surface amines on polystyrene nanoparticles in their interactions with mesenchymal stem cells. Biomacromolecules 11:748–753
7. Jiang X, Weise S, Hafner M et al (2010) Quantitative analysis of the protein corona on FePt nanoparticles formed by transferrin binding. J Roy Soc Interface 7:S5–S13
8. Verma A, Stellacci F (2010) Effect of surface properties on nanoparticle–cell interactions. Small 6:12–21
9. Lovrić J, Bazzi HS, Cuie Y et al (2005) Differences in subcellular distribution and toxicity of green and red emitting CdTe quantum dots. J Mol Med 83:377–385
10. Verma A, Uzun O, Hu Y et al (2008) Surface structure-regulated cell membrane penetration by monolayer protected nanoparticles. Nat Mater 7:588–595
11. Choleris E, Little SR, Mong JA et al (2007) Microparticle-based delivery of oxytocin receptor antisense DNA in the medial amygdala blocks social recognition in female mice. Proc Natl Acad Sci U S A 104:4670–4675
12. Breus VV, Heyes CD, Nienhaus GU (2007) Quenching of CdSe/ZnS core/shell quantum dot luminescence by water-soluble thiolated ligands. J Phys Chem C 111:18589–18594
13. Wang TT, Jiang X (2013) Size-dependent stability of water-solubilized CdTe quantum dots and their uptake mechanism by live HeLa cells. ACS Appl Mater Interfaces 5:1190–1196
14. Jiang X, Röcker C, Hafner M et al (2010) Endo- and exo-cytosis of zwitterionic quantum dot nanoparticles by live HeLa cells. ACS Nano 4:6787–6797
15. Wang T, Bai J, Jiang X et al (2012) Cellular uptake of nanoparticles by membrane penetration: a study combining confocal microscopy with FTIR spectroelectrochemistry. ACS Nano 6:1251–1259

Part IV

QDs for Small Animals Applications

Chapter 14

In Vivo Approaches to Assessing the Toxicity of Quantum Dots

David K. Scoville, Christopher M. Schaupp, François Baneyx, and Terrance J. Kavanagh

Abstract

The small size and heavy metal composition of quantum dots (QDs) combined with their growing consumer product and biomedical research applications have generated concern over their safety. In an occupational setting where QD-enabled products are being manufactured, inhalation is a likely route of exposure. Since current research indicates that QDs could cause inflammation and toxicity in the respiratory tract, it is important that a variety of methods be available to further characterize this potential respiratory hazard. This chapter focuses primarily on in vivo methods for modeling the inhalation and assessing the pulmonary toxicity of QDs.

Key words Quantum dots, Bronchoalveolar lavage, Cytospin, Intranasal instillation, Intratracheal instillation, Flow cytometry, Tissue fixation

1 Introduction

Quantum dots (QDs) are a class of nanomaterials known for their fluorescent and semiconductor properties. QDs traditionally consist of a cadmium alloy core (e.g., Cadmium Selenium (CdSe), Cadmium Telluride (CdTe), or CdSeTe), capped with a shell of higher band gap material (e.g., ZnS). QD fluorescence spectra, which are very narrow and cover the visible and near-infrared range, are dependent on the size and composition of the core and capping shells of the particle [1–6]. Capitalizing on their superior quantum yield and resistance to photobleaching, bio-conjugated QDs have been used extensively to fluorescently label intra- and extracellular targets in vitro and have served as drug delivery tools [7–11]. QDs have also been used for in vivo animal imaging primarily in the context of lymph node mapping and tumor antigen labeling and appear to be stable for extended periods of time [12, 13]. Removing the need for external excitation, the use of luciferase conjugation and bioluminescence to achieve auto-excitation of

Adriana Fontes and Beate Saegesser Santos (eds.), *Quantum Dots: Applications in Biology*, Methods in Molecular Biology, vol. 1199, DOI 10.1007/978-1-4939-1280-3_14, © Springer Science+Business Media New York 2014

QDs is a new direction of QD research that improves their clinical utility [14]. However, some of the same characteristics that give QDs unique properties (e.g., nanometer size, heavy metal core, high surface area) also contribute to uncertainty regarding their long-term, potentially deleterious effects on environmental and public health. Such concerns have prevented the introduction of QDs into the clinical setting and into some commercial products where occupational exposure during manufacturing may be a concern. Thus, further investigation of the toxicity of QDs will be critical in determining the fate of this promising nanotechnology.

Numerous studies investigating QD toxicity in vitro have concluded that QDs can be cytotoxic. However, the level of toxicity is dependent on dose, cell type, and surface chemistry [15–20]. In vivo toxicity has also been investigated using intravenous (IV) injection, dermal exposure, intranasal (IN) and intratracheal (IT) instillation (as surrogate techniques for inhalation), and inhalation [21–30]. Intravenous injection is an important route of QD exposure for potential therapeutic applications, such as drug delivery and antibody or nucleic acid conjugation. Injected QDs have been examined for their toxic-kinetic/dynamic profiles and potential systemic toxicity using traditional toxicological endpoints including hematology, clinical chemistry, and histopathology [21, 22, 27–29]. In general, IV administration of QDs has not proven particularly toxic in rodents and nonhuman primates, although thrombogenicity has been observed at high doses [28]. While not yet utilized in published QD toxicity research, retro-orbital injection has been suggested as a more reliable and humane method than tail vein injection for mouse strains with dark skin (e.g., C57BL/6 mice) [31, 32]. Multiple ex vivo studies of QD dermal absorption using porcine or human skin mounted on flow-through diffusion cells have been performed, with varying conclusions [33, 34]. Given the complexity of the integumentary system, questions remain regarding the applicability of these models for in vivo dermal absorption. Of the few in vivo studies of dermal QD absorption that have been performed, research by the National Toxicology Program suggests that polyethylene glycol (PEG)-coated CdSe QDs are able to penetrate dermabraded skin, but importantly, not intact skin of SKH-1 mice [35].

While concerns related to IV and dermal exposures to QDs in the clinical environment are warranted, an important route of exposure that is more likely in occupational settings is inhalation [36]. Importantly, studies employing IN and IT installation in rodents have demonstrated pulmonary injury using endpoints including histological identification of inflammation and granuloma formation in the lung as well as increased levels of inflammatory cytokines, neutrophils, DNA damage, total protein, and LDH in bronchoalveolar lavage fluid (BALF) [23–26, 30]. Excess total protein and LDH in BALF indicate damage to the alveolar-capillary barrier and cytotoxicity.

Since pulmonary toxicity appears to be a sensitive endpoint for assessing QD toxicity, techniques to measure these endpoints will be the main focus in this chapter (Fig. 1). Specifically, bronchoalveolar lavage (BAL) and follow-on analyses of cellular and non-cellular fractions in BALF (including total cell count, cell differential, and detection of inflammatory cells), using techniques such as flow cytometry, the lactate dehydrogenase (LDH) assay, and Bradford assay for total protein, are detailed in Subheading 3. Techniques for embedding tissue in Tissue-Tek® optimal cutting temperature (OCT) compound for cryosectioning and formalin fixation for paraffin embedding and sectioning, both necessary steps for evaluation of tissue pathology, are also covered in detail. Techniques for detection of cytokines and other changes in gene expression are identified in Subheading 3 of this chapter but are not detailed since they are common molecular biology techniques and/or are beyond the scope of this chapter. In addition, methods for measuring the amount of QD constituent metals in tissue, which are important for toxico-kinetics/dynamics of QDs, are noted. Dosing methods that model QD inhalation (i.e., IN and IT instillation) are also outlined in Subheading 3. A recently published study that has used true inhalation of QDs includes a detailed description of the apparatus employed in their delivery [30].

When designing any study, the dose metric is important and with in vivo QD research, there are different ways to report dose. If the metal content of the QDs is known, doses can be expressed in terms of equivalents of constituent metals per body weight (e.g., 6 mg cadmium equivalents/kg body weight). Conversely, if metal quantities are unknown, doses can be expressed as mass or volume of QDs given in a known concentration per animal or per kg bodyweight [25, 27].

This chapter focuses primarily on methods for assessing pulmonary toxicity in vivo in rodent models. An overview of these methods can be seen in Fig. 1.

2 Materials

2.1 Intranasal Instillation of QDs

1. Quantum Dots.
2. Sterile physiological saline (0.9 %) for dispersion of QDs.
3. Vortexer with attachment for tube containing QD solution.
4. Anesthetic (e.g., Ketamine/Xylazine, pentobarbital, Isoflurane, or sodium methohexital) (*see* **Note 1**).
5. Syringe with needle for injectable anesthetics or anesthesia machine for inhalable anesthetic (e.g., Isoflurane).
6. Scale for animal weight (if dosing by body weight).
7. Micropipetter and tips for nasal instillation of QDs.

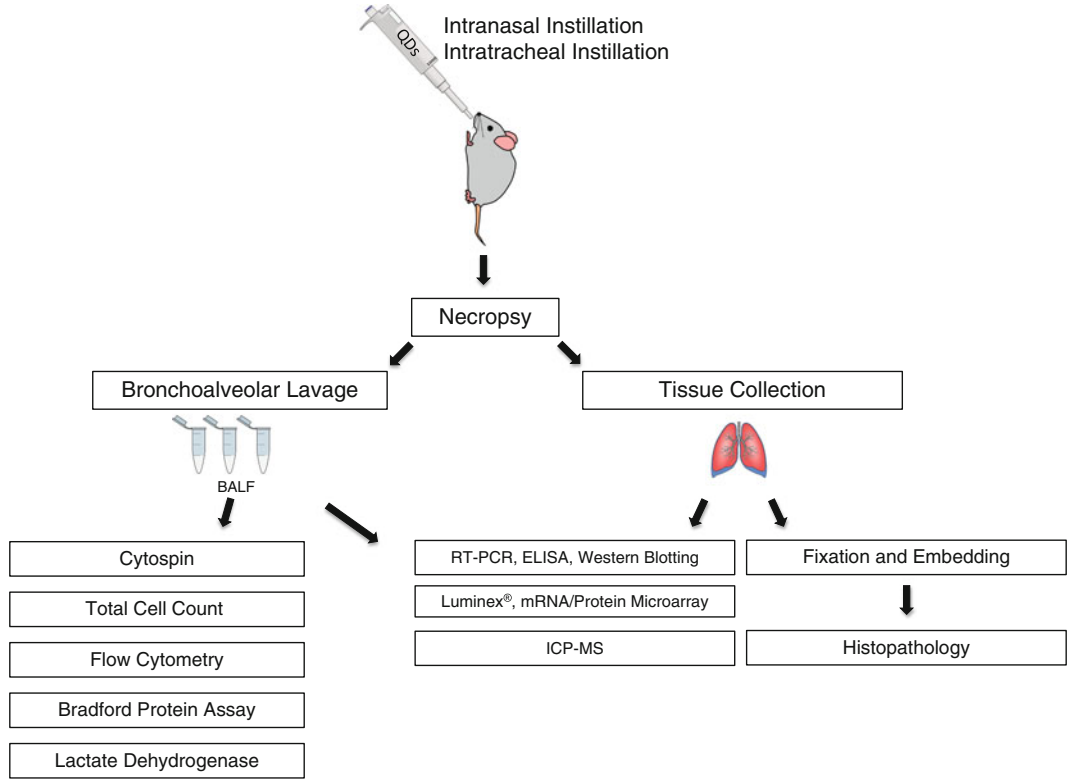

Fig. 1 Evaluating pulmonary toxicity after QDs exposure

2.2 Intratracheal Instillation of QDs

1. Quantum Dots.
2. Sterile phosphate buffered saline (sterile physiological saline at 0.9 %) or sterile deionized water for dispersion of QDs (*see* **Note 2**).
3. Vortexer with attachment for tube containing QD solution.
4. Anesthetic (e.g., Ketamine/Xylazine, pentobarbital, isoflurane, or sodium methohexital) (*see* **Note 1**).
5. Syringe with needle for injectable anesthetics; or anesthesia machine for inhalable anesthetic (isoflurane).
6. Scale for animal weight (if dosing by body weight).
7. Catheter for intratracheal instillation.

2.3 Bronchoalveolar Lavage (BAL) of Lungs of QD-Treated Animals

1. Phosphate Buffered Saline (*see* **Note 2**).
2. Syringe.
3. Catheter or Luer stub.
4. Surgical thread.
5. Scissors.
6. Microscissors.
7. Collection Tubes (1.7–2 mL microcentrifuge tubes for mice; 15–50 mL conical tubes for rats).

2.4 Cell Differential in BALF Using CytoSpin Slides

1. Microscope slides.
2. Cytocentrifuge (e.g., Shandon Cytospin, Thermo Scientific).
3. Cytospin Funnel (Thermo Scientific).
4. Cytospin Filter Paper (Thermo Scientific).
5. Cytoclip (Thermo Scientific).
6. Diff-Quik Solutions (Siemens AG).
7. Light microscope.

2.5 Total Cell Count in BALF

1. Hemocytometer.
2. Trypan Blue 0.4 % in Phosphate Buffered Saline (*see* **Note 2**).
3. Micropipette and tips.
4. Light microscope.

2.6 Identification of Macrophages and Neutrophils Using Flow Cytometry

1. Centrifuge.
2. Micropipette and tips.
3. BD FACS™—BD FACS Lysing Solution.
4. PAB (Phosphate Buffered Saline + 1 % Bovine Serum Albumin + 0.1 % Sodium Azide) (*see* **Notes 2** and **3**).
5. PAB with 5 % of Rat Serum.
6. 96-well V-bottom microtiter plate.
7. Adhesive covers for 96-well plates.
8. Vortexer with attachment for 96-well plate.
9. Anti-CD11b antibody conjugated with phycoerythrin (PE) (AbCam, Cambridge, MA).
10. Biotinylated anti-mouse Gr1 antibody and streptavidin conjugated to AlexaFluor350 (BioLegend, San Diego, CA).
11. Anti-F4/80 antibody conjugated to Alexafluor 488 (eBioscience, San Diego, CA).
12. Flow Cytometer capable of fluorophore excitation at 350 and 488 nm (e.g., argon ion laser).

2.7 Total Protein in BALF

1. BioRad Protein Assay Dye Reagent (BioRad, Hercules, CA).
2. Clear polystyrene 96-well microtiter plate.
3. Micropipette and tips.
4. Multichannel or repeat pipette for adding reagent (optional).
5. Plate reader capable of reading absorbance at 590 nm.

2.8 LDH in BALF

1. CytoTox ONE or CytoTox 96 Non-Radioactive Cytotoxicity Assay Kit (Promega, Madison, WI) or Cytotoxicity Detection Kit (LDH) (Roche, Indianapolis, IN).
2. LDH for standard curve (Roche, Indianapolis, IN).

3. Plate reader capable of measuring absorbance of CytoTox 96 or Cytotoxicity Detection Kit.
4. Plate reader capable of measuring fluorescence of CytoTox ONE.
5. Micropipette and tips.

2.9 Embedding Lung Tissue in OCT for Cryosectioning

1. TissueTek® OCT (Sakura Finetek, Torrance, CA).
2. TissueTek® Cryomold.
3. Dry ice.
4. Ethanol 95 %.
5. Thin metal plate (pipette tip box insert or other source).

2.10 Fixation of Lung Tissue in Formalin for Paraffin Embedding

1. Neutral Buffered Formalin at 10 % (*see* **Note 4**).
2. Syringe (50 mL).
3. Ring stand or other support.
4. IV tubing.
5. Luer valve.
6. Catheter.
7. Ethanol 70 %.

3 Methods

No animal procedures should be conducted without prior Institutional Animal Care and Use Committee (IACUC) approval.

3.1 Intranasal Instillation of QDs

1. Animals should be adequately anesthetized using reagents of choice.
2. Disperse QDs to desired concentration in sterile saline or PBS. Half of the dose should be instilled in each nostril using a micropipette tip—previous studies have reported nasal instillation volumes for mice between 10 and 40 μL/nostril [23]. Equivalent volumes of saline should be instilled in each nostril in control animals. Animals should be positioned vertically for 1 min post-instillation to ensure adequate delivery to the respiratory tract.

3.2 Intratracheal Instillation of QDs

1. Animals should be adequately anesthetized using reagents of choice.
2. QDs should be diluted to desired concentration in sterile physiological saline or PBS. Intratracheal instillation volumes for QDs have been reported around 30 μL for mice and around 300 μL for rats [25, 26]. Equivalent volumes of saline or PBS should be instilled in control animals. An extensive review of techniques is available [37].

3.3 Bronchoalveolar Lavage (BAL) of Lungs of QD Treated Animals

1. Animals should be euthanized using IACUC approved methods. Care should be exercised when using cervical dislocation so as to minimize trauma to vessels in the cervical region to reduce the potential for blood in the lavage.
2. Surgically expose the trachea taking care not to cut major vessels in the area. A small cut should be made in the trachea near the larynx. A catheter should be inserted and surgical thread used to tie around the trachea to secure the catheter. For most adult mice and rats, an 18 G catheter is adequate.
3. An appropriate volume of PBS or saline (1–1.2 mL for mice and 6–8 mL for rats) should be loaded into a volume-appropriate syringe. The syringe should be inserted into a catheter that is tied into the trachea, and the lungs should be slowly inflated and deflated with the PBS three times, constituting one bronchoalveolar lavage (*see* **Note 5**). After the last inflation, the lavage should collected and placed in the collection tube. Usually two or three lavages are performed per animal. Lavages can be kept in separate collecting tubes or pooled. Often the first lavage is kept separate to avoid diluting proteins of interest. Bronchoalveolar lavage fluid (BALF) collection tubes should be kept on ice. If desired, one lung or individual lobes can be clamped or tied off prior to lavage.
4. An alternative method not requiring the catheter be tied into the trachea can also be used for lavage in mice [38]. Using this method, the catheter remains attached to the syringe. PBS or saline for each lavage is then drawn through the catheter into the syringe and the catheter is then inserted into a small incision in the trachea proximal to the larynx, and the lavage is performed. Care should be taken to minimize the loss of lavage fluid during the procedure (*see* **Note 5**).

3.4 Cell Differential in BALF Using CytoSpin Slides

1. Prior to any centrifugation of BALF, an aliquot of the first lavage should be taken for analyzing different cell populations (e.g., macrophages, neutrophils, eosinophils, lymphocytes).
2. BALF aliquots should be loaded into Shandon Cytospin cartridges that are preloaded with filters and microscope slides and centrifuged at ~80 × *g* for 5 min.
3. Cytospin slides should be stained with Diff-Quik Fixative and counted under a light microscope. Slides should be dipped for 5, 6, and 5 s in Diff-Quik solutions I, II, and III, respectively. Typically 250–500 cells are counted and both total number and percentages of each cell type of interest are reported.

3.5 Total Cell Count in BALF

1. The lavage samples should be centrifuged at ~500 × *g* at 4 °C for 10 min. The supernatant from the first lavage should be kept and stored at −80 °C for any further analyses. The other lavage supernatants may be discarded (*see* **Note 6**).

2. Cellular fractions of all lavages from each animal should be pooled and resuspended in 1 mL of BD FACS Lysing Solution to lyse RBCs. Cells in RBC lysis buffer should be incubated for 3 min at room temperature (~25 °C). After an additional 10 min centrifugation at ~500 × *g* in a microcentrifuge, the cell pellets should be resuspended in 260 μL PAB. An aliquot should be taken and total cell count determined using a hemocytometer. Viability may be assessed with the addition of Trypan blue 0.4 % solution (1:1) to the sample aliquot.

3.6 Identification of Macrophages and Neutrophils Using Flow Cytometry

1. After resuspension in PAB, cell samples should be transferred to a V-bottom 96-well microtiter plate (one sample per well), covered with an adhesive plate cover and centrifuged at ~360 × *g* for 10 min. Cells should be resuspended in 50 μL PAB containing 5 % rat serum for blocking, vortexed at lowest setting for 10–12 s, and incubated on ice for 15 min (*see* **Note 7**).
2. Next, 25 μL of a primary antibody mix of anti-F4/80-Alexafluor 488 (1 μL/sample) antibody, biotinylated anti-mouse Ly6G/Ly6C (Gr1) antibody (0.5 μL/sample), and anti-CD11b-phycoerythrin (PE) (1 μL/sample) antibody in PAB (22.5 μL/sample) should be added to the samples in the 96-well plate. The plate should be lightly vortexed at lowest setting for 10–12 s and incubated for 15 min on ice protected from light. Finally, 25 μL of a secondary antibody mix of streptavidin-Alexafluor 350 (5 μL/sample) in PAB (20 μL/sample) is added to the plate. Following an additional 10–12 s light vortex, the plate is incubated for a final 15 min on ice. The sample is then removed from the plate and put into a tube that is compatible with the flow cytometer. The sample well is then washed with 200 μL phosphate buffered saline which is also added to the flow cytometry tube. The sample is then diluted with an additional 200 μL for a final volume of 500 μL and analyzed on a flow cytometer.
3. Macrophages are identified as $F4/80^+/CD11b^+$ or $F4/80^+/Gr1^-$ fluorescence. Neutrophils can be identified as having $CD11b^+/Gr1^+$, $CD11b^+/F4/80^-$, or $F4/80^-/Gr1^+$. This process has been described previously [38].

3.7 Total Protein in BALF Supernatants

1. Add 10 μL supernatant sample to 96-well plate in triplicate.
2. Add 200 μL protein assay reagent.
3. Incubate for 10 min.
4. Measure absorbance at 590 nm on plate reader.
5. A standard curve of BSA should be created (standard concentrations from 0 to 0.35 mg/mL) and treated the same as BALF samples for calculation of total protein quantities.

3.8 LDH in BALF

1. LDH can be measured in BALF supernatants, but an aliquot must be taken before freezing, since freezing drastically reduces LDH activity. Aliquots should be stored at 4 °C.
2. Manufacturer's instructions should be followed using the kit of choice. Most commercial kits are designed to quantify percent cell lysis and use a detergent to lyse 100 % of the cells as a positive control (typically used for in vitro cell culture studies). For in vivo studies, a standard curve employing purchased LDH can be used for quantitation of absolute LDH activity in the lavage.

3.9 Embedding Lung Tissue in OCT for Cryosectioning

1. Both lungs, one lung, or specific lobes may be embedded in OCT.
2. Dry ice with 95 % ethanol should be placed under the thin metal plate or other thermally conductive supportive surface underneath the cyromold.
3. If lavage is being performed, the existing cut in the trachea should be utilized to inflate the lung with OCT. Otherwise, a cut should be made in the trachea and a syringe and catheter should be used to gently inflate the lung with OCT.
4. A small amount of OCT covering the bottom should be placed in the mold with care to minimize the occurrence of bubbles.
5. After the lung is placed on top of the existing OCT layer, OCT should be placed on top of the tissue, filling the cryomold. Again, care should be taken to minimize or eliminate bubbles since these make sectioning more difficult.
6. Cryosections may be examined for pathology or for QD fluorescence, although tissue auto-fluorescence may interfere.

3.10 Fixation of Lung Tissue in Formalin for Paraffin Embedding

1. If lavage is being performed, the existing cut in the trachea should be utilized to fill the tissue with formalin.
2. In the case where the catheter is not tied into the trachea, Neutral Buffered Formalin 10 % can be taken into a syringe and the lungs can be inflated while still attached to the trachea or after they have been dissected (*see* **Note 8**).
3. If the catheter or Luer stub is tied into the trachea, Formalin can be put in a syringe and hung on a ring stand or other support with tubing and released into the lung(s) using a Luer valve once the Luer stub or catheter is attached to the suspended formalin filled syringe. This is usually performed after dissection of the lungs that are still attached to the trachea. A variation on this method that could be applied to experiments where the catheter is not tied into the trachea consists of attaching an additional piece of tubing beyond the Luer valve and attaching a catheter to the tubing and placing this inside the preexisting or fresh cut in the trachea and inflating the lung(s) prior to dissection. Inflation is usually done at 20–30 cm static pressure for 1 h.

4. Inflated tissues should be kept in formalin for 24 h and transferred to 70 % ethanol before being placed into a tissue cassette and processed for paraffin embedding.

3.11 Detection of Inflammatory Cytokines or Other Changes in Gene Expression in BALF or Tissue

Inflammatory cytokines can be measured in BALF and tissue using a variety of techniques including ELISA, quantitative Reverse Transcriptase-Polymerase Chain Reaction (qRT-PCR), and Western blotting. Higher throughput methods include the multiplex Luminex platform, and traditional mRNA and protein microarray methods [39].

3.12 Detection of Cadmium in Tissue

As a surrogate for directly measuring intact cadmium-based QDs in tissue by fluorescence, elemental cadmium levels can be measured. Inductively coupled plasma-mass spectrometry (ICP-MS) is the standard method, and EPA method 6020A (*see* **Note 9**) has been followed in previous studies to measure Cd in lung tissue [23].

4 Notes

1. Anesthetics in the gas form should be used in a fume hood or the anesthesia machine should have a scavenging device attached to remove excess anesthetic from the inhalation chamber.
2. We use Gibco® 10× Dulbecco's Phosphate Buffered Saline (80 g/L NaCl, 2 g/L KCl, 21.6 g/L Na_2HPO4, 2 g/L KH_2PO_4) and dilute to 1× and then autoclave before use.
3. A mask and eye protection should be worn along with gloves and lab coat when measuring Sodium Azide as it is highly acutely toxic if inhaled or if it contacts skin.
4. We use Formalin Solution, neutral buffered, 10 % (Sigma-Aldrich) that consists of: 100 mL/L Formaldehyde (37–40 %), Distilled or Deionized water 900 mL/L, 4.0 g/L Sodium Phosphate (monobasic), and 6.5 g/L Sodium Phosphate (dibasic, anhydrous).
5. In general for a 1 mL lavage, ~700 μL is an adequate volume to move out of the lugs during deflations that are not the final deflation where as much fluid as possible should be removed and put in the collection tube. Care should be taken to remove all air bubbles from syringes before starting lavage.
6. A vacuum flask set up may be used to discard supernatant from lavages where fluid is not going to be saved for future analysis.
7. After cells have been centrifuged for 10 min at ~360×*g*, the supernatant may be discarded by the removal of the adhesive cover and one light inverted shake of the plate over a sink. Excess liquid may be removed from the plate by gently wiping the plate on a dry paper towel.

8. It is recommended to inflate the lungs through the trachea while they are still attached. It is difficult to find the main bronchial opening into the lungs once they have been dissected. Also, one lung may be clamped off and used for another purpose not requiring fixation.
9. The .pdf file for EPA Method 6020A can be found at: http://www.epa.gov/osw/hazard/tmethods/sw846/pdfs/6020a.pdf.

References

1. Bruchez M Jr, Moronne M, Gin P, Weiss S, Alivisatos AP (1998) Semiconductor nanocrystals as fluorescent biological labels. Science 281(5385):2013–2016
2. Dabbousi BO, Rodriguez-Viejo J, Mikulec FV, Heine JR, Mattoussi H, Ober R, Jensen KF, Bawendi MG (1997) (CdSe)ZnS core–shell quantum dots: synthesis and characterization of a size series of highly luminescent nanocrystallites. J Phys Chem B 101(46):9463–9475
3. Hoshino A, Hanada S, Yamamoto K (2011) Toxicity of nanocrystal quantum dots: the relevance of surface modifications. Arch Toxicol 85:707–720
4. Medintz IL, Uyeda HT, Goldman ER, Mattoussi H (2005) Quantum dot bioconjugates for imaging, labelling and sensing. Nat Mater 4:435–446
5. Smith AM, Duan H, Rhyner MN, Ruan G, Nie S (2006) A systematic examination of surface coatings on the optical and chemical properties of semiconductor quantum dots. Phys Chem Chem Phys 8(33):3895–3903
6. Kim S, Fisher B, Eisler H-J, Bawendi M (2003) Type-II quantum dots: CdTe/CdSe(core/shell) and CdSe/ZnTe(core/shell) heterostructures. J Am Chem Soc 125(38):11466–11467
7. Wu X, Liu H, Liu J, Haley KN, Treadway JA, Larson JP, Ge N, Peale F, Bruchez MP (2003) Immunofluorescent labeling of cancer marker Her2 and other cellular targets with semiconductor quantum dots. Nat Biotechnol 21(1):41–46
8. Chen F, Gerion D (2004) Fluorescent CdSe/ZnS nanocrystal: peptide conjugates for long-term, nontoxic imaging and nuclear targeting in living cells. Nano Lett 4(10):1827–1832
9. Chakravarthy KV, Davidson BA, Helinski JD, Ding H, Law W-C, Yong K-T, Prasad PN, Knight PR (2011) Doxorubicin-conjugated quantum dots to target alveolar macrophages and inflammation. Nanomedicine 7:88–96
10. Weiming X, Lizhi L, Brown NJ, Christian S, Hornby D (2012) Quantum dot-conjugated anti-GRP78 scFv inhibits cancer growth in mice. Molecules 17(1):796–808
11. Savla R, Taratula O, Garbuzenko O, Minko T (2011) Tumor targeted quantum dot-mucin 1 aptamer-doxorubicin conjugate for imaging and treatment of cancer. J Control Release 153:16–22
12. Gao X, Cui Y, Levenson RM, Chung LWK, Nie S (2004) In vivo cancer targeting and imaging with semiconductor quantum dots. Nat Biotechnol 22(8):969–976
13. Kim S, Lim YT, Soltesz EG, De Grand AM, Lee J, Nakayama A, Parker JA, Mihaljevic T, Laurence RG, Dor DM, Cohn LH, Bawendi MG, Frangioni JV (2004) Near-infrared fluorescent type II quantum dots for sentinel lymph node mapping. Nat Biotechnol 22(1):93–97
14. So MK, Xu C, Loening AM, Gambhir SS, Rao J (2006) Self-illuminating quantum dot conjugates for in vivo imaging. Nat Biotechnol 24(3):339–343
15. Shiohara A, Hoshino A, Hanaki K, Suzuki K, Yamamoto K (2004) On the cyto-toxicity caused by quantum dots. Microbiol Immunol 48:669–675
16. Clift MJ, Boyles MS, Brown DM, Stone V (2010) An investigation into the potential for different surface-coated quantum dots to cause oxidative stress and affect macrophage cell signalling in vitro. Nanotoxicology 4(2):139–149
17. Kirchner C, Liedl T, Kudera S, Pellegrino T, Muñoz Javier A, Gaub HE, Stölzle S, Fertig N, Parak WJ (2005) Cytotoxicity of colloidal CdSe and CdSe/ZnS nanoparticles. Nano Lett 5:331–338
18. McConnachie LA, White CC, Botta D, Zadworny ME, Cox DP, Beyer RP, Hu X, Eaton DL, Gao X, Kavanagh TJ (2012) Heme oxygenase expression as a biomarker of exposure to amphiphilic polymer-coated CdSe/ZnS quantum dots. Nanotoxicology 7(2):181–191

19. Lovric J, Bazzi HS, Cuie Y, Fortin GR, Winnik FM, Maysinger D (2005) Differences in subcellular distribution and toxicity of green and red emitting CdTe quantum dots. J Mol Med (Berl) 83(5):377–385
20. Smith WE, Brownell J, White CC, Afsharinejad Z, Tsai J, Hu X, Polyak SJ, Gao X, Kavanagh TJ, Eaton DL (2012) In vitro toxicity assessment of amphiphillic polymer-coated CdSe/ZnS quantum dots in two human liver cell models. ACS Nano 6(11):9475–9484
21. Hauck TS, Anderson RE, Fischer HC, Newbigging S, Chan WC (2010) In vivo quantum-dot toxicity assessment. Small 6(1):138–144
22. Su Y, Peng F, Jiang Z, Zhong Y, Lu Y, Jiang X, Huang Q, Fan C, Lee ST, He Y (2011) In vivo distribution, pharmacokinetics, and toxicity of aqueous synthesized cadmium-containing quantum dots. Biomaterials 32(25):5855–5862
23. McConnachie LA, Botta D, White CC, Weldy CS, Wilkerson HW, Yu J, Dills R, Yu X, Griffith WC, Faustman EM, Farin FM, Gill SE, Parks WC, Hu X, Gao X, Eaton DL, Kavanagh TJ (2013) The glutathione synthesis gene gclm modulates amphiphilic polymer-coated CdSe/ZnS quantum dot-induced lung inflammation in mice. PLoS One 8(5):e64165. doi:10.1371/journal.pone.0064165
24. Jacobsen NR, Moller P, Jensen KA, Vogel U, Ladefoged O, Loft S, Wallin H (2009) Lung inflammation and genotoxicity following pulmonary exposure to nanoparticles in ApoE−/− mice. Part Fibre Toxicol 6(2):1–17
25. Roberts JR, Antonini JM, Porter DW, Chapman RS, Scabilloni JF, Young SH, Schwegler-Berry D, Castranova V, Mercer RR (2013) Lung toxicity and biodistribution of Cd/Se-ZnS quantum dots with different surface functional groups after pulmonary exposure in rats. Part Fibre Toxicol 10(5):1–17
26. Ho CC, Chang H, Tsai HT, Tsai MH, Yang CS, Ling YC, Lin P (2013) Quantum dot 705, a cadmium-based nanoparticle, induces persistent inflammation and granuloma formation in the mouse lung. Nanotoxicology 7(1):105–115
27. Ye L, Yong K-T, Liu L, Roy I, Hu R, Zhu J, Cai H, Law W-C, Liu J, Wang K, Liu J, Liu Y, Hu Y, Zhang X, Swihart MT, Prasad PN (2012) A pilot study in non-human primates shows no adverse response to intravenous injection of quantum dots. Nat Nanotechnol 7:453–458
28. Geys J, Nemmar A, Verbeken E, Smolders E, Ratoi M, Hoylaerts MF, Nemery B, Hoet PHM (2008) Acute toxicity and prothrombotic effects of quantum dots: impact of surface charge. Environ Health Perspect 116(12):1607–1613
29. Lu Y, Su Y, Zhou Y, Wang J, Peng F, Zhong Y, Huang Q, Fan C, He Y (2013) In vivo behavior of near infrared-emitting quantum dots. Biomaterials 34(17):4302–4308
30. Ma-Hock L, Brill S, Wohlleben W, Farias PMA, Chaves CR, Tenório DPLA, Fontes A, Santos BS, Landsiedel R, Strauss V, Treumann S, van Ravenzwaay B (2012) Short term inhalation toxicity of a liquid aerosol of CdS/$Cd(OH)_2$ core shell quantum dots in male Wistar rats. Toxicol Lett 208(2):115–124
31. Price JE, Barth RF, Johnson CW, Staubus AE (1984) Injection of cells and monoclonal antibodies into mice: comparison of tail vein and retroorbital routes. Proc Soc Exp Biol Med 177(2):347–353
32. Yardeni T, Eckhaus M, Morris HD, Huizing M, Hoogstraten-Miller S (2011) Retro-orbital injections in mice. Lab Anim 40(5):155–160
33. Ryman-Rasmussen JP, Riviere JE, Monteiro-Riviere NA (2006) Penetration of intact skin by quantum dots with diverse physicochemical properties. Toxicol Sci 91(1):159–165
34. Prow TW, Monteiro-Riviere NA, Inman AO, Grice JE, Chen X, Zhao X, Sanchez WH, Gierden A, Kendall MA, Zvyagin AV, Erdmann D, Riviere JE, Roberts MS (2012) Quantum dot penetration into viable human skin. Nanotoxicology 6(2):173–185
35. Gopee NV, Roberts DW, Webb P, Cozart CR, Siitonen PH, Latendresse JR, Warbitton AR, Yu WW, Colvin VL, Walker NJ, Howard PC (2009) Quantitative determination of skin penetration of PEG-coated CdSe quantum dots in dermabraded but not intact SKH-1 hairless mouse skin. Toxicol Sci 111(1):37–48
36. Hardman R (2006) A toxicologic review of quantum dots: toxicity depends on physicochemical and environmental factors. Environ Health Perspect 114(2):165–172
37. Driscoll KE, Costa DL, Hatch G, Henderson R, Oberdorster G, Salem H, Schlesinger RB (2000) Intratracheal instillation as an exposure technique for the evaluation of respiratory tract toxicity: uses and limitations. Toxicol Sci 55(1):24–35
38. Weldy CS, White CC, Wilkerson H-W, Larson TV, Stewart JA, Gill SE, Parks WC, Kavanagh TJ (2011) Heterozygosity in the glutathione synthesis gene Gclm increases sensitivity to diesel exhaust particulate induced lung inflammation in mice. Inhal Toxicol 23(12):724–735
39. Servoss SL, Gonzalez R, Varnum S, Zangar RC (2009) High-throughput analysis of serum antigens using sandwich ELISAs on microarrays. Methods Mol Biol 520:143–150

Chapter 15

Quantum Dots for Imaging Neural Cells In Vitro and In Vivo

Angela O. Choi*, Kevin D. Neibert*, and Dusica Maysinger

Abstract

Quantum dots (QDs) have been used for optical imaging of neural cells in vitro and in vivo. This chapter lists the basic materials, instrumentation and step-by-step procedures to image live microglia cells and to show the functional and biochemical changes in microglia exposed to QDs. Details are also provided for the real-time imaging of cerebral ischemic lesions in animals and for the assessment of lesion reduction after therapeutic interventions. Microglia are brain cells which detect, internalize, and eliminate particulate matter, thereby maintaining homeostasis in the central nervous system. Although the protocols for imaging microglia shown here are developed for QDs without specific ligands or antibodies, the principles are the same for imaging other QDs.

Key words Quantum dot, Microglia, Ischemia, Cortex, Intranasal delivery, Nano-neuroscience, Nanotechnology, Live-cell imaging

1 Introduction

Neurons and glial cells in the brain form intricate networks and communicate via electrical or chemical pathways. The underlying intercellular and intracellular physical and chemical interactions play a critical role in the execution of cognitive functions and in the maintenance of physiological homeostasis in the nervous system. To deal with any form of neural dysfunction, one would ideally wish to "see" and measure relevant markers of these interactions that would reflect neural disturbances at the earliest stage possible, thereby allowing therapeutic interventions to be instituted as soon as possible. This centuries-long search for a noninvasive brain imaging technique with a longitudinal character has resulted in some success, such as optogenetic approaches in transgenic animals [1, 2]. Nano-neuroscience, a relatively new area of interdisciplinary research, bridges biological sciences and nanotechnology. Nanotechnological products, including quantum dots (QDs), have been used to assess relevant structures and functions of the

*Author contributed equally with all other contributors.

Adriana Fontes and Beate Saegesser Santos (eds.), Quantum Dots: Applications in Biology, Methods in Molecular Biology, vol. 1199, DOI 10.1007/978-1-4939-1280-3_15, © Springer Science+Business Media New York 2014

nervous system [3]. QDs have also been used for optical imaging of astrocytes [4], microglia [5], and neurons [6] in vitro and in vivo.

The key problem in imaging individual cell types in the nervous system is the lack of specific, stably attached markers on QDs, which recognize glia and neurons in their multiple states of activation and pathologies. However, using nontoxic PEGylated, QDs it is possible to distinguish activated and surveyor microglia. Activated microglia have different morphologies and tend to internalize QDs to a greater extent than the surveyors. Without functionalization, QDs can enter microglial cells by endocytosis or phagocytosis, depending on the state of QD aggregation in the biological environment [5]. In this chapter, basic procedures to assess QD internalization by microglia are described. The mechanisms of QD endocytosis have been explored by several groups including ours [7–10]. This chapter provides detailed information on how to use fluorescent probes for organelles in combination with QDs to determine their subcellular fate. These initial steps in investigating microglial responses to QDs provide a first attempt to resolve the complex interplay between microglia and other neural cells. Microglia maintain brain homeostasis by recognizing and eliminating harmful agents (endogenous and exogenous) in the surrounding microenvironment [11]. Monitoring of microglia in their active and surveyor states is therefore essential to establish a threshold within which an insult triggers repair mechanisms in the absence of deleterious consequences. The protocols described here employ cadmium selenide QDs, but similar procedures can be used for imaging microglia utilizing cadmium-free QDs, once these become more easily accessible for routine biological experiments in vitro and in vivo [12].

2 Materials

Although traditional organic dyes and fluorescent proteins are widely used in biology, they have considerable limitations. QDs have emerged as an attractive alternative due to their tunable optical properties, superior brightness, and photostability. The properties of QDs change in different biological media as a result of the interactions with the media components (e.g., salt composition, proteins), and should be considered when imaging QDs in live cells and in animals. Specific concerns regarding QD-protein interactions are briefly discussed in **Note 1**.

The methods for in vitro and in vivo imaging of QDs detailed below are suitable for both QDs produced in the laboratory and those commercially available (*see* **Note 2**). For this protocol, we have selected amino-terminus PEGylated QDs (Qdot705, Life Technologies, Q2176MP), which are ideal for

in vitro and in vivo imaging due to their high photostability and near-infrared emission, which would avoid spectral overlap with biological autofluorescence.

2.1 In Vitro Imaging

2.1.1 Cell Culture

Murine microglia cells (N9) (*see* **Note 3**) should be cultured in T-75 cell culture flasks containing Iscove's Modified Dulbecco's Media (IMDM), supplemented with 5 % of fetal bovine serum (FBS) and 1 % penicillin–streptomycin (P/S). Culture flasks should be maintained at 37 °C in a humidified atmosphere (5 % CO_2).

2.1.2 Culture Dish for Imaging

Glass-bottom microwell culture dishes are ideal for live-cell imaging with the confocal microscope (*see* **Note 4**). The dishes should be coated with rat tail collagen prior to cell seeding.

2.1.3 PKH Cell Membrane Labeling Mix

We recommend modifying the preparation instructions from those described in the PKH kit (Sigma, PKH67GL-1KT). Take 1 μL PKH dye solution (1 mM) and dilute to 500 μL with diluent C in a sterile microcentrifuge tube. Mix thoroughly by pipetting up and down. Keep the PKH mix on ice and protect from light. Always prepare a fresh solution of PKH mix prior to imaging. Bovine serum albumin (BSA) at 1 % is prepared in phosphate-buffered saline (PBS) and used as a "stop solution" for the staining.

2.1.4 Instrumentation for Live-Cell Imaging In Vitro

QDs can be imaged using fluorescent, confocal, and multiphoton microscopes equipped with the appropriate lasers and filters for the selected QDs. We used the following microscopy equipment and settings: LSM 710 multi-photon upright confocal microscope, 30 mW argon ion laser, 63×/1.4 numerical aperture (NA) VIS-IR W Plan-Apochromat aqueous immersion objective, excitation/emission 488/505 nm, 3 % laser power, 950 photomultiplier gain, Zen imaging software (*see* **Note 5**).

2.2 In Vivo Imaging

2.2.1 Animals

One- to two-month-old SKH1 hairless mice (strain code 477, Charles River) were used for the in vivo imaging studies. This hairless strain of mice was selected for these studies to avoid interference from the autofluorescence of animal hair. SKH1 mice are immunocompetent and euthymic, and are therefore ideal candidates for repeated imaging and longitudinal experiments, especially after surgery with recovery [13]. The mice were maintained on a 12-h light/dark cycle and were allowed access to food and water ad libitum. In total, six adult male SKH1 mice, weighing between 25 and 30 g, were used for this study. All animal protocols used in this study were approved by the McGill University Animal Care Committee and followed the guidelines of the Canadian Council on Animal Care (http://www.ccac.ca/en_/standards/guidelines).

2.2.2 Surgical Materials

1. Ethanol 70 %.
2. Chlorhexidine 2 %.
3. Gas anesthesia machine.
4. Induction chamber.
5. Bain system (with nose cone).
6. Isoflurane.
7. Compressed oxygen gas.
8. F/AIR anesthesia gas filter.
9. Sterile isotonic saline (0.9 % saline).
10. Heat pad.
11. Ophthalmic ointment.
12. Sterilized cotton swabs.
13. Scalpel.
14. 5 mm Vannas spring scissors.
15. Dumont #5 forceps.
16. Halsted-mosquito hemostats.
17. Rotary micromotor dental drill.
18. Dental trephine burr.
19. Synthetic absorbable sutures.
20. Lidocaine-bupivacaine mixture (<2 mg/kg).
21. Carprofen (5 mg/kg).
22. 26.5 G needle.
23. 1 mL syringe.
24. Surgical tape.

2.2.3 Instrumentation for Optical Molecular Imaging In Vivo

Optix MX3 system (Advanced Research Technologies Inc) or any of the IVIS Spectrum systems (Perkin Elmer) equipped with appropriate lasers and filters can be used for fluorescence imaging with QDs.

3 Methods

3.1 Live Cell In Vitro Imaging

Fluorescence microscopy is among the most widely used techniques for high-resolution, noninvasive imaging of live cells. Here we outline the procedures for real-time imaging of microglia (Fig. 1).

3.1.1 Preparation of Collagen-Coated Microwell Dish

1. The coating of dishes and cell seeding should be carried out under sterile conditions in a biological safety cabinet.
2. Dilute 1 mg/mL rat tail collagen tenfold with 0.1 N acetic acid.

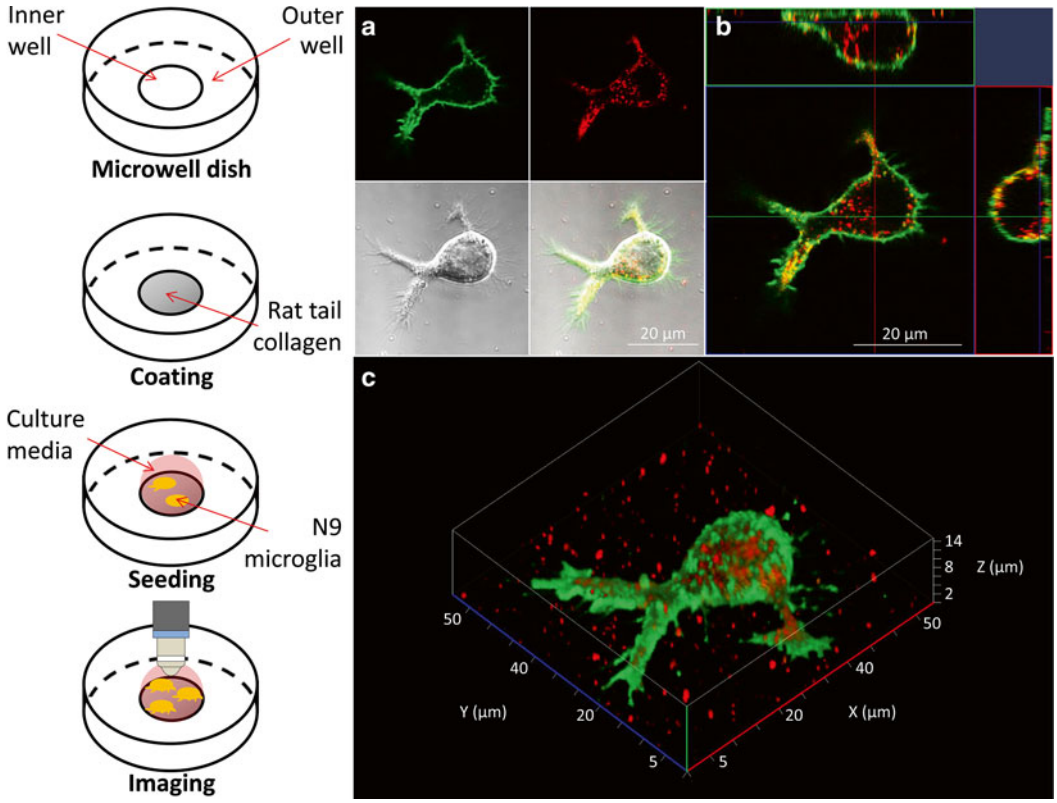

Fig. 1 Live-cell confocal microscopy of QDs in microglia. N9 microglia cells were incubated with QD-PEG (100 nM; 3 h) in serum-containing media (IMDM + 5 % FBS). (**a**) Split view displays the individual channels of a multichannel image as well as the superimposed image. QD-PEG is shown in *red*, PKH-labeled plasma membrane in *green*, and phase contrast in *grey*. (**b**) Ortho view displays a z stack of images in an orthogonal view. (**c**) z-stack series can be compiled and displayed as 3D reconstructions

3. Add 300 µL of 1× collagen to the microwell dish. Gently rotate the dish at an angle to ensure full coverage of the surface.
4. Protect the dish from light and incubate at room temperature (RT) for 90 min.
5. Wash the coated surface twice with IMDM containing serum (*see* **Note 6**).
6. The coated microwell should be prepared at least 30 min prior to cell seeding to allow time for complete drying.
7. Seed 10,000 cells per dish in 500 µL of IMDM containing serum.

3.1.2 Live-Cell Imaging Using Confocal Microscope

1. Provide 48 h for cells to adhere before imaging (*see* **Note 7**).
2. Turn on the power switch on the confocal microscope and power up selected lasers.
3. Allow at least 30 min for laser power levels to stabilize.

4. Start imaging software.
5. Set confocal stage temperature to 37 °C.
6. Prepare PKH cell membrane labeling mix as described above.
7. Aspirate cell culture media and add 200 μL of PKH mix to the dish.
8. The PKH mix can contain additional labeling dyes for co-labeling of cellular structures and subcellular organelles (*see* **Note 8**).
9. Incubate with PKH mix (+/– co-labeling dyes) for 10 min at RT.
10. Add 300 μL of PBS containing 1 % of BSA (PBS-BSA), do not aspirate the PKH mix.
11. Wait for 10 min, then aspirate the solution, and wash the cells with another 500 μL of 1 % BSA-PBS.
12. Add 500 μL of fresh, serum-free IMDM media (*see* **Note 9**).
13. Place the microwell dish at the microscope and position under the aqueous immersion objective.
14. Slowly lower the objective into the media (*see* **Note 10**).
15. Adjust the focus to the focal plane of the cell monolayer.
16. Lock microscope stage and microwell positions.
17. Slowly inject QDs into the cell media at a 45° angle.
18. For time course experiments, z-stacks should be acquired every 5–10 min (*see* **Note 11**).
19. Refocus and establish z-stack positions before each time point (*see* **Note 12**).
20. Gallery images, orthogonal projections, and 3D reconstructions can be complied using the Zen imaging software (Zeiss) or other software.
21. This protocol is useful for tracking QD uptake in real time and in determining their intracellular destination (*see* **Notes 13** and **14**).

3.2 In Vivo Imaging of Cerebral Brain Lesions

Noninvasive, longitudinal imaging provides invaluable information on the development of central nervous system pathologies and on the effectiveness of therapeutic interventions. In vivo imaging is particularly useful for the diagnosis of neurological diseases since histopathological methods are invasive and have limited applications for the brain due to restricted accessibility [14]. Each year over 5.8 million people suffer from strokes, and over 80 % of these are ischemic stroke episodes caused by the interruption of blood flow to the brain (WHO 2012, American Heart Association 2012). One of the biggest challenges preventing timely treatment of ischemic strokes is the delay in detecting lesions and microlesions, which are often

asymptomatic, but can develop into full strokes if left untreated [15]. Current neuroimaging methods for lesion detection, both in humans and in animals, mostly rely on measuring late-stage changes in physiological functions, such as perfusion and hemorrhage imaging [16], and utilize costly methods including computed tomography (CT) scanning and magnetic resonance imaging (MRI). We describe here an alternative, cost-effective, high-resolution, noninvasive, and fluorescence-based imaging method for the detection of cerebral microlesions in live animals. Using near-infrared-emitting QDs administered intranasally, lesioned mice could be monitored (i.e., repeatedly imaged) for weeks [17]. The retention of QDs at and near the lesion core suggests that phagocytic microglia take up the QDs and accumulate in the penumbra (i.e., regions bordering the infarct). Live imaging of the stroke penumbra can be useful to monitor stroke propagation and long-term prognosis, but more importantly, to evaluate efficacies of current and new stroke therapeutics. The procedure applied for unilateral cortical devascularizing lesion was modified from the previous procedure described in the literature [18].

3.2.1 Unilateral Cortical Devascularizing Lesion

1. Sterilize all surgical instruments by soaking in ethanol 70 % for 15 min.
2. Place the mouse into the induction chamber.
3. Open the oxygen tank and the isoflurane vaporizer. Adjust the oxygen flow meter to 0.8 L/min, and the isoflurane vaporizer to 3 %.
4. Once the mouse is deeply anesthetized (pinch the foot pad to test reflexes), using a cotton swab, apply ophthalmic ointment to cover the eyes, then transfer the mouse to the nose cone-bain system, and maintain under anesthesia. Administer warm, sterile isotonic saline subcutaneously (0.2 mL per 10 g of body weight) (*see* **Note 15**). A pre-warmed heat pad should also be used to keep the animal warm. The isoflurane vaporizer can be reduced to 2–2.5 % for maintenance.
5. Swab the skin on the head of the mouse with chlorhexidine 2 %.
6. Use a sterile scalpel to create a sagittal incision in the middle of the skull (approximately 1.5 cm in length). Place the mouse into the stereotaxic frame. Select stereotaxic coordinates using the Mouse Brain Atlas [19], and mark the site by gently twisting a 26.5 G needle against the skull (do not push down).
7. Create a bone flap by gently drilling the skull at the marked site using the dental drill with a trephine burr. Do not push down on the skull while drilling (*see* **Note 16**).
8. Remove the bone flap carefully with forceps to expose the dura of the motor cortex.

9. Verify the stereotaxic coordinates again, and disrupt the terminal pia-arachnoid vessels by gently pricking with a fresh sterile needle.
10. Stop any bleeding with a cotton swab. Apply a few drops of lidocaine-bupivacaine mixture (<2 mg/kg) in the open wound. Draw the skin together using sterile forceps, and close the wound with continuous suturing using hemostats (*see* **Note 17**).
11. Administer 5 mg/kg of carprofen subcutaneously as postoperative analgesic. Repeat carprofen administration daily for the next 72 h.
12. The animal could be imaged immediately (kept under anesthesia) or be placed into its cage for recovery. Monitor until it regains consciousness and mobility, and monitor daily for signs of infection, pain, or distress.

3.2.2 Administration of QDs

For direct, noninvasive access to the brain, we administered QDs and/or nano-therapeutics intranasally [17]. For comparisons, intravenous and intraparenchymal administrations of QDs were also carried out (Fig. 2).

Intranasal administration

1. Place the mouse into the induction chamber, and adjust the oxygen flow to 0.8 L/min and the isoflurane vaporizer to 3 %.
2. Once the animal is immobilized, open the chamber lid and place the mouse in a prone position. Administer 5 μL of QDs (8 μM) dropwise to the nostril using a micropipette (Fig. 2).

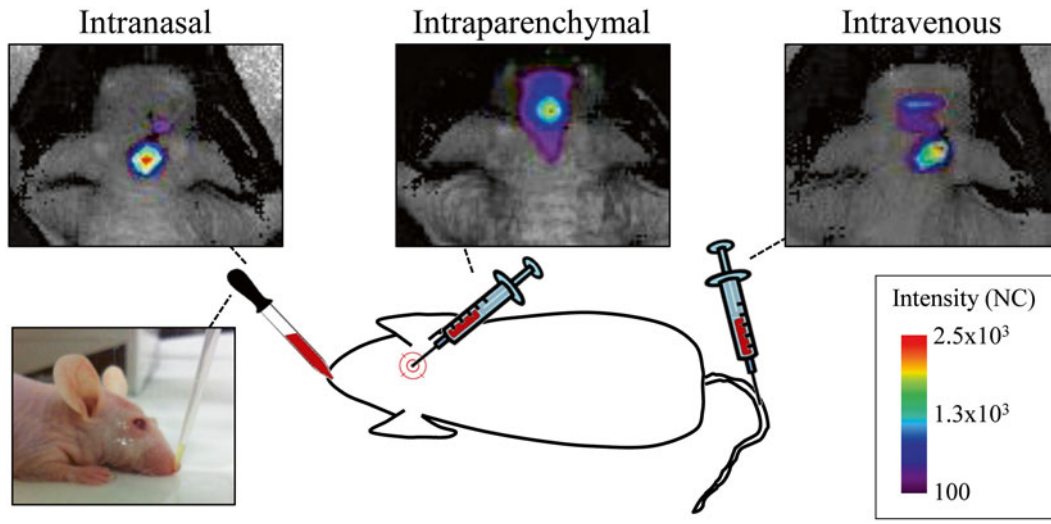

Fig. 2 Modes of QD administration for in vivo imaging of brain lesions. Real-time live fluorescence images of lesioned SKH1 mice after intranasal, intraparenchymal, or intravenous administration of QD-PEG for 24 h. Fluorescence intensity was measured as the number of counts (NC) in the region of interest selected at the head

Allow the animal to fully inhale each drop before administering the next drop (approximately 10 s in between) (*see* **Note 18**).

3. Place the animal in the imaging machine and image immediately (set this as time 0).

Intravenous administration

1. Warm up the animal with a heat lamp for 5–10 min to dilate the tail veins.
2. Place the mouse in a flat-bottom restrainer, and swab the tail with chlorhexidine 2 %.
3. Locate a tail vein (dorsal or lateral veins) by rotating the tail left or right and by applying light pressure. While holding down the tail with one hand, insert a 26.5 G needle (beveled side up) syringe loaded with 100 μL of QDs (0.4 μM) into the vein. Slowly and steadily inject the QDs into the vein (10–20 s) (*see* **Note 19**).
4. Release the tail. Anesthetize the animal in the induction chamber and image immediately (set this as time 0).

Intraparenchymal (intracranial) administration

1. Immediately after disruption of the pia-arachnoid vessels (Subheading 3.2.1, **step 9**), administer 5 μL of QDs (8 μM) to the lesion site using a micropipette. Stop all bleeding in the wound before QD administration.
2. Wait for 30 s. Apply a few drops of lidocaine-bupivacaine mixture (<2 mg/kg) in the open wound and close the wound with continuous suturing. Administer 5 mg/kg of carprofen subcutaneously as described previously.
3. Transfer the animal to the imaging machine and image immediately (set this as time 0).

3.2.3 In Vivo Fluorescence Imaging

The procedure described here provides details for in vivo imaging using the Optix MX3 system.

1. Power on the computer (MX3 imager), and double click on the "OptiScan" icon to start up the program.
2. Click and hold down the "Turn Power On" button for 3 s to power the system components. Allow 10–15 min for the system and lasers to warm up. At this point, do not open the access door of the imager.
3. Once the system is in "Ready" mode (indicated by the status bar on the bottom right), click on the "Scan" button and follow the instructions to set up a new study or scan.
4. In the laser drop-down menu, select the laser and filter set appropriate for the QDs. For Qdot705, choose the 480 nm excitation laser, coupled with the 695-LP (long pass) filter, and select the 50- or 400-ns time window (*see* **Note 20**).

5. Under "Specimen—Identification," name the scan for the study. Select the "In vivo" option, then select the single bed type, set the temperature to 37 °C, and check the mouse detection option. Allow 5–10 min for the scanning bed to warm up.
6. At this point, the mouse is placed in the induction chamber and anesthetized as described previously (oxygen flow 0.8 L/min, isoflurane vaporizer 3 %).
7. Open the gas valve connected to the MX3 imager to allow isoflurane flow into the specimen chamber.
8. Once the animal is deeply anesthetized, apply ophthalmic ointment, and place the mouse on the scanning bed inside the specimen chamber in the prone position. Make sure that its nose is fitted inside the nose cone to maintain anesthesia during imaging. The limbs and tail should be taped down to avoid reflexive twitching which may reposition the animal during the scan.
9. Click "Next" to continue.
10. Under "ROI Settings," select "Polygon" under ROI Type. "Scan Resolution" should be selected at 1.5 mm or lower (*see* **Note 21**).
11. Use the cursor to draw a region of interest (ROI) at the head. Click "Scan" to verify the selected ROI. Allow a minimum of 10 min for the initial quick scan. Then click "Next" to initiate a Full Quantitative scan. A full scan can take as long as 15–20 min depending on the size and resolution of the ROI.
12. Click "Finish" to complete the scan. Wait until "Ready" mode (check status bar) before opening the access door. Remove the animal from the chamber and place in its cage. Monitor the recovery until it regains consciousness and mobility.
13. The same animal can be used for repeated imaging at different time points (*see* **Note 22**).
14. Wipe down and clean all instruments and equipment parts with chlorhexidine 2 %.
15. Data analysis should be carried out using the OptiView software. Background signal removal, fluorescence lifetime analysis, depth-concentration analysis, and 3D reconstruction of the lesion can be generated using this software (Fig. 3) (*see* **Note 23**).

3.3 Ex Vivo Imaging of QD Distribution in Tissues

1. Euthanize the animal using CO_2 asphyxiation followed by cervical dislocation.
2. Dissect the tissues of interest and place them on a black, non-reflective surface (e.g., black paper, matte plastic).
3. Start up the MX3 imager as described previously. No isoflurane anesthesia is necessary for ex vivo imaging.

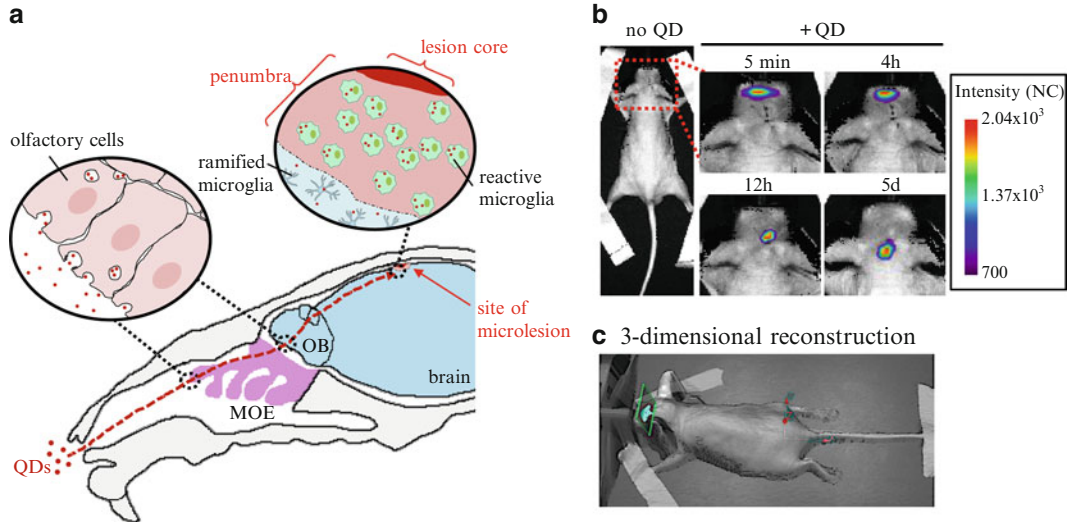

Fig. 3 Intranasal transport of fluorescent quantum dots to the brain lesion. (**a**) Schematic illustration of the nose-to-brain delivery of nanoparticles in the mouse. QDs administered in small volumes (5 μL) intranasally are taken up by cells in the main olfactory epithelium (MOE), and then transported transcellularly through the olfactory bulb and to posterior brain regions. Following the rapid necrosis occurring at the lesion core, neuroglia activation is triggered and reactive glia proliferate and migrate to the vicinity of the core. The penumbra region is populated by reactive microglia with enhanced phagocytic activity, thereby increasing the uptake and accumulation of QDs in this region. (**b**) Real-time live fluorescence images of lesioned SKH1 mice after intranasal administration of QD-PEG at the times indicated. The fluorescence intensity was measured as the number of counts (NC) from the region of interest (ROI) selected at the head. (**c**) Three-dimensional reconstruction based on the live fluorescent images of a lesioned mouse with intranasal administration of QDs after 24 h. The ROI is selected at the head for 3D analysis. Reproduced from Choi et al. [17] with permission from Bentham Science

4. At the "Specimen" window, select the "In vitro" option and proceed with the ROI selection. Multiple ROIs should be drawn for individual organs, and the "Scan Resolution" should be 1.5 mm or less.
5. Proceed with the quick scan and finish with the full quantitative scan.
6. Analyze the data using the OptiView software. The imaging data should always be complemented with biochemical tissue analysis. For quantitative analyses of the QD constituents, graphite furnace atomic absorption spectrometry should be performed (Fig. 4a).

4 Notes

1. Proteins present in biological fluids can rapidly adsorb onto the QD surface and modify to some extent both QD surface properties and size. Consequently, the "biological identity" of QDs often does not relate to their "synthetic identity"

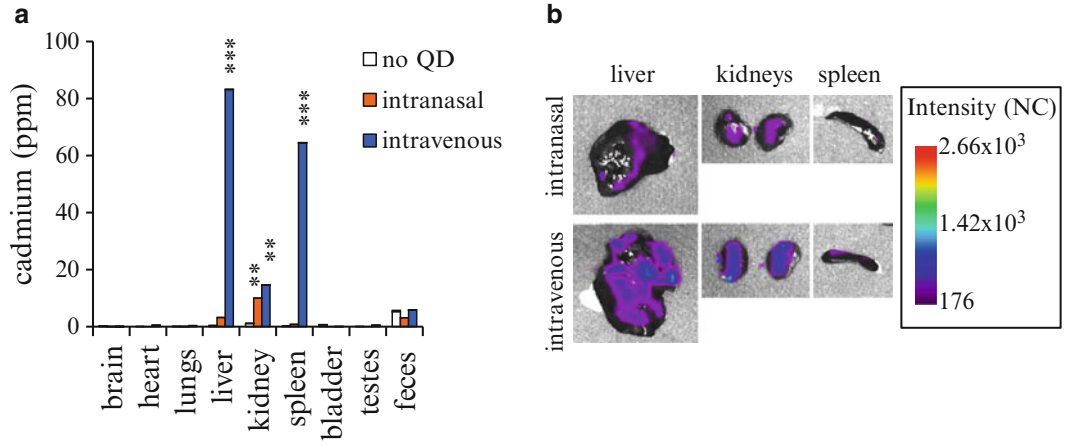

Fig. 4 Distribution of quantum dots in tissues. (**a**) Cadmium content (parts per million) of organs dissected from mice after intranasal or intravenous administration of QD-PEG. Total cadmium ion content from each organ was determined using graphite furnace atomic adsorption. Values represent means ± SEM. $^{**}p < 0.01$ and $^{***}p < 0.001$ indicate significance when compared to organs of untreated animals. (**b**) Fluorescence images of selected organs dissected from animals administered with QD-PEG intranasally or intravenously. Reproduced from Choi et al. [17] with permission from Bentham Science

determined with QD dispersions in a nonphysiological context (e.g., buffered water) [20–26]. We recommend asymmetrical flow field-flow fractionation (AF4) for detailed QD characterization to better determine the interactions between QDs and the biological milieu. AF4 is a technique that involves hydrodynamical separation of the constituents of a mixture as they migrate through in a thin channel. This technique is described in detail by our group in a previous chapter [27].

2. A wide range of high-quality QDs are now available from commercial sources such as Life Technologies (QDot Probe) and Sigma (Lumidot).
3. Given the limited availability and difficultly of culturing primary microglia, immortalized cell lines are an attractive alternative for in vitro imaging applications. N9 microglia are commonly used in neuroscience research because they display cell surface markers and share phenotypic characteristics that are similar to primary human microglia cells [28].
4. We recommend using microwell cell culture dishes with an inner diameter of 20 mm. Reduced cell culture volume (≤500 μL) requires relatively small amounts of reagents and materials, and is still adequate for the immersion of objectives.
5. Laser power should never exceed 5 % for live-cell imaging. Higher laser intensities, which are needed for high-resolution z-stack acquisition, can damage the cell in longitudinal imaging

experiments. The photomultiplier gain and numerical aperture can be adjusted accordingly to adjust signal intensity.

6. IMDM media will change color from light red/pink to orange at lower pH. During the first wash after rat tail collagen coating of the dishes, the media may change color when in contact with the acetic acid.
7. N9 cells are mostly rounded in morphology immediately following seeding and will slowly flatten or extend on the dish (1–4 processes per cell). Due to the low seeding density in each dish (10,000 cells/dish), full confluence will not be attained even after 48 h, thereby permitting imaging of individual cells.
8. We recommend using additional dyes for co-labeling multiple cellular components in live cells. In our experience, Hoechst 33342 (5 μM, 10 min, ex/em = 350/450 nm), a blue-emitting fluorescent dye, is a suitable label for the nucleus, due to limited spectral overlap with most QD types. Additional vital dyes can also be used to label subcellular organelles such as mitochondria (MitoTracker), lipid bodies (BODIPY), and acidic compartments such as lysosomes (LysoTracker). These dyes are commercially available (Life Technologies) in a wide range of emission spectra and are compatible with different biological systems.
9. Unstable QDs tend to form large-order aggregates in the presence of serum proteins, and should be imaged in serum-free media in order to minimize aggregation. Serum-supplemented media is otherwise preferred, as these are optimal cell culture conditions for long-term experiments.
10. If the media spills over the inner well when lowering the objective, aspirate and carefully dry the outer well with a Kim Wipe.
11. We recommend taking a minimum of ten sections per z-stack with an optimal slice diameter between 0.30 and 0.60 μm. This provides superior image quality for subsequent 3D reconstructions and minimizes z-plane distortion between slices.
12. Microglia constantly survey their microenvironment and may change their position. Thus re-focusing the image frame is necessary between each time point.
13. QDs with different surface properties are taken up at different rates through multiple modes of internalization (for more details, *see* [29–32]). The optimal time for endocytic loading should be determined beforehand for each QD type.
14. Pitfalls of cellular imaging: Confocal fluorescence microscopy is the tool of choice to track the fate of QDs in in vitro and in vivo systems, but does not permit quantitative evaluation of QD uptake by living cells, given the artefacts associated with quantitative measurements based on QD emission intensities.

As such, multiple complementary methods, including flow cytometry (FACS), graphite furnace atomic absorption spectrometry (for the determination of intracellular metal ions), and transmission electron microscopy (TEM), must be used to study nanoparticle entry into and elimination from the cell.

15. For surgical procedures (under anesthesia) longer than 60 min, administer another dose of warm saline subcutaneously every hour. Fluids can also be administered in the days following surgery if animals are showing signs of pain or distress.
16. The mouse skull is a very thin piece of bone, and pushing down with the drill or the needle can easily cause excessive damage to the brain tissue. Slow, controlled drilling is sufficient to create and dislodge a bone flap.
17. Absorbable sutures will dissolve within 7–10 days and therefore do not need to be removed manually.
18. Intranasal administration in mice without anesthesia is challenging, as the mouse will attempt to lick the droplet off the nostril instead of inhaling it. A fully conscious mouse may try to bite the pipette tip even when restrained firmly. The mouse should be placed in a prone position, and a small volume (5 μL) should be administered dropwise in the nostril in order to facilitate the uptake of the QDs by the main olfactory epithelium (Fig. 3a). QDs are then expected to transport transcellularly through the olfactory bulb and to deeper and posterior brain regions [17]. By tilting the mouse back (to a more supine position) during intranasal administration, the solution will follow the trachea down to the lungs due to gravitational force. For verification, mice should be imaged in the supine position immediately following intranasal QD administration. Mice with fluorescence signal in the torso region are eliminated from the intranasal group.
19. For intravenous injections, if a bubble or a blister forms in the tail vein, stop the injection as this indicates that the needle is no longer in the vein. To inject a steady flow of solution, secure the syringe between the index and middle fingers, insert the needle (beveled side up) into the vein, and push the plunger slowly with the thumb.
20. The "time window" is the time frame within which the fluorescence lifetime (and decay) will be captured. The fluorescence lifetime of most organic fluorophores is typically between 0.3 and 6 ns, which is much shorter than the typical QD lifetime of ≥100 ns. By selecting a longer time window (e.g., 50, 400 ns) when measuring QD fluorescence, the QD signal can be separated from background and autofluorescence based on fluorescence lifetime.

21. For 3-dimensional reconstruction using the OptiView analysis software, scans should be captured at higher resolutions (between 0.5 and 1.5 mm).
22. For repeated in vivo imaging, the same animal should be used as its own pre-injection, "background signal" control. Simply image each animal prior to surgery and/or before QD administration.
23. For a comprehensive evaluation of lesion progression, the in vivo imaging data should be complemented with biochemical assays, histochemical assays, and animal behavioural studies (e.g., motor control and function) [17].

Acknowledgements

This work was supported in part by grants from CIHR (119425) and NSERC (strategic). AOC was supported by an FRSQ doctoral award.

References

1. Deisseroth K, Feng G, Majewska AK et al (2006) Next-generation optical technologies for illuminating genetically targeted brain circuits. J Neurosci 26(41):10380–10386
2. Hillman EM (2007) Optical brain imaging in vivo: techniques and applications from animal to man. J Biomed Opt 12(5):051402
3. Walling MA, Novak JA, Shepard JR (2009) Quantum dots for live cell and in vivo imaging. Int J Mol Sci 10(2):441–491
4. Maysinger D, Behrendt M, Lalancette-Hebert M, Kriz J (2007) Real-time imaging of astrocyte response to quantum dots: in vivo screening model system for biocompatibility of nanoparticles. Nano Lett 7(8):2513–2520
5. Minami SS, Sun B, Popat K et al (2012) Selective targeting of microglia by quantum dots. J Neuroinflamm. doi:10.1186/1742-2094-9-22
6. Pathak S, Cao E, Davidson MC et al (2006) Quantum dot applications to neuroscience: new tools for probing neurons and glia. J Neurosci 26(7):1893–1895
7. Zhang LW, Monteiro-Riviere NA (2009) Mechanisms of quantum dot nanoparticle cellular uptake. Toxicol Sci 110(1):138–155
8. Jiang X, Rocker C, Hafner M et al (2010) Endo- and exocytosis of zwitterionic quantum dot nanoparticles by live HeLa cells. ACS Nano 4(11):6787–6797
9. Al-Hajaj NA, Moquin A, Neibert KD et al (2011) Short ligands affect modes of QD uptake and elimination in human cells. ACS Nano 5(6):4909–4918
10. Behrendt M, Sandros MG, McKinney RA et al (2009) Imaging and organelle distribution of fluorescent InGaP/ZnS nanoparticles in glial cells. Nanomedicine (Lond) 4(7):747–761
11. Nimmerjahn A, Kirchhoff F, Helmchen F (2005) Resting microglial cells are highly dynamic surveillants of brain parenchyma in vivo. Science 308(5726):1314–1318
12. Li L, Daou TJ, Texier I et al (2009) Highly luminescent $CuInS_2$/ZnS core/shell nanocrystals: cadmium-free quantum dots for in vivo imaging. Chem Mater 21(12):2422–2429
13. Schaffer BS, Grayson MH, Wortham JM et al (2010) Immune competency of a hairless mouse strain for improved preclinical studies in genetically engineered mice. Mol Cancer Ther 9(8):2354–2364
14. Klohs J, Rudin M (2011) Unveiling molecular events in the brain by noninvasive imaging. Neuroscientist 17(5):539–559
15. Vermeer SE, Longstreth WT Jr, Koudstaal PJ (2007) Silent brain infarcts: a systematic review. Lancet Neurol 6(7):611–619
16. Liebeskind DS (2009) Imaging the future of stroke: I. Ischemia. Ann Neurol 66(5): 574–590

17. Choi AO, Maysinger D (2013) Intranasal fluorescent nanocrystals for longitudinal in vivo evaluation of cerebral microlesions. Pharm Nanotechnol 1(2):93–104
18. Maysinger D, Piccardo P, Liberini P et al (1994) Encapsulated genetically engineered fibroblasts: release of nerve growth factor and effects in vivo on recovery of cholinergic markers after devascularizing cortical lesions. Neurochem Int 24(5):495–503
19. Paxinos G, Franklin KBJ (2012) Paxinos and Franklin's the mouse brain in stereotaxic coordinates, 4th edn. Academic Press, Whaltham, MA
20. Walkey CD, Olsen JB, Guo H et al (2012) Nanoparticle size and surface chemistry determine serum protein adsorption and macrophage uptake. J Am Chem Soc 134(4): 2139–2147
21. Walkey CD, Chan WC (2012) Understanding and controlling the interaction of nanomaterials with proteins in a physiological environment. Chem Soc Rev 41(7):2780–2799
22. Tenzer S, Docter D, Rosfa S et al (2011) Nanoparticle size is a critical physicochemical determinant of the human blood plasma corona: a comprehensive quantitative proteomic analysis. ACS Nano 5(9):7155–7167
23. Cedervall T, Lynch I, Lindman S et al (2007) Understanding the nanoparticle-protein corona using methods to quantify exchange rates and affinities of proteins for nanoparticles. Proc Natl Acad Sci USA 104(7): 2050–2055
24. Lundqvist M, Stigler J, Elia G et al (2008) Nanoparticle size and surface properties determine the protein corona with possible implications for biological impacts. Proc Natl Acad Sci USA 105(38):14265–14270
25. Lundqvist M, Stigler J, Cedervall T et al (2011) The evolution of the protein corona around nanoparticles: a test study. ACS Nano 5(9):7503–7509
26. Casals E, Pfaller T, Duschl A et al (2010) Time evolution of the nanoparticle protein corona. ACS Nano 4(7):3623–3632
27. Moquin A, Winnik FM, Maysinger D (2013) Separation science: principles and applications for the analysis of bionanoparticles by asymmetrical flow field-flow fractionation (AF4). Methods Mol Biol 991:325–341
28. Stansley B, Post J, Hensley K (2012) A comparative review of cell culture systems for the study of microglial biology in Alzheimer's disease.JNeuroinflamm.doi:10.1186/1742-2094-9-115
29. Maysinger D, Lovric J, Eisenberg A, Savic R (2007) Fate of micelles and quantum dots in cells. Eur J Pharm Biopharm 65(3): 270–281
30. Duncan R, Richardson SC (2012) Endocytosis and intracellular trafficking as gateways for nanomedicine delivery: opportunities and challenges. Mol Pharm 9(9):2380–2402
31. Iversen T, Skotland T, Sandvig K (2011) Endocytosis and intracellular transport of nanoparticles: present knowledge and need for future studies. Nano Today 6(2):176–185
32. Muro S (2012) Challenges in design and characterization of ligand-targeted drug delivery systems. J Control Release 164(2):125–137

Chapter 16

A Short-Term Inhalation Study Protocol: Designed for Testing of Toxicity and Fate of Nanomaterials

Lan Ma-Hock, Thomas Hofmann, Robert Landsiedel, and Bennard van Ravenzwaay

Abstract

The Short-Term Inhalation Toxicity Study Design described here was specifically developed for the testing of nanoparticles. It consists of a 5-day inhalation exposure with a subsequent 3-week exposure-free period. The protocol has been optimized for the detection of toxic effects in the respiratory tract by incorporation of additional endpoints like collection of bronchoalveolar lavage and measurement of biomarkers indicative for pro-inflammatory and inflammatory changes. Analytical determination of the test compound concentrations in the lung and other organs can be included in the study design for the determination of organ burden and fate of the tested nanomaterial. Over 20 nanomaterials have been tested with this method. In case of those compounds, where data of 90-day inhalation studies were available, the qualitative effects were comparable in both study types. Likewise, the No Observed Adverse Effect Levels were similar between the two study types, showing that the short-term design is suitable for a first risk assessment.

Key words Toxicity study, Respiratory tract, Nanomaterial toxicity, Inhalation exposure, Inflammatory changes

1 Introduction

Quantum Dots are crystalline nanoparticles with semiconductor properties and exhibit extraordinary optical and mechanical properties. However, being nanoparticles, the increased application of Quantum Dots may raise concerns regarding potential health effects, since they can much more easily penetrate biological barriers when compared to their bulk counterparts. Among the potential exposure routes, inhalation is considered to be the most relevant. Toxicological studies using inhalation exposure have been performed with different nanoparticles and have revealed that in principle local inflammation in the lung is the most prominent effect. However, additional important factors have to be considered: First, although inhaled nanoparticles are usually phagocytized by alveolar macrophages, circumvention of this process and

Adriana Fontes and Beate Saegesser Santos (eds.), *Quantum Dots: Applications in Biology*, Methods in Molecular Biology, vol. 1199, DOI 10.1007/978-1-4939-1280-3_16, © Springer Science+Business Media New York 2014

subsequent translocation of particles in other tissues and organs have also been observed. Second, the extent of local inflammation is dependent on many factors, like surface area [1], charge [2], surface lipophilicity/hydrophilicity [3], surface chemistry (e.g., partial oxidation, structural defects, and impurities) [3–5], shape [6, 7], agglomeration state [8, 9], particle size distribution [10], and finally the amount of lung burden [11]. Therefore, a detailed physicochemical characterization of the test materials and the aerosol is crucial for proper evaluation of the study results. Since inhalation toxicity is determined by a complex interaction of these factors, experimental toxicological testing is considered as the preferred option for identifying and avoiding unsafe applications and for selecting safe alternatives for given applications.

Inhalation safety assessment usually is performed based on results of 28- or 90-day inhalation toxicity studies, which require a considerable amount of resources. In order to enable testing of a higher number of nanomaterials, a short-term inhalation testing protocol was developed by BASF in collaboration with the German Federal Ministry of Education and Research project NanoCare and the European Sixth Framework Programme project NanoSafe2. Basically this study design consists of a nose-only inhalation exposure of rats to different aerosol concentrations, 6 h per day, for 5 days, followed by a 23-day period without exposure. The predictivity of this short-term inhalation test for long-term effects is significantly increased by introduction of sensible parameters indicative for pro-inflammatory and pro-fibrotic changes in bronchoalveolar lavage fluid and lung tissue. The results of this study type may serve as a basis for a quantitative risk assessment [12–15]. This study design is currently discussed at the OECD level as draft for a guidance document.

2 Materials

2.1 Animals

The study is performed with rodents routinely used in toxicology studies. Preferred species is the rat, since the historical database of this species is huge. Due to their higher minute volume, male rats are considered more sensitive to local effects on the respiratory tract and are therefore preferred as the more sensitive gender. The age of the animals at study start is 7–9 weeks, with body weights not deviating more than 20 % from the mean weight in each group. Rats are randomly assigned to the different test groups. Environmental conditions are 19–22 °C temperature and 30–70 % relative humidity.

2.2 Inhalation System

The rats are exposed in a dynamic nose-only inhalation chamber system. For this purpose, the animals are placed in cylindrical exposure tubes which are radially placed outside the inhalation

chamber. Thus only the noses of the animals are inside the chamber. The chamber itself consists of a stainless steel cylinder with a volume of approximately 90 L. The aerosol of nanoparticles is introduced at the top of the chamber and exhausted at the bottom. Several types of nose-only inhalation systems exist, continuous-flow and flow-past chambers being the most commonly used ones.

3 Methods

3.1 Generation and Monitoring of the Aerosol

1. The generation of the aerosol can be achieved by different generators, e.g., brush generators, swinging bed generators, or by dispersion of liquid nanosuspensions by atomizers. Basically, pressurized air enters the generator and transports the aerosolized particles into the inhalation chamber. A suction device at the bottom of the chamber draws off the aerosol. A schematic diagram of the inhalation system is depicted in Fig. 1. Different concentrations of the aerosol can be achieved by adjusting the amount of pressurized air entering the aerosol generator. The control group is exposed to air only (*see* **Note 1**).
2. Operating the chamber under a slightly positive pressure prevents a dilution of the test atmosphere in the breathing region of the animals by prevention of bypass air entering through the exposure tubes.

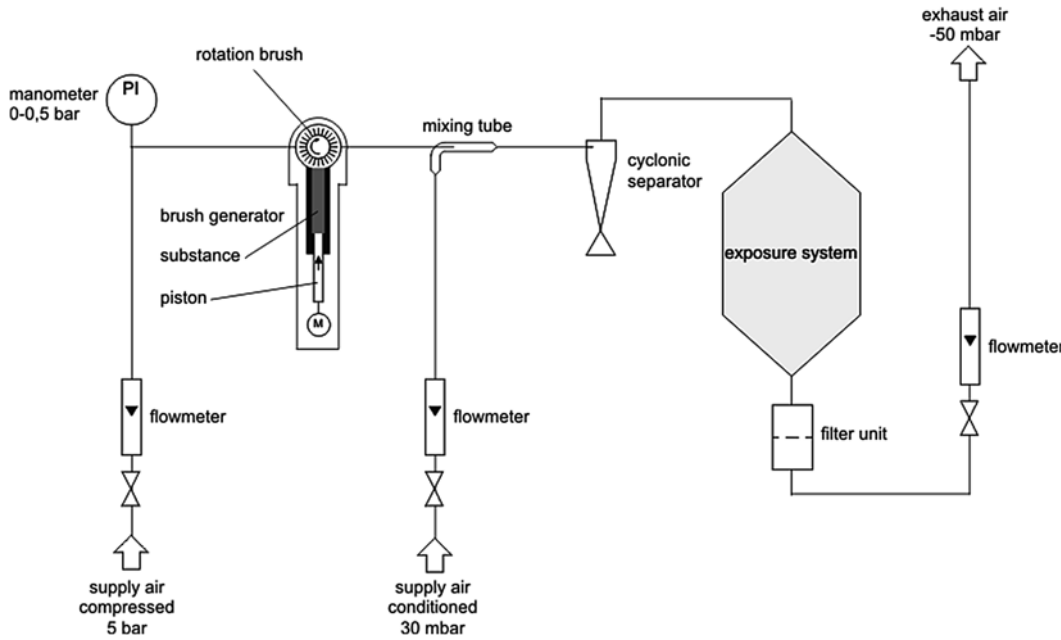

Fig. 1 Schematic diagram of the inhalation system

3. Exposure time is 6 h per day, for 5 days. Airflow through the chambers is controlled at regular intervals in order to ensure stable atmospheres.
4. During exposure, the accuracy and constancy of the aerosol concentration in the chamber is monitored gravimetrically at regular (e.g., hourly) intervals. For this purpose, a defined amount of the test atmosphere is drawn through a filter sampling device temporarily mounted to the inhalation chamber. The actual concentration of the aerosol is then calculated by dividing the collected mass on the filter through the sample volume. Constancy of the aerosol concentration can additionally be monitored continuously by scattered light photometers.
5. The particle size distribution of the nanoparticle aerosol is measured normally twice during the study using a cascade impactor. Analogous to the gravimetric measurements described above, the test atmosphere is drawn through the impactor and separated on several pre-weighed stages according to different particle size ranges. The amount of collected mass per stage is thereafter used for the calculation of the mass median aerodynamic diameter (MMAD) and its geometric standard deviation (SG), which are key parameters for the characterization of aerosols. In order to differentiate the smaller particle size ranges and to measure free nanoparticles, an optical particle sizer (OPC) and/or a scanning mobility particle sizer (SMPS) may be appropriate in addition to the cascade impactor.
6. During the study the animals are observed for clinical signs before, during, and after exposure. Body weights and food consumption are recorded at start and end of exposure, weekly thereafter, and at study end.

3.2 Necropsy

1. After the last exposure (Day 5) and on Day 28, groups of three rats are necropsied. Liver, kidney, brain, lungs, spleen, thymus, and mediastinal lymph node are weighed. Head (with oropharynx), lungs, larynx, trachea, liver, kidneys, adrenal glands, mediastinal lymph node, thymus, brain, spleen, heart, thyroid gland, and all gross lesions are fixated in 10 % buffered formalin, embedded in paraffin, and processed for histopathological examination.
2. Tissue slices are stained with hematoxylin-eosin and examined microscopically. Special attention is given to the respiratory tract (four levels of the nasal cavity, three levels of larynx, trachea with bifurcation, lung).
3. Transmission electron microscopy can be performed on additional satellite groups of rats on a case-by-case basis.
4. On Day 5 and Day 28, groups of five rats are used for clinical pathology and bronchoalveolar lavage.

3.3 Clinical Pathology

1. Blood samples are taken from the retrobulbar venous plexus in anesthetized rats after overnight fasting. Thereafter the animals are killed by exsanguination under deep anesthesia.
2. Blood samples are used for determination of hematological (red cell count, reticulocytes, total and differential white cell count, clotting parameters) and clinical chemistry parameters indicative for systemic inflammation (haptoglobin, C-reactive protein).

3.4 Bronchoalveolar Lavage Fluid

1. Bronchoalveolar lavage fluid (BALF) is collected by instillation and retraction of approximately 6 mL physiological saline into the lung via a tracheal cannula after exsanguination of the rats. This procedure is repeated once and the recovered fluids combined. BALF is centrifuged by approximately $200 \times g$.
2. The pellet is used for determination of total cell count after resuspension, and cytocentrifuge preparations are stained after Wright for microscopic differentiation. Evaluated parameters comprise macrophages, polymorphonuclear neutrophils, lymphocytes, eosinophils, monocytes, and atypical cells.
3. The supernatant is used for the determination of protein, lactate dehydrogenase, alkaline phosphatase, *N*-acetyl-β-glucosaminidase, and γ-glutamyltransferase.
4. Additionally, BALF and the homogenized lavaged lung tissue are examined for biomarkers indicative for inflammation, fibrotic processes, and pulmonary toxicity. With respect to this, among others the following parameters have been proved to be useful: rat monocyte chemoattractant protein-1 rat MCP-1, rat cytokine-induced neutrophil chemoattractant-1/interleukin-8 (CINC-1/IL-8), macrophage colony stimulating factor (M-CSF), and rodent osteopontin. The monitoring panel has been arranged so that different functional groups of antigens are covered, i.e., CC-chemokines (MCP-1); CXC-chemokines (IL-8/CINC-1); hematopoiesis (M-CSF); proliferation of sessile cells (osteopontin).

3.5 General Consideration

The Short-Term Inhalation Study Design was developed as a considerably less labor- and time-intensive alternative to the classical 28-day study. This protocol has been optimized by incorporation of additional endpoints like collection of BALF and measurement of biomarkers indicative for pro-inflammatory and inflammatory changes. Over 20 nanomaterials have been tested with this method. In case of those compounds, where data of 90-day inhalation studies were available, the qualitative effects were comparable in both study types. Likewise, the No Observed Adverse Effect Levels were similar between the two study types, showing that the short-term design is suitable for a first risk assessment (*see* **Notes 2–4**).

4 Notes

1. In case of marked agglomeration of primary particles, a pre-separator may be used before the aerosol enters the inhalation chamber.
2. The results of a short-term inhalation study with cadmium-based Quantum Dots [16] have demonstrated that also these materials can be adequately characterized by this study design.
3. Since Quantum Dots contain heavy metals which may have distinctly long elimination half-lives in the organism (e.g., for Cd greater than 20 years), determination of these metals in the respiratory tract after the last exposure and thereafter may be indicated on a case-by-case basis. These examinations can also be used for the detection of translocation of the inhaled nanoparticles into other organs like brain or spleen.
4. Metal ions (e.g., Cd^{2+}) can be released from Quantum Dots in the organism, which may lead to local and/or systemic toxicity. This possibility should be taken into account.

References

1. Oberdorster G, Ferin J, Lehnert BE (1994) Correlation between particle size, *in vivo* particle persistence, and lung injury. Environ Health Perspect 102(Suppl 5):173–179
2. Karakoti AS, Hench LL, Seal S (2006) The potential toxicity of nanomaterials – the role of surfaces. JOM 58:77–82
3. Bottini M, Bruckner S, Nika K et al (2006) Multi-walled carbon nanotubes induce T lymphocyte apoptosis. Toxicol Lett 160:121–126
4. Muller J, Huaux F, Fonseca A et al (2008) Structural defects play a major role in the acute lung toxicity of multiwall carbon nanotubes: toxicological aspects. Chem Res Toxicol 21: 1698–1705
5. Fenoglio I, Greco G, Tomatis M et al (2008) Structural defects play a major role in the acute lung toxicity of multiwall carbon nanotubes: physicochemical aspects. Chem Res Toxicol 21:1690–1697
6. Poland CA, Duffin R, Kinloch I et al (2008) Carbon nanotubes introduced into the abdominal cavity of mice show asbestos-like pathogenicity in a pilot study. Nat Nanotechnol 3:423–428
7. Mühlfeld C, Poland CA, Duffin R et al (2012) Differential effects of long and short carbon nanotubes on the gas-exchange region of the mouse lung. Nanotoxicology 6:867–879
8. Wick P, Manser P, Limbach LK et al (2007) The degree and kind of agglomeration affect carbon nanotube cytotoxicity. Toxicol Lett 168:121–131
9. Mercer RR, Scabilloni J, Wang L et al (2008) Alteration of deposition pattern and pulmonary response as a result of improved dispersion of aspirated single walled carbon nanotubes in a mouse model. Am J Physiol Lung Cell Mol Physiol 294:87–97
10. Elder A, Gelein R, Finkelstein JN et al (2005) Effects of subchronically inhaled carbon black in three species. I. Retention kinetics, lung inflammation, and histopathology. Toxicol Sci 88:614–629
11. Morrow PE (1988) Possible mechanisms to explain dust overloading of the lungs. Fundam Appl Toxicol 10:369–384
12. Ma-Hock L, Burkhardt S, Strauss V et al (2009) Development of a short-term inhalation test in the rat using nano-titanium dioxide as a model substance. Inhal Toxicol 21:102–118
13. Van Ravenzwaay B, Landsiedel R, Fabian E et al (2009) Comparing fate and effects of three particles of different surface properties: nano-TiO_2, pigmentary TiO_2 and quartz. Toxicol Lett 186:152–159
14. Landsiedel R, Ma-Hock L, Kroll A et al (2010) Testing metal-oxide nanomaterials for human safety. Adv Mater 22:2602–2627
15. Klein CL, Wiench K, Wiemann M et al (2012) Hazard identification of inhaled nanomaterials: making use of short-term inhalation studies. Arch Toxicol 86:1137–1151
16. Ma-Hock L, Brill S, Wohlleben W et al (2012) Short term inhalation toxicity of a liquid aerosol of CdS/$Cd(OH)_2$ core shell quantum dots in male Wistar rats. Toxicol Lett 208:115–124

Part V

Quantum Dots for FRET Applications

Chapter 17

Quantitative Measurement of Proteolytic Rates with Quantum Dot-Peptide Substrate Conjugates and Förster Resonance Energy Transfer

Miao Wu, Eleonora Petryayeva, Igor L. Medintz, and W. Russ Algar

Abstract

An important challenge in biology is the development of probes for visualizing and quantitatively tracking enzyme activity. Proteases are an important class of enzyme with value as both diagnostic and therapeutic targets. In this chapter, we describe the preparation of quantum dot (QD)-peptide substrate conjugates as probes for measuring proteolytic activity. QDs have several highly advantageous optical properties that make these materials especially well suited for applications in bioanalysis and bioimaging. Further, peptide substrates for proteases can be controllably self-assembled to QDs and this capability, in combination with Förster resonance energy transfer (FRET), enables the design of quantitative in vitro assays capable of directly reporting on proteolytic activity. We present a detailed method for the preparation, calibration, and application of such QD probes, along with methods of analysis to generate progress curves for the proteolytic digestion of substrate. Representative data are illustrated for two different proteases and two different QD-fluorescent dye FRET pairs. The general methodology is likely to be applicable with other hydrolytic enzymes in addition to proteases. Overall, the method is straightforward to implement with commercially available materials and does not require specialized expertise.

Key words Quantum dot, Förster resonance energy transfer, Peptide, Proteolysis, Progress curve

1 Introduction

Fluorescence spectroscopy and imaging are versatile and very sensitive techniques for biological studies. Well-known applications include cellular imaging and tissue staining, fluorescence activated cell sorting and flow cytometry, in situ hybridization, microarrays, and numerous fluorescent assays [1–5]. Despite the great success of these applications, it has been recognized that organic fluorescent dyes have a number of shortcomings; for example, a tendency to photobleach, sensitivity to their environment, and technical challenges in multiplexing (e.g., crosstalk, multiple excitation sources) [6]. In recent years, semiconductor quantum dots (QDs) have emerged as alternatives to organic fluorophores,

Adriana Fontes and Beate Saegesser Santos (eds.), *Quantum Dots: Applications in Biology*, Methods in Molecular Biology, vol. 1199, DOI 10.1007/978-1-4939-1280-3_17, © Springer Science+Business Media New York 2014

offering robust luminescence with several favorable characteristics. In this chapter, we describe a method for tracking the activity of proteases with QD-peptide conjugates, including preparation of these probes and examples of assays from calibration through to analysis of fluorescence data. Proteases rival kinases as one of the largest functional gene families within the human genome and the function of most proteases are still not fully characterized. Aberrant proteolytic activity is associated with various cancers, Alzheimer's disease, arthritis, and the pathogenesis of malaria and HIV, among many other conditions, such that proteases are important diagnostic and therapeutic targets [7, 8]. Sensitive probes that can quantitatively measure proteolytic activity are thus critically needed as research tools.

1.1 Quantum Dots

QDs are brightly luminescent colloidal semiconductor nanocrystals. These materials typically range from 2 to 10 nm in diameter and are synthesized as a core/shell structure for most biological applications [9–11]. Common examples include CdSe/ZnS QDs and alloyed $CdSe_{1-x}S_x$/ZnS QDs, both of which have photoluminescence (PL) in the visible spectrum. The core nanocrystal determines the optical properties of the QD, while the shell passivates the core and enhances those properties. The favorable optical properties of QDs include, but are not necessarily limited to, spectrally narrow emission that can be tuned to different wavelengths on the basis of nanocrystal size and composition; light absorption across a broad range of wavelengths, characterized by large one-photon (10^5–10^6 M^{-1} cm^{-1}) and two-photon (10^3–10^4 GM) absorption coefficients; and excellent resistance to photobleaching [9]. QDs are particularly well suited for multicolor or multiplexed applications, for ensemble and single-molecule imaging and, notably, for Förster resonance energy transfer (FRET) probes [12]. Consequently, QDs have been of great interest for developing new methods of bioanalysis.

High-quality QDs are synthesized in organic solvents and are not dispersible in water [13, 9]. One common method for rendering QDs water dispersible is to exchange their hydrophobic ligands from synthesis with hydrophilic ligands such as dihydrolipoic acid (DHLA), various derivatives of DHLA, or other bifunctional thiol compounds [9, 14–16]. When such coatings are applied to QDs, bioconjugates can frequently be prepared through the self-assembly of polyhistidine-appended peptides, proteins, and oligonucleotides [17, 18]. Polyhistidine-appended biomolecules exhibit high affinity for the ZnS shell of QDs ($K_d \sim 10^{-9}$–10^{-8} M) and reach equilibrium binding with QDs within minutes [18]. An important consequence of this high affinity is that the average number of biomolecules per QD (i.e., conjugate valence) can be reliably controlled on the basis of the mixing stoichiometry between the biomolecule and the QD. This capability facilitates both the design of

QD-bioconjugates and the analysis of data collected with those conjugates. These advantages will become clear in this chapter as we self-assemble polyhistidine-appended peptides to QDs as part of a quantitative FRET assay for proteolytic activity.

1.2 Förster Resonance Energy Transfer

FRET is a distance-dependent, nonradiative energy transfer mechanism between a donor fluorophore and acceptor chromophore [19]. It has become famous for its ability to serve as a so-called molecular ruler for measuring protein folding [20], its role in molecular beacons [21], and its utility in studying protein–protein interactions via fusions with, for example, cyan fluorescent protein (CFP, donor) and yellow fluorescent protein (YFP, acceptor) [22]. The efficiency of energy transfer depends on the distance, r, between donor and acceptor, as well as the intrinsic properties of the donor–acceptor pair. The latter are accounted for in the Förster distance, R_0, which represents the distance at which the energy transfer efficiency is 50 % [19]. One of the key criteria for a good FRET pair with large R_0 is that the donor emission has spectral overlap with the acceptor absorption. The relationship between the donor–acceptor distance, r, the Förster distance, and FRET efficiency is given by Eq. 1. Note that n is the number of equivalent acceptors interacting with a donor. Experimentally, FRET can be measured from quenching of donor emission, also shown in Eq. 1, where I is an emission intensity, D denotes a donor-only quantity, and DA denotes a donor quantity measured in the presence of acceptor [19].

$$E = \frac{nR_0^6}{nR_0^6 + r^6} = 1 - \frac{I_{\mathrm{DA}}(\lambda)}{I_D(\lambda)} \tag{1}$$

When the acceptor is fluorescent, FRET can also be measured from the sensitization of acceptor emission, concomitant with donor quenching. The ratio of acceptor and donor emission is given by Eq. 2, where AD denotes an acceptor quantity measured in the presence of donor and Φ is a quantum yield. In Eq. 2, the total integrated emission from the donor and acceptor is needed, whereas any wavelength (or band of wavelengths) associated with only donor emission can be used in Eq. 1.

$$\frac{\int I_{\mathrm{AD}}(\lambda)\,\mathrm{d}\lambda}{\int I_{\mathrm{DA}}(\lambda)\,\mathrm{d}\lambda} = n\frac{\Phi_A}{\Phi_D}\left(\frac{R_0}{r}\right)^6 \tag{2}$$

1.3 Assaying Proteolytic Activity

This chapter describes a method for a FRET-based assay of proteolytic activity using QD-peptide substrate conjugates. The peptides are labeled with a suitable fluorescent dye acceptor for a given QD donor and self-assembled to the QDs through polyhistidine-ZnS affinity coordination to generate FRET probes. QDs are excellent

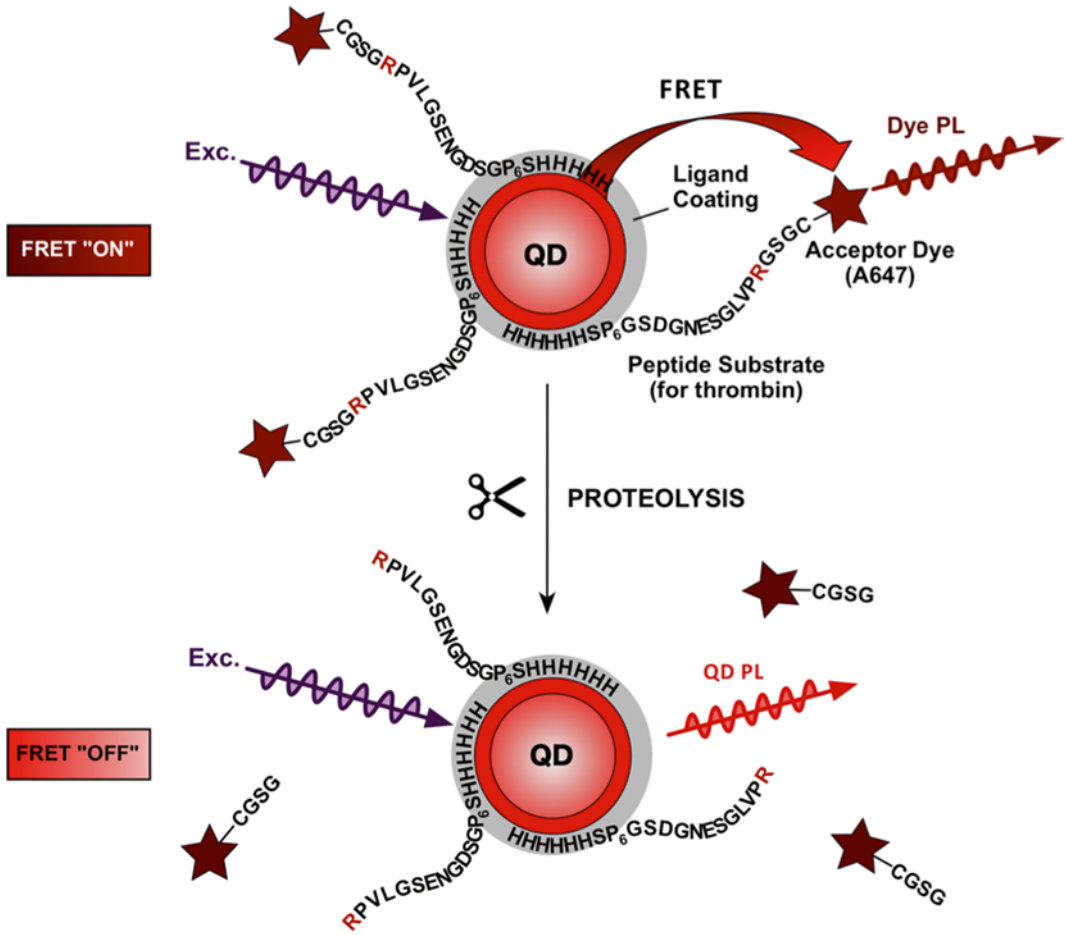

Fig. 1 Illustration of a QD-peptide substrate conjugate and FRET-based signaling of proteolysis. A red-emitting QD is shown conjugated to a peptide substrate for thrombin. The peptide is labeled with a fluorescent dye, A647, at a C-terminal cysteine residue and self-assembled to the QD through a hexahistidine sequence at its N-terminus. In the absence of thrombin (protease), FRET occurs between the QD donor and dye acceptor. Proteolysis at the recognition site in the peptide sequence (the *highlighted* arginine residue, *R*) separates the dye from the QD and FRET can no longer occur. Emission shifts from the dye to the QD and changes in the A647/QD PL ratio provides an analytical signal for tracking proteolysis

FRET donors by virtue of (a) their narrow emission, which permits large spectral overlap with minimal emission crosstalk; (b) their broad absorption, which permits efficient donor excitation with minimal direct excitation of acceptor; and (c) their nanoscale surface area, which permits the self-assembly of multiple acceptors per QD to enhance FRET efficiency ($n > 1$ in Eqs. 1 and 2). As illustrated in Fig. 1, proteolytic activity cleaves the peptide, separating the QD donor and dye acceptor with loss of FRET. Assays for several different proteases have been reported using this format [23–27]. Here, we outline experimental and data analysis methods

that can be used to calibrate and extract quantitative enzyme kinetic data from two-color fluorescence measurements with QD-peptide-dye conjugate-FRET pairs—something that has remained challenging to date. Although based on the fundamental expressions in Eqs. 1 and 2, our methodology is entirely empirical and does not require knowledge of Förster distances or quantum yields. Highly parallel analysis can be implemented using a fluorescence plate reader, as we describe here with assays for thrombin and trypsin as two model proteases, and with two examples of QD-dye FRET pairs.

2 Materials

2.1 Reagents

1. Ultrapure water: sterile, specific resistance ≥18 MΩ cm^{-1}.
2. Acetonitrile (CH_3CN), HPLC grade.
3. Borate buffer (BB1): 50 mM borate, pH 9.2, 250 mM NaCl.
4. Borate buffer (BB2): 50 mM borate, pH 9.2.
5. Borate buffer (BB3): 50 mM borate, pH 8.5, 13.7 mM NaCl, 0.27 mM KCl.
6. Tris buffer: 20 mM 2-amino-2-hydroxymethyl-propane-1, 3-diol (Tris), pH 8.5, 50 mM NaCl, 1 mM $CaCl_2$.
7. Hydrophobic QDs (*see* **Note 1**). As an example, we use commercially available alkyl-ligand coated CdSeS/ZnS QDs (Cytodiagnostics Inc., Burlington, ON, Canada), including those with green emission (gQD) and red emission (rQD).
8. Dihydrolipoic acid (DHLA; *see* **Note 2**).
9. L-Glutathione, reduced (GSH).
10. Tetramethylammonium hydroxide (TMAH): 25 % w/w solution in methanol.
11. Chloroform, reagent grade.
12. Dye-labeled peptide substrate(s) with a hexahistidine terminus (*see* **Notes 3** and **4**). As an example, we use the peptides listed in Table 1 (Biosynthesis Inc., Lewisville, TX). These peptides are abbreviated as "Sub_{THR}(A647)," a thrombin substrate labeled with Alexa Fluor 647 dye, and as "Sub_{TRP}(A555)," a trypsin substrate labeled with Alexa Fluor 555.

Table 1
Peptide substrate sequences (divided into modules as indicated) and dye modifications

Peptide	Abbreviation	Sequence (N-terminal to C-terminal)
Thrombin substrate	Sub_{THR}(A647)	H_6·SP_6·GSDGNESGLVP**R**GSG·C(A647)
Trypsin substrate	Sub_{TRP}(A555)	H_6·SP_6·SGWDSGWDSGWDSG**R**LG·C(A555)

13. Reagents for preparation of poly(acrylamide) gels: acrylamide, bisacrylamide, ammonium persulfate (APS), tetramethylethylenediamine (TEMED).
14. Agarose: molecular biology grade, low electroendoosmosis (EEO).
15. Tris-borate-EDTA (TBE) buffer (10× stock): 0.89 M Tris base, 0.89 M borate, 0.02 M EDTA. Prepare a 1× dilution for agarose gels (*see* **Note 5**).
16. Aqueous glycerol solution, 20 % v/v: prepare >100 μL of a 1:4 dilution with ultrapure water.
17. Thrombin from bovine plasma: 36.7 kDa, 40–300 NIH units/mg protein.
18. Trypsin from bovine pancreas: 23.8 kDa, TPCK treated, ≥10,000 BAEE units/mg protein.
19. N_{α}-Tosyl-L-lysine chloromethyl ketone hydrochloride (TLCK).

2.2 Equipment

1. Micropipettes and tips.
2. Low-binding polypropylene microcentrifuge tubes, 1.7 mL capacity. We use Costar 3207 (Corning, NY, USA).
3. Apparatus for agarose gel electrophoresis.
4. Apparatus for poly(acrylamide) gel electrophoresis.
5. Power supply for gel electrophoresis.
6. UV-visible spectrophotometer. We use an Infinite M1000 Pro plate reader (Tecan Ltd., Morrisville, NC, USA).
7. Fluorescence plate reader. We use an Infinite M1000 Pro plate reader.
8. 96-well microtiter plates. We use Corning 3650 plates for fluorescence measurements and Corning 3679 plates for UV-visible absorption measurements.

3 Methods

3.1 Selection of a QD-Dye FRET Pair

1. Choose a QD with a peak PL emission wavelength suitable for the plate reader available (*see* **Note 6**).
2. Choose a dye according to the following criteria: (a) overlap between the dye absorption spectrum and the QD emission spectrum; (b) a minimum in the dye absorption in the blue/ultraviolet region of the spectrum; (c) minimal overlap between the QD PL and dye fluorescence; and (d) dye emission suitable for the plate reader available. As shown in Fig. 2, we use green emitting QDs paired with A555 and red emitting QDs paired with A647.

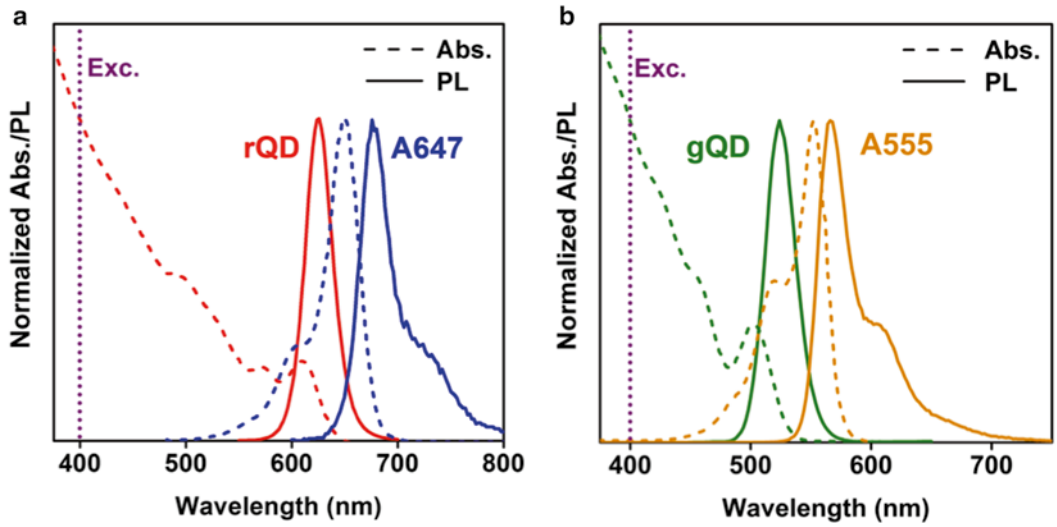

Fig. 2 Normalized absorption and PL emission spectra for (**a**) rQD-A647 FRET pair and (**b**) gQD-A555 FRET pair. An excitation wavelength of 400 nm is used for both FRET pairs. In both panels, note the minimum in the absorbance of the dye at 400 nm, the overlap between the QD emission and dye absorption, and the nearly resolved peak emission between the QDs and dyes

3.2 Ligand Exchange with Glutathione

Water dispersed QDs are needed for conjugation with peptide substrates and subsequent assays of proteolytic activity. GSH can be used as a ligand to render water dispersed QDs. This section describes a method for modifying hydrophobic QDs with glutathione. Here, we use GSH-coated QDs for assaying thrombin activity. An alternative coating method using DHLA is described in Subheading 3.3.

1. Add 100 μL of 1–5 μM hydrophobic QDs in organic solvent to a 1.7 mL microcentrifuge tube or small glass vial with similar capacity (*see* **Note 7**).
2. Dilute the QDs from **step 1** with 900 μL of chloroform.
3. Prepare a solution of ca. 80 mg of GSH in 300 μL of TMAH solution. The final concentration of GSH is ca. 870 mM.
4. Add the GSH/TMAH solution to the QDs.
5. Mix and let stand at room temperature for 8–12 h.
6. Add 200 μL of borate buffer (BB1) and mix. Let the aqueous and organic phases separate. The QDs will be in the aqueous layer.
7. Remove and discard the organic layer (bottom).
8. Add ca. 700–800 μL of ethanol to the aqueous QDs. Mix and centrifuge at 4,800 rcf for 10 min.

9. Draw the supernatant off the pellet of precipitated QDs from **step 8** and discard.
10. Redisperse the QDs in 100 μL of borate buffer (BB1).
11. Repeat **steps 8–10** twice (a total of three precipitation and wash steps). On the final repetition, redisperse the QDs in 200 μL of borate buffer (BB2; *see* **Note 8**).
12. Determine the concentration of the aqueous QD suspension using UV-visible absorption spectrophotometry and the extinction coefficient provided by the manufacturer.
13. Store at 4 °C. Do not freeze.

3.3 Ligand Exchange with DHLA

This section describes a method for rendering hydrophobic water dispersed QDs using DHLA as a ligand. We use DHLA-coated QDs to assay trypsin activity.

1. Add 100 μL (1–5 μM) of hydrophobic QDs in organic solvent to a small glass reaction vessel (*see* **Note 9**).
2. Add 100 μL of neat DHLA to the QDs.
3. Close the reaction vessel to the ambient environment and purge with inert gas (*see* **Note 10**).
4. Heat the reaction mixture to 70 °C for 2 h (*see* **Note 11**).
5. Cool in an ice bath.
6. Add 200 μL of TMAH solution.
7. Add 200 μL of borate buffer (BB1).
8. Add ca. 1 mL of chloroform and mix. Let the aqueous and organic phases separate. The QDs will be in the aqueous phase.
9. Transfer the aqueous layer as two aliquots of approximately equal volume (ca. 200 μL each) to microcentrifuge tubes. Discard the organic layer.
10. Add ca. 700–800 μL of ethanol to each tube. Mix and centrifuge at 4,800 rcf for 4 min.
11. Draw the supernatant off the pellet of precipitated QDs from **step 10** and discard.
12. Redisperse the QDs in 100 μL of borate buffer (BB1).
13. Repeat **steps 10–12** twice (a total of three precipitation and wash steps). On the final repetition, redisperse the QDs in 200 μL of borate buffer (BB2; *see* **Note 8**).
14. Determine the concentration of the aqueous QD solution using UV-visible absorption spectrophotometry and the extinction coefficient provided by the manufacturer.
15. Store at 4 °C. Do not freeze.

3.4 Predigestion of Peptide Substrate

Predigested peptide is needed for calibration experiments where FRET signals are correlated to the number of native and digested substrates assembled per QD.

1. Prepare ≥50 μL of buffered enzyme solution. We prepared ca. 25 μM (1 mg/mL) thrombin in borate buffer (BB3) and ca. 54 nM (2.5 μg/mL) trypsin in Tris buffer (*see* **Note 12**).
2. Dissolve solid dye-labeled peptide substrate (10 nmol) in 5 μL of 50 % v/v aqueous acetonitrile (prepared with sterile ultrapure water). Dilute with 45 μL of buffer (BB3 for thrombin; Tris buffer for trypsin).
3. Add 50 μL of enzyme solution from **step 1** to the peptide solution from **step 2** (100 μM final concentration of peptide substrate). This mixture will be a stock solution of predigested peptide substrate (*see* **Note 13**).
4. Dissolve a second portion of solid dye-labeled peptide substrate (10 nmol) in 5 μL of 50 % v/v aqueous acetonitrile and dilute with 95 μL of buffer (100 μM final concentration of peptide substrate; BB3 for thrombin, Tris buffer for trypsin). This mixture will be a stock solution of native peptide substrate.
5. Leave both samples (**steps 3** and **4**) overnight (>12 h) at room temperature (s*ee* **Note 14**).
6. Prepare a fresh solution of enzyme inhibitor. For trypsin and thrombin, we use 25 mM TLCK dissolved in DMSO (*see* **Note 15**).
7. Add an excess of enzyme inhibitor to the digested peptide sample. We use 5 μL TLCK solution from **step 6** for trypsin and thrombin (final concentration ca. 1 mM). Let stand for 1 h at room temperature (*see* **Note 16**).
8. With thrombin, we repeated **step 7** twice at 60 min intervals (three additions of inhibitor in total).

3.5 Confirming Predigestion of Peptide Substrate

Poly(acrylamide) gel electrophoresis is used to confirm that the native peptide substrate is fully hydrolyzed to two product fragments by predigestion with enzyme (Subheading 3.4).

1. Prepare a 5 % poly(acrylamide) gel with 1× TBE buffer.
2. Prepare samples with 1 nmol peptide in 20 μL of buffer (*see* **Note 17**).
3. Add 8 μL of 20 % v/v glycerol to a final concentration of ca. 6 % v/v.
4. Load the gel and run at 10 V/cm for 40–60 min.
5. Image under UV light. The native and predigested substrate should have different electrophoretic mobilities (*see* **Note 18**). An example of poly(acrylamide) gel with native and digested substrate for trypsin is shown in Fig. 3a.

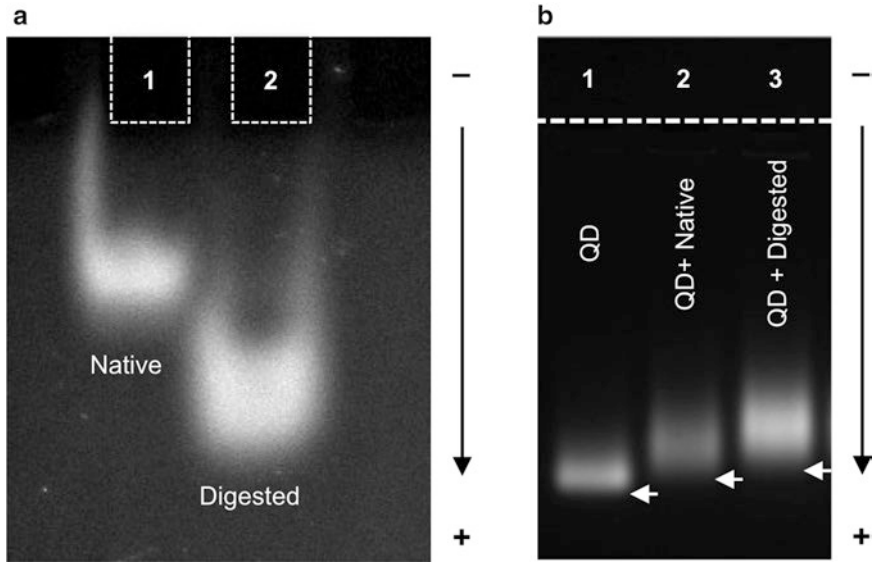

Fig. 3 Fluorescence images of (**a**) poly(acrylamide) gel showing complete predigestion of native trypsin substrate, Sub_{TRP}(A555), and (**b**) 1.5 % agarose gel showing differences in electrophoretic mobility between rQDs, and native and predigested rQD-$Sub_{THR}(A647)_8$ conjugates. In panel (**b**), note that the native rQD-SubTHR$(A647)_8$ conjugates have the weakest emission due to efficient FRET. The lower mobility of the predigested rQD-$Sub_{THR}(A647)_8$ conjugates is because the A647 dye label is anionic

3.6 Confirming Self-Assembly of Peptides to QDs

Agarose gel electrophoresis is used to confirm that the native and digested (polyhistidine fragment) peptides self-assemble to the QDs.

1. Prepare a 1.5 % agarose gel with 1× TBE buffer.
2. Prepare samples with 10 pmol of QD or QD-peptide conjugate in 15–20 μL of buffer.
3. Add 4–5 μL of 20 % v/v glycerol to a final concentration of ca. 4 % v/v.
4. Load the gel and run at 7 V/cm for 20–30 min. GSH and DHLA modified QDs run toward the anode (positive potential).
5. Image under UV light. The self-assembly of peptides to GSH or DHLA modified QDs will decrease their electrophoretic mobility. Figure 3b shows an example of an agarose gel with unmodified QDs, QDs assembled with native peptide substrate, and QD assembled with predigested substrate (*see* **Note 19**).

3.7 Calibration Curve

1. Prepare dilutions of native and digested peptide at convenient working concentrations. We typically dilute to between 2 and 4 μM (*see* **Note 20**).
2. Prepare a series of calibration samples by mixing QDs (20 pmol; *see* **Note 21**) with different ratios of native and predigested peptide substrates according to **steps 3–6**, where N_0 is the

Table 2
Example of a set of calibration samples

Sample	(i)	(ii)	(iii)	(iv)	(v)	(vi)	(vii)	(viii)	(ix)
Quantum dots									
eqv.	1	1	1	1	1	1	1	1	1
pmol	20	20	20	20	20	20	20	20	20
Native peptide									
eqv.	0	1	2	3	4	5	6	7	8
pmol	0	20	40	60	80	100	120	140	160
Predigested peptide									
eqv.	8	7	6	5	4	3	2	1	0
pmol	160	140	120	100	80	60	40	20	0

valence of QD-peptide substrate conjugates to be used for enzyme assays (*see* Subheading 3.9).

3. Add N equivalents of native peptide substrate (20 N pmol) and X equivalents of predigested peptide substrate (20X pmol) to microcentrifuge tubes for $N=0$ to $N=N_0$, where $N+X=N_0$ (*see* **Note 22**). Table 2 is an example of a sample set for a calibration experiment.
4. Dilute the mixture of native and digested peptide substrates with buffer to the desired final volume *less* V_{QD}, the volume of QDs to be added. We typically add

$$V_{Buffer} = 110\ \mu L - V_{QD} - V_{Native} - V_{Digest}$$

where V_{Native} and V_{Digest} are the volumes of native and digested peptide already added in **step 3** (*see* **Note 23**).
5. Add QDs (20 pmol as $V_{QD} = 20\ \text{pmol}/C_{QD}$, where C_{QD} is the stock concentration of QDs) to each sample and mix immediately.
6. Let the calibration samples stand at room temperature for at least 0.5–1.0 h (*see* **Notes 24** and **25**).
7. Transfer an aliquot of each calibration sample to a well in a microtiter plate. We transfer 100 μL of calibration sample into the wells of our 96-well plates.
8. Measure the photoluminescence spectrum of each calibration sample using a fluorescence plate reader. An excitation wavelength of 400 nm works well with many combinations of QD and fluorescent dye (*see* **Note 26**). Examples of calibration

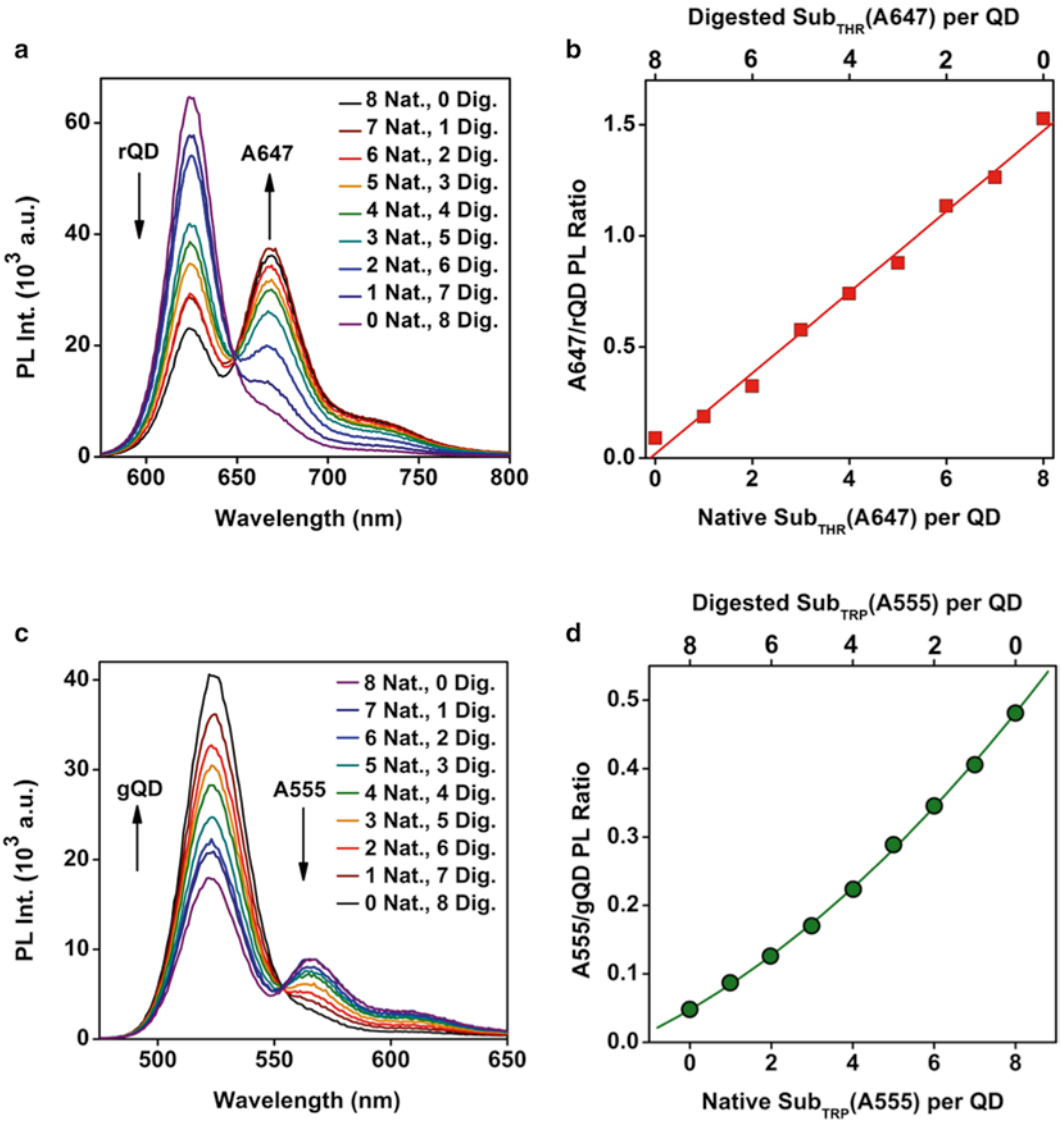

Fig. 4 Examples of calibration data. (**a**) PL spectra and (**b**) PL intensity ratios for the rQD-A647 FRET pair and different stoichiometric ratios of native (Nat.) and predigested (Dig.) Sub_{THR}(A647) at a total valence of eight peptides per QD. The data in panel (**b**) is approximately linear. (**c**) PL spectra and (**d**) PL intensity ratios for the gQD-A555 FRET pair and different stoichiometric ratios of native and predigested Sub_{TRP}(A555) at a total valence of eight peptides per QD. The data in panel (**d**) is quadratic. For both sets of conjugates, note the decrease in QD PL and increase in FRET-sensitized acceptor PL as the number of native peptides per QD increases

spectra for rQD-Sub_{THR}(A647) and gQD-Sub_{TRP}(A555) conjugates are shown in Fig. 4a, c, respectively.

9. Record the optimized plate reader settings from **step 8** for future use (Subheading 3.9).
10. Proceed to Subheading 3.8 for data analysis.

3.8 Analysis of Calibration Data

1. We define an acceptor/donor PL intensity ratio, ρ, according to Eq. 3, where I_λ is the PL intensity at wavelength, λ. The subscripts D and A denote FRET donor (i.e., QD) and acceptor (i.e., fluorescent dye) as noted in the introduction (Subheading 1.2). The values of λ_D and λ_A are typically selected to coincide with the peak emission wavelengths for both (*see* **Note 27**). Equation 3 includes a correction factor, σ_{D,λ_A}, to account for spectral crosstalk (*see* **step 2**). Since this method is empirical, there is no need to account for the total integrated emission of donor and acceptor; rather, a single wavelength (or band of wavelengths) can be used for both.

$$\rho = \frac{I_{\mathrm{AD}}}{I_{\mathrm{DA}}} = \frac{I_{\mathrm{AD},\lambda_A} - \sigma_{D,\lambda_A} I_{\mathrm{DA},\lambda_D}}{I_{\mathrm{DA},\lambda_D}} \tag{3}$$

2. The QD often has a small amount of emission at λ_A. The correction factor, σ_{D,λ_A}, is determined from the measured PL emission spectrum of the QD alone and calculated using Eq. 4.

$$\sigma_{D,\lambda_A} = \frac{I_{D,\lambda_A}}{I_{D,\lambda_D}} \tag{4}$$

3. The value of ρ, the PL ratio, is determined for each calibration sample and plotted versus the number of native substrates per QD, N, where there are $N_0 - N$ digested substrates in the same sample. Examples of PL ratio calibration data for rQD-$\mathrm{Sub_{THR}}$(A647) and gQD-$\mathrm{Sub_{TRP}}$(A555) conjugates are shown in Fig. 4b, d, respectively.
4. The calibration data, ρ versus N, can generally be fit to either a linear function of N, Eq. 5, or a quadratic function of N, Eq. 6 (*see* **Note 28**). The terms m (slope), q (intercept), a, b, and c are constants from least squares fitting. The regression equation allows for determination of the number of native substrates per QD as a function time, $N(t)$, from measurements of the acceptor/donor PL ratio during kinetic enzyme assays. The calibration data in Fig. 4b with rQD-$\mathrm{Sub_{THR}}$(A647) was fit with a linear function (Eq. 5), whereas the calibration data in Fig. 4d with gQD-$\mathrm{Sub_{TRP}}$(A555) conjugates was fit with a quadratic function (Eq. 6).

$$\rho = mN + q \tag{5}$$

$$\rho = aN^2 + bN + c \tag{6}$$

3.9 Kinetic Enzyme Assay

1. Prepare a batch of QD-peptide substrate conjugates by mixing QDs with native peptide substrate according to **steps 2–4**. Here, we use valences of $N_0 = 8$ for both thrombin substrate

and trypsin substrate. We prepare enough material for S samples, where $S-2$ enzyme concentrations and a negative control (0 μM enzyme) are measured and an "extra" aliquot is kept in reserve (*see* **Note 29**).

2. Add $S\times N_0\times 20$ pmol of native peptide substrate to a microcentrifuge tube.
3. Add $S\times(55\ \mu L - V_{QD} - V_{Native})$ of buffer, where V_{QD} is the volume of QD solution to be added per sample, and V_{Native} is the volume of native peptide.
4. Add $S\times 20$ pmol of QDs (as $S\times V_{QD} = S\times 20\ \text{pmol}/C_{QD}$) and mix immediately; let stand at room temperature for 0.5–1.0 h (*see* **Note 25**).
5. Prepare a fresh stock solution of enzyme. For thrombin and trypsin, we weigh 1.0–1.5 mg of solid into a microcentrifuge tube (*see* **Note 30**) using an analytical balance. The solid enzyme is then dissolved in buffer and the concentration more accurately determined by measuring the absorbance at 280 nm.
6. Prepare a dilution of enzyme solution at 2× the highest concentration desired for enzyme assays.
7. Prepare a series of successive twofold dilutions of enzyme solution down to the lowest enzyme concentration desired for assays (*see* **Note 31**). With thrombin, we prepare 11 dilutions ranging from 40 to 0.04 μM (corresponding to 20 to 0.02 μM after **step 10**). With trypsin, we prepare 11 dilutions ranging from 0.84 μM to 0.84 nM (corresponding to 0.42 μM to 0.42 nM after **step 10**).
8. Pipette 50 μL of each enzyme dilution into adjacent wells in a 96-well microtiter plate. One well is filled with buffer as a negative control (*see* **Note 32**).
9. Add 50 μL of QD-peptide substrate conjugate to the negative control well. Take initial PL measurements of this sample with the fluorescence plate reader to confirm optimal settings (*see* **step 9** of Subheading 3.7 and **Note 33**).
10. Add 50 μL of QD-peptide substrate conjugate to each microtiter plate well with enzyme (*see* **Note 34**).
11. Immediately begin a time series of PL measurements at λ_D and λ_A (*see* **Note 35**). We use 400 nm excitation and $\lambda_D = 624$ nm and $\lambda_A = 668$ nm for thrombin (rQD-A647 FRET pair) and $\lambda_D = 525$ nm and $\lambda_A = 568$ nm for trypsin (gQD-A555 FRET pair). Measurements are repeated every 1–3 min over ca. 3–6 h (*see* **Note 36**). Examples of raw kinetic PL data for thrombin digestion of rQD-Sub_{THR}(A647) conjugates and for trypsin digestion of gQD-Sub_{TRP}(A555) conjugates are shown in Fig. 5a–b and c–d, respectively.
12. Proceed to Subheading 3.10 for data analysis.

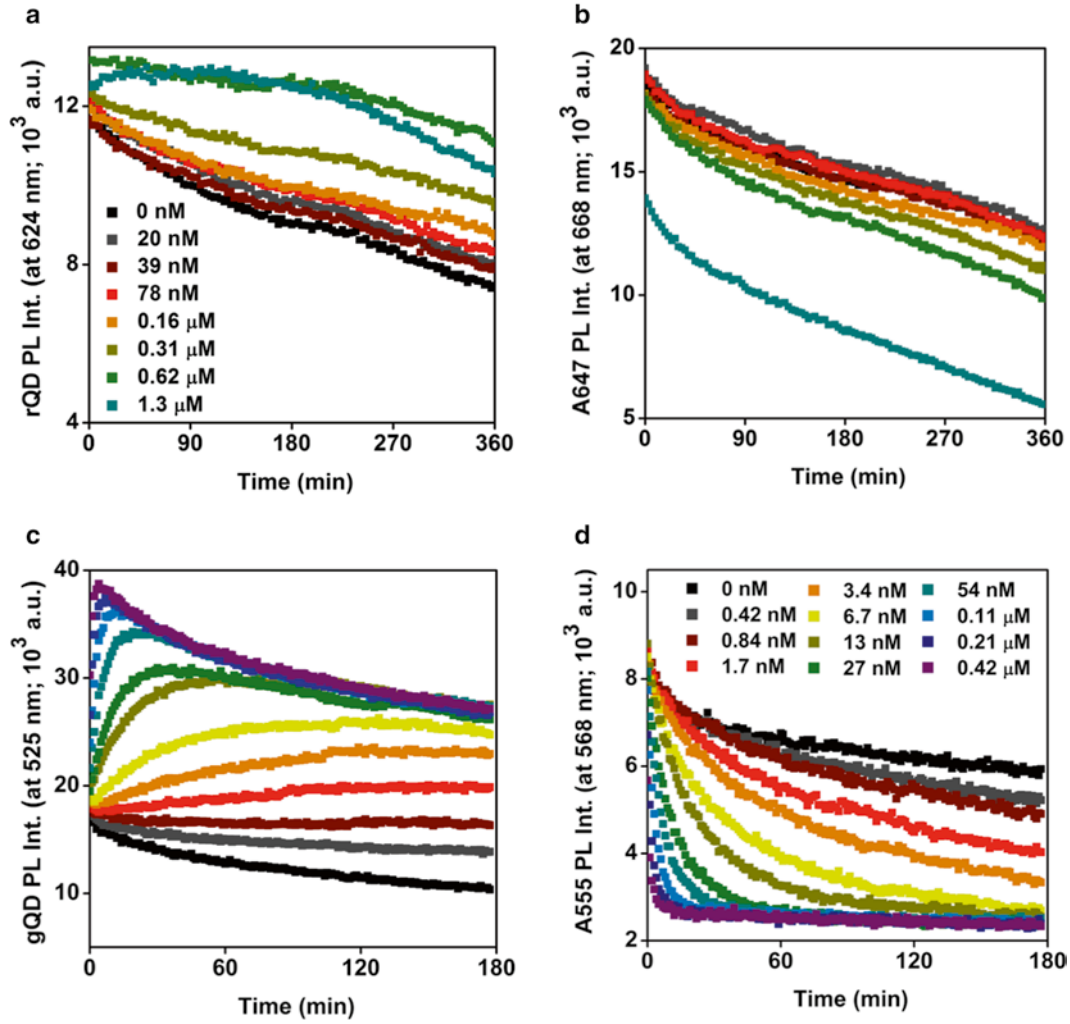

Fig. 5 Examples of raw PL data for kinetic enzyme assays. (**a**) rQD PL intensity at 624 nm and (**b**) uncorrected A647 PL intensity at 668 nm for initial rQD-$[Sub_{THR}(A647)]_8$ conjugates during a thrombin assay. (**c**) gQD PL intensity at 525 nm and (**d**) uncorrected A555 PL intensity at 568 nm for initial gQD-$[Sub_{TRP}(A555)]_8$ conjugates during a trypsin assay. Data is shown for several enzyme concentrations. The A647 and A555 PL data is not corrected for any crosstalk with QD PL. In both experiments, QD PL increases relative to the control and acceptor dye PL decreases relative to the control. The magnitude of these changes can vary significantly and be superimposed with drift in both signals. However, the ratio of the two signals is quite robust, as evident in Fig. 6

3.10 Analysis of Kinetic Data

1. For each time point, t, and enzyme concentration, $[E]$, calculate the PL intensity ratio, $\rho(t)$, from the corresponding PL intensities at λ_A and λ_D using Eq. 7. The values for $I_{AD}(t)_{[E]}$ and $I_{DA}(t)_{[E]}$ are obtained from the data generated in **step 11** of Subheading 3.9. The value for σ_{D,λ_A} is obtained from **steps 1** and **2** in Subheading 3.8. We typically process this data using spreadsheet software (e.g., Microsoft Excel) with time,

intensity at λ_D, and intensity at λ_A down three adjacent columns. The result of Eq. 7 is calculated in a fourth column for each row and repeated across the various enzyme concentrations. Calculations in subsequent steps are also done for each row (i.e., time point) and enzyme concentration.

$$\rho(t)_{[E]} = \frac{I_{\mathrm{AD}}(t)_{[E]}}{I_{\mathrm{DA}}(t)_{[E]}} = \frac{I_{\mathrm{AD},\lambda_A}(t)_{[E]} - \sigma_{D,\lambda_A} I_{\mathrm{DA},\lambda_D}(t)_{[E]}}{I_{\mathrm{DA},\lambda_D}(t)_{[E]}} \tag{7}$$

2. Calculate the normalized PL intensity ratio, $P(t)_{[E]}$, using Eq. 8. The normalization is relative to the control sample with 0 nM enzyme, $\rho(t)_{[0\ \mathrm{nM}]}$, with an adjustment to the initial time point ($t=0$), $\rho(0)_{[0\ \mathrm{nM}]}$. Figure 6a shows normalized kinetic PL ratio data for rQD-$\mathrm{Sub_{THR}}$(A647) conjugates as a function of thrombin concentration; Fig. 6b shows analogous data for gQD-$\mathrm{Sub_{TRP}}$(A555) conjugates as a function of trypsin concentration.

$$P(t)_{[E]} = \frac{\rho(t)_{[E]}}{\rho(t)_{[0\ \mathrm{nM}]}} \cdot \rho(0)_{[0\ \mathrm{nM}]} \tag{8}$$

3. Convert the normalized PL ratio data, $P(t)$, to the number of acceptors per QD, $N(t)$. If the calibration data was linear and fit with Eq. 5, then $N(t)$ is given by Eq. 9. If the calibration data was quadratic and fit with Eq. 6, then $N(t)$ is given by Eq. 1. The values for the fitting parameters were obtained in **step 4** of Subheading 3.8.

$$N(t)_{[E]} = \frac{P(t)_{[E]} - q}{m} \tag{9}$$

$$N(t)_{[E]} = \frac{1}{2a}\left(-b + \sqrt{b^2 - 4a\left(c - P(t)_{[E]}\right)}\right) \tag{10}$$

4. Calculate the amount of digested peptide per QD, $X(t)_{[E]}$, using Eq. 11. The concentration of product can be calculated by multiplying by the concentration of QDs in the assays, Eq. 12. Representative progress curves for the thrombin- and trypsin-catalyzed hydrolysis of rQD-$\mathrm{Sub_{THR}}$(A647) and gQD-$\mathrm{Sub_{TRP}}$(A555) conjugates are shown in Fig. 7.

$$X(t)_{[E]} = N(0)_{[0\ \mathrm{nM}]} - N(t)_{[E]} \tag{11}$$

$$[\mathrm{Product}] = X(t)_{[E]} \cdot [\mathrm{QD}] \tag{12}$$

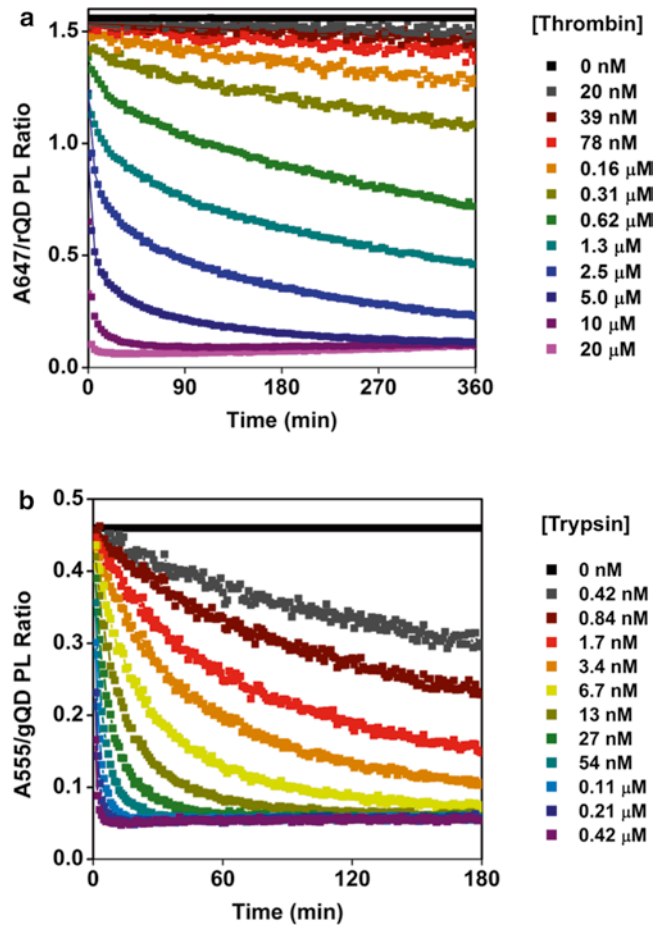

Fig. 6 (**a**) Normalized changes in the A647/rQD PL intensity ratio over time for initial rQD-$[Sub_{THR}(A647)]_8$ conjugates in assays with a series of different thrombin concentrations. Some of the data in panel (**a**) is derived from Fig. 5a–b. (**b**) Normalized changes in the A555/gQD PL intensity ratio over time for initial gQD-$[Sub_{TRP}(A555)]_8$ conjugates in assays with a series of different trypsin concentrations. The data in panel (**b**) is derived from Fig. 5c–d

5. For further analysis, initial rates of substrate digestion/product formation can be determined from tangents to the initial portion of the progress curves. Alternatively, the data can be analyzed with an integrated kinetic model, as has been described elsewhere [28–31]. The nature of these analyses largely depends on the experiment of interest and a further general protocol is not readily described.
6. To conclude, we note that the steps described above can potentially be adapted to measuring the kinetics of other types of enzyme in addition to proteases (*see* **Note 37**).

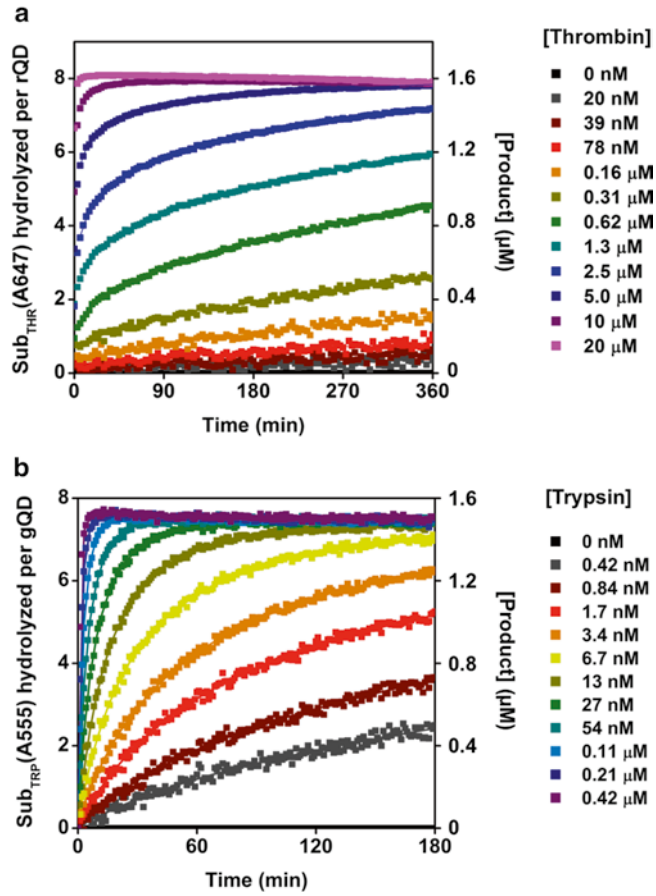

Fig. 7 Examples of processed kinetic data. (**a**) Progress curves showing changes in the number of peptide substrates cleaved per rQD over time, at different thrombin concentrations, for rQD-[Sub$_{THR}$(A647)]$_8$ conjugates. The progress curves were calculated from the data in Figs. 4b and 6a. (**b**) Progress curves showing changes in the number of peptide substrates cleaved per gQD over time, at different trypsin concentrations, for gQD-[Sub$_{TRP}$(A555)]$_8$ conjugates. The progress curves were calculated from the data in Figs. 4d and 6b

4 Notes

1. Commercially available QDs are typically sold by vendors as either hydrophobic materials (with native ligands from synthesis) or hydrophilic materials with polymer coatings. The former need to be modified with hydrophilic ligands such as GSH and DHLA in order to permit self-assembly of polyhistidine-appended biomolecules in aqueous media. Pre-made hydrophilic ligand-coated QDs are not available commercially. Note that some hydrophilic carboxylated polymer-coated QDs can

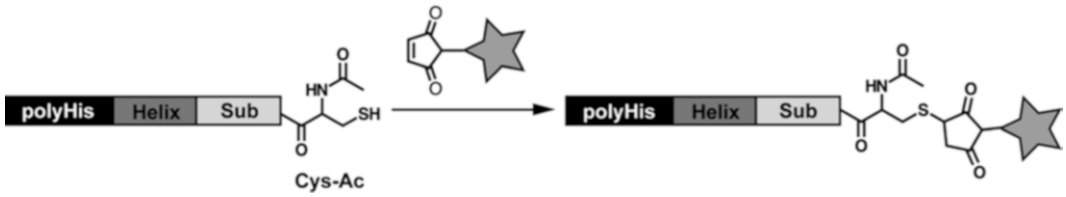

Fig. 8 Peptide design and labeling scheme. An acetylated cysteine residue (Cys-Ac) is shown as the labeling site

be supplemented with Ni^{2+} to make use of polyhistidine self-assembly, as described elsewhere [32, 33]. The use of these materials is beyond our scope here.

2. DHLA is available commercially but can also be readily synthesized from lipoic acid precursor at much lower cost and in greater quantity [34]. The reader should also note that various zwitterionic and poly(ethylene glycol)-appended derivatives of DHLA can be synthesized and used to render water dispersed QDs [15, 16]. However, these protocols are much more involved.
3. We design our peptides with four "modular" components: (a) a terminal hexahistidine sequence for self-assembly to QDs; (b) a helical linker segment (e.g., polyproline or alanine/2-aminoisobutyric acid rich sequence); (c) a hydrophilic sequence containing an internal cleavage site for the enzyme of interest; and (d) a terminal cysteine residue for site-selective labeling with a maleimide dye (*see* Fig. 8) [26, 27, 31].
4. Although peptides can be purchased with fluorescent dye modifications, we label our peptides in-house using commercially available maleimide dye packs (Life Technologies, Carlsbad, CA), as shown in Fig. 8. Labeling is followed by purification over Ni^{2+}-nitrilotriacetic acid media and desalting. The procedure can be found elsewhere [25, 35].
5. The QDs can tolerate ethylenediaminetetraacetic acid (EDTA) over the course of running the gel. However, long-term storage in EDTA-containing buffer is not recommended.
6. We use a monochromator-based plate reader and have no technical restrictions on dye selection. Filter-based plate readers may have limitations.
7. We have successfully used polypropylene centrifuge tubes, glass culture tubes, and glass vials as reaction vessels. The polypropylene is sufficiently resistant to organic solvent over the course of the ligand exchange at room temperature.
8. The colloidal stability of QDs stabilized with small anionic ligands such as GSH and DHLA decreases as pH decreases and ionic strength increases. We therefore recommend storing

these QDs in basic borate buffer with low ionic strength. The use of buffers with added NaCl during purification of QDs from excess ligands is to assist in precipitation.

9. We typically use glass culture tubes as reaction vessels.
10. The glass culture tube is sealed with an appropriately sized Suba-Seal septum (Sigma-Aldrich), which allows for the attachment of gas-in and gas-out lines using needles. Argon or nitrogen may be used as the inert gas and helps protect both the QDs and DHLA ligands from oxidation.
11. The elevated temperature is important for effective ligand exchange with DHLA. We do not recommend carrying out ligand exchange with DHLA at room temperature.
12. The amount of enzyme needed to effect digestion of the peptide substrate will vary from enzyme to enzyme.
13. For predigestion, we advise using the minimum amount of enzyme possible. Even though the enzyme activity is inhibited prior to preparation of calibration samples, the protein itself is still transferred over to the samples and can interfere, for example, through adsorption on the QDs. The degree to which adsorption is a concern will depend on the enzyme and surface chemistry on the QD.
14. Other temperatures may be used as appropriate. For example, many enzymes exhibit optimal activity near 37 °C. Longer or shorter incubation times may also be used as appropriate, provided the digestion goes to completion (a polyacrylamide gel can be used for confirmation, as described here). The native sample is incubated under the same conditions (without enzyme) as the digested sample to accommodate any potential degradation of the fluorescent dye label or other effects during the incubation.
15. TLCK irreversibly inhibits both trypsin and thrombin. Irreversible small molecule inhibitors such as TLCK are generally preferred. Protein inhibitors may be prone to adsorption onto the surface of QDs, which can affect the assembly of native peptide, the adsorption of digested peptide, and PL signals.
16. A large excess of TLCK ensures inhibition of all enzyme in the predigested sample, which is critical for obtaining a calibration curve. Any remaining active enzyme will digest native substrate and accurate calibration will not be possible.
17. We found it necessary to use a high concentration of peptide because our gel imaging system does not have the optimal excitation wavelength and emission filters for the A555 and A647 dyes. The use of lower concentrations of peptide is possible with better optimized imaging systems.

18. The dye-labeled fragment of the predigested peptide will generally have higher mobility than the native peptide. However, the relative mobilities may vary with sequence and dye selection (dyes are often cationic or anionic).
19. The difference in mobility between QDs assembled with native peptides versus predigested peptides can be quite small. To a large extent, the difference will depend on the position of the cleavage site along the length of the peptide sequence and relative to any charged residues. Any charge on the dye label will also affect the relative mobility.
20. Pipetting accuracy is important for obtaining an accurate and precise calibration curve. We recommend that the concentrations of working solutions of native and digested pipette be chosen to allow for the addition of at least 5 μL of peptide solution per equivalent (relative to the QD). For samples with 20 pmol of QD, this corresponds to a 4 μM solution of peptide. Volumes smaller than 5 μL tend to increase experimental error.
21. Larger or smaller quantities of QDs can be used depending on instrument sensitivity and the desired assay stoichiometry and conditions. We recommend working at concentrations ≥100 nM to ensure efficient peptide self-assembly ($K_d \sim 1$–10 nM).
22. The purpose of adding predigested peptide is to account for any adsorption of the dye-labeled fragment on the QD that results in a background FRET signal. In our experience, the magnitude of such effects can vary with the QD surface chemistry, peptide sequence, and choice of the fluorescent dye label.
23. We prepare 110 μL of each sample to facilitate precise transfer of 100 μL to a well in a 96-well microtiter plate.
24. Assembly will normally appear complete within minutes; however, incubating for 0.5–1.0 h ensures that equilibrium is reached. At equilibrium, the exact number of peptides per individual QD is determined by Poisson statistics. For example, mixing QDs with one equivalent of peptide will largely yield a mixture of conjugates with valences of 0, 1, and 2 peptides per QD. The effect of the Poisson statistics becomes small at average conjugate valences >4. The empirical calibration procedure inherently accounts for the Poisson statistics of peptide self-assembly. An in-depth discussion of the Poisson distribution can be found elsewhere [36].
25. For maximum precision, it is advisable to incubate the calibration samples and the conjugates for assays for equal lengths of time to account for any non-idealities during preparation.
26. An excitation wavelength of 400 nm yields negligible direct excitation of A555 and A647. With other dyes, it is advisable to collect fluorescence excitation spectra to find the wavelength corresponding to minimum excitation.

27. If there is a large degree of overlap between the QD and fluorescent dye emission, it may be desirable to choose λ_A to coincide with a shoulder on the red side of dye emission peak to minimize crosstalk.
28. The theoretical relationship between the acceptor/donor PL ratio, ρ, and number of acceptors per QD, N, is linear. However, a weakly quadratic function often fits experimental data better. Deviations from linearity result from the adsorption of dye-labeled digested peptide fragments on the QDs, as well as changes in the properties of the dye as more labeled peptides are assembled per QD (e.g., self-quenching, changes in donor-acceptor separation).
29. The extra aliquot kept in reserve has a few purposes. First, it ensures that a full 50 μL of QD-peptide conjugate solution can be added to every sample well in a microtiter plate. Second, the extra aliquot can be used to replace a sample if an error is made in preparation. Finally, the extra aliquot can be used for quality control and characterization of the QD-peptide substrate conjugates, including monitoring colloidal stability over a certain time period, gel electrophoresis, etc.
30. Beware of static when weighing solid enzyme.
31. Dilutions can be prepared individually in microcentrifuge tubes or altogether in the microtiter plate. As an example of the latter, consider an assay across one row a 96-well microtiter plate. A 100 μL amount of a solution with 2× the highest desired concentration of enzyme is added to the rightmost well (e.g., A12). A volume of 50 μL of buffer is added to the remaining wells. Next, 50 μL amount of the enzyme solution is transferred to the well to its immediate left (e.g., A11) and mixed. A of μL amount of this diluted enzyme solution is further transferred to the next well on the left (e.g., A10) and mixed. This process continues across the row (e.g., from A11 to A2), leaving the leftmost well (e.g., A1) with only buffer. The "excess" 50 μL from the solution with the lowest concentration of enzyme is discarded (i.e., all wells contain 50 μL). The enzyme concentration will be halved by the addition of an equal volume of QD-peptide conjugate solution to start the assays.
32. A negative control with 0 μM of enzyme is important to account for any changes in PL over the course of the experiment that are not related to proteolytic activity.
33. This step can be used to confirm wavelength selection for PL measurements and, importantly, set the instrument gain so that its dynamic range accommodates the recovery of the QD PL with loss of FRET during proteolysis. The expected magnitude of recovery can be estimated from calibration data (Fig. 4).

34. We add the QD-peptide substrate conjugates in order from lowest to highest enzyme concentration. While a short delay between the addition of enzyme and start of PL measurements is unavoidable, this order of addition provides the shortest delay for the highest enzyme concentrations, minimizing the overall effect of the time delay on results. Use of a multichannel pipette may be useful for improving aliquoting speed since enzyme can be delivered to multiple wells simultaneously.
35. Prior to adding enzyme, ensure that the plate reader settings have been completely optimized and that measurements can begin with the push of a single button.
36. The duration of the assay and the time interval for measurements will depend on the enzyme system under study and the reaction conditions. In general, as the duration of the assay increases, the time interval between measurements should also increase. Always check that the time required for measurement of every well is less than the measurement interval, preferably by a factor of 5 or more. This requirement may limit the number of wells that can be measured per assay. Ideally, the time required for measurement at each time point should be much faster than the time needed for digestion.
37. It is expected that the assay methodology described in this chapter can be readily adapted to other hydrolase enzymes; for example, nucleases. In this case, peptide substrate would be replaced by oligonucleotide substrate and calibration curves would be derived from samples with mixtures of native and predigested dye-labeled oligonucleotide. In addition, kinase activity could potentially be measured using dye-labeled adenosine triphosphate with non-phosphorylated and pre-phosphorylated peptide substrates for calibration. Non-kinetic assays based on QDs and FRET have been reported for nuclease [37, 38] and kinase activity [39, 40].

Acknowledgements

M.W., E.P., and W.R.A. acknowledge the Natural Sciences and Engineering Council of Canada (NSERC) and the University of British Columbia for financial support of their research. E.P. is also grateful to NSERC for support through a graduate fellowship. I.L.M. acknowledges the Office of Naval Research (ONR), the Naval Research Laboratory (NRL), the NRL Nanosciences Institute (NSI), the Defense Advanced Research Projects Agency (DARPA), and the Defense Threat Reduction Agency Joint Science and Technological Office (DTRA-JSTO) Military Interdepartmental Purchase Requisition (MIPR) #B112582M.

References

1. Day RN, Davidson MW (2009) The fluorescent protein palette: tools for cellular imaging. Chem Soc Rev 38:2887–2921
2. Rao JH, Dragulescu-Andrasi A, Yao HQ (2007) Fluorescence imaging in vivo: recent advances. Curr Opin Biotechnol 18:17–25
3. Volpi EV, Bridger JM (2008) FISH glossary: an overview of the fluorescence *in situ* hybridization technique. Biotechniques 45:385–409
4. Nagl S, Schaeferling M, Wolfbeis OS (2005) Fluorescence analysis in microarray technology. Microchim Acta 151:1–21
5. Chattopadhyay PK, Hogerkorp CM, Roederer M (2008) A chromatic explosion: the development and future of multiparameter flow cytometry. Immunology 125:441–449
6. Resch-Genger U, Grabolle M, Cavaliere-Jaricot S, Nitschke R, Nann T (2008) Quantum dots versus organic dyes and fluorescent labels. Nat Methods 5:763–775
7. Turk B (2006) Targeting proteases: successes, failures and future prospects. Nat Rev Drug Discov 5:785–799
8. McKerrow JH, Caffrey C, Kelly B, Like P, Sajid M (2006) Proteases in parasitic diseases. Annu Rev Pathol Mech Dis 1:497–536
9. Algar WR, Susumu K, Delehanty JB, Medintz IL (2011) Semiconductor quantum dots in bioanalysis: crossing the valley of death. Anal Chem 83:8826–8837
10. Rosenthal SJ, Chang JC, Kovtun O, McBride JR, Tomlinson ID (2011) Biocompatible quantum dots for biological applications. Chem Biol 18:10–24
11. Zrazhevskiy P, Sena M, Gao XH (2010) Designing multifunctional quantum dots for bioimaging, detection, and drug delivery. Chem Soc Rev 39:4326–4354
12. Petryayeva E, Algar WR, Medintz IL (2013) Quantum dots in bioanalysis: a review of applications across various platforms for fluorescence spectroscopy and imaging. Appl Spectrosc 67:215–252
13. Evans CM, Cass LC, Knowles KE, Tice DB, Chang RPH, Weiss EA (2012) Review of the synthesis and properties of colloidal quantum dots: the evolving role of coordinating surface ligands. J Coord Chem 65:2391–2414
14. Susumu K, Medintz IL, Delehanty JB, Boeneman K, Mattoussi H (2010) Modification of poly(ethylene glycol)-capped quantum dots with nickel nitrilotriacetic acid and self-assembly with histidine-tagged proteins. J Phys Chem C 114:13526–13531
15. Susumu K, Oh E, Delehanty JB, Blanco-Canosa JB, Johnson BJ, Jain V, Hervey WJ, Algar WR, Boeneman K, Dawson PE, Medintz IL (2011) Multifunctional compact zwitterionic ligands for preparing robust biocompatible semiconductor quantum dots and gold nanoparticles. J Am Chem Soc 133:9480–9496
16. Mei BC, Susumu K, Medintz IL, Delehanty JB, Mountziaris TJ, Mattoussi H (2008) Modular poly(ethylene glycol) ligands for biocompatible semiconductor and gold nanocrystals with extended pH and ionic stability. J Mater Chem 18:4949–4958
17. Algar WR, Prasuhn DE, Stewart MH, Jennings TL, Blanco-Canosa JB, Dawson PE, Medintz IL (2011) The controlled display of biomolecules on nanoparticles: a challenge suited to bioorthogonal chemistry. Bioconjugate Chem 22:825–858
18. Sapsford KE, Pons T, Medintz IL, Higashiya S, Brunel FM, Dawson PE, Mattoussi H (2007) Kinetics of metal-affinity driven self-assembly between proteins or peptides and cdse-zns quantum dots. J Phys Chem C 111: 11528–11538
19. Cheung HC (1991) Resonance energy transfer. In: Lakowicz JR (ed) Topics in fluorescence spectroscopy, vol 2. Plenum Press, New York, pp 127–176
20. Schuler B, Eaton WA (2008) Protein folding studied by single molecule FRET. Curr Opin Struct Biol 18:16–26
21. Didenko VV (2001) DNA probes using fluorescence resonance energy transfer (fret): designs and applications. Biotechniques 31: 1106–1121
22. Truong K, Ikura M (2001) The use of FRET imaging microscopy to detect protein–protein interactions and protein conformational changes in vivo. Curr Opin Struct Biol 11:573–578
23. Boeneman K, Mei BC, Dennis AM, Bao G, Deschamps JR, Mattoussi H, Medintz IL (2009) Sensing caspase 3 activity with quantum dot-fluorescent protein assemblies. J Am Chem Soc 131:3828–3829
24. Medintz IL, Clapp AR, Brunel FM, Tiefenbrunn T, Uyeda HT, Chang EL, Deschamps JR, Dawson PE, Mattoussi H (2006) Proteolytic activity monitored by fluorescence resonance energy trransfer through quantum-dot-peptide conjugates. Nat Mater 5:581–589
25. Sapsford KE, Farrell D, Sun S, Rasooly A, Mattoussi H, Medintz IL (2009) Monitoring

of enzymatic proteolysis on a electroluminescent-CCD microchip platform using quantum dot-peptide substrates. Sens Actuators B 139:13–21

26. Sapsford KE, Granek J, Deschamps JR, Boeneman K, Blanco-Canosa JB, Dawson PE, Susumu K, Stewart MH, Medintz IL (2011) Monitoring botulinum neurotoxin A activity with peptide-functionalized quantum dot resonance energy transfer sensors. ACS Nano 5:2687–2699
27. Algar WR, Ancona MG, Malanoski AP, Susumu K, Medintz IL (2012) Assembly of a concentric Förster resonance energy transfer relay on a quantum dot scaffold: characterization and application to multiplexed protease sensing. ACS Nano 6: 11044–11058
28. Duggleby RG (2001) Quantitative analysis of the time courses of enzyme-catalyzed reactions. Methods 24:168–174
29. Goličnik M (2010) Explicit reformulations of time-dependent solution for a Michaelis–Menten enzyme reaction model. Anal Biochem 406:94–96
30. Goličnik M (2011) Explicit analytic approximations for time-dependent solutions of the generalized integrated Michaelis–Menten equation. Anal Biochem 411:303–305
31. Algar WR, Malanoski A, Deschamps JR, Blanco-Canosa JB, Susumu K, Stewart MH, Johnson BJ, Dawson PE, Medintz IL (2012) Proteolytic activity at quantum dot-conjugates: kinetic analysis reveals enhanced enzyme activity and localized interfacial "hopping". Nano Lett 12:3793–3802
32. Boeneman K, Delehanty JB, Susumu K, Stewart MH, Medintz IL (2010) Intracellular bioconjugation of targeted proteins with semiconductor quantum dots. J Am Chem Soc 132:5975–5977
33. Yao HQ, Zhang Y, Xiao F, Xia ZY, Rao JH (2007) Quantum dot/bioluminescence resonance energy transfer based highly sensitive detection of proteases. Angew Chem Int Ed 46:4346–4349
34. Clapp AR, Goldman ER, Mattoussi H (2006) Capping of CdSe-ZnS quantum dots with DHLA and subsequent conjugation with proteins. Nat Protoc 1:1258–1266
35. Algar WR, Blanco-Canosa JB, Manthe RL, Susumu K, Stewart MH, Dawson PE, Medintz IL (2013) Synthesizing and modifying peptides for chemoselective ligation and assembly into quantum dot-peptide bioconjugates. In: Hamad-Schifferli K, Bergese P (eds) Methods molecular biology, vol 1025. Springer, New York, doi:10.1007/1978-1001-62703-62462-62703_62705
36. Pons T, Medintz IL, Wang X, English DS, Mattoussi H (2006) Solution-phase single quantum dot fluorescence resonance energy transfer. J Am Chem Soc 128:15324–15331
37. Gill R, Willner I, Shweky I, Banin U (2005) Fluorescence resonance energy transfer in CdSe/ZnS–DNA conjugates: probing hybridization and DNA cleavage. J Phys Chem B 109:23715–23719
38. Huang S, Xiao Q, He ZK, Liu Y, Tinnefeld P, Su XR, Peng XN (2008) A high sensitive and specific QDs FRET bioprobe for MNase. Chem Commun 5990–5992
39. Freeman R, Finder T, Gill R, Willner I (2010) Probing protein kinase (CK2) and Alkaline phosphatase with CdSe/ZnS quantum dots. Nano Lett 10:2192–2196
40. Lowe SB, Dick JAG, Cohen BE, Stevens MM (2012) ACS Nano 6:851–857

Chapter 18

Solid-Phase Supports for the in situ Assembly of Quantum Dot-FRET Hybridization Assays in Channel Microfluidics

Anthony J. Tavares, M. Omair Noor, Uvaraj Uddayasankar, Ulrich J. Krull, and Charles H. Vannoy

Abstract

Semiconductor quantum dots (QDs) have long served as integral components in signal transduction modalities such as Förster resonance energy transfer (FRET). The majority of bioanalytical methods using QDs for FRET-based techniques simply monitor binding-induced conformational changes. In more recent work, QDs have been incorporated into solid-phase support systems, such as microfluidic chips, to serve as physical platforms in the development of functional biosensors and bioprobes. Herein, we describe a simple strategy for the transduction of nucleic acid hybridization that combines a novel design method based on FRET with an electrokinetically controlled microfluidic technology, and that offers further potential for amelioration of sample-handling issues and for simplification of dynamic stringency control.

Key words Quantum dots, Microfluidics, Hybridization, Förster resonance energy transfer, Silane chemistry, Immobilization, Spatial detection

1 Introduction

Microfluidic systems provide a powerful platform for the development and analysis of biological assays [1–3]. The capability to precisely control and manipulate small volumes of chemical and/or biological reagents through fabricated microchannels embedded within a chip offers unlimited possibilities. Microfluidic technologies are attractive because they have small requirements for solvents and reagents, potential for parallel operation, portability, short reaction times, and lower detection limits and produce fewer waste products [4]. Integration capability is the basic idea behind microfluidics, which allows the possibility of an extended range of individual laboratory protocols (i.e., handling of sample materials, chemical reactions, separation, and detection) to be incorporated onto a single platform [5].

Adriana Fontes and Beate Saegesser Santos (eds.), *Quantum Dots: Applications in Biology*, Methods in Molecular Biology, vol. 1199, DOI 10.1007/978-1-4939-1280-3_18, © Springer Science+Business Media New York 2014

Incorporating functional nanomaterials, such as semiconductor quantum dots (QDs), into a microfluidic system offers the possibility of developing innovative strategies for the transduction of nucleic acid hybridization. QDs possess unique optical properties that make them well suited as donors in Förster resonance energy transfer (FRET). In microfluidics, QDs can act as an integrated sensing component, concomitantly serving as an active transduction element and a nanoscaffold for biorecognition [6, 7]. Nucleic acid hybridization assays using QD-FRET have been reported on various solid-phase substrates [7–13]. The common aims of these systems are to ensure stable immobilization of the QDs on the solid substrate support, allowing these nanoscaffolds to maintain their inherent ability to interact via sequence specificity with available probes (i.e., complementary oligonucleotides) while simultaneously preventing nonspecific adsorption. On-chip QD-FRET assays have afforded detection limits (LOD) an order of magnitude lower than those on optical fiber assays [7, 14]. Spatially distributed FRET-sensitized photoluminescence (PL) profiles along microchannels have been used for the quantitative transduction of nucleic acid hybridization in single-color and multiplexed formats, and presently demonstrate 10 fmol LOD of oligonucleotide target [7].

Herein, we describe the step-by-step fabrication of a microfluidic based solid-phase QD-FRET nucleic acid hybridization assay. The stepwise assembly is shown in Fig. 1, beginning with deposition of biotinylated surface ligands for QD immobilization. Assembly of the solid-phase assay within each channel is achieved by sequentially dispensing streptavidin-functionalized QDs (SAv-QDs) and biotinylated oligonucleotide probe, which are delivered using electroosmotic flow (EOF) and electrophoretic force (EPF), respectively. The biotin–avidin interaction is selected to offer stable bioconjugates, and the streptavidin also ameliorates nonspecific adsorption of oligonucleotides. Introduction of sample solution containing oligonucleotide targets results in rapid interfacial hybridization that is complete within a few minutes. The target oligonucleotides in the injected sample become deposited on the channel surface and eventually the sample plug may be completely consumed by this process as the plug moves through the channel. This results in coverage along the length of a channel, with the length of coverage varying as a function of the quantity of the target oligonucleotide that was injected. A cyanine dye 3 (Cy3) tag on the target oligonucleotide is brought into close proximity to the immobilized QD donor by hybridization to the probe. Excitation using a 405 nm laser enables FRET from the QD to the Cy3 acceptor, and emission from Cy3 serves as an analytical signal. The length of this FRET-sensitized Cy3 spatial profile from the channel interior is used to quantify the amount of nucleic acid present in a sample.

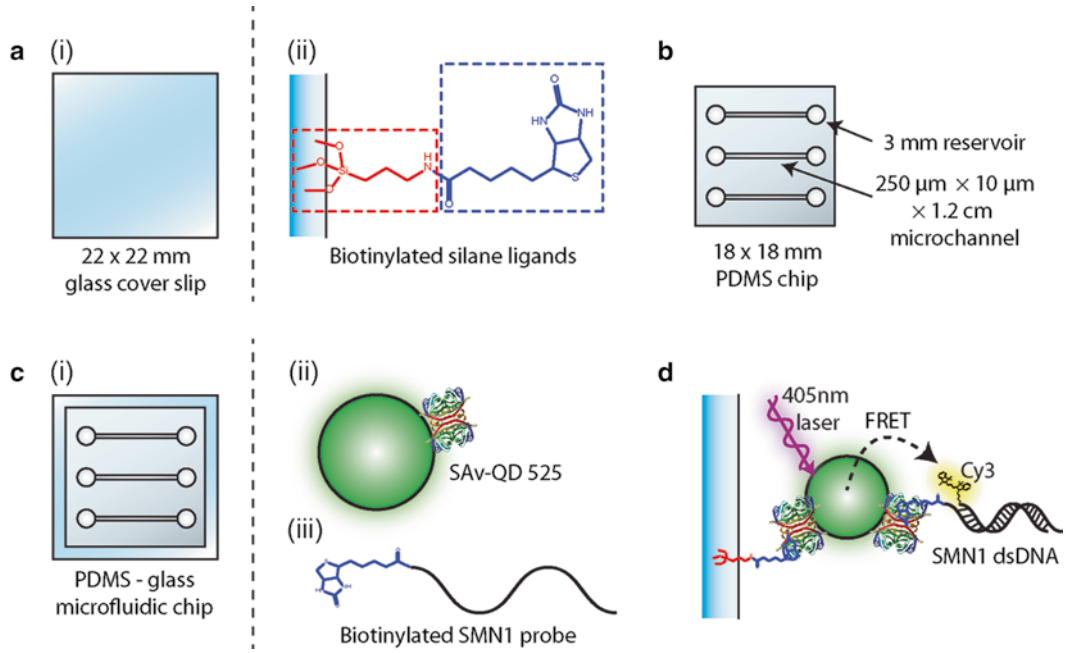

Fig. 1 Assembly of a solid-phase QD-FRET hybridization assay in a PDMS-glass microfluidic chip. (**a**) (*i*) An etched 22 × 22 mm glass cover slip is derivatized with biotin ligands (*ii*) by initial deposition of APTMS (*red*) and then amide coupling through an activated succinimidyl ester of biotin (*blue*). (**b**) A PDMS microfluidic chip is cast to contain three microchannels measuring 250 µm wide, 10 µm high, and 1.2 cm in length terminated with 3 mm diameter dispensing reservoirs. (**c**) Reversible oxidation of the PDMS stamp using air plasma enables sealing to the derivatized glass cover slip (*i*) and permits further assembly of the in-channel assay where (*ii*) SAv-QDs are then introduced using EOF, and then (*iii*) biotinylated oligonucleotide probes are introduced by electrophoresis. (**d**) Injection of complementary target nucleic acid labeled with Cy3 results in hybridization. This provides the necessary proximity for energy transfer from the immobilized QD to the Cy3 acceptor, and the emission of the Cy3 serves as the analytical signal to transduce hybridization

2 Materials

2.1 Modification of Glass Cover Slips

1. Thirty-two cover slips and doped p-type silicon wafers (as example, we used, respectively, Fisherfinest™ Premium Cover Glasses from Fisher Scientific, Ottawa, ON, Canada, and wafers from Empak, Chanhassen, MN) cut to the same dimensions (22 × 22 mm).
2. Four cover slip mini-racks: As example we used the C-14784 model from Life Technologies, Burlington, ON, Canada, with custom-fabricated Teflon® "arms."
3. Organic clean solution: A 1:1:5 solution of NH_4OH (ammonium hydroxide), H_2O_2 (hydrogen peroxide, 30 % v/v), and dH_2O (deionized water) for a total volume of 420 mL (*see* **Note 1**).

4. Ionic clean solution: A 1:1:5 solution of HCl (concentrated hydrochloric acid), H_2O_2 (30 % v/v), and dH_2O for a total volume of 420 mL (*see* **Note 1**).
5. Washing solvents (reagent grade): Methanol, dichloromethane, and diethyl ether.
6. APTMS solution: 7.5 mL (2.5 % v/v) of (3-aminopropyl)trimethoxysilane (APTMS) and 1 mL of Hunig's base (*N′N′*-diisopropylethylamine) made up to 300 mL with anhydrous toluene (*see* **Note 2**).
7. Biotin-NHS: 2.5 g biotin, 1.5 g *N*-hydroxysuccinimide (NHS), 1.9 mL *N′N′*-diisopropylcarbodiimide (DIC), 0.5 mL Hunig's base, and 100 mL of anhydrous dimethylformamide (DMF).
8. Biotinylation solution: 400 mg biotin succinimidyl ester (Biotin-NHS), 0.25 mL Hunig's base, and 300 mL of anhydrous DMF.

2.2 Preparation of a Microfluidic Chip

1. Microfluidic template (and microfluidics master mold).
2. SYLGARD® 184 Silicon Elastomer Kit (Dow Corning, Newton, MA).
3. Adhesive tape.
4. Metal bore with a diameter of 3 mm.
5. Plasma cleaner (Harrick Plasma, Ithaca, NY).
6. Biotin-modified cover slips.

2.3 In Situ Assay Assembly

1. High voltage sequencer (HVS448-3000, Livermore, CA).
2. At least one pair of electrodes made from platinum wire.
3. Borate buffer: 50 mM Borate, pH 9.25. Weigh 10.1 g of sodium tetraborate and dissolve in 900 mL of dH_2O. Mix and adjust to pH 9.25. Make up to 1 L with dH_2O (*see* **Note 3**).
4. Tris-borate buffer: 100 mM Tris borate, pH 7.4, 20 mM NaCl. Weigh 12.1 g of Tris base, 6.18 g of boric acid, and 1.17 g of NaCl and dissolve in 900 mL of dH_2O. Mix and adjust to pH 7.4. Make up to 1 L with dH_2O (*see* **Note 3**).
5. SAv-QD suspension: 100 nM streptavidin conjugated QDs (Qdot® 525 ITK™ Streptavidin Conjugate Kit was utilized as an example, from Life Technologies, Burlington, ON, Canada) in 50 mM borate buffer, pH 9.25 (*see* **Note 4**).
6. 3 μM SMN1 probe (nucleic acid sequence: biotin-5′-ATTTTGTCTGAAACCCTGT-3′ with a biotin added to the 5′-end using a C6 (standard) spacer arm is utilized as an example, from Integrated DNA Technologies, Coralville, IA) in 100 mM Tris-borate buffer, pH 7.4 (*see* **Note 5**).

7. 250 nM—2 μM custom SMN1-Cy3 target (nucleic acid sequence: Cy3-3′-TAAAACAGACTTTGGGACA-5′ with a Cy3 fluorophore added to the 3′-end is utilized as an example, from Integrated DNA Technologies, Coralville, IA) in 100 mM Tris-borate buffer, pH 7.4 (*see* **Note 6**).
8. Epi-fluorescence microscope (as example we used Nikon Eclipse L150, from Nikon, Mississauga, ON, Canada).

3 Methods

3.1 Modification of Glass Cover Slips

1. Insert a combination of 32 glass cover slips and silicon wafers into the four cover slip mini-racks with custom-fabricated Teflon® "arms" (*see* **Note 7**).
2. Place the cover slip mini-racks fitted with cover slips into a 1 L glass beaker. Add the organic clean solution and heat on a hot plate at 85 °C for 10 min. Remove the flask from the hot plate and allow the mixture to cool for 5 min. Rinse the cover slips twice with copious amounts of dH_2O.
3. Repeat the aforementioned procedure, but instead use the ionic clean solution. Rinse the cover slips twice with copious amounts of dH_2O. Decant the solution. Rinse the cover slips twice with methanol via bath sonication, 10 min each time. Decant the remaining methanol, then rinse twice with dichloromethane and twice with diethyl ether, and store the cover slips in a vacuum oven at 65 °C until further use (*see* **Note 8**).
4. Place the mini-racks containing the cover slips inside a 1 L wide-mouth glass reagent bottle and purge five times for 5 min each in the anti-chamber of a nitrogen glove box (*see* **Note 9**). After purging is completed, add the APTMS solution to the glass reagent bottle. Swirl the bottle gently and then stopper the bottle before removing it from the inert atmosphere.
5. In a fume hood, assemble a heating mantle onto an orbital shaker and a condenser linked to argon inlet and outlet lines. Heat the mantle to ca. 100 °C and turn on the argon flow (control the rate using an oil bubbler). Quickly remove the stopper on the reagent bottle and fit the condenser into the neck of the flask. Seal the joint with a band of Teflon® tape and adjust the flow rate of argon to a moderate flow. Insulate the neck of the flask with glass wool or metal foil and place this assembly on an orbital shaker. Reflux the reaction mixture for 6 h under argon, noting the start time of the reaction as the first visible sign of solvent condensation. Afterwards, remove the heating mantle and allow the chamber to cool down to

room temperature (23 °C) under argon. Decant the solution and transfer the cover slips to a 500 mL beaker and rinse twice with methanol and then bath sonicate in methanol twice more, 10 min each time. Finally, wash the cover slips once with dichloromethane and once with diethyl ether and store in a desiccator until further use (*see* **Note 8**). The cover slips are now amine functionalized.

6. Coupling of biotin to the amine-terminated cover slips first requires synthesis of the activated succinimidyl ester (biotin-NHS) [15] as either an external step or in the presence of the amine-derivatized cover slips (*see* **Note 10**). Add 2.5 g biotin (10 mmol) and 1.5 g NHS (13 mmol) to a 250 mL Schlenk or round-bottom flask along with 75 mL of anhydrous DMF. Degas the mixture with argon for 10 min. Heat the reaction mixture to 50 °C to ensure complete dissolution and then add 1 mL of Hunig's base to the flask. With stirring, add 1.9 mL (12 mmol) of *N′N′*-diisopropylcarbodiimide (DIC) dropwise. After the addition is complete, equip an air or a water reflux condenser and heat the mixture to 60 °C for ca. 2 h. Remove the reaction mixture from heat and allow it to cool to room temperature (23 °C). The volume of the solution was reduced via rotary evaporation (external bath temperature 55 °C) (*see* **Note 11**). Recrystallize the crude off-white precipitate using 100 mL of isopropanol. Leave the vessel at −20 °C overnight. Filter the crystals by vacuum filtration and wash twice with ca. 20 mL of cold isopropanol. The product can be characterized using proton NMR. Store the product in a desiccator until further use. NMR ^{1}H (400 MHz in deuterated dimethyl sulfoxide, DMSO-d_6) δ: 1.37–1.64 (m; 6H), 2.54–2.57 (d; 1H), 2.63–2.67 (t; 2H), 2.79–2.87 (m; 5H), 3.07–3.10 (m; 1H), 4.11–4.14 (m; 1H), 4.27–4.30 (m; 1H), 6.34 (s; 1H), 6.39 (s; 1H) ppm.
7. Dissolve 400 mg of biotin-NHS in 300 mL of anhydrous DMF and add the solution to amine-terminated cover slips in a dry 500 mL beaker. Add 250 μL of Hunig's base, cap the beaker with a watch glass, and place the mixture on an orbital shaker for 24 h. Decant the solution and rinse the slides with DMF, reagent grade. Bath sonicate the slides two times in isopropanol, 10 min each time. Rinse twice with dichloromethane and then twice with diethyl ether before storing cover slips in a desiccator for future use.

3.2 Preparation of a Microfluidic Chip

3.2.1 Fabrication of Microfluidic Templates

Microfluidic templates (masters) are commonly prepared using photolithography, which requires a clean room facility. The details for the fabrication of microfluidic templates can be found elsewhere [16]. Additional specifications and instructions about the use of Su-8 photoresist can be found on the vendor's website: www.microchem.com. For the work described herein, glass substrates were

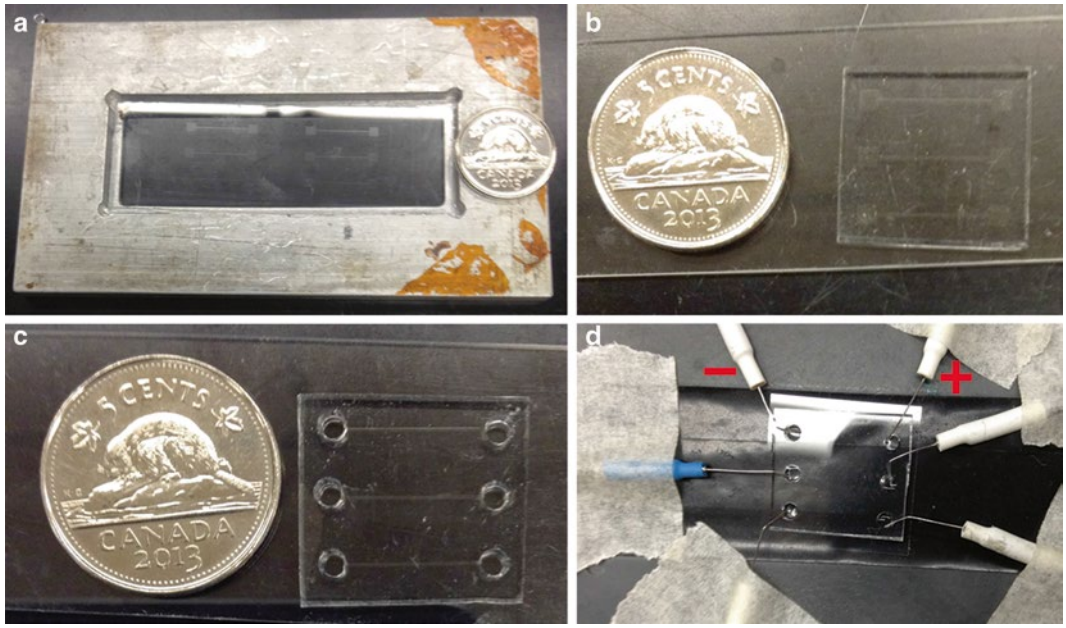

Fig. 2 (**a**) A glass-based microfluidic positive relief template inside an aluminum block mold. PDMS is packed inside the mold and later is cut to the dimensions shown in (**b**). A small metal bore of 3 mm diameter is used to create reservoirs in the cured PDMS as shown in (**c**). Attachment of negative (cathode) and positive (anode) platinum electrodes across each microchannel (**d**). Tape is used to fix the electrodes within the reservoir

used for the development of microfluidic templates. The length, width, and height of the microfluidic channels described in this work were 1.2 cm, 250 μm, and 10 μm, respectively.

3.2.2 Casting of Polydimethylsiloxane (PDMS) by Replica Molding

1. Add 10.0 g SYLGARD® 184 silicone elastomer base and 1.0 g SYLGARD® 184 silicone elastomer curing agent to a 100 mL disposable plastic beaker. Use a glass rod to thoroughly mix these materials for 10 min. Degas the mixture under vacuum until it becomes clear.
2. Place a glass template containing a positive relief pattern of the desired channel design within an aluminum casing block (Fig. 2a) and pour ~3.5 g of the PDMS on top of the template. Allow the PDMS to spread evenly across the surface of the template (*see* **Note 12**).
3. Cure the PDMS in an oven at 120 °C for 30 min.
4. After the aluminum casing block has reached room temperature (23 °C), remove the template and cured PDMS stamp from the casing and cut out the excess PDMS from the sides of the template using a razor blade (Fig. 2b).
5. Cut PDMS to dimensions that are slightly smaller than a cover slip, ca. 18 × 18 mm, and punch out the PDMS reservoirs at the end of the channels using a metal bore (Fig. 2c).

3.2.3 Sealing the PDMS to a Biotin-Modified Cover Slip

1. Remove any macroscopic particles from the surface of the cast PDMS and an unmodified glass cover slip using adhesive tape to lift such debris.
2. Clean the PDMS and the unmodified glass cover slip with ethanol and dry the substrates under a stream of nitrogen gas.
3. Gently press the PDMS (channels facing down) (*see* **Note 13**) in contact with the unmodified glass cover slip. Remove any air bubbles between the two substrates by gently dabbing the face of the PDMS stamp with a piece of aluminum foil.
4. Place the assembled PDMS-glass cover slip into a plasma cleaner and air oxidize the substrates for 2 min at ca. 0.2–0.3 mTorr (*see* **Note 14**). The intention is to plasma oxidize the channels.
5. Remove the PDMS-glass cover slip assembly from the plasma cleaner and peel off the PDMS stamp from the unmodified glass slide.
6. Immediately cover the PDMS (channels down) with a biotin-modified cover slip.
7. Once again, gently dab the top face of the PDMS stamp with aluminum foil to remove any air bubbles that may be trapped between the PDMS and biotin-modified glass cover slip.

3.3 In Situ Assay Assembly

1. Add 7 μL of borate buffer to three reservoirs on one side of the PDMS chip, allowing capillary action to drive the buffer to the adjacent reservoirs (*see* **Note 15**). Dispense 7 μL of borate buffer to the remaining three reservoirs on the other side of the chip. Insert the electrodes into the right (anode) and left (cathode) reservoirs, respectively. Secure the electrode wires with tape to insure that the electrodes remain in each reservoir (Fig. 2d). Apply 200 V DC to the working set of electrodes for 2 min and note the current, which should generally range from 8 to 10 μA. Disable the applied voltage, remove the contents from all reservoirs using the same micropipette, and dispense into a waste container.
2. Dispense 7 μL of a 100 nM SAv-QD suspension into the right reservoir (anode) and 7 μL of borate buffer in the left reservoir (cathode) (*see* **Note 16**). Apply 200 V DC to the electrodes for 10 min. The delivery of QDs by EOF to the cathodic electrode can be monitored with the use of a handheld UV lamp to track fluorescence. If no visible QD PL is seen from the channel interior *see* **Note 17**. Disable the applied voltage and allow the chip to stand undisturbed for an additional 10 min to ensure QD immobilization within the channel. Remove the contents of all reservoirs and dispense 7 μL of borate buffer into both reservoirs. Apply 200 V DC for an additional 5 min to remove excess SAv-QDs from the channel. Disable the volt-

age and remove the contents from all reservoirs. Dispense borate buffer into all reservoirs and obtain PL spectra throughout all channels to ensure successful immobilization (*see* **step 6** for instrumentation and analysis details). If QD PL is not visible from the interior of each channel then *see* **Note 18** for troubleshooting.

3. Add 7 μL of SMN1 probe oligonucleotide (3 μM) in Tris-borate buffer into the left reservoir (cathode) and 7 μL of Tris-borate buffer to the right reservoir (anode). Apply 200 V DC for 5 min to introduce the oligonucleotide electrophoretically into the channel. Disable the voltage and allow the chip to stand undisturbed for an additional 5 min to allow the nucleic acid to couple to the immobilized SAv-QDs. Remove the contents from all reservoirs and replace all reservoirs with 7 μL of Tris-borate buffer. Apply 200 V DC for an additional 5 min to wash out excess oligonucleotide. Disable the voltage and empty the contents of all reservoirs.
4. Dispense 7 μL of Cy3-labeled SMN1 target oligonucleotide (variable concentrations) into the left reservoir (cathode) and 7 μL of Tris-borate buffer into the right reservoir (anode). Apply 200 V DC for 3 min to introduce the target oligonucleotide. Disable the voltage, empty the contents of all reservoirs, and replace them with Tris-borate buffer. Apply 200 V DC for an additional 1 min to wash out excess target nucleic acid. Disable the voltage, empty all reservoir contents, and replenish with fresh Tris-borate buffer before quantitative optical analysis of PL changes.
5. Steady-state PL spectra and/or PL image profiles (Fig. 3a–c) are acquired from the on-chip assay using a custom-built epifluorescence microscope based on the Nikon Eclipse L150 model (Nikon, Mississauga, ON, Canada). Eq. 1 was used for calculation of the FRET ratio (R), and represents data analysis (Fig. 3d) with background-subtracted PL spectra [7]:

$$R = \left(\frac{\sum_{\lambda=560}^{590} \mathrm{PL}(\lambda)}{\sum_{\lambda=510}^{540} \mathrm{PL}(\lambda)} \right)_{DA} - \left(\frac{\sum_{\lambda=560}^{590} \mathrm{PL}(\lambda)}{\sum_{\lambda=510}^{540} \mathrm{PL}(\lambda)} \right)_{D} \quad (1)$$

where the wavelength (λ) ranges of maximum acceptor (Cy3) and donor (QD) PL are given by 560–590 nm and 510–530 nm, respectively. The first term in Eq. 1 with subscript *DA* describes a PL measurement made after excitation of the donor in the presence of the acceptor, while the second term with the subscript *D* denotes a spectrum collected in the absence of the acceptor. FRET ratios were used as the quantitative data for assay response that made use of PL intensity for samples that

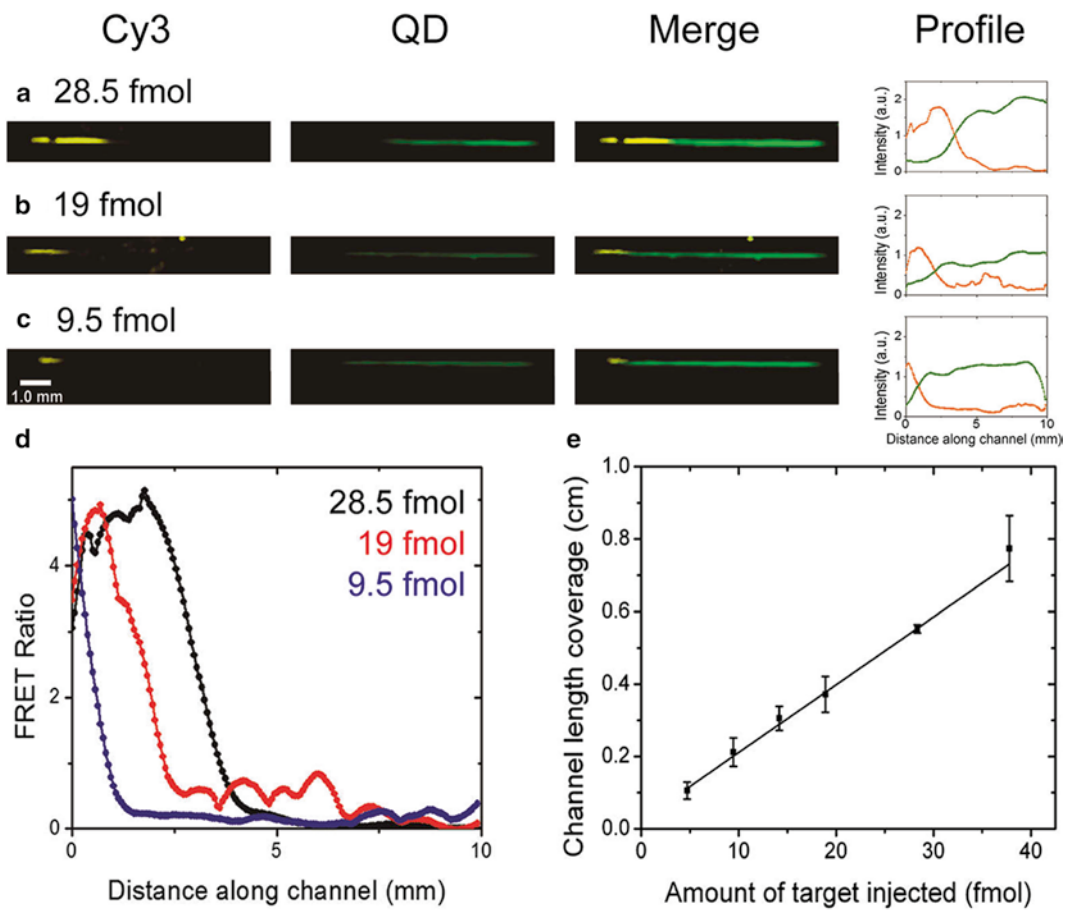

Fig. 3 Epi-fluorescence image of FRET-sensitized PL of Cy3, QD, and merge, with corresponding Cy3 and QD channel intensity profiles (Cy3: *orange*, QD: *green*) for the injection of (**a**) 28.5 fmol, (**b**) 19 fmol, and (**c**) 9.5 fmol of Cy3-labeled target oligonucleotide. The images have been background corrected. (**d**) In-channel FRET ratio profiles for the injection of 28.5, 19.0, and 9.5 fmol of Cy3-labeled target oligonucleotide. (**e**) Quantitative transduction of nucleic acid hybridization as a function of the length of channel covered by Cy3 PL. The channel length coverage was determined from a point where the Cy3 acceptor PL had decayed to 50 % of the initial intensity for that respective concentration. The target concentrations injected were between 0.25 and 2.0 μM at a fixed volume of 19 nL (reproduced from Tavares et al. [7] with permission from American Chemical Society)

contained fully complementary, noncomplementary, and partially mismatched oligonucleotide targets. This approach allowed assignment of a corresponding contrast ratio.

6. The spatial profile of FRET-sensitized PL along the channel length can be used for quantitative analysis of target concentration and differs from the use of intensity as an analytical signal that changes with target concentration (Fig. 3). After the hybridization reaction, PL images of a microfluidic chip

using the QD (525/20) or Cy3 (570/20) band-pass filters (as example, we used emission filters from Chroma Technologies Corp., Bellows Falls, VT) are acquired. The resulting images are processed using ImageJ (National Institutes of Health, Bethesda, MD) to determine the length of coverage associated with each of the PL channels. Select the line tool in ImageJ and manually draw a line from the edge of each reservoir with the appropriate pixel width to span the channel width. Then select plot profile to output a text file of position against intensity for the drawn line. Repeat this same protocol for the other wavelength channel using the exact same XY coordinates. Then normalize each individual plot profile and superimpose the two intensity profiles as a function of distance for comparison. Identify the crossover point by comparing the intensity profiles for the two wavelength channels, with the Cy3 PL profile starting with a high intensity and dropping to a lower value as a function of distance and the QD PL profile showing the reverse trend (Fig. 3a–c). This crossover position is used as the analytical signal, making concurrent use of data from both the QD and Cy3 emission (Fig. 3e). Plotting the crossover point position against the concentration of injected DNA or the amount (mol) of DNA enables assay calibration for a fixed set of operational parameters consisting of applied voltage, ionic strength, pH, and injection time.

4 Notes

1. A large amount of heat is released when reactive compounds (acids/bases) are mixed with water. Always add acids/bases to water and never the reverse.
2. We find that it is best to prepare this solution in a glove box.
3. Buffer solutions should be autoclaved and filtered through an Acrodisc® 0.2 μm syringe filter (Pall Corp, Ann Arbor, MI) before use.
4. QDs exist with various emission wavelengths. Use QDs that best fit your application. Prepare solutions in a glass vial (plastic vials have been shown to cause aggregation). The streptavidin protein has an extraordinarily high affinity for biotin, with multiple binding sites exhibiting a binding constant of ~10^{-14}–10^{-15} M. Coating the surface of the QDs with streptavidin makes them suitable for very specific attachment of biotin-labeled probes (e.g., oligonucleotides).
5. A wide variety of nucleic acid hybridization assays can be developed, depending on the identity of the probe and target sequences.

6. The choice and position of the fluorophore are essential and must correspond to the choice of QD. FRET can only occur when the QD donor and fluorophore acceptor possess sufficient spectral overlap and are brought in close proximity to one another (within a few nanometers) [17]. Our team has also developed label-free (the analyte of interest is void of a fluorescent label) nucleic acid hybridization assays [18].
7. When placing cover slips into holders ensure spacing between adjacent substrates since glass contact can impede surface modification and will result in irreproducibility of QD immobilization in the later assay assembly steps. Teflon® "arms" ensure the prevention of damage to the cover slips from contact within the reaction chamber during agitation. Samples of silicon wafers can be added to a batch of glass cover slips to follow the chemical modification and immobilization steps. Note that the sensitivity of the silanization reaction to moisture (ambient humidity) can cause an unnecessary amount of polymerization and multilayer formation. The reaction chemistry of glass and oxidized silicon is similar and allows silicon wafers to be surrogates of glass for physical characterization of coatings. The reflective nature of the silicon substrate enables ellipsometric measurements of the homogeneous surface thickness after the silanization and biotinylation steps. Generally, an increase of 10 nm in surface thickness is seen for deposition of APTMS and 3–5 nm for biotin using a silicon wafer that is treated as the glass samples. The conductive nature of the silicon also enables SEM (scanning electron microscopy) imaging of in-channel QDs. However, QDs must be delivered into the microfluidic channels of PDMS-silicon chips by pressure flow since the conductivity of silicon shorts the applied voltage.
8. After the final diethyl ether rinse, allow the solvent to evaporate from the cover slips in the fume hood before placing them in a desiccator or a vacuum oven. To ensure successful silane coupling in the subsequent step, avoid prolonged exposure to ambient atmosphere since the etched silanols can reoxidize and may prevent further modification.
9. An alternative silanization protocol can be used in the absence of an inert environment [19]. Since the procedure uses volatile solvents, the procedure should be performed in a fume hood. Place the cover slips (fitted into mini-rack holders) in a glass beaker. The silanization solution is prepared by mixing acetic acid (0.1 % v/v) and APTMS (5 % v/v) in isopropanol. The solution should be prepared immediately prior to use. The cover slips are incubated with the silanization solution that is placed on an orbital shaker for 30 min at room temperature (23 °C). Longer incubation times would provide a higher density of functional groups, but this tends to produce a

nonuniform layer of surface chemistry. After incubation, the cover slips are thoroughly and repeatedly washed by sonicating (water bath sonicator) the cover slips in a solution of isopropanol five times, 2 min each time. Wash once with dichloromethane and once with diethyl ether. Allow the cover slips to dry in the fume hood. The cover slips are then cured in an oven at 120 °C for 2 h. Store the amine-modified cover slips in a vacuum desiccator until future use.

10. In our earlier work, amide formation between the amine-terminated cover slips and biotin was conducted in situ, where the activation of the carboxylic acid to the succinimidyl ester using carbodiimide chemistry was conducted in a reaction chamber containing the glass cover slips at room temperature, 23 °C [7]. More recently, we have synthesized the succinimidyl ester of biotin in a separate step for two reasons: (a) the solubility of biotin in DMF and thus its subsequent activation is poor at room temperature (23 °C) and (b) in situ activation is not economical in terms of reagent cost. We have observed that increasing the temperature of the succinimidyl ester activation to ca. 60 °C provides for yields of biotin-NHS in excess of 90 % in comparison to 40 % at room temperature (23 °C). Coupling of biotin-NHS to APTMS-terminated slides proceeds sufficiently at room temperature (23 °C). Albeit in situ activation at an increased temperature under inert conditions is possible, the current apparatus (reaction chamber) requires 300 mL of anhydrous DMF for complete substrate immersion and this is again wasteful. In moving to this new experimental method for slide preparation, we have also noticed that the PL intensity of the resulting immobilized SAv-QDs has increased ca. 1.5-fold (unpublished results).
11. When synthesizing biotin-NHS, if a vacuum pump and/or cold trap system is unavailable, the product can be precipitated from an excess of diethyl ether at 0 °C. However, yields less than 40 % are realized. Purchasing this reagent from a vendor is an alternative.
12. Casting of PDMS can also be done in a petri dish. The elastomer mixture can be poured on the glass template that is placed within the dish such that the elastomer covers the template. However, for curing the PDMS, the temperature should be kept at 60 °C and the PDMS should be cured for 3 h.
13. This arrangement allows air plasma to oxidize the channel area only, rendering it hydrophilic and advantageous for the injection of aqueous solutions. This procedure also renders the top face of the PDMS stamp hydrophobic. This step is important as it prevents solution from spreading on top of the PDMS stamp upon sample addition to the reservoirs.

14. Sealing of PDMS to a chemically functionalized glass substrate can be done either by irreversible [7] or reversible [20] bonding methods. In the case of irreversible bonding, the PDMS and glass surfaces are both subjected to plasma oxidation to generate surface silanol groups [21]. The two plasma-oxidized surfaces are then brought in contact with each other to make an irreversible seal. A condensation reaction of the two silanol groups between the two substrates results in a formation of a siloxane bond and is responsible for an irreversible seal. In the case of reversible bonding, van der Waals interactions are responsible for the bonding between the two substrates. For the work presented in this study, reversible bonding was found to offer a more reproducible seal as compared to an irreversible seal.
15. It is important to initially fill either all three left or right reservoirs since rapid dispensing of solution to both reservoirs of a single channel can trap air within the channel. Enabling capillary action to drive the dispensed solution through the channel and into the adjacent reservoir eliminates this issue.
16. Application of an electric field results in cathodic EOF since the PDMS surface is negatively charged at pH >4. The SAv-QDs are slightly negatively charged, but their net mobility is by EOF instead of EPF. EPF is used to deliver the strongly polyanionic oligonucleotides.
17. If no visible QD PL is seen using the handheld UV lamp, it could suggest poor oxidation of PDMS resulting in insufficient EOF for delivery. Check to see if the plasma cleaner is operating at the appropriate vacuum range.
18. If no QD PL is visible after the washing step, this could suggest that the streptavidin on the surface of the QDs is no longer active. Check the SAv-QDs stock vial to ensure no visible aggregation. Conjugation of the SAv-QDs with biotinylated oligonucleotides in solution can be used to assess protein-binding activity. An agarose gel can then be run to see if conjugation was successful since the QD-oligonucleotide constructs will now migrate to the anode under an applied electric field, as demonstrated before [7].

Acknowledgements

The authors gratefully acknowledge financial support of their research program by the Natural Sciences and Engineering Research Council of Canada (NSERC). A.J.T. and U.U. are also thankful to NSERC for provision of graduate fellowships. M.O.N. is grateful to the Ontario Ministry of Training, Colleges and Universities (MTCU) for provision of an Ontario Graduate Scholarship (OGS).

References

1. Peter M (2001) Microfluidics – downsizing large-scale biology. Nat Biotechnol 19: 717–721
2. Meldrum DR, Holl MR (2002) Microscale bioanalytical systems. Science 297:1197–1198
3. Sia SK, Whitesides GM (2003) Microfluidic devices fabricated in poly(dimethylsiloxane) for biological studies. Electrophoresis 24:3563–3576
4. Whitesides GM (2006) The origins and the future of microfluidics. Nature 442:368–373
5. Erickson D, Li D (2004) Integrated microfluidic devices. Anal Chim Acta 507:11–26
6. Vannoy CH, Tavares AJ, Noor MO, Uddayasankar U, Krull UJ (2011) Biosensing with quantum dots: a microfluidic approach. Sensors 11:9732–9763
7. Tavares AJ, Noor MO, Vannoy CH, Algar WR, Krull UJ (2012) On-chip transduction of nucleic acid hybridization using spatial profiles of immobilized quantum dots and fluorescence resonance energy transfer. Anal Chem 84:312–319
8. Algar WR, Krull UJ (2009) Interfacial transduction of nucleic acid hybridization using immobilized quantum dots as donors in fluorescence resonance energy transfer. Langmuir 25:633–638
9. Algar WR, Krull UJ (2009) Toward a multiplexed solid-phase nucleic acid hybridization assay using quantum dots as donors in fluorescence resonance energy transfer. Anal Chem 81:4113–4120
10. Algar WR, Krull UJ (2010) Developing mixed films of immobilized oligonucleotides and quantum dots for the multiplexed detection of nucleic acid hybridization using a combination of fluorescence resonance energy transfer and direct excitation of fluorescence. Langmuir 26:6041–6047
11. Algar WR, Krull UJ (2011) Interfacial chemistry and the design of solid-phase nucleic acid hybridization assays using immobilized quantum dots as donors in fluorescence resonance energy transfer. Sensors 11:6214–6236
12. Petryayeva E, Algar WR, Krull UJ (2013) Adapting fluorescence resonance energy transfer with quantum dot donors for solid-phase hybridization assays in microtiter plate format. Langmuir 29:977–987
13. Noor MO, Shahmuradyan A, Krull UJ (2013) Paper-based solid-phase nucleic acid hybridization assay using immobilized quantum dots as donors in fluorescence resonance energy transfer. Anal Chem 85:1860–1867
14. Chen L, Algar WR, Tavares AJ, Krull UJ (2011) Toward a solid-phase nucleic acid hybridization assay within microfluidic channels using immobilized quantum dots as donors in fluorescence resonance energy transfer. Anal Bioanal Chem 399:133–141
15. Susumu K, Mei BC, Mattoussi H (2009) Multifunctional ligands based on dihydrolipoic acid and polyethylene glycol to promote biocompatibility of quantum dots. Nat Protoc 4:424–436
16. Erickson D, Sinton D, Li D (2003) Joule heating and heat transfer in poly(dimethylsiloxane) microfluidic systems. Lab Chip 3:141–149
17. Clapp AR, Medintz IL, Mattoussi H (2006) Forster resonance energy transfer investigations using quantum dot fluorophores. ChemPhysChem 7:47–57
18. Vannoy CH, Chong L, Le C, Krull UJ (2013) A competitive displacement assay with quantum dots as fluorescence resonance energy transfer donors. Anal Chim Acta 759:92–99
19. Petryayeva E, Krull UJ (2012) Quantum dot and gold nanoparticle immobilization for biosensing applications using multidentate imidazole surface ligands. Langmuir 28: 13943–13951
20. Noor MO, Krull UJ (2011) Microfluidics for the deposition of density gradients of immobilized oligonucleotide probes; developing surfaces that offer spatial control of the stringency of DNA hybridization. Anal Chim Acta 708:1–10
21. McDonald JC, Whitesides GM (2002) Poly(dimethylsiloxane) as a material for fabricating microfluidic devices. Acc Chem Res 35:491–499

INDEX

A

Antibody(ies) 26, 34–36, 41, 42, 47, 50–52, 55–65, 68–78, 80, 82, 129–139, 180, 183, 186
  functional fragments 56–58
  reduction 57, 58

B

BAL. *See* Broncho-alveolar lavage (BAL)
Biocompatible 13–29
Bioconjugate 6, 34, 103–108, 216, 242
Bioconjugation 6, 34, 103–109
Biophotonics tools 3–8
Biotinylated lipid particles (BLPs) 113–126
Broncho-alveolar lavage (BAL) 181, 182, 185, 208, 210

C

Cadmium telluride (CdTe) 5, 35, 37–40, 48–50, 96–98, 105–109, 114, 155, 166–168, 179
Capillary electrophoresis 33–52
Carbodiimide 56, 68–71, 76, 253
CdTe. *See* Cadmium telluride (CdTe)
Cell culture 26, 116, 142–148, 152, 153, 157, 159, 166, 167, 170, 171, 187, 193, 196, 202, 203
Cell labeling 56, 132, 143, 150, 152
Cell tracking 141
Cellular imaging 67–82, 203–204, 215
Co-culture 142, 146–154
Confocal fluorescence microscopy 115, 148, 203–204
Confocal fluorescent microscopy 142
Confocal microscopy 104, 121, 122, 126, 165, 171, 193, 195–196
Conjugate 15, 16, 18, 26–29, 33–52, 55, 56, 58, 59, 61–65, 67–82, 109, 116, 129, 131, 134–139, 215–237, 244
Conjugation 5, 15, 26, 29, 35, 36, 40–43, 47–52, 55–65, 67–69, 71–73, 75–79, 103–108, 129–139, 179, 180, 221, 254
Cortex 197
Coupling 18, 34, 67–82, 106, 107, 114, 121, 154, 243, 246, 252, 253
Cytospin 183, 185
Cytotoxicity 156, 157, 160, 161, 180, 183, 184

D

Detergent dialysis 114, 118, 120
Diagnostic nanoprobes 58, 130–132, 136–138
Diffusion coefficient 88, 89, 125
3-(4,5-Dimethylthiazol-2-yl)-5-(3-carboxymethoxyphenyl)-2-(4-sulfophenyl)-2H-tetrazolium (MTS) 156–160
(3-(4,5-Dimethylthiazol-2-yl)-2,5-diphenyltetrazolium bromide) (MTT) 156

E

EDC. *See* 1-Ethyl-3-(3-dimethylaminopropyl)carbodiimide (EDC)
Epidermal growth factor 114, 122, 123, 125
1-Ethyl-3-(3-dimethylaminopropyl) carbodiimide (EDC) 34, 36, 40–43, 47, 52, 68, 69, 71, 72, 75, 76, 79, 82, 106, 107

F

FCS. *See* Fluorescence correlation spectroscopy (FCS)
Flow cytometry 63–65, 130, 131, 136, 181, 183, 186, 204, 215
Fluorescence correlation spectroscopy (FCS) 85–90, 104
Fluorescence plate reader 104, 107, 109, 219, 220, 225, 228
Fluorescent recovery after photobleaching (FRAP) 142, 148–151, 153
Förster resonance energy transfer (FRET) 7, 14, 47–49, 94, 120, 215–237, 242, 249, 250, 252
FRAP. *See* Fluorescent recovery after photobleaching (FRAP)
Full-size antibodies 55–65

Adriana Fontes and Beate Saegesser Santos (eds.), *Quantum Dots: Applications in Biology*, Methods in Molecular Biology, vol. 1199, DOI 10.1007/978-1-4939-1280-3, © Springer Science+Business Media New York 2014

H

Highly oriented conjugates....129, 130
Hybridization 49, 215, 241–254
Hydrodynamic radius measurement 85–90

I

Imaging 7, 13, 14, 34, 55, 60, 67–82, 114, 122, 123, 126, 141–144, 148, 150, 152, 153, 155, 179, 191–205, 215, 216, 234, 252
Immobilization....27, 71, 73, 109, 242, 248, 249, 252
Immuno assay.... 34, 49–51, 109
Inflammatory changes 211
Inhalation
  exposure....207, 208
  study 207–212
Intranasal delivery 201
Intranasal instillation....181, 184
Intratracheal instillation 182, 184
In vitro.... 56, 113, 141, 142, 155–162, 179, 180, 187, 191–205
In vivo 56, 113, 141, 156, 179–189, 191–205
Ischemia 196

L

Lactate dehydrogenase (LDH)....156, 157, 159–161, 180, 181, 183–184, 187, 211
Laser-induced fluorescence (LIF)..... 34–36, 45–47, 50
Laser-induced luminescence....33–52
LDH. *See* Lactate dehydrogenase (LDH)
Lipoic acid....13–29, 233
Live cell imaging 142, 150, 153, 193, 195–196, 202
Living HeLa cells....166

M

Mesenchymal stem cells (MSCs) 141–154
Microfluidics 46, 241–254
Microglia 192–195, 197, 201–203
Microscopy....7, 45, 46, 89, 103, 116, 122, 137, 153, 170, 171, 183, 185, 193, 196
MTS. *See* 3-(4,5-Dimethylthiazol-2-yl)-5-(3-carboxymethoxyphenyl)-2-(4-sulfophenyl)-2H-tetrazolium (MTS)
MTT. *See* (3-(4,5-Dimethylthiazol-2-yl)-2,5-diphenyltetrazolium bromide) (MTT)

N

Nano-cell interaction....166
Nanomaterials 4, 103, 157, 179, 207–212, 242
Nanomaterial toxicity....207–212
Nano-neuroscience....191
Nanoparticle....3, 5, 7, 14, 34, 35, 37, 45, 113, 114, 129–131, 141, 155, 156, 165, 166, 171, 172, 201, 204, 207, 209, 210, 212
Nanoprobe....55–58, 62, 64, 129–132, 136–138
Nanotechnology 4, 33, 180, 191
Neural cells....191–205

O

Optical properties....3–5, 49, 93, 107, 192, 216, 242
Oriented conjugation....55–65, 129–139

P

Peptide....26, 29, 34, 41, 113, 150, 216–219, 221, 223–228, 230, 232–237
Photo-induced ligand exchange 15
Progress curve....230–232
Protein 13, 15–18, 23, 26–27, 29, 34, 35, 52, 59, 60, 69, 72–75, 103–109, 113, 180, 181, 183, 185, 186, 188, 192, 201, 203, 211, 216, 217, 220, 234, 251, 254
Protein conjugation 15
Proteolysis 218, 236

Q

Quantum dot-antibody conjugate 55–65, 67–82
Quantum yield....13, 14, 22, 93–100, 133, 141, 165, 179, 217, 219

R

Red blood cells (RBCs) 152, 166, 171–172, 186
Respiratory tract 184, 208, 210, 212

S

sdAb. *See* Single-domain antibody (sdAb)
Semiconductor quantum dots (QDs) 13, 155, 166, 215, 242
Semiquantitative fluorescence 103–109
Silane chemistry 252
Single-domain antibody (sdAb) 129–139
Solid-phase supports 241–254
Spatial detection 242

T

Targeted delivery 113
Thermal lens....93–100
Tissue fixation 181, 184, 187–188
Toxicity study 207–212

Z

Zwitterion ligands 13–29